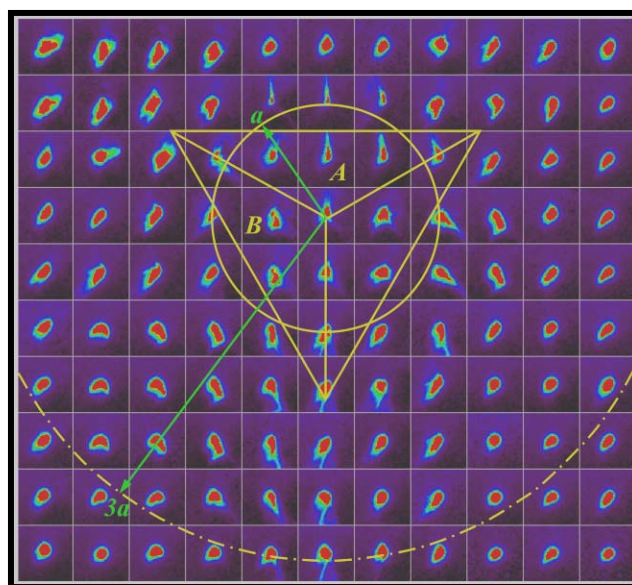
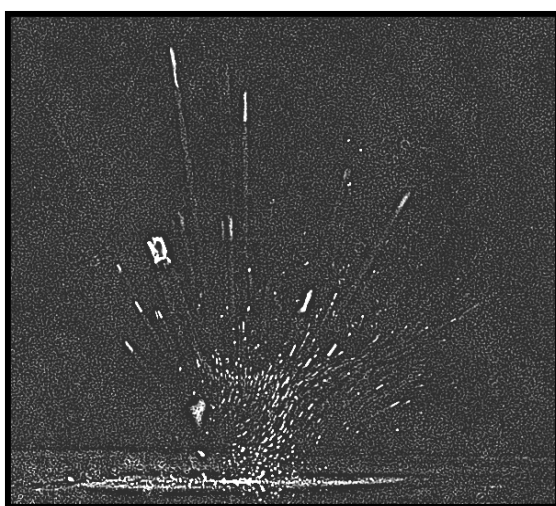
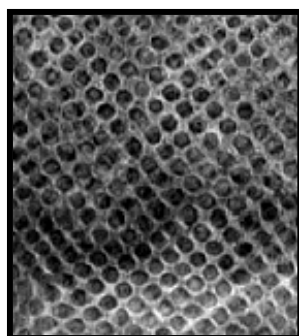
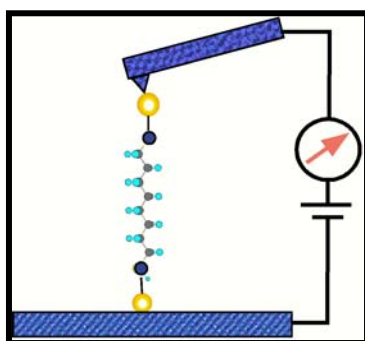
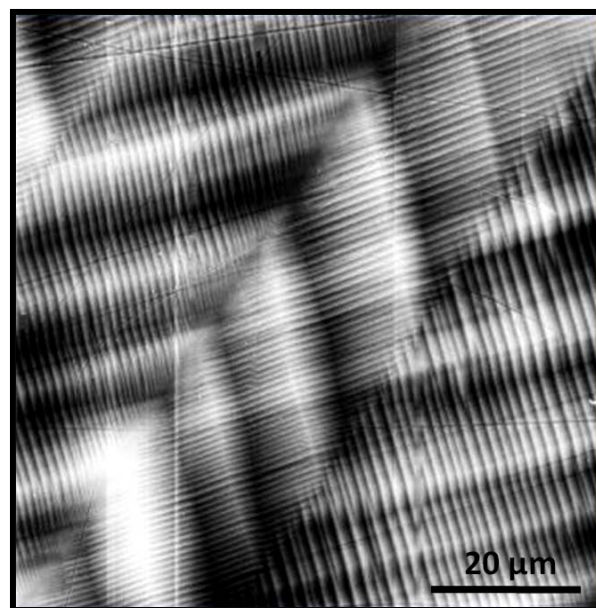
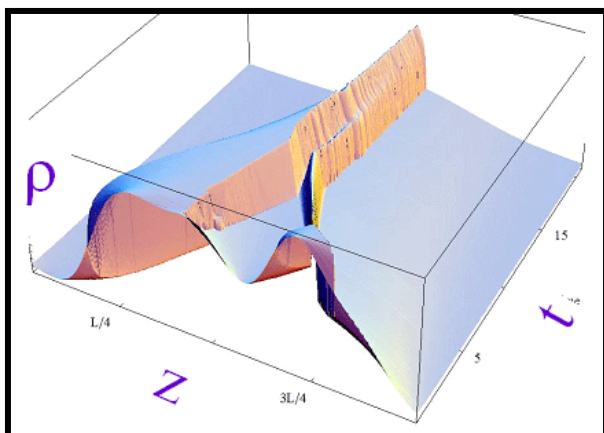


Behavior of Defects in Materials

Contractors Meeting – 2008

April 13-16, 2008

Airlie Conference Center, Warrenton, VA



Office of Basic Energy Sciences

Division of Materials Sciences and Engineering

Cover

Top Right - AFM Image of Twins in Ni-Mn-Ga Magnetic Shape Memory Alloy (Müllner, et al., Boise State University)

Bottom Right - Streaked Laue spots associated with locating a white x-ray microbeam at various locations in an indentation in single crystal copper (Nix, et al., Stanford University)

Bottom Left - High speed photographic image (1000 frames/sec) of particles being ejected from a beta-eucryptite composite that has experienced an indentation (Reimanis, et al., Colorado School of Mines)

Middle Left - Simultaneous conductance and force measurement of a molecular junction during breakdown using a conducting AFM setup (Tao, et al., Arizona State University)

Middle Right - Overfocused bright-field TEM images of voids in CaF₂ recorded during *in situ* TEM with electron fluence of $2 \times 10^{21} \text{e}^-/\text{cm}^2$. A superlattice of nanovoids has developed through a self- organization process. (Wang, et al., University of Michigan)

Top Left - The formation and coarsening of dislocation walls as a function of time in a simulation including both glide and climb (Sethna et al., Cornell University)

Foreword

This volume comprises the scientific content of the 2008 Mechanical Behavior and Radiation Effects Contractors Meeting sponsored by the Division of Materials Science and Engineering (DMS&E) in the Office of Basic Energy Sciences (BES) of the U. S. Department of Energy (DOE). The meeting, held on April 13-16, 2008, at the Airlie Conference Center, Warrenton, Virginia, is the second Contractors Meeting on this topic and is one among a series of research theme-based Contractors Meetings being held by DMS&E. The meeting's focus is on research in mechanical behavior and radiation effects of materials, and it also features research that cuts across several other BES core research program areas where appropriate and relevant.

The studies of mechanical behavior and radiation effects have a long and important history with respect to the generation, transmission, utilization and conservation of energy. It is a tribute to the researchers that they have continued to move the field forward into a number of important areas, as can be seen by the diversity of projects being presented at this meeting.

The purpose of the Mechanical Behavior and Radiation Effects Contractors Meeting is to bring together researchers funded by DMS&E in this important area of research on a periodic basis (approximately every three years) in order to facilitate the exchange of new results and research highlights, to nucleate new ideas and collaborations among the participants, and to identify needs of the research community. The meeting will also help DMS&E in assessing the state of the program, identifying new research directions and recognizing programmatic needs. The discussion sessions are a complement to the programmatic presentations and I would like to especially acknowledge the help of Bill Nix, Bill Weber and Rob Ritchie for facilitating the discussions.

I would like to express my sincere thanks to all of the attendees, especially the invited speakers, for their active participation and sharing their ideas and new research results. The effort and advice of the meeting chair, Dr. Amit Misra, of Los Alamos National Laboratory, in helping to bring these ideas together is deeply appreciated. I would also like to express my sincere gratitude to Ms Christie Ashton in DMS&E; and Sophia Kitts, Lois Irwin and Barbara Cohen of the Oak Ridge Institute of Science and Education (ORISE) for their dedicated and outstanding work in taking care of all the logistical aspects of the meeting.

John Vetrano
Program Manager
Mechanical Behavior and Radiation Effects
Division of Materials Sciences and Engineering
Office of Basic Energy Sciences
U.S. Department of Energy

Table of Contents

Table of Contents

Foreword	i
Table of Contents	ii
Agenda	v
Poster Session I	xi
Poster Session II	xii

Keynote Speakers

<i>Seeing is Believing: Micro-compression in the Spotlight of a Synchrotron</i> Helena Van Swygenhoven	1
<i>Smaller is Stronger: Observations and Possible Explanations</i> C. A. Volkert	2

Grant Projects

<i>Microstructural Evolution and Mechanical Response of Complex Alloys Under Prolonged Particle Irradiation</i> Robert Averback and Pascal Bellon	3
<i>Nano Vacancy Clusters and Trap Limited Diffusion of Si Interstitials in Silicon</i> Wei-Kan Chu	7
<i>Nanomaterial Thin-Film Structures: Fracture and Complex Environment</i> Reinhold H. Dauskardt	10
<i>Effect of Rare-Earth Additions on the Microstructural Evolution and Mechanical Properties of Al-Sc Alloys Containing Nanosize Precipitates</i> David C. Dunand and David N. Seidman	11
<i>Particle-Induced Modification of Complex Ceramics: Response of Materials to Extreme Conditions</i> Rodney C. Ewing, Lumin Wang and Jie Lian	15
<i>Plasticity in Ultra Fine Grained Materials</i> Marisol Koslowski	19
<i>Nano-mechanics of Tunable Adhesion Using Non-Covalent Forces</i> Kenneth M. Liechti, D. Xu, M. Wakamatsu, M. J. Krische and M. Y. Ngai	23

<i>Recent Results on Hydrogen-Induced Cracking of High-Strength Steels</i> Xin Yu Liu, Jun Kameda and C. J. McMahon, Jr.	27
<i>The Inverse Magnetoplastic Effect of Magnetic Shape-Memory Alloys</i> Peter Müllner	29
<i>Roles of Nanoclusters in Shear Banding and Plastic Deformation of Bulk Metallic Glasses</i> T. G. Nieh	33
<i>Mechanical Properties of Materials with Nanometer Scale Microstructures</i> William D. Nix	37
<i>Understanding Size Effects in Cleavage Cracking in Thin Film Materials</i> Yu Qiao	41
<i>The Coupling Between Interfacial Charge and Mechanical Deformation at High Temperatures in Ceramics</i> Rishi Raj	45
<i>Mechanical Behavior in Lithium Aluminum Silicate Composites</i> Ivar Reimanis	47
<i>Nanomechanics: Elasticity and Friction in Nano-objects</i> Elisa Riedo	50
<i>Continuum Plasticity: From Grain Boundaries and Coarsening to Cellular Structures and Recrystallization</i> James P. Sethna	54
<i>Shape Memory in Nanoscale Metallic Alloys</i> Alexander Thompson, Karthik Guda Vishnu and Alejandro Strachan	58
<i>Electrical, Mechanical and Thermal Properties of Single Molecules</i> Nongjian (NJ) Tao	62
<i>Multiscale Modeling of Dislocation Behavior in Non-Magnetic Transition Metals and Ferromagnetic Iron</i> V. Vitek	66
<i>Nanostructure Patterning Under Energetic Particle Beams: Radiation Effects Versus Self-Organization</i> Lumin Wang	70
<i>Near-Surface Plasticity and its Applications in Surface Treatment</i> Honghui Yu	74
<i>Investigating Deformation and Failure Mechanisms in Nanoscale Multilayer Metallic Composites</i> H. M. Zbib, D. F. Bahr, S. Medyanik, F. Akasheh, I. Mastorakos, Shuai Shao, Nicole Overman, Cory Overman, A. Misra and R. G. Hoagland	78

Laboratory Projects

<i>Microstructural Design of Advanced Ceramics</i> Paul F. Becher	82
<i>Atomistic Simulations of Irradiated Materials on the Reactor Timescales</i> Vasily Bulatov	86
<i>Mechanics of Small Length Scales</i> David M. Follstaedt, Elizabeth A. Holm, Jianyu Huang and John P. Sullivan	90
<i>Multiscale Mechanical Properties and Alloy Design</i> E. P. George, H. Bei, J. R. Morris, C. T. Liu, J. A. Horton, G. M. Pharr and Y. F. Gao	94
<i>On the Relevance of Interfaces to the Properties of Nanolayered Composites</i> R. G. Hoagland, A. Misra, M. J. Demkowicz and J. Wang	98
<i>New X-ray and Neutron Tools for Exploring Local Structures in Materials</i> Gene E. Ice	99
<i>Stable Nanoclusters in Metallic Matrices</i> C. T. Liu, C. L. Fu, M. K. Miller, J. H. Schneibel, M. J. Mills, X. L. Wang and M. Kremer	100
<i>Deformation Physics of Ultra-fine Scale Materials</i> Amit Misra	104
<i>LBNL Mechanical Behavior of Materials Program</i> R. O. Ritchie, A. P. Tomsia, E. Saiz, D. C. Chrzan and J. W. Ager	108
<i>Radiation Damage Effects in Ceramics and Non-Metals</i> Kurt E. Sickafus and Blas P. Uberuaga	112
<i>A Multi-scale Study of the Role of Microstructure in the Deformation Behavior of Hexagonal Materials</i> Carlos N. Tomé	115
<i>Defects and Defect Processes in Ceramics</i> William J. Weber, Ram Devanathan, Fei Gao, Weilin Jiang and Yanwen Zhang	119
Author Index	122
Participant List	123

Behavior of Defects in Materials Contractors Meeting – 2008

Agenda

U. S. Department of Energy
Office of Basic Energy Sciences
Behavior of Defects in Materials Contractors Meeting
Airlie Conference Center, Warrenton, VA
April 13-16, 2008

Sunday Evening, April 13, 2008

3:00 - 6:00 pm	Registration
6:00 - 7:00 pm	*****Dinner*****
7:00 - 7:15 pm	John Vetrano and Amit Misra: Welcome
7:15-7:45 pm	Harriet Kung: News from Office of Basic Energy Sciences
7:45 - 8:30 pm	Helena Van Swygenhoven, Paul Scherrer Institute, Switzerland <i>Seeing is Believing: Micro-Compression in the Spotlight of a Synchrotron</i>
8:30 - 9:15 pm	Cynthia Volkert - University of Göttingen, Germany <i>Smaller is Stronger: Observations and Possible Explanations</i>

Monday, April 14, 2008

Session I	Interface and Surface Effects in Mechanical Behavior <u>Chair</u> : Amit Misra, Los Alamos National Laboratory
7:00 - 8:00 am	*****Breakfast*****
8:15 - 8:45 am	Hussein Zbib, Washington State University, <i>Investigating Deformation and Failure Mechanisms in Nanoscale Multilayer Metallic Composites</i>
8:45 - 9:15 am	Elizabeth Holm, Sandia National Laboratory <i>Energy and Mobility of Flat Grain Boundaries</i>
9:15 - 9:45 am	Kevin Hemker, Johns Hopkins University <i>Stress-Coupled Grain Boundary Migration</i>

9:45 - 10:15 am	Easo George, Oak Ridge National Laboratory <i>Investigations of Small-Scale Plasticity in Single-Crystal Mo-Alloy Micro-pillars</i>
10:15 - 10:30 am	*****Break*****
10:30 - 11:00 am	Ian Baker, Dartmouth College <i>Structure/Property Relationships in High Strength Nanostructured Spinodal FeNiMnAl Alloys</i>
11:00 - 11:30 am	Rishi Raj, University of Colorado <i>The Coupling between Interfacial Charge and Mechanical Deformation at High Temperatures in Ceramics</i>
11:30 - 12:00 am	Marisol Koslowski, Purdue University <i>Plasticity in Ultra Fine Grained Materials</i>
12:00 - 1:00 pm	*****Lunch*****
1:00 - 3:30 pm	Discussion and Interactions
3:30 - 5:30 pm	Poster Session I <u>Chair:</u> Rishi Raj, University of Colorado
5:30 - 6:30 pm	*****Dinner*****
Session II	Interfaces and New Techniques <u>Chair:</u> David Bahr, Washington State University
6:30 - 7:00 pm	(Invited) Andrew Minor, LBNL <i>In situ TEM nanomechanics</i>
7:00 - 7:30 pm	(Invited) Gene Ice, Oak Ridge National Laboratory <i>New x-ray and Neutron Tools for Exploring Local Structures in Materials</i>
7:30 - 9:30 pm	Panel discussion: <i>Interfaces and New Techniques</i> <u>Chair:</u> William D. Nix, Stanford University

Presentations:

William D. Nix, Stanford University

Length Scale Effects on Strength and Plasticity of Crystalline Materials

Richard G. Hoagland, Los Alamos National Laboratory

On the Relevance of Interfaces to the Properties of Nanolayered Composites

Ian M. Robertson, University of Illinois Urbana-Champaign

Deformation Experiments in situ in the Transmission Electron Microscope

Q&A / Discussion

9:30 pm

Continue Poster Session I / Cash Bar

Tuesday, April 15, 2008

Session III

Radiation Effects

Chair: Rod Ewing, University of Michigan

7:00 - 8:00 am

*****Breakfast*****

8:15 - 8:45 am

Robert Averback, University of Illinois-Urbana Champaign
Microstructural Evolution and Mechanical Response of Complex Alloys under Prolonged Particle Irradiation

8:45 - 9:15 am

Wei-Kan Chu, University of Houston
Nano Vacancy Clusters and Trap Limited Diffusion of Si Interstitials in Silicon

9:15 - 9:45 am

Yanwen Zhang, Pacific Northwest National Laboratory
Damage Evolution and Recovery in Complex Oxides Under Irradiation

9:45 - 10:15 am

Kurt Sickafus, Los Alamos National Laboratory
Radiation Damage Effects in Ceramics and Non Metals

10:15 - 10:30 am

*****Break*****

Session IV

Structure/Property Relations

Chair: Richard LeSar, Ames Laboratory

10:30 - 11:00 am

Peter Müllner, Boise State University
The Inverse Magnetoplastic Effect of Magnetic Shape-Memory Alloys

11:00 - 11:30 am

Alejandro Strachan, Purdue University
Shape Memory in Nanoscale Metallic Alloys

11:30 - 12:00 Noon

Elisa Riedo, Georgia Institute of Technology
NanoMechanics: Elasticity and Friction in Nano-Objects

12:00 - 1:00 pm

*****Lunch*****

1:00 - 3:30 pm

Discussion and Interactions

3:30 - 5:30 pm

Poster Session II

Chair: Alejandro Strachan, Purdue University

5:30 - 6:30 pm

*****Dinner*****

Session IV cont'd

Structure/Property Relations

Chair: Daryl Chrzan, Lawrence Berkeley National Lab

6:30 - 7:00 pm

Irene J. Beyerlein, Los Alamos National Laboratory
Plasticity Constitutive Models of Hexagonal Materials

7:00 - 7:30 pm

C.T. Liu, Oak Ridge National Laboratory
Stable Nanoclusters in Ferritic Alloys: Formation Mechanism and Mechanical Behavior

7:30 – 9:30 pm

Panel Discussion: *Defects in Irradiated and/or Deformed Materials*

Chair: William J. Weber, Pacific Northwest National Lab

Presentations:

William J. Weber, Pacific Northwest National Laboratory
Effects of Electronic Excitations and Charge Transfer on Defects and Phase Transformations in Irradiated Ceramics

Vaclav Vitek, University of Pennsylvania
Precursors of Atomic Level Modeling of Dislocations, Interfaces and Radiation Damage and Development of the Link with Engineering Calculations

Lumin Wang, University of Michigan
Nanostructure Patterning under Energetic Particle Beam Irradiation

Q&A / Discussion

9:30 pm

Continue Poster Session II / Cash Bar

Wednesday, April 16, 2008

Session VI

Fracture

Chair: Charlie McMahon, University of Pennsylvania

7:00 - 8:00 am

*****Breakfast*****

8:15 - 8:45 am

Rob Ritchie, Lawrence Berkeley National Laboratory
Hierarchical/Hybrid Structural materials

8:45 - 9:15 am

Yu Qiao, University of California-San Diego
Understanding Size Effects in Cleavage Cracking in Thin Film Materials

9:15 - 9:45 am

Reinhold Dauskardt, Stanford University
Nanomaterial Thin-Film Structures: Fracture and Complex Environments

9:45 - 10:00 am

*****Break*****

10:00 - 10:30 am

Ivar Reimanis, Colorado School of Mines
Mechanical Behavior in Lithium Aluminum Silicate Composites

10:30 - 11:30 am

Discussion session on *Aspects of Fatigue and Fracture*
Leader: Rob Ritchie, Lawrence Berkeley National Laboratory

11:30 – 11:45 am

Concluding Remarks

11:45 am

Box lunches Available

Poster Session I
Jefferson Room
Monday, April 14, 3:30 – 5:30 pm

P-I-1 - Kenneth Liechti, University of Texas-Austin, *Nano-Mechanics of Tunable Adhesion using Non Covalent Forces*

P-I-2 - Bill Nix, Stanford University, *Length Scale Effects on Strength and Plasticity of Crystalline Materials*

P-I-3 - James Sethna, Cornell University, *Continuum Plasticity: From Grain Boundaries and Coarsening to Cellular Structures and Recrystallization*

P-I-4 - Nongjian Tao, Arizona State University, *Electromechanical Properties of Single Molecules*

P-I-5 - Honghui Yu, City College of New York, *Near Surface Plasticity and Its Implications in Surface Treatment*

P-I-6 - Nathan Mara, Los Alamos National Laboratory, *Stress-strain Response and TEM Characterization of Deformed Cu-Nb Multilayers*

P-I-7 - Hongbin Bei, Oak Ridge National Laboratory, *Reversible Strain softening and Shear Banding in Deformed and Annealed Bulk Metallic Glasses*

P-I-8 - T.G. Nieh, University of Tennessee – Knoxville, *Bypassing Shear Band Nucleation and Suctility Improvement in Bulk Metallic Glasses*

P-I-9 - Paul Becher, Oak Ridge National Laboratory, *Microstructural Design of Advanced Ceramics*

P-I-10 - David Dunand, Northwestern University, *Effect of Rare-Earth Additions on the Microstructural Evolution and Mechanical Properties of Al-Sc Alloys Containing Nanosize Precipitates*

P-I-11 - Jianyu Huang, Sandia National Laboratory, *In-Situ Atomic-Scale Nanomechanics of Carbon Nanotubes and Nanowires*

Poster Session II
Jefferson Room
Tuesday, April 15, 3:30 – 5:30 pm

P-II-1 - Pascal Bellon, University of Illinois-Urbana Champaign, *Microstructural Evolution and Mechanical Response to Complex Alloys under Prolonged Particle Irradiation*

P-II-2 - Charles McMahon, University of Pennsylvania, *Micromechanisms of the Ductile-Brittle Transition in Hydrogen-Induced Fracture of Steels*

P-II-3 - Vaclav Vitek, University of Pennsylvania, *Multiscale Modeling of Dislocation Behavior in Non-magnetic Transition Metals and Ferromagnetic Iron*

P-II-4 - Rodney Ewing, University of Michigan, *Particle-induced Modification of Complex Ceramics: Response of Materials to Extreme Conditions*

P-II-5 - Lumin Wang, University of Michigan, *Nanostructure Patterning under Energetic Particle Beam Irradiation*

P-II-6 - Richard LeSar, Ames Laboratory, *Mechanical Behavior and Defects in Solids*

P-II-7 - Daryl Chrzan, Lawrence Berkeley National Laboratory, *Modeling the Mechanical Properties of Hybrid Composites*

P-II-8 - Vasily Bulatov, Lawrence Livermore National Laboratory, *Atomistic Simulations of Irradiated Materials on the Reactor Timescales*

P-II-9 - Blas Uberuaga, Los Alamos National Laboratory, *Modeling Radiation Damage in Materials*

P-II-10 - Laurent Capolungo, Los Alamos National Laboratory, *Nucleation and Propagation of Twins in Hexagonal Materials*

P-II-11 - Bill Weber, Pacific Northwest National Laboratory, *Radiation Tolerance, Recrystallization, and Phase Transformations in Ceramics*

P-II-12 - Mike Demkowicz, Los Alamos National Laboratory, *Combining Experiments with Atomistic Modeling to Design Radiation Damage Resistant Composite Materials*

P-II-13 – David Olmsted, Sandia National Laboratories, *How Close are Two-Grain Boundaries? (In the Five-Dimensional Macroscopic Crystallographic Space)*

Keynote Speakers

**Seeing is believing:
micro-compression in the spotlight of a synchrotron.**

Helena Van Swygenhoven

Paul Scherrer Institut, CH-5232 Villigen PSI, Switzerland

Plasticity in single crystal micron sized pillars has gained considerable interest since the development of a new micro-compression technique with a flat punch equipped nanoindenter. For all fcc metals measured, the initial flow stress increases with decreasing pillar diameter. Plastic deformation is characterized by slip events that are reflected in discrete strain bursts. Large scattering amongst the data is reported, where pillars of similar orientation are deforming according to different slip systems, sometimes shearing-off or barrelling. To address the scattering and to understand the mechanism behind the increase in strength, an in-situ micro-compression device has been developed at the Swiss Light Source (SLS) allowing for the continuous measurement of time-resolved white beam Laue diffraction patterns during compression of pillars, capturing the initial microstructure and the changes in microstructure during deformation.

Smaller is Stronger: Observations and Possible Explanations

C.A. Volkert, University of Göttingen, Germany

The observation that yield stresses in metals increase with decreasing size has been confirmed in a variety of metals with different grain and sample sizes. Both the generality and the few notable exceptions to this trend can be used to gain insight into possible mechanisms. The successes and limitations of models based on dislocation interaction-limited and dislocation nucleation-limited deformation will be discussed in an effort to clarify whether a single process can account for the "smaller is stronger" trend.

University Grant Projects

Microstructural evolution and mechanical response of complex alloys under prolonged particle irradiation

Award number: DEFG02-05ER46217

Robert Averback
Department of Materials Science and Eng.
University of Illinois at Urbana-Champaign
104 S. Goodwin Ave, Urbana IL, 61801
averback@uiuc.edu

Pascal Bellon
Department of Materials Science and Eng.
University of Illinois at Urbana-Champaign
405 W. Green St, Urbana, IL 61801
Bellon@uiuc.edu

I. Overview: This program addresses issues critical to the development new nuclear reactors that can provide safe, sustainable, and economically viable energy production in the near future. For this purpose we are developing a generic, multiscale modeling approach to simulate the evolution of microstructures in complex alloys for a wide range of irradiation environments. The work is organized in four tasks. In Task 1, we develop and validate a quantitative multiphase phase field model that will be capable of tracking the evolution of point-defects, defect-clusters, precipitates, and dislocations, and we introduce a new efficient algorithm to integrate these kinetic equations in real-space. In Task 2, we and collaborators at LLNL integrate this phase field model with *ParaDis*, the dislocation dynamics code recently developed at LLNL. This integration will provide the computational muscle needed to gain insights into the physics of strain hardening, dynamic recovery, and dislocation reactions, self-organization and patterning. In Task 3 we perform molecular dynamics and kinetic Monte Carlo simulations of three dimensional microstructural evolution for model alloys over actual time scales. This model will provide input data, mechanisms, and validation of the phase field model. Task 4 consists of experiments that will provide critical input data for the modeling and validation tests of specific approximations in the models. These experiments utilize the most advanced imaging and diffraction techniques, such as three-dimensional atom probe microscopy, transmission electron microscopy, and diffuse x-ray scattering. The machinery developed in this program will be applied to evaluate the viability of nanoscale self organization for producing radiation resistant materials.

II. Progress to date:

A. Phase field model:

We have introduced a new phase field description that combines the standard continuous approach for chemical and point defect diffusion with a discrete approach for point-defect clusters. This mixed approach makes it possible to obtain a realistic description of the evolution of defect clusters during irradiation, based on the primary recoil spectrum of the particular projectile/target combination. It also allows us to retain a nanoscale description of the microstructure. We have applied this new phase field model to study the effect of primary recoil spectrum on segregation and precipitation either enhanced or induced by irradiation. An example of this new code is illustrated in Fig. 1.

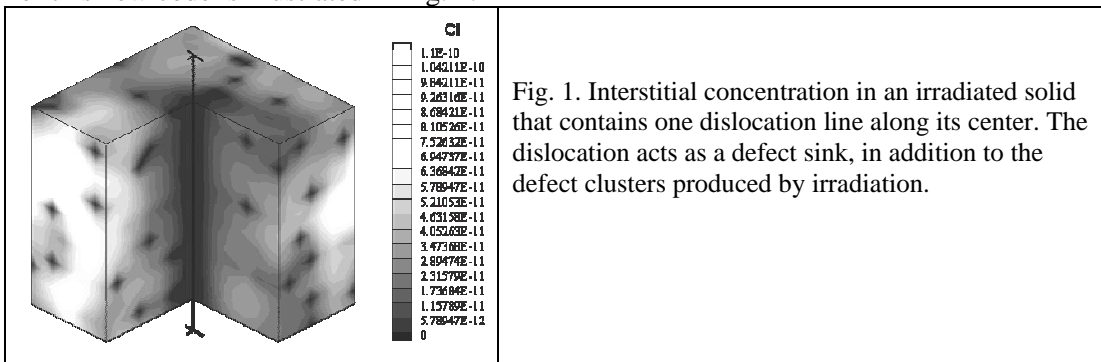
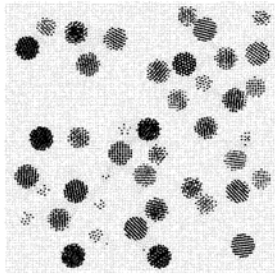
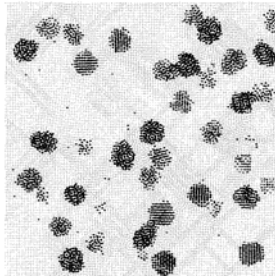
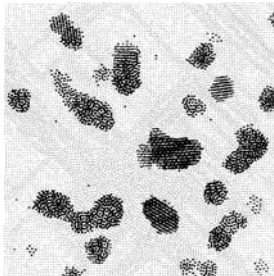


Fig. 1. Interstitial concentration in an irradiated solid that contains one dislocation line along its center. The dislocation acts as a defect sink, in addition to the defect clusters produced by irradiation.

B. Atomic level simulations

MD simulations of irradiated dilute Cu-Mo alloys: In connection with the experimental program, we have performed large scale MD simulations to examine phase stability in two-phase Cu-Mo alloys. We first show that bombardment of homogeneous Cu-Mo alloys with 50 keV Cu atoms leads to precipitation of Mo, even at low temperature where thermal diffusion is suppressed. This is a consequence of the low solubility of Mo in Cu and Mo transport during the thermal spike. We next show that small (1nm) Mo precipitates aggregate during bombardment at 200 K, but do not coagulate into dense precipitates, see Fig. 2(b). In contrast, irradiation at 750 K leads to dense precipitates, Fig. 2(c). This behavior is a consequence of the high melting temperature of Mo, i.e., during room temperature bombardment, the Mo precipitates can move in the liquid Cu produced by the thermal spike and aggregate, but since the Mo precipitates do not melt, they do not coagulate. At 750 K, on the other hand, Mo does melt during the thermal spike and coagulation occurs. These results suggest that Mo precipitates thus grow by a cluster aggregation mechanism and not the usual LSW mechanism. As a consequence, the nanoscale precipitate structure is stable to very high temperatures, agreeing with the experimental results discussed below.

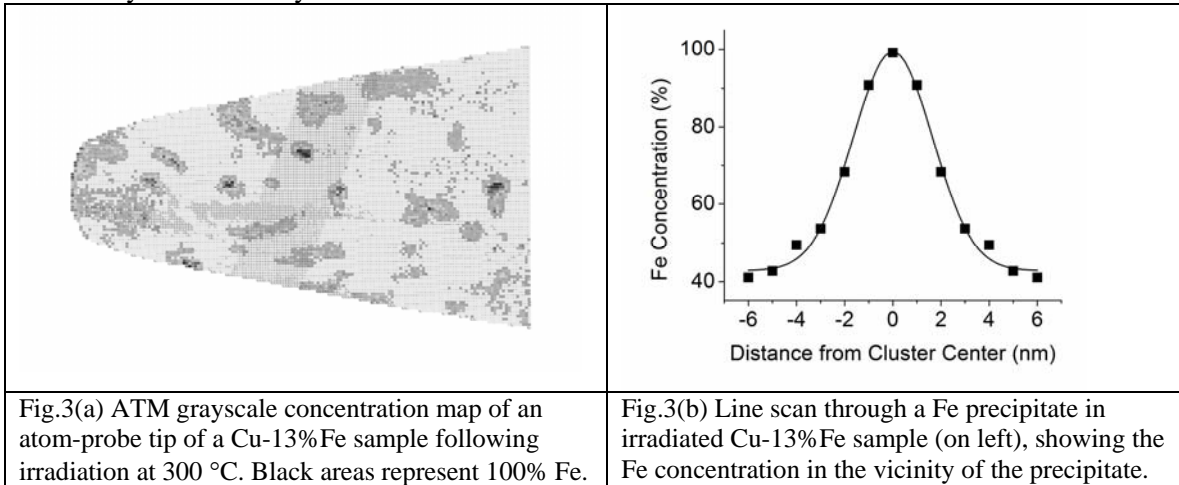
Kinetic Monte Carlo simulations of radiation-induced segregation: This work considered homogeneous nucleation of precipitate phases (see publ. (1)). In this study the interesting finding was that homogeneous nucleation of precipitates could form in systems that normally form ideal solutions under equilibrium conditions. Moreover, these precipitates are generally ramified structures. Small changes in the heat of mixing, however, dramatically altered the precipitate structure to one that is compact. This unusual behavior can be attributed to the extremely large chemical potential of interstitials in metals, and may provide an explanation for so-called “mushy” zones observed in dilute Fe-Cu alloys.

		
Fig.2(a) As prepared state: Cu containing 1 nm Mo precipitates. The precipitates are 10% atom fraction	Fig.2(b) Microstructure following bombardment with 50 keV Cu at 200 K. Precipitates aggregate but maintain ramified structure.	Fig.2(c) Same as Fig. 2b, but bombardment at 750 K.

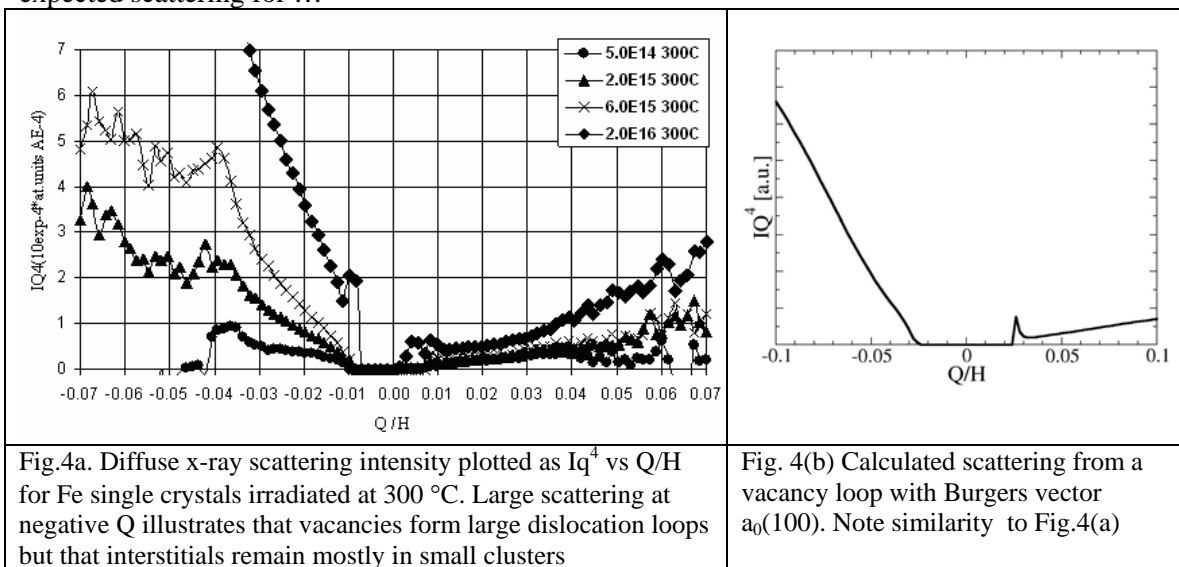
C. Experimental progress

Irradiation induced self organization at the nanoscale: It has long been known that the detrimental effects of irradiation damage in crystalline materials could be suppressed by the inclusion of high concentrations of unbiased defect sinks and/or defect traps in the microstructure. The difficulty with this approach, however, has been that such specially designed microstructures are generally not stable under prolonged irradiation. This program is looking into the potential of utilizing alloys that undergo self organization of the compositional field under irradiation during high temperature irradiation. We have been employing atom probe microtome (ATM) and x-ray diffraction to address the potential of this approach. These results, moreover, enable quantitative validation of the phase field model. Dilute Cu-Fe alloys provide an excellent test of the model since Fe precipitates coherently in Cu, however, the size distribution and concentration of the precipitates are difficult to measure by diffraction and so we employ ATM as illustrated in Fig.3.

At 300 °C, the Fe precipitates approach a steady size of ≈ 5 nm, although precipitates are not uniform in size or concentration. In another Cu eutectic alloy, Cu-10%Mo, we find using x-ray diffraction that precipitates are stable with size, ≈ 5 nm, up to at least 600°C, owing to the low diffusivity and solubility of Mo in Cu.



Diffuse x-ray scattering of defect in Fe: One of the most difficult tasks in the study of irradiation damage is identifying small defect clusters and determining their properties, i.e., structure and mobility. Yet understanding defect clusters is crucial for both predicting the response of materials to irradiation and establishing benchmarks for multiscale simulations, including our own. Diffuse x-ray scattering remains one of the few methods capable of providing such information. We have been performed such measurements on 2 MeV Kr irradiated Fe single crystalline thin films, which we have grown in our laboratory. Results from recent experiments are illustrated in Fig. X, where the scattering is plotted as a function of distance from a (110) reciprocal lattice vector, H, i.e. $Q = K - H$, where K is the scattering vector. The data obtained after irradiation at 300 °C to different doses show more scattering at $-Q$ than $+Q$ signifying that the size of the defect clusters (loops) are much larger for vacancies than interstitials. More detailed interpretation of these scattering data is greatly facilitated by computer simulation. For example, Fig. 4 shows the expected scattering for ...



III. Future Plans:

Phase field model: Using the newly developed phase field model and code, we will perform a systematic study to determine the conditions leading to heterogeneous irradiation-induced precipitation (IIP) in an undersaturated solid solution. In particular, we will focus on the effects of temperature, displacement rate, and primary recoil spectrum, and compare with existing data for IIP, for instance for Ni-Si solid solutions irradiated with 1 MeV electrons and 500 keV Ni ions. In parallel, we will collaborate with V. Bulatov at LLNL to include stress effects on diffusion, using his newly developed real-space approach, based on fast multipole expansion. We will also work with LLNL to fully optimize the parallel version of our code, in order to take full advantage of the computing power of current computer machines.

Atomic scale simulations: Kinetic Monte Carlo (KMC) computer simulations will be performed to set benchmarks for the phase field modeling. We will examine a simple eutectic alloy for which both interstitials and vacancies couple to the solute and form precipitates at defect clusters. This system is sufficiently complex that the outcome is not trivial, yet sufficiently simple to examine the behavior of the phase field model. For this work, we will employ a new parallel KMC code developed by our collaborators at LLNL. We will also employ KMC, in combination with MD, to further explore the mechanism of precipitate coarsening in systems like Cu-Mo during high temperature irradiation. Lastly, we will employ MD to explore the strength and deformation mechanisms of nanocomposite alloy systems.

Experimental work: The experimental studies have been just getting underway and most of the work discussed above will be continued in our second year. Particular attention will be focused on ATM studies of Cu-10%Mo alloy for which we will explore whether room temperature irradiation of the alloy leads to a ramified structure, as suggest by the simulations, and whether high temperature irradiations lead to compact precipitates with small size. We will also begin investigations on the stability of nanoscale oxide inclusions in Cu and Fe. For these studies we will employ our cluster deposition system to fabricate the specimens.

The work on diffuse x-ray scattering will be continued investigating the effect of alloying additions on the defect structure in Fe.

IV. Publications:

P. Krasnochtchekov, R.S. Averback, and P. Bellon, The role of interstitials in phase segregation of binary alloys under ion irradiation conditions from KMC simulations, *Phys. Rev. B* **75**, 144107 (2007)

P. Krasnochtchekov, P. Bellon and R.S. Averback, "Precipitate Stability and Morphology in Irradiation Environments" *JOM* **59**: 46-50 (2007)

A. Badillo, Y. Liu, P. Krasnochtchekov, R. S. Averback, P. Bellon, "Generalized phase field modeling for microstructural evolutions in irradiated alloys", invited talk and proceeding publication for the 3rd Int. Conf. on Multiscale Materials Modeling, Freiburg, Germany, Sept. 18th 2006, p. 679.

Title: Nano Vacancy Clusters and Trap Limited Diffusion of Si Interstitials in Silicon

Principal Investigator: Wei-Kan Chu
Department of Physics and Texas Center for Superconductivity
University of Houston
Houston, TX 77204
TEL: 713-743-8252 (O); FAX: 713-743-8201;
E-mail: wkchu@uh.edu

Program Scope

The objective of this project is to develop a method to characterize nano vacancy clusters and the dynamics of their formation in ion-irradiated silicon. It will impact (1) semiconductor device processing involving ion implantation, and (2) device design concerning irradiation hardness in harsh environments. It also aims to enhance minority participation in research and curricula on emerging materials and ion beam science. Vacancy defects are of scientific and technological importance since they are ubiquitous when the host materials are exposed to particle irradiation. Studies on vacancy clustering in the past decades were mainly theoretical and the approach heavily relied on the total-energy calculation methods. The lack of experimental data is mainly due to the formidable task in measuring the cluster size and density using modern metrological techniques, including transmission electron microscopy and positron annihilation spectroscopy. To surmount these challenges, we propose a novel approach to tackle the metrological problems on the nano vacancy clusters, especially in determining densities and sizes of the nano vacancies based on the premise that the vacancy-clusters act as diffusion-trapping centers. For a silicon substrate containing vacancy-clusters, the diffusion of interstitials (from the surface) can be classified into three phases: (1) an ultrafast phase-I in which the trapping centers have little effect on the diffusion of interstitials; (2) a prolonged phase-II in which the loss rate of interstitials by trapping balances the influx of interstitials from the surface; and (3) a phase-III diffusion in which surface influx of interstitials depletes the trapping centers and interstitials consequently propagate deeper into the bulk. By measuring diffusion profiles of Si interstitials as a function of diffusion time, void sizes and void densities can be obtained through fitting.

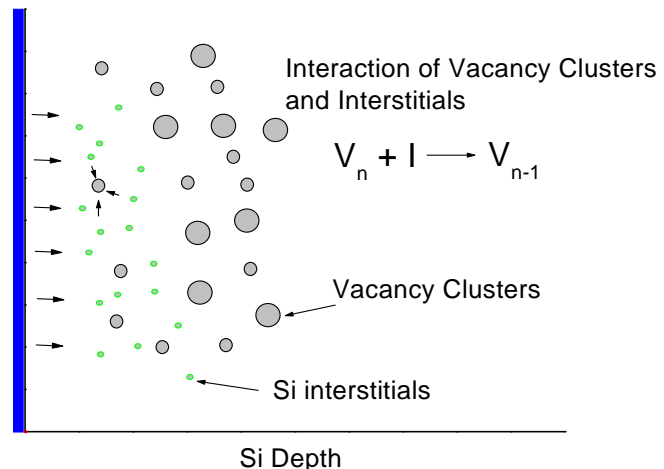
Recent Progress

(1) We have finished the characterization of voids through three consecutive steps.

(a) First, high energy self ion irradiation is used to create a wide vacancy-rich region, and to form voids by post implantation annealing.

(b) In an additional annealing step in oxygen ambient, Si interstitials are injected in by surface oxidation.

Surface oxidation to inject Si interstitials



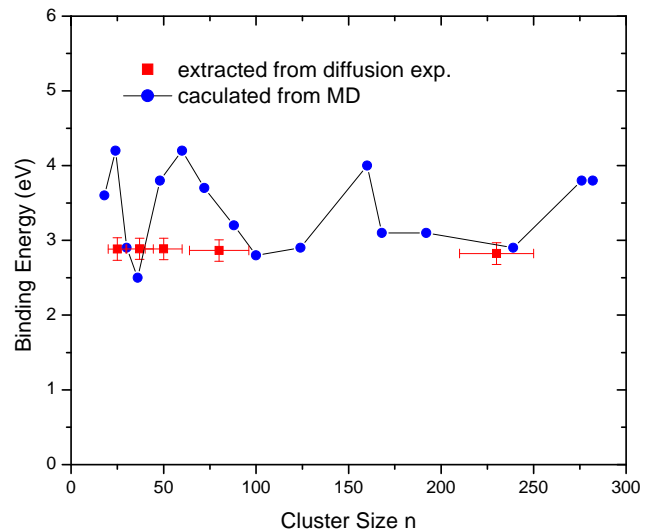
A schematic show of void-limited penetration of Si interstitials from the surface. Modeling of interstitial diffusion is able to extract void sizes and densities.

(c) Analyzing trap-limited diffusion of Si interstitials, which is experimentally detectable by studying the diffusion of multiple boron superlattices grown in Si, and enables us to characterize the nano voids, e.g. their sizes and densities.

(2) We have experimentally derived the binding energy of vacancy clusters as a function of sizes. Comparison with theoretical prediction has been conducted.

(a) We used Sb-doped Si superlattice markers to detect the free vacancy concentration at the annealing stages when void growth and decay have reached the equilibrium. Under such a quasi static state, the free vacancy concentration is determined by the binding energy of voids. Therefore, we derived the binding energy of voids as a function of mean void size.

(b) We have conducted large scale molecular dynamic simulations based on the potential derived from modified embedded atom methods. The binding energies of vacancy in voids as a function of void size have been obtained and compared with the experimental data.



The binding energy of vacancy clusters as a function of cluster size. The values are extracted from the diffusion experiments, and in a comparison with the values calculated from MD simulations.

(3) We have studied the stability of voids under high temperature annealing. It shows voids formed by MeV Si self ion implantation are very stable (up to 900 °C for 5 min anneal). This suggests that voids can survive high budget thermal processes in device fabrication. Thus, MeV implantation can be introduced in on-line processing with large flexibility, for the purpose of defect engineering.

(4) Details of atomic scale diffusion, such as migration lengths and jumping frequencies for two most important dopants, boron (B) and antimony (Sb), in the presence of voids, have been studied. These studies reveal the fundamentals of impurity-defect interactions and will impact defect engineering based approaches for a better control of doping profiles in fabricating microelectronics.

Future Plans

Multiscale modeling of void growth needs to be completed. This involves using continuum methods to predict void evolution, based on kinetics obtained through large scale molecular dynamic simulation. With experimental and modeling data obtained through the project, we are proceeding to accomplish the ultimate objective of the project, which is to better understand and be able to predict evolution of voids in silicon.

References to Publications of DOE Sponsored Research

1. L. Shao, M. Nastasi, P.E. Thompson, Q. Y. Chen, Jiarui Liu and Wei-Kan Chu, "Application of High Energy Ion Beam for the Control of Boron Diffusion"; Nucl. Instrum. Methods. Phys. Res. B, 242, 670 (2006).
2. L. Shao, M. Nastasi, P.E. Thompson, I. Rusakova, Quark Y. Chen, Jiarui Liu and Wei-Kan Chu, "The Energy Dependence of Excessive Vacancies Created by High Energy Ion Implantation"; Nucl. Instrum. Methods. Phys. Res. B, 242, 506 (2006).
3. L. Shao, M. Nastasi, J.K. Lee, T. Hochbauer, P.E. Thompson, I. Rusokova, H.W. Seo, Q.Y. Chen, J.R. Liu and Wei-Kan Chu, "Ion-cut of Si Facilitated by Interfacial Defects of Si Substrate/epitaxial Layer Grown by Molecular Beam Epitaxy"; Nucl. Instrum. Methods. Phys. Res. B, 242, 509 (2006).
4. L. Shao, M. Nastasi, X.M. Wang, J. Liu and Wei-Kan Chu, "A Model for Damage Caused by Cluster Implantation: Non-linear Effect due to Damage Overlap"; Nucl. Instrum. Methods. Phys. Res. B, 242, 503 (2006).
5. H.W. Seo, Q.Y. Chen, M.N. Iliev, L. W. Tu and C. L. Hsiao, J.K. Meen, and W.K. Chu, "Epitaxial GaN nanorods free from strain and luminescent defects"; Appl. Phys. Lett. 88,153124 (2006).
- 6 L. Zhu, M. Martin, M. Hollander, Q. Y. Wang, Q. Chen, K. Ma, X. K. Yu, J. R. Liu, Wei-Kan Chu, L. Shao, "Instability of junctions formed by low energy B implant and low temperature solid phase epitaxy growth", Journal of Vacuum Science & Technology B, 25 (2007) 1276-1279.
7. H. Chou, C. B. Wu, F. P. Yun, Z. H. Zhang, Wei-Kan Chu, "Particular strain relaxation for La_{0.8}Ba_{0.2}MnO₃ films on SrTiO₃(100) substrates", Applied Physics Letters, 91 (2007) 242505
8. K.R. Wang, S.J. Lin, L.W. Tu, M. Chen, Q.Y. Chen, T.H. Chen, M.L. Chen, H.W. Seo, N.H. Tai, S.C. Chang, I. Lo, D.P. Wang, and Wei-Kan Chu, "InN Nanotips as Excellent Field Emitters", Appl. Phys. Lett., in press.
9. L. H. Chu, E. Y. Chang, Y. H. Wu,, J. C. Huang, Q. Y. Chen, W. K. Chu, H. W. Seo, and C. T. Lee, "Study of interfacial reactions on Pt-based Schottky contacts on InGaP", Appl. Phys. Lett. 92, 1 (2008)

Papers submitted or in preparation for publication

10. K. Ma, X. Yu, Q. Chen, X. Wang, J. Liu and Wei-Kan Chu, L. Shao, P.E. Thompson, "A Temperature Independent Migration Length for the Diffusion of Antimony in Silicon", in preparation.
- 11.L. Shao, P.E. Thompson, Q. Chen, K. Ma and W.K. Chu, "Energetics of Large Vacancy Clusters in Si", in preparation.
12. L. Shao, P.E. Thompson, Q. Chen, K. Ma, J. Liu and Wei-Kan Chu, "Stabilities of Vacancy Clusters Formed in MeV Si Self-ion-implanted Si", Appl. Phys. Lett., submitted.

Nanomaterial Thin-Film Structures: Fracture and Complex Environments

Principal Investigator: Professor Reinhold H. Dauskardt
Department of Materials Science and Engineering
Stanford University
Stanford, CA 94305 - 2205

Considerable research efforts are being directed at exploiting nanostructured organosilicate thin films containing nanometer sized porosity or organic second phases for emerging nanoscience and energy technologies. Applications include biosensors, size-selective membranes, microfluidic structures, fuel cells, and microelectronics. While their potential and wide application in nanoscience is clear, little is currently understood regarding the mechanical and particularly fracture behavior of these nanostructured films, how they may be characterized, how they are related to the underlying glass and nanostructure, and how they are influenced by the presence of reactive chemical environments.

The present proposed program addresses the deficit in fundamental understanding of these properties by proposing an aggressive program involving two classes of very promising nanostructured glass films based on the incorporation of either *terminal* or *bridging* organic groups, the presence of nanometer sized porosity or organic second phases with controlled length scales, a wide range of film structures, and detailed fracture and nanostructural characterization in a range of complex aqueous solution chemistries. The research program will also include the development of a new and novel thin film fracture technique involving patterned test structures embedded in macroscopic fracture specimens which is expected to be a major advance for quantitative testing of thin film structures. Experimental research will be complimented with kinetic and multi-scale computational modeling with the intended application of new reactive potentials that have recently been developed by collaborators. The ultimate aim of the proposed research is to provide a fundamental basis from which the mechanical reliability of thin-film nanostructured materials in complex gaseous and aqueous environments may be understood.

Effect of Rare-Earth Additions on the Microstructural Evolution and Mechanical Properties of Al-Sc Alloys Containing Nanosize Precipitates

Prof. David C. Dunand (PI), dunand@northwestern.edu
Prof. David N. Seidman (co-PI), d-seidman@northwestern.edu

Department of Materials Science & Engineering
Northwestern University, Evanston IL 60208

Program Scope

This program focuses on the effect of micro-alloying rare-earth elements (RE) to dilute Al-Sc alloys containing nanosize L_{12} -structured $Al_3(Sc,RE)$ precipitates, in terms of precipitation, coarsening, chemical partitioning, segregation and strength, both at ambient and elevated temperature. Both experimental (atom probe, electron microscopy, mechanical testing) and theoretical (coarsening and dislocation-based models) approaches are taken to describe these phenomena.

Recent Progress

The microhardness of Al–0.06 Sc–0.02 RE alloys (at.%, with RE (rare-earth) = Y, Sm, Gd, Tb, Dy, Ho, Er, Tm, Yb, Lu) was measured as a function of aging time at 300 °C (Fig. 1). As compared to Al–0.08 Sc, the ternary alloys exhibit: (i) the same incubation time, except for alloys with Tb, Ho, Tm, Yb and Lu which hardens much faster; (ii) the same or reduced peak micro-hardnesses (which are higher than for Al–0.06 Sc); and (iii) the same over-aging behavior. Local Electron Atom Probe (LEAP) measurements (Fig. 2) show that RE partition to the $Al_3(Sc_{1-x}RE_x)$ precipitate where they segregate to the precipitate core. The accelerating effect on incubation time shown by some of the RE is due to the early formation of Al_3RE precipitates (as shown by LEAP), on which Al_3Sc subsequently grow epitaxially. Creep experiments show that the partial replacement of Sc with RE has no deleterious effect on the excellent creep resistance of these alloys up to 300°C, which is expressed by the presence of threshold stresses.

An Al–11.3Li–0.110Sc (at. %) alloy was double-aged to induce first α' - Al_3Sc and then δ' - Al_3Li precipitates. Atom-probe tomography (Fig. 3) revealed both single-phase δ' -precipitates and core-shell α'/δ' -precipitates (with respective average radii of 16 and 27 nm, and respective volume fractions of 12 and 9%) conferring a high strength to the alloy. Although the δ' -shells contain little Sc (~0.027 at. %), the α' -precipitate cores have a high Li content, with an average composition of $Al_{0.72}(Sc_{0.17}Li_{0.11})$, Fig. 4. The Li concentrations within the δ' -phase and the Li interfacial excess at the δ'/α' -interface both exhibit wide precipitate-to-precipitate variations.

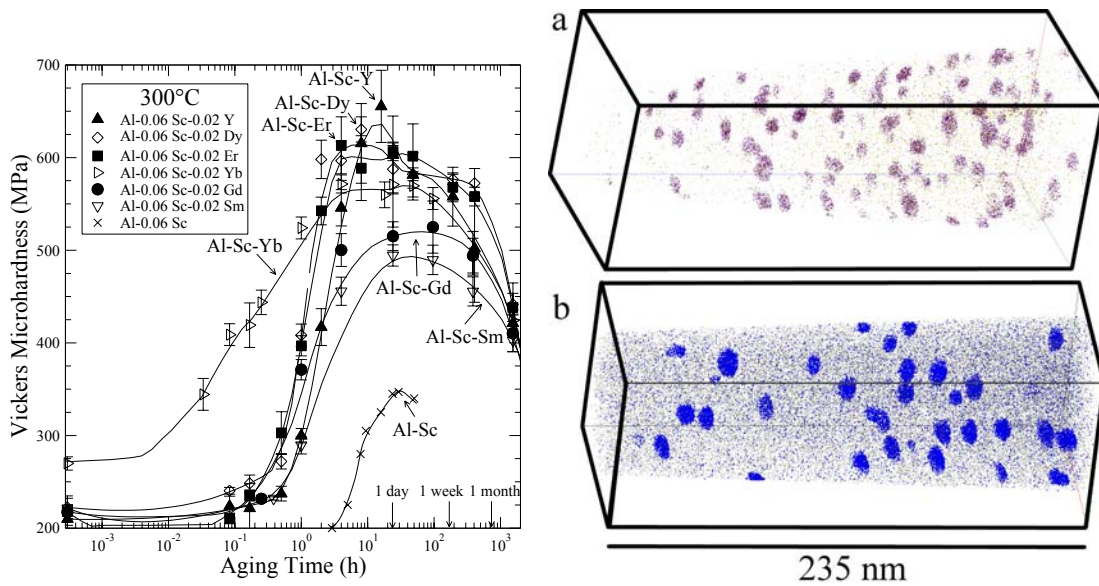


Fig. 1: Vickers microhardness (MPa) versus aging time at 300°C for Al-0.06 Sc-0.02 RE (at.%). Error bars are 1 standard-deviation from the mean. AlScYb forms Al_3Yb early (Yb is most likely a faster diffuser than Sc, while the other five rare-earth metals are probably slower than Sc), which is why there is significantly more hardening in this alloy before 1 h.

Fig. 2: Atom-probe tomograms of (a) Al-0.06 Sc-0.02Er (at.%) aged for 24 h at 300°C and (b) Al-0.06 Sc-0.02Gd (at.%), aged for 96 h at 300°C. Note the higher number density of finer precipitates in the sample containing Er.

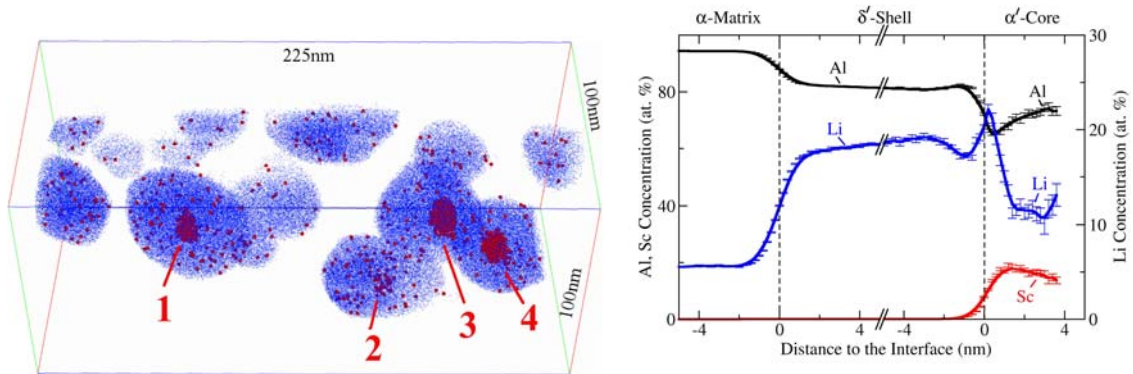


Fig. 3: LEAP tomographic reconstruction of doubly-aged specimen showing ten single-phase δ' -precipitates and four numbered dual-phase δ'/α' -precipitates (only a small portion of the α' -core of precipitate 2 is contained in the reconstructed volume). Li atoms are in blue, Sc atoms are in red, and Al atoms are omitted for clarity, as are all matrix atoms; the atomic diameters are not to scale.

Fig. 4 - Combined proximity histograms of six core-shell precipitates displaying the average concentration of Al, Li, and Sc as a function of distance from the α -matrix/ δ' -shell and δ' -shell/ α' -core interfaces (as defined by 12.5 at.% Li and 9 at.% Sc isoconcentration surfaces, respectively). The interruption of the x-axis in the δ' -shell removes, on average, 11 nm from the proxigram in a region where the concentration profiles are stable.

Future Plans

Starting in March 15, 2008, we will focus our efforts on a new program (with C. Wolverton as additional co-PI) which builds upon the current DOE research project sponsored. We will investigate the effect of adding large quantities of Li (up to ~12 at.%) to dilute Al-Sc and Al-Sc-RE alloys (with RE = Yb), with the ultimate goal of improving mechanical properties at ambient and elevated temperature, while also reducing density.

Scientifically, the goal of the project is to understand the complex interplay between the various $L1_2$ nano-size precipitates in these systems (Al_3Li , Al_3Sc and Al_3RE) both in terms of microstructure (nucleation/growth/coarsening) and mechanical properties (shearable vs. non-shearable). This will be accomplished by both experimental techniques (electron microscopy, atom probe tomography, mechanical testing) and modeling (first-principles methods, lattice kinetic Monte-Carlo and continuum dislocation mechanics). The output of the project will be an experimentally-validated suite of predictive models from which Al-Li-Sc-RE alloys can be designed with optimal microstructural stability and deformation/creep resistance behavior, while being castable and heat-treatable (and thus less expensive and more ductile than powder-metallurgy alloys based on rapidly-solidified powders). A similar strategy has been very successful used in cast nickel-base superalloys.

We will study the interaction, during deformation at low and elevated temperatures, between dislocations and core-shell precipitates. With an outer Al_3Li shell that is shearable, dislocation intersecting the $Al_3(Sc,RE)$ core will be blocked; we will compare this situation to that found in Al-Li alloys where simple precipitates are fully shearable. We will also address the effect of the elastic strain field of the precipitates (due to lattice mismatch with the matrix) upon dislocations, this effect providing enhanced creep resistance at elevated temperature. Models will be developed that will provide quantitative prediction for yield strength and creep resistance.

Additionally, in both above cases, we will investigate the microstructural evolution during nucleation, growth and coarsening of these complex precipitates, with particular attention to the issues of interfacial segregation, elemental partitioning and interdiffusion, number density and average precipitate size. In some cases, the situation may be complicated by the presence of two or more populations of precipitates with distinct chemical composition.

Our scientific goal is to achieve a comprehensive atomic-level understanding of the synergistic interactions among partitioning, segregation, interdiffusion, coarsening, heterophase interfacial free energy and resistance to dislocation shearing or climbing for these new quaternary alloys with core-shell precipitates. This understanding will lead to the creation of predictive, physics-based models of microstructural temporal evolution based on basic thermodynamic and kinetic properties and micromechanical, dislocation-based models of mechanical properties. These basic properties will be computed from first-principles density functional theory calculations: diffusivities of the alloying elements, lattice parameters, precipitate/matrix interfacial free energies and segregation, and solute-defect interactions (*e.g.*, solute-vacancy binding energies). The development

of these models will allow for the rational and efficient design of Al-Li alloys microalloyed with Sc and Yb (and other RE), without the inefficient Edisonian research effort that would be needed to screen all possible heat-treatments and compositions. Our models should also provide guidance for the rational design of other alloy systems containing core-shell precipitates.

References to publications of DOE sponsored research 2005-present

1. M.E. Van Dalen, D.C. Dunand, D.N. Seidman, "Effect of Ti Additions on the Microstructure and Creep Behavior of a Precipitation-Strengthened Al-Sc Alloy", *Acta Materialia*, **53**, 4225-4235 (2005).
2. K.E. Knipling, D.C. Dunand, D.N. Seidman, "Criteria for Developing Castable, Creep-Resistant Aluminum Alloys – A Review", *Zeitschrift für Metallkunde*, **97**, 3, 246-265 (2006).
3. R.A. Karnesky, M.E. van Dalen, D.C. Dunand, D.N. Seidman, "Effects of Substituting Rare-Earth Elements for Scandium in a Precipitation-Strengthened Al-0.08at.% Sc Alloy", *Scripta Materialia* **55** 437–440 (2006).
4. M.E. Van Dalen, D.C. Dunand, D.N. Seidman, "Nanoscale Precipitation and Mechanical Properties of Al-0.06 at.% Sc Alloys Microalloyed with Yb or Gd", *Journal of Materials Science*, **41** 7814-7823 (2006).
5. R.A. Karnesky, D.N. Seidman, D.C. Dunand, "Creep of Al-Sc Microalloys with Rare-Earth Element additions", *Materials Science Forum*, **519-521** 1035-1040 (2006).
6. Y. Harada, D.C. Dunand, "Microstructure and Hardness of Scandium Trialuminide with Ternary Rare-Earth Additions", *Materials Science Forum*, **539-543** 1565-1570 (2007).
7. R.A. Karnesky, L. Meng, D.C. Dunand, "Strengthening Mechanisms in Aluminum Containing Coherent Al₃Sc Precipitates and incoherent Al₂O₃ Dispersoids", *Acta Materialia* **55**, 1299–1308 (2007).
8. K.E. Knipling, D.C. Dunand, D.N. Seidman, "Precipitation Evolution in Al-Zr and Al-Zr-Ti alloys during Isothermal Aging at 375-425°C", *Acta Materialia*, **56**(1), 114-127 (2008).
9. K.E. Knipling, D.C. Dunand, D.N. Seidman, "Precipitation Evolution in Al-Zr and Al-Zr-Ti alloys during Isothermal Aging at 450-600°C", *Acta Materialia*, in print.
10. Y. Harada, D.C. Dunand, "Microstructure of Al₃Sc with Ternary Rare-Earth Additions", *Intermetallics*, accepted for publication pending modifications.
11. M.E. Krug, D.C. Dunand, D.N. Seidman, "Composition Profiles within Al₃Li and Al₃Sc/Al₃Li Nanoscale Precipitates in Aluminum", *Applied Physics Letters*, accepted.

Particle-induced Modification of Complex Ceramics: Response of Materials to Extreme Conditions

Rodney C. Ewing, Lumin Wang and Jie Lian
rodewing@umich.edu, lmwang@umich.edu, jlian@umich.edu

Departments of Geological Sciences, Nuclear Engineering & Radiological Sciences and
Materials Sciences & Engineering, University of Michigan, Ann Arbor, MI 48109

Program Scope

Our research program on radiation effects on complex ceramics mainly focuses on the determination of the fundamental processes by which radiation interacts with complex oxide, silicate and phosphate minerals and ceramics. The investigations include systematic studies of radiation damage in minerals, ion beam irradiations of minerals and synthetic ceramics, and actinide-doping experiments. The damage mechanisms and the evolution of the microstructure are studied by a wide array of electron beam and spectroscopic techniques, mainly advanced techniques in electron microscopy and Raman spectroscopy. The new aspects of our research program investigations are response of materials to extreme pressure and the very high-energy irradiation of materials at elevated pressures (up to 100 GPa) using diamond anvil cells. We have established the fundamental connection between radiation-induced and pressure-induced phase transitions, including order-disorder transformations and the formation of aperiodic domains. The model structures under investigation include pyrochlore, apatite, and zircon, as well as their derivative and polymorphic structure-types (e.g., murataite, reidite and xenotime). The correlations between chemical composition, structure (e.g., close packing vs. open-framework structure), chemical bonding (ionic vs. covalent) and materials properties (e.g., phase stability) under interacting irradiation, pressure and temperature will be elucidated. The results of this research program should be generally applicable to the understanding of the behavior of ceramics in radiation fields (e.g., fission reactor materials; nuclear fuels and SiC coatings; long-term stability of ceramic, nuclear waste forms; sensitivity of electrical and optical devices to radiation fluxes in space).

Recent Progress

During last three years, we have performed systematic ion beam irradiations on the pyrochlore ($A_2B_2O_7$) and murataite ($A_3B_6C_2O_{22-x/2}$, $F\bar{4}3m$) ceramics, and investigated the microstructural evolution as a function of irradiation damage and temperature. Both pyrochlore and murataite-structure types are the derivative of parent fluorite structure but with ordered arrangements of cation and anions. Particularly, pyrochlore structures display diverse chemistry and structural flexibility by accommodating extensive cation and anion substitutions in the crystal structure. The diverse crystal chemistry and structural flexibility provide a great platform for us to investigate how the chemical composition and structural variation (cation substitutions, structural distortion, chemical bonding, etc) affect the radiation response behavior of materials such as the crystalline-to-amorphous and order-disorder structural transitions. Furthermore, we have synthesized murataite polytypes, anion-deficient fluorite-structured oxides, and investigated the effects of different degrees of structural disordering on ion beam-induced amorphization and the order-disorder structural transition. Systematic ion irradiation studies of lanthanide pyrochlores with $B = Ti, Zr,$ and Sn combining with in-situ TEM observations have indicated

that the radiation response of the pyrochlore compounds is highly dependent on compositional changes. Both the ionic size and cation electronic configurations (e.g., bond-types) affect the structural distortion from the ideal fluorite structure and thus the response of pyrochlore-structure types to ion beam irradiation [1]. An ion beam-induced pyrochlore-to-fluorite structural transition occurs in all irradiated pyrochlore compositions, and the independent kinetics of the cation and anion disordering processes were discussed. A dramatic increasing critical amorphization dose for $\text{Gd}_2\text{Ti}_2\text{O}_7$ was found under dual beam irradiations simulating α -decay events, in which the electronic excitation and ionization of energetic He^+ greatly enhance the defect annealing behavior and thus the structural stability under extreme irradiation environment.

We also performed systematic swift heavy ion irradiations in the $\text{Gd}_2(\text{Zr}_x\text{Ti}_{1-x})_2\text{O}_7$ binary system exposed to ^{58}Ni , ^{129}Xe , ^{197}Au , ^{208}Pb , and ^{238}U projectiles with specific energy 11.1 MeV/u and characterized the radiation damage-induced structural transformation processes by ex-situ Synchrotron X-ray diffraction and Raman spectroscopy. A comparable structural modification occurred in pyrochlore compositions with pure electronic excitations and ionizations induced by swift heavy ions and nuclear collision processes under low energetic heavy ions. The observed structural transitions strongly depend on the pyrochlore compositions, and the effects of electronic energy loss on the structural modification have been clarified [2].

We reported dramatically different behaviors between isostructural $\text{Gd}_2\text{Ti}_2\text{O}_7$ and $\text{Gd}_2\text{Zr}_2\text{O}_7$ pyrochlore at pressures up to 44 GPa, in which the substitution of Ti for Zr significantly increases structural stability [3]. Upon release of pressure, a self-amorphization process occurred in the compressed $\text{Gd}_2\text{Ti}_2\text{O}_7$, while the high-pressure phase of $\text{Gd}_2\text{Zr}_2\text{O}_7$ transforms gradually to a disordered defect-fluorite structure. A consistent trend in the phase stability and structural transformation processes for titanate and zirconate pyrochlores at high pressures and in high radiation fields. Pyrochlore compositions that can accommodate disordering are resistant to forming an amorphous phase at high pressures or high irradiation fluxes. The response of such structures to extreme environments, such as high pressures or irradiation fields, is directly related to the energetics of the disordering process. Quantum mechanics calculations revealed that the response of pyrochlore to high pressures was controlled by the intrinsic energetics of defect formation. The performance of materials in extreme environments can much improved by a consideration of the atomic-scale disordering mechanism and energetics.

We have also made great progresses in understanding the materials behavior under extreme conditions of combining pressure, temperature and irradiation. For example, swift heavy ion beam-induced nanocrystallization or order-disorder structural transformation in ZrSiO_4 and $\text{Gd}_2\text{Zr}_2\text{O}_7$, respectively, stabilize the phase stability and enhances the compressibility upon subsequent pressurization [4]. While, simultaneous exposure to pressure and ion beams lead to a quite different material response: in pressurized zircon (ZrSiO_4), e.g., the ions trigger the formation of the scheelite-structured high-pressure phase reidite, which cannot be induced by the applied pressure or ions alone. Beside the nucleation of other high-pressure/temperature phases, modifications such as long-range amorphization and decomposition into nanocrystals have been observed. We also showed that the simultaneous combination of relativistic heavy ions, high pressure, and high temperature can be used to simulate fission-track formation in minerals under conditions relevant to the Earth's deep crust (e.g., zircon) [5]. The fundamental knowledge of the phase stability and transformation processes under these conditions can be used to create a new class of materials that have novel properties, and allow us to design materials with excellent radiation performance and resistant to extreme thermo-mechanical stress or pressure.

Future Plans

Our future research will focus on developing a fundamental understanding of materials behavior under synergetic extreme environments consisting of intense irradiation fields, high temperatures and high pressures. We will investigate irradiation-induced phase transformations utilizing a wide spectrum of radiation sources and nano-scale analytical techniques. We will specifically focus on the effects of high-temperature and high-pressure on radiation-induced structural transformations. The fundamental aspects of materials response behavior will be studied by advanced techniques of electron microscopy (HAADF-STEM, EELS and EFTEM), a variety of spectroscopies (Raman, Synchrotron X-ray and IR), and a novel experimental design for very high-energy irradiation of materials at elevated pressures (up to 100 GPa) using diamond anvil cells. The correlations between chemical composition, structure (e.g., close packing vs. open-framework structure), chemical bonding (ionic vs. covalent) and materials properties (e.g., phase stability) under interacting irradiation, pressure and temperature will be elucidated. Quantum mechanics calculations will be initiated to model the energetics of the damage mechanisms and disordering processes of materials. Combining the advanced experimental design and characterization tools, a synergetic model from the perspectives of non-equilibrium thermodynamics and kinetics will be developed to understand the phase stability and transformation processes of materials under intensive radiation and extreme pressure environments. From a more fundamental perspective, irradiation and pressure represent a unique means of creating non-equilibrium states of matter, providing new possibilities for tailoring novel materials with new properties. The combination of intense irradiation, high pressure, and high temperature opens up unprecedented possibilities for the study of the interaction of nano-scale structures and surfaces with different types of irradiation over a range of temperatures and pressure. An important aspect of our future studies lies at the design of materials for extreme conditions with enhanced performance. The integration of the concept of non-equilibrium thermodynamics, introduced by pressure or/and irradiation, offers new pathways for the investigation of fundamental phenomena and for the development of new materials with improved properties, such as the stabilization of metastable high-temperature phases (e.g., tetragonal zirconia at elevated pressures) or self-organized nanostructures with novel morphologies and functionalities.

References

- [1] J. Lian, K. B. Helean, B. J. Kennedy, *et al.*, *J. Phys. Chem. B* 2006, 110, 2343.
- [2] M. Lang, F. X. Zhang, J. Lian, *et al.*, *Phys. Rev. B.*, in preparation.
- [3] F.X. Zhang, J. Wang, J. Lian *et al.*, *Phys. Rev. Lett.* 100 (2008) 045503.
- [4] M. Lang, F. X. Zhang, J. Lian *et al.*, *Earth. Planet. Sci. Lett.* (2008), in press.
- [5] M. Lang, J. Lian, F. X. Zhang, *et al.*, *Geology.* (2008), submitted.

DOE Sponsored Publications in 2006-2008

1. M. Lang, F. X. Zhang, J. Lian, R. C. Ewing, R. Neumann, C. Trautmann, (2008) “Energetic Beam Irradiation Stabilizes Pressurized Zircon”, *Earth Planetary Science Letters*, in press.
2. F. X. Zhang, J. W. Wang, J. Lian, M. K. Lang, U. Becker, R. C. Ewing, “Phase stability and pressure dependence of defect formation in $Gd_2Ti_2O_7$ and $Gd_2Zr_2O_7$ pyrochlores“, *Physical Review Letters* 100 (2008) 045503.
3. F. X. Zhang, M. Lang, U. Becker, R. C. Ewing, and J. Lian, “High pressure phase transitions and compressibilities of $Er_2Zr_2O_7$ and $Ho_2Zr_2O_7$ ”, *Applied Physics Letters* 92 (2008) 011909.

4. N. Li, X. Y. Xiao, X. T. Zu, L. M. Wang, R. C. Ewing, J. Lian, and F. Gao, "First-principles study of electronic properties of $\text{La}_2\text{Hf}_2\text{O}_7$ and $\text{Gd}_2\text{Hf}_2\text{O}_7$ ", *Journal of Applied Physics* 102 (2007) 063704.
5. H. Y. Xiao, L. M. Wang, X. T. Zu, J. Lian, R. C. Ewing, "Theoretical investigation of structural, energetic and electronic properties of titanate pyrochlores", *Journal of Physics Condensed Matter* 19 (2007) 346203.
6. F. X. Zhang, J. Lian, U. Becker, R. C. Ewing, J. Z. Hu, and S. K. Saxena, "High-pressure structural changes in the $\text{Gd}_2\text{Zr}_2\text{O}_7$ pyrochlore", *Physical Review B* 76 (2007) 214104.
7. W. Jiang, Y. Zhang, M. H. Engelhard, W. J. Weber, G. J. Exarhos, J. Lian and R. C. Ewing, "Behavior of Si and C atoms in ion amorphized SiC", *Journal of Applied Physics* 101 (2007) 023524.
8. J. Lian, S. V. Yudintsev, S. V. Stefanovsky, L. M. Wang, and R. C. Ewing "Ion beam irradiation of U-, Th- and Ce-doped pyrochlores", *Journal of Alloy and Compounds*, 444 (2007) 429-433.
9. J. Lian, F. X. Zhang, Lumin Wang, and R. C. Ewing "Ion beam irradiation of La- and Th-doped $\text{Y}_2\text{Ti}_2\text{O}_7$ titanates", *Journal of Nuclear Materials*, 362 (2006) 438-4444.
10. F. X. Zhang, J. Lian, U. Becker, Lumin Wang, R. C. Ewing, *et al.* "Structure change of layered perovskites of $\text{La}_2\text{Ti}_2\text{O}_7$ at high pressures", *Journal of Solid State Chemistry*, 180 (2007) 576-581.
11. F.X. Zhang, J. W. Wang, U. Becker, J. Lian, R. C. Ewing, L. M. Wang, J. Hu, and S. Saxena, "Pressure-induced splitting and buckling of Cu-O chains in one-dimensional compound SrCuO_2 ," *Journal of the American Chemical Society* 129 (2007) 13923-13926.
12. F. X. Zhang, J. Lian, U. Becker, L. M. Wang, R. C. Ewing, *et al.*, "Structural distortions and phase transformations in $\text{Sm}_2\text{Zr}_2\text{O}_7$ pyrochlore at high pressures", *Chemical Physics Letters* 441 (2007) 216-220.
13. W. Jiang, W. J. Weber, J. S. Young, L. A. Boatner, J. Lian, L. M. Wang, and R. C. Ewing, "Irradiation-induced nanostructures in cadmium niobate pyrochlores", *Nucl. Instrum. Method Phys. Res. B* 250 (2006) 188-191.
14. W. Jiang, Y. Zhang, W. J. Weber, J. Lian and R. C. Ewing "Direct evidence of N aggregation and diffusion in Au^+ irradiated GaN", *Appl. Phys. Lett.*, 89 (2006) 021903.
15. F. X. Zhang, J. Lian, U. Becker, L. M. Wang, R. C. Ewing, *et al.* "Pressure-induced structural transitions and phase decomposition in the $\text{Cd}_2\text{Nb}_2\text{O}_7$ pyrochlore" *Physical review B* 74 (2006) 174116.
16. J. Lian, W. J. Weber, W. Jiang, L. M. Wang, L. A. Boatner, R. C. Ewing, "Radiation-induced effects in pyrochlore and nano-Scale materials engineering", *Nucl. Instrum. Method Phys. Res. B* 250 (2006) 128-136.
17. J. Lian, L. M. Wang, X. C. Sun, Q. K. Yu, R. C. Ewing, "Patterning Metallic Nanostructures by Ion Beam-induced Dewetting and Rayleigh Instability", *Nano Letters* 6 (2006) 1047.
18. J. Lian, W. Zhou, L. M. Wang, L. A. Boatner, and Rodney C. Ewing "Simultaneous Formation of Surface Ripples and Metallic Nanodots Induced by Phase Decomposition and Focused Ion Beam Patterning", *Appl. Phys. Lett.* 88, 093112 (2006).
19. J. Lian, K. B. Helean, B. J. Kennedy, L. M. Wang, A. Navrotsky, and R. C. Ewing, "Effect of Structure and Thermodynamic Stability on the Response of Lanthanide Stannate Pyrochlores to Ion Beam Irradiation", *Journal of Physics Chemistry B* 110 (2006) 2343-2350.
20. J. Lian, L. M. Wang, R. C. Ewing and L. A. Boatner, Microstructural Evolution of Ion Implanted $\text{Gd}_2\text{Ti}_2\text{O}_7$, *Nucl. Instrum. Method Physics B* 242 (2006) 448-451.

Plasticity in ultra fine grained materials

Marisol Koslowski

School of Mechanical Engineering Purdue University
585 Purdue Mall, West Lafayette, IN 47906

Many of the fundamental mechanisms underlying the inelastic behavior of materials are mediated by defects with mechanisms that operate at atomistic scales. Conversely, continuum theories rest on the assumption that the relevant fields that describe the state of the material vary slowly at atomic scale. Therefore, continuum theories break down in the microscopic range and fail to describe the relevant phenomena at this scale. It is clear that atomistic and continuum theories need connection, this connection is attempted, for example, by the multiscale modeling framework in which the materials behavior is divided in hierarchical length scales and the higher length scale is informed by averages of the preceding length scale [1]. However, in this process the local detail of the microstructure and its relation with the macroscopic behavior is lost. This is particularly important when the scale of the volume of analysis approaches the microstructure and the continuum assumption diminishes as in micron and submicron size grains in polycrystalline materials.

Our goal is to develop a predictive continuum plasticity model to address the evolution of dislocations in confined geometries and their interaction with grain boundaries. This model constitutes an important step towards the integration of the ***microstructural evolution as well as the effect of high surface to volume ratio in the mechanical response*** into continuum mechanical modeling for crystalline materials.

When the characteristic size or certain characteristic length, such as the grain size, approaches the micron or sub micron range, metals display a strong size dependency given by an increase in the yield stress as the characteristic size decreases following a power law:

$$\sigma_y \propto d^{-a}$$

where σ_y is the yield stress, d is a characteristic length of the specimen and a is an exponent reported to be between 0.5 and 1. This relation, known as Hall-Petch relation [2, 3], is well established experimentally in polycrystalline materials with sub micron and micron grain size. It is observed that for an average grain size in the micron regime the yield stress of the metal increases as the grain size decreases following a power law with exponent $a=0.5$. Therefore, a physically based theory of plastic deformation for crystalline materials should include a description of these boundary conditions on dislocation fields to properly represent the microstructures and how they affect the macroscopic response.

Figure 1 shows the relation between the yield stress and the characteristic size for different experiments [4, 5, 6, 7] in metallic materials and our simulations with the phase-field model [8]. The value of the exponent in the power law relation spans from 0.5 for single crystals to 1 for free standing thin films. This

shows that surface effects play a key role in the mechanical response of materials.

Figure 1 illustrates the ability of the phase field theory to account for size effects in plastic deformation. A great advantage of our method is that we do not need the introduction of length scale parameters. Size dependency results from the non-local dislocation interactions and the formation of microstructures due to confined geometries, affecting the overall response.

Classical continuum theories originally developed to describe bulk materials have been enhanced to incorporate the experimentally observed size effect at micron and submicron scales through the introduction of length scale parameters [9, 10, 11, 12, 13, 14, 15, 16]. We will show a comparison between the gradient theory of plasticity developed by Gurtin [16] and the phase-field theory of dislocations developed by Koslowski et.al [17, 8] for a constrained layer geometry. This problem represents a metallic film bonded to a substrate that acts as a rigid constraint and it is of importance to represent the behavior of passivated thin films. The same boundary condition is also used to simulate other interfaces that are impenetrable to dislocations including grain boundaries. For this particular geometry we are able to predict in closed form the value of the length scale and strength parameters defined in the strain gradient theory and their dependency on the geometry and material properties.

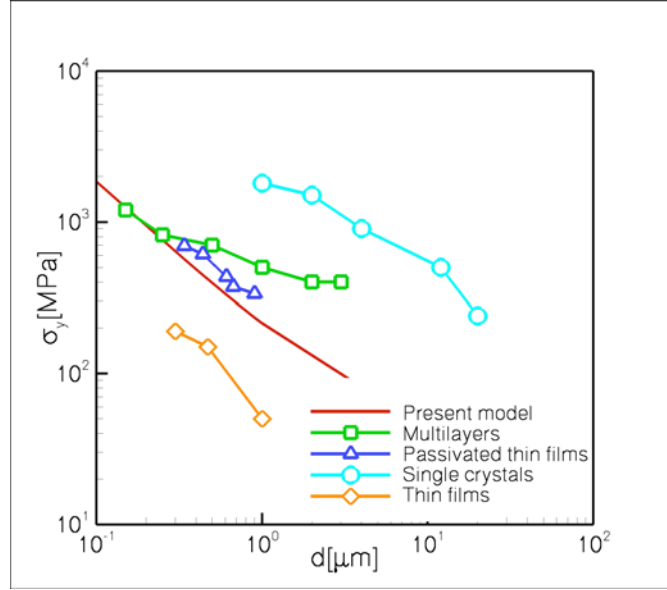


Figure 1: Yield stress dependency on size for different experimental conditions: thin films [5], single crystals [4], multilayers [6] and passivated thin films [7] and compared to our simulations [8]

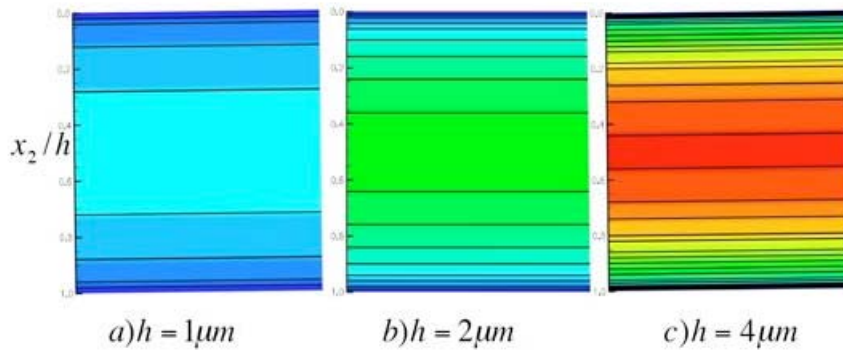


Figure 2: Effect of thin film thickness on dislocation profile.

Figure 2 shows the profiles of the plastic strain obtained with the phase-field model, for the same applied stress, in the constrained channel geometry. The lines represent the position of dislocations along the channel thickness. The phase-field model predicts dislocation pile-ups of opposite sign forming at the top and bottom interfaces. As expected from experiments, for the same applied stress the average plastic deformation increases with increasing thickness.

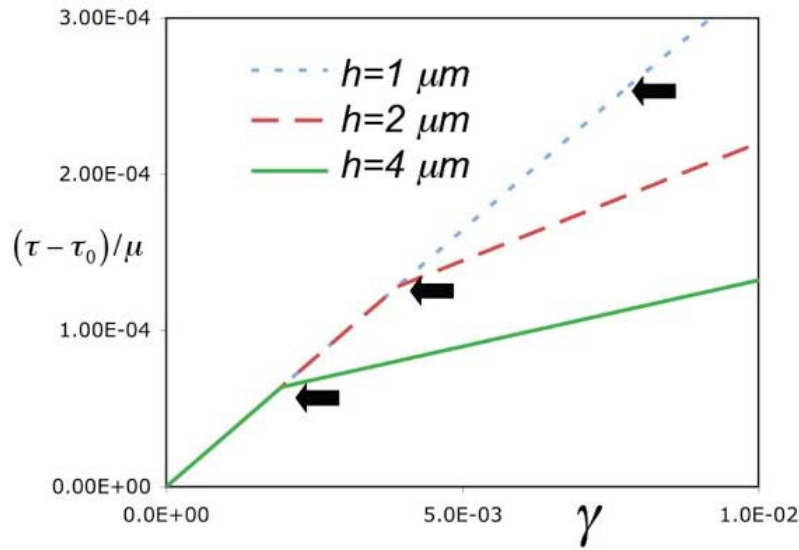


Figure 3: Effect of thickness on stress-strain curve.

Figure 3 shows the stress/strain response for thin film thickness $h = 1, 2,$ and $4\mu m$. It is interesting to notice the hardening effect due to the formation of dislocation pile-ups as well as the effect of size in the yield stress as a result of the nucleation of dislocations. The arrows in Figure 3 display the onset of plastic deformation. For the particular case of $h = 1\mu m$ the slope does not change after yielding, even though dislocations are nucleated. This effect is a consequence of the high hardening rate produced by the dislocation pile-up due to the constraint in the motion of dislocations. This effect is also observed in free standing thin films experiments [5] and may explain why even though dislocations are being nucleated the stress/strain response seems elastic.

References

- [1] Ortiz, M., Cuitino, A. M., Knap, J. and Koslowski, M., "Mixed atomistic-continuum models of material behavior: The art of transcending atomistics and informing continua". *MRS Bulletin* **26**(3) 216 (2001).
- [2] Hall E. O., *Proc. Phys. Soc. London Sect. B* **64**, 747 (1951).
- [3] Petch, N. J., *J. Iron Steel Inst.*, **174**(25) 8 (1953).
- [4] Uchic, M. D., Dimiduk, D. M., Florando, J. N. and Nix, W. D., *Science*, **305** (2004).
- [5] Espinosa, H. D., Prorok, B. C., Peng, B., *J. Mech. Phys. Solids*, **52** 667 (2004).
- [6] Xiang, Y. and Vlassak, J. J. *Acta Materialia*, **54** 5449 (2006)
- [7] Huang, H. and Spaepen, F., *Acta Mater.*, **48** 3261 (2000).
- [8] M. Koslowski and A. Hunter, submitted to Journal of the Mechanics and Physics of Solids (2007)
- [9] Fleck, N. A., Muller, G. M., Ashby, M. F., Hutchinson, J. W., *Acta Met. Mater.* **42** (2) 475 (1994).
- [10] Stölken, J. S., Evans, A. G., *Acta Mater.* **46** 5109 (1998).
- [11] Hutchinson, J. W., *International Journal of Solids and Structures*, **37** 225 (2000).
- [12] Nix, W. D. and Gao, H., *J. Mech. Phys. Solids*, **46** 411(1998).
- [13] Fleck, N. A. and Hutchinson, J. W., *J. Mech. Phys. Solids*, **41** 1825 (1994).
- [14] Acharya, A. and Bassani, J. *J. Mech. Phys. Solids*, **48** 1565 (2000).
- [15] Gurtin, M. E., *J. Mech. Phys. Solids*, **50** 5 (2002).
- [16] Needleman A, Gil Sevillano *J. Scripta Mater.* **48**(109) (2003).
- [17] Koslowski, M., Cuitino, A. and Ortiz, M., *J. Mech. Phys. Solids*, **50**(12) (2002).

Nano-mechanics of Tunable Adhesion using Non Covalent Forces

Principal Investigators

Kenneth M. Liechti, D. Xu and M. Wakamatsu, Aerospace Engineering and Engineering Mechanics, University of Texas, Austin, TX 78712, kml@mail.utexas.edu

M. J. Krische and M. Y. Ngai, Chemistry and Biochemistry, University of Texas, Austin, TX 78712, mkrische@mail.utexas.edu

Objective

The objective of this program is to examine, via experiment and atomistic and continuum analysis, coordinated noncovalent bonding over a range of length scales with a view to obtaining modulated, patterned and reversible bonding at the molecular level.

Scope

The first step in this project will be to develop processes for depositing self-assembled monolayers (SAMs) bearing carboxylic acid and amine moieties on Si (111) surfaces and probe tips of an interfacial force microscope (IFM). This will allow the adhesive portion of the interactions between functionalized surfaces to be fully captured in the force-displacement response (force profiles) that are measured by the IFM. The interactions will be extracted in the form of traction-separation laws using combined molecular and continuum stress analyses. In this approach, the results of molecular dynamics analyses of SAMs subjected to simple stress states are used to inform continuum models of their stress-strain behavior. Continuum analyses of the IFM experiment are then conducted, which incorporate the stress-strain behavior of the SAMs and traction-separation laws that represent the interactions between the tip and functionalized Si surface. Agreement between predicted and measured force profiles is taken to imply that the traction-separation laws have been properly extracted. The traction-separation laws obtained in this way will be correlated to the number/areal density of attractive ammonium-carboxylate interactions used to bind the surfaces.

Scale up to larger contact areas will be considered by forming Si/SAM/Si sandwiches and then separating them via fracture experiments. The traction-separation laws obtained from the IFM experiments will be used to predict the fracture response (load-displacement and crack growth history) of the sandwiches. Comparisons will then be made with the measured responses for a range of areal densities of attractive ammonium-carboxylate interactions.

Progress

Progress has been made in the three areas of SAM deposition, IFM nano indentation experiments and the development of a high vacuum fracture experiment. These are each summarized below.

SAM deposition

The two SAMs that are being considered here consist of an alkyl chain with ten CH₂ groups that are terminated with either carboxyl or amine groups. The substrate is a 125mm, p/boron <111> 5-11 ohm-cm, 550-600 μm, double side polished, silicon wafer that presents the Si(111) surface for deposition. The deposition starts with a piranha solution and ammonia fluoride (NH₄F) treatments of the Si surface. The piranha cleans off the native oxide layer and replaces it with a 2-nm silica layer that is OH terminated and then the ammonium fluoride provides a hydrogen terminated surface with a roughness of approximately 0.4 nm. This latter step was preferable to HF etch, which gave rise to much rougher surfaces. This sets the stage for the deposition of a 10-undecylenic trifluoroethyl ester SAM [Si(CH₂)₁₀(CO)O(CH₂CF₃)] using a

2,2,2-trifluoroethyl undec-10-enoate solution whose (CH₂CF₃) group can be replaced by carboxyl or amine terminuses. A solution of 0.25 M t-BuOK in dimethyl sulfoxide (DMSO) is used to remove the fluorine terminated SAM and replace it with a carboxyl terminus to form a 10-undecylenic acid SAM [Si(CH₂)₁₀(CO)OH]. We have explored the formation of amine and diamine surfaces. The latter is more promising and makes use of a neat N,N-dimethyl-1,2-ethyldiamine solution (1 ml) with 50mg of pyridinium p-toluenesulfonate to remove the fluorine and leave a 10-undecylenic N-(2-(dimethylamino)ethyl amide SAM [Si(CH₂)₁₀(CO)(NH)(CH₂)₂-NMe₂] SAM on the silicon wafer. The presence of the expected monolayers is checked using XPS (surface chemistry), AFM (surface roughness) and ellipsometry (layer thickness). The results to date are summarized in Table 1 where the measured thickness is compared with chain length. The agreement between the two, coupled with the roughness data indicates that monolayers are indeed being formed. We are now examining the statistical aspects of the data in order to establish confidence limits.

Sample	SAM thickness (nm)	Chain length (nm)	Roughness (nm)
CF3	2.20	2.21	0.31
COOH	1.87	1.94	0.42
NMe2	2.59	2.46	0.35

Table 1. SAM thickness and roughness

IFM Experiments and Analysis

Pending deposition of the carboxy and amine terminated SAMs, we present some results of IFM experiments and analysis on monolayers of octadecyltrichlorosilane (OTS) These were stable monolayers with an rms roughness less than 0.1 nm [1], very similar in quality to those deposited in an anhydrous manner, but with a different solvent that required less stringent environmental control [2]. The presence of a monolayer was confirmed by X-ray photoelectron spectroscopy (XPS), ion scattering spectroscopy (ISS) and AFM imaging of patterned and blanket monolayers. Ellipsometry was used to determine the thickness of the OTS monolayer, which was 2.5±0.1 nm, due to a 16° tilt from the normal.

The coated specimens were probed with an IFM using electrochemically etched tungsten wires with tip radii ranging from 100 to 200 nm. The IFM clearly distinguished [3] the presence of the OTS monolayer in the compressive regime. There were some interesting differences in the tensile (adhesive) regime. For the uncoated silicon, there was an adhesive step in the response of about 0.2 μN as a water bridge presumably formed in the ambient humidity in which the experiment was conducted. There was a slightly smaller initial step when the OTS-coated specimen was probed. We think that this was due to a reduction in the 16° tilt as the tungsten tip approached. The water explanation is also possible, but probably to a lesser extent, due to the hydrophobic nature of OTS. Adhesive hysteresis was clearly observed in the unloading responses of bare and coated silicon, presumably due to more water being attracted to the contact region during contact.

The analysis of the IFM force profiles had to account for the fact that specimens consisted of an OTS monolayer covering the SiO₂ layer (2.0±0.1 nm) that had been grown in the piranha solution. These two thin layers on top of the silicon meant that substrate effects would be present, thereby disallowing [4] the use of classical contact mechanics theories (Hertz, JKR, DMT and Maugis developed for monolithic bodies) for extracting the mechanical behavior of the OTS layer. Accordingly, a finite element analysis of the IFM experiment was conducted that

incorporated normal surface interactions via a triangular traction-separation law. The area underneath the curve gives the thermodynamic work of adhesion $\omega = 0.5 \sigma_0 \delta_c$, between the tungsten tip and the OTS, where σ_0 is the maximum stress and δ_c is the critical opening displacement. In all analyses, the tungsten tip, silicon and silica were assumed to be linearly elastic and isotropic. The OTS was first assumed to be linearly elastic and isotropic and its modulus was extracted by matching finite element solutions for the force profiles with measured ones. However, the match between the numerical solutions and measured force profiles was not satisfactory. The OTS was therefore taken to be an isotropic hypo-elastic material based on the results of a molecular dynamics analysis of uniaxial compression straining of the OTS.

The stress-strain behavior of the OTS under uniaxial compressive strain as obtained from the molecular analysis was quite nonlinear and reminiscent of rubbery materials. There were several discontinuities in the response, which are probably due to configurational changes. At higher stress levels, the three normal stresses were nearly the same, indicating an approach to incompressibility. The tangent modulus and Poisson's ratio of the hypo-elastic model were extracted from the molecular analysis results. The values of the tangent modulus reflected the nonlinear behavior with an initial modulus of 1 GPa, rising to 30 GPa at high compressive strains. The Poisson's ratio remained constant at 0.44. These values of tangent modulus and Poisson's ratio were used in a hypo-elastic model of uniaxial compressive strain and provided very reasonable agreement up to about 40% nominal strain, which was sufficient for modeling the IFM experiment.

This continuum representation (hypo-elastic material with traction-separation law) of the behavior of an OTS monolayer was then used in a finite element analysis of the IFM experiment. The finite element solution compared well with the measurements (Fig. 3) even in the low compressive force regime without any further adjustments to the hypo-elastic model. The agreement between analysis and experiment is remarkable, given that the constitutive law that was used in the continuum model was based directly on molecular dynamics simulations without any adjustment. This result suggests that the behavior of the OTS is indeed simple enough that differences in the time scales of the molecular dynamics analyses and the actual experiments are not important. It appears that a class of problems has been opened up where spatial and temporal scales can be crossed in a relatively simple manner, and molecular dynamics analyses may be used to motivate continuum representations of self-assembled monolayers in a simple but direct manner.

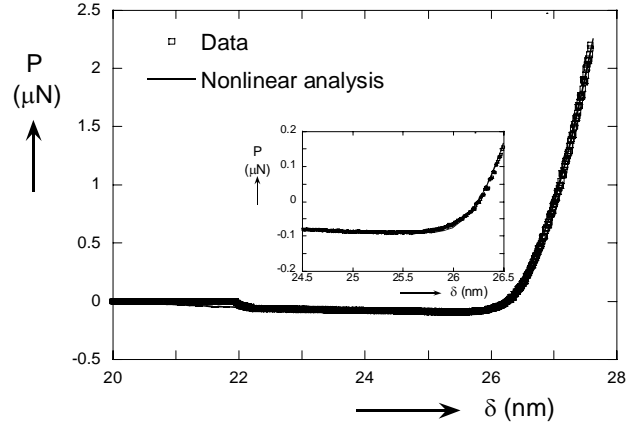


Figure 1. The solution for the IFM force profile with a hypo-elastic representation of the OTS is compared with measurements.

The values of the tangent modulus reflected the nonlinear behavior with an initial modulus of 1 GPa, rising to 30 GPa at high compressive strains. The Poisson's ratio remained constant at 0.44. These values of tangent modulus and Poisson's ratio were used in a hypo-elastic model of uniaxial compressive strain and provided very reasonable agreement up to about 40% nominal strain, which was sufficient for modeling the IFM experiment.

	σ_0 (MPa)	δ_0 (nm)	δ_t (nm)	ω (mJ/m ²)
Bare silicon	60	3	7	210
OTS/silicon	35	5	7	122.5

Table 1. Extracted adhesion parameters for bare and coated silicon.

The parameters for the traction-separation laws for bare and coated silicon are listed in Table 1. The work of adhesion between the tungsten tip and the bare silicon was higher than the value obtained for tungsten probing an OTS monolayer. Such values are consistent with the formation of water bridges and the ordering reflects the hydrophobic nature of OTS.

High Vacuum Fracture Rig

The development of a fracture rig for separating two functionalized surfaces that have been pressed together is nearing completion. In view of concerns regarding the effect of water molecules on the interactions between the functionalized surfaces, the experiment will have the capability of being conducted in high vacuum (10^{-6} Torr). A schematic of the fracture specimen and device is shown in Figure 4. The four point bending configuration consists of a carrier beam that transmits a uniform bending moment to the specimen. The load is provided by a piezoelectric motor that is rated for high vacuum. A view port will allow the crack opening displacement to be measured using infra red crack opening interferometry [5]. The specimen and carrier beam have been designed on the basis of surface interactions between tungsten and OTS and a parametric study based on those values [6]. The facility has been constructed and is currently undergoing trials using mica specimens.

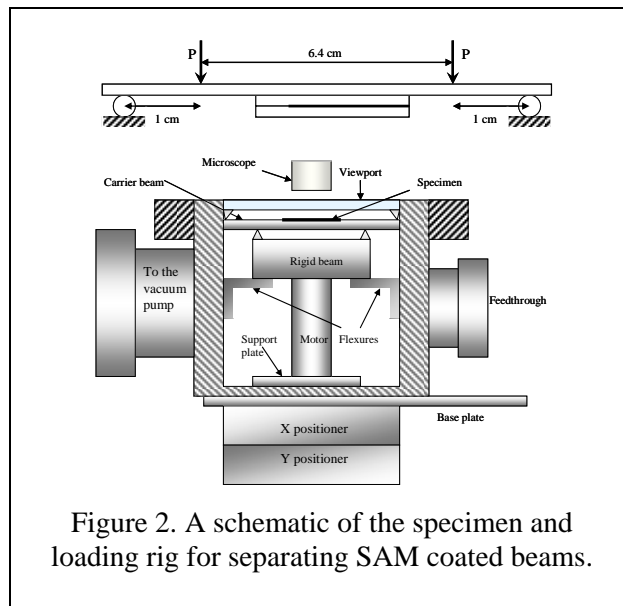


Figure 2. A schematic of the specimen and loading rig for separating SAM coated beams.

1. Wang, M., et al., Self-Assembled Silane Monolayers: Fabrication with Nanoscale Uniformity. *Langmuir*, 2005. 18: p. 1848-1857.
2. Wang, Y., and Lieberman, M., Growth of Ultrasooth Octadecyltrichlorosilane Self-Assembled Monolayers on SiO₂. *Langmuir*, 2003. 19: p. 1159-1167.
3. Wang, M., Liechti, K. M., Srinivasan, V., White, J. M., Rossky, P. J., Stone, T. M., A hybrid molecular-continuum analysis of IFM experiments of a self-assembled monolayer. *J. Appl. Mech.*, 2006. 73: p. 769-777.
4. Wang, M., Liechti, K. M., White, R. M., and Winter, R. M., Nanoindentation of polymeric thin films with an interfacial force microscope. *J. Mech. Phys. Solids*, 2004: p. 52(10), 2329-2354.
5. Liechti, K.M., On the Use of Classical Interferometry Techniques in Fracture Mechanics. *Experimental Techniques in Fracture, III*, ed. J.S. Epstein. 1993, New York: VCH Publishers. Chapter 4, 95-124.
6. Russo, M.E., Delamination between self-assembled monolayers, in *Aerospace Engineering*. 2007, University of Texas: Austin.

DOE support for this work has been acknowledged in Russo's thesis [6] and the Proceedings of the 31st Annual Meeting of the Adhesion Society, which took place in February 2008 in Austin, Texas.

Grant Number DE-FG02-01ER45924 to the University of Pennsylvania

Project Title: "Micromechanisms of the Ductile-Brittle Transition in Hydrogen-Induced Fracture of Steels"

PI: Charles J. McMahon, Jr.
cmcMahon@lrsm.upenn.edu

Recent Results on Hydrogen-Induced Cracking of High-Strength Steels

XinYu Liu, Jun Kameda, and C. J. McMahon, Jr.
Department of Materials Science and Engineering
University of Pennsylvania 3231 Walnut Street
Philadelphia PA 19104

Abstract

The central theme of this work is the characterization of the ductile-to-brittle transition of high-strength steels in hydrogen. The brittle mode is stress-controlled intergranular decohesion, which is the mode generally known as hydrogen embrittlement. The ductile mode is displacement-controlled, plasticity-related cracking along planes of high shear stress, and it is transgranular with respect to the prior austenite grain boundaries. One can imagine a diagram in three-parameter space characterized by the strength of the steel, the hydrogen fugacity, and the purity of the grain boundaries. The diagram has a parabolic surface separating the ductile from the brittle regions, the former nearer the origin where the strength and hydrogen fugacity are both low and the grain boundaries are pure.

Working with the Tohoku University group of Kenji Abiko, we have found that one can produce a 4340-type steel that is effectively ideally pure as far as grain boundaries are concerned, and that this will still fail by brittle intergranular fracture in even low-fugacity hydrogen at high strength levels. Therefore, in the high-purity limit, there is some microstructural factor (or factors) that causes grain-boundary weakness. We are exploring the effects of cyclic thermal treatments to overcome this weakness and will present the results to date.

This finding allows us to eliminate the purity variable by using an effectively pure steel and therefore to concentrate on the two-dimensional diagram in which yield strength (or applied stress intensity) is plotted against hydrogen fugacity to establish the parabolic boundary separating the ductile and brittle regions. The steel being used is a 5%Ni, Cr, Mo, V HY130-type steel containing no Mn or Si,

and having a yield strength greater than 150ksi, or 1050MPa. This steel is not brittle in 20psi hydrogen, and we are exploring collaborations to do testing at higher pressures.

Publications:

“Hydrogen-Induced Cracking in a Very-High-Purity High-Strength Steel,” X-Y. Liu, J. Kameda, J.W. Anderegg, S. Takaki, K. Abiko and C.J. McMahon, Jr., accepted by *Matls Sci Eng A*, March, 2008

“Evidence for the Intergranular Segregation of Tin to Grain Boundaries of a Cu-Sn Alloy and Its Consequences for Dynamic Embrittlement,” XY Liu, Douglas Tham, Douglas Yates, and C. J. McMahon, Jr., *Matls Sci & Eng A* **458**, 2007, 123-125.

“Time-Dependent Intergranular Brittle Fracture,” C, J, McMahon, Jr. ICF11, Turin, 2005

“Comments on “Identification of SAGBO-induced damage zone ahead of crack tip to characterize sustained loading crack growth in alloy 783,” C. J. McMahon, Jr., *Scripta Mat.* 54, 2006, 305 – 307.

“Improving resistance to dynamic embrittlement and intergranular oxidation of nickel based superalloys by grain boundary engineering type processing,” U. Krupp, P.E.-G Wagenhuber, W. M. Kane, and C. J. McMahon, Jr., *Matls Sci & Technology*, 21, 2005, 1-8.

“On the mechanism of quench cracking in Rene 95 nickel based superalloy,” W. M. Kane, U. Krupp, T. Jacobs, and C. J. McMahon, Jr. *Matls Sci Eng A*, 402, 2005, 42-46.

“Quench Cracking in Steel as a Case of Hydrogen Embrittlement,” XinYu Liu and C. J. McMahon, Jr. *Matls Sci Eng A* 2008, accepted.

The inverse magnetoplastic effect of magnetic shape-memory alloys

Peter Müllner

Department of Materials Science and Engineering

Boise State University

1910 University Dr., MS 2075

Boise, Idaho 83725

petermullner@boisestate.edu

Program Scope and Definition

Inverse magnetoplasticity is the deformation-induced change of magnetization occurring in the martensitic phase of magnetic shape-memory alloys. Inverse magnetoplasticity is the inverse effect to magnetic-field-induced deformation (magnetoplasticity). The goal of this project is to investigate the underlying mechanisms of inverse magnetoplasticity, its potential, and limitations both, experimentally and theoretically. Project objectives cover the synthesis of high-quality single crystals, the control of twin microstructure, systematic magneto-mechanical experiments, and numerical modeling. The outcomes of this project are defect-based experimental and theoretical understanding of the micromechanisms of inverse magnetoplasticity, effects of thermo-magneto-mechanical training on twin-microstructure and magneto-mechanical properties, and knowledge about potential and limits of inverse magnetoplasticity of magnetic shape-memory alloys. The outcomes will significantly affect (i) further research in the field of magnetic shape-memory alloys and (ii) novel solutions in sensor, memory, and power generation technologies.

Recent Progress

A) Experimental

Training experiments were performed with Ni-Mn-Ga single crystals. Samples with approximate size of 3 mm x 4 mm x 6 mm were annealed under a compressive stress of up to 12 MPa and cooled through the martensitic transformation while maintaining the compressive stress (thermo-mechanical training). The stress was applied along the shortest direction. Subsequently, the sample was tested in a compression test where the load was applied parallel to the longest edge of the sample. Thermo-mechanical training and deformation experiments were repeated several times. The twinning stress decreased during the first couple of thermo-mechanical treatments. Thereafter, training lead to hardening. This sample did not exhibit magnetic-field-induced recovery of the strain. A second sample deformed by twinning at lower stress than the first and displayed significant magnetic-field-induced recovery. The two samples were prepared from different sites within one single crystal, which was grown via a modified Bridgman technique. The variance of the results is attributed to inhomogeneities with respect to composition, defects, and/or structure throughout the original single crystal.

A casting furnace was acquired and installed. First casting experiments were performed with $\text{Ni}_{51}\text{Mn}_{28}\text{Ga}_{21}$ alloys. A device for encapsulating ingots in quartz tubes in an inert argon atmosphere was assembled and is currently being tested. A device for measuring the inverse magnetoplastic effect was designed and built.

B) Numerical Simulation

A defect model for a hierarchical twin microstructure of thermoelastic martensite was developed [1,2]. The model makes use of the disclination description of twins [3-5]. Two micrographs of typical twin patterns are shown in Figs. 1a and 1b. The corresponding schematics and disclination contents are shown in Figs. 1c and 1d. Disclinations are present where twins meet and form disclination walls. A dislocation-disclination dynamics code was written using the programming language C#. The code makes use of a disclination quadrupole approximation for a twin double layer as elementary unit of the twin microstructure. In this approximation, two disclination quadrupoles represent a twin double layer (Fig. 2a). Twinning disconnections are introduced when the twin boundary is inclined (Fig. 2b). Disconnections are the equivalent to dislocations when located in interfaces. A series of numerical simulations were run for a range of slope angles α (see Fig. 2b for a definition of α). The resulting stress-strain curves are displayed in Figs. 3a and 3b. For small α , the shear stress increases gradually with strain while the twin boundary is displayed. For increasing α , the hardening rate increases gradually until the slope angle reaches 45° . Above 45° , a threshold stress is required to initiate twinning. For the critical angle of 45° , the mutual interaction force of dislocations (representing the twinning disconnections) vanishes. Below 45° , the mutual interaction force is repulsive, whereas above 45° , the mutual interaction force is attractive. Thus, for large slope angle, the disconnections are being pulled into the vertical interface and form a disclination quadrupole. This is a metastable defect arrangement. Therefore, a threshold stress is required to pull individual disconnections out of the interface and to initiate twin boundary motion.

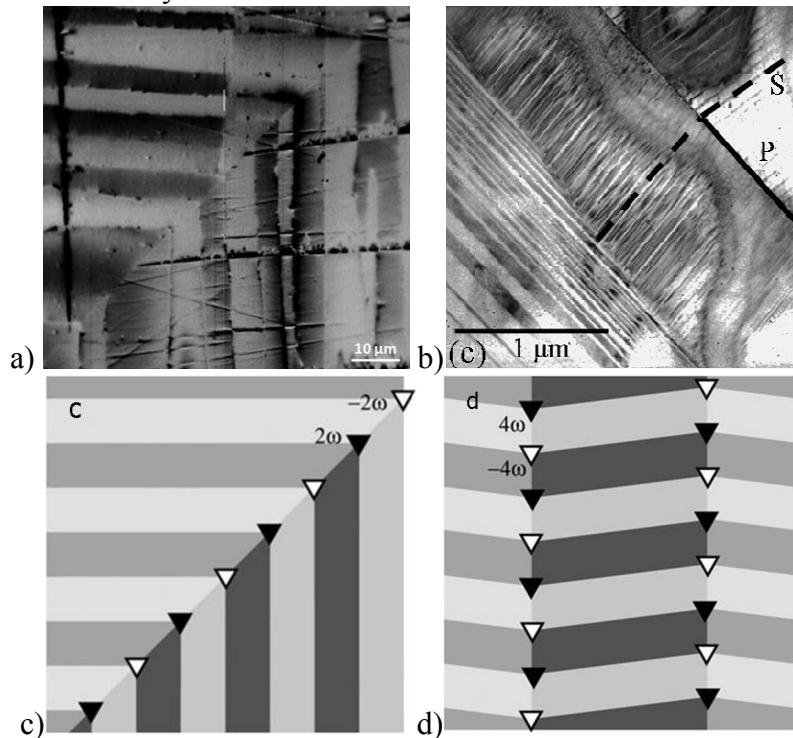


Figure 1: Hierarchical twin microstructure of Ni-Mn-Ga magnetic shape-memory alloys. (a) Magnetic-force microscopy image of a twin arrangement where secondary twins meet orthogonally across a boundary of primary twins. (b) Transmission electron micrograph of a twin arrangement where secondary twins (S) in neighboring primary twins (P) are almost parallel. (c,d) Schematics of the structures in (a) and (b). The positive and negative disclinations are indicated with solid and open triangles.

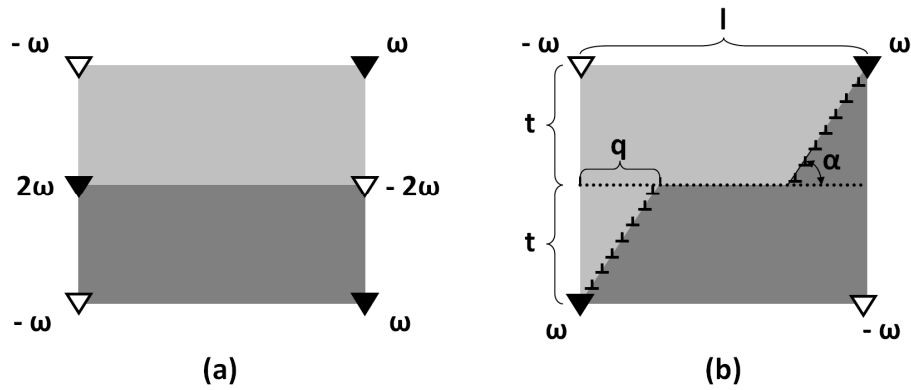


Figure 2: Quadrupole approximation of the twin-microstructure. (a) The elementary unit of a double twin layer of the pattern in Figure 1d. The double layer is bound by two vertically arranged disclination quadrupoles. In each quadruple, the central two disclinations have the same sign and are positioned at the same location, i.e. they appear as one disclination with strength $\pm 2\omega$. In (b), the twin boundary is inclined by the angle α . Therefore, the twin boundary is decorated with twinning disconnections (displayed with dislocation symbols).

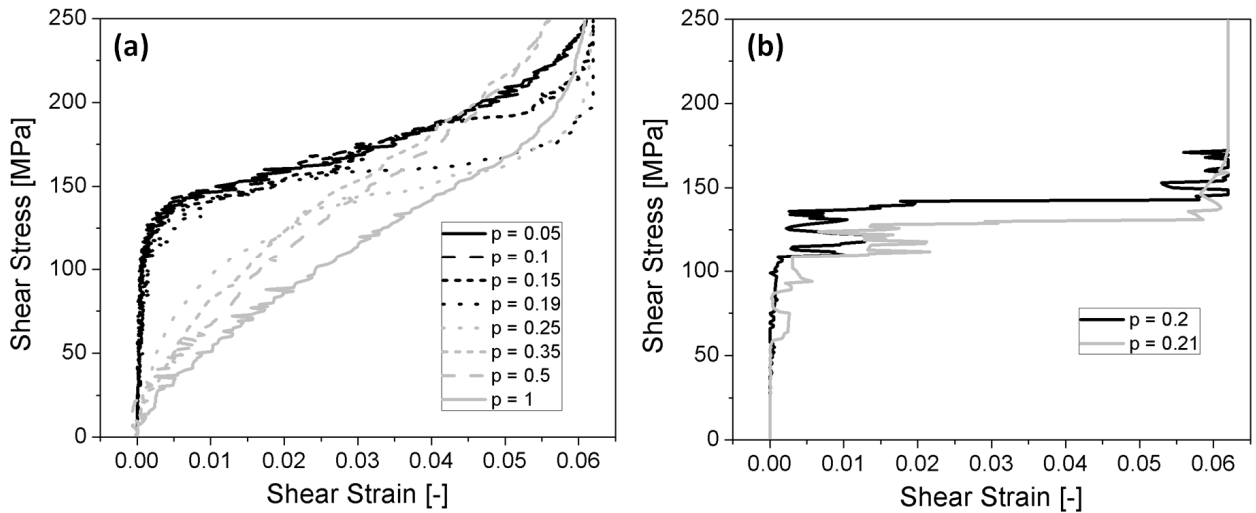


Figure 3: Stress-strain results of numerical simulations. (a) For large $p = 2q/l$ (corresponding to small α , see Fig. 2b for a definition of the parameters), the shear stress increase gradually with increasing strain and decreasing p . The shear stress-shear strain curve displays a threshold stress for small p (corresponding to large α). (b) At the transition value of $p = 0.2$ (corresponding to $\alpha = 45^\circ$), there is increased noise. This is a numerical artifact resulting from increased bypassing events due to small mutual interaction forces between neighboring dislocations.

Future Plans

1. Upon completion of the encapsulation device, systematic annealing experiments will be performed with the goal to create large grains from which single crystalline samples will be prepared.
2. Systematic training experiments will be performed to establish a particular twin microstructure. The twin microstructure will be characterized using atomic-force microscopy, magnetic-force microscopy, scanning electron microscopy, optical microscopy, and transmission electron microscopy.

3. Systematic deformation experiments will be performed with the trained samples to evaluate the twinning threshold stress and magnetic-field-induced recovery as a function of twin microstructure (i.e. twin thickness and twin aspect ratio).
4. Eliminating the numerical issue of disconnection bypassing.
5. Numerical simulation experiments will be performed with the goal to study the effects of twin thickness and twin aspect ratio on twinning threshold stress.
6. The results of the numerical simulations will be compared with the mechanical experiments.
7. Magneto-mechanical experiments will be performed to evaluate the effect of twin microstructure and mechanical properties on the inverse magnetoplastic effect.

References – publications resulting from this project

- [1] P. Müllner, A. S. Geleynse, D. R. Carpenter, M. S. Hagler, M. Chmielus, MRS Fall 2007 Meeting, “Modeling magnetoplasticity and magnetoelasticity with disconnections and disclinations”, invited talk, in press for proceedings.
- [2] P. Müllner and G. Kostorz, “Microstructure of magnetic shape-memory alloys: between magnetoelasticity and magnetoplasticity”, in “Advance Shape Memory Materials”, ed. V. A. Chernenko, submitted February 2008.

References – other publications

- [3] P. Müllner and A. E. Romanov, “Internal twinning in deformation twinning”, *Acta Mater.* 48/9 (2000) 2323-2337.
- [4] P. Müllner, “Disclination models for deformation twinning”, *Solid State Phenomena* 87 (2002), 227-238.
- [5] P. Müllner, “Between microscopic and mesoscopic descriptions of twin-twin interaction”, *Int. Journal of Mater. Res. (formerly Z. f. Metallkunde)*, 97/3 (2006) 205-216.

Roles of nanoclusters in shear banding and plastic deformation of bulk metallic glasses

T.G. Nieh

Department of Materials Science, University of Tennessee, Knoxville, TN 37996

tnieh@utk.edu

Scope

The objective of this research is to establish a basic understanding of shear banding in bulk metallic glasses (BMGs) at an atomistic scale. Based upon previous observations of the presence of nanoclusters (about 1 nm in the length scale) in shear bands induced by nanoindentation and thermographic measurements showed that the shear band temperature in metallic glasses (Pd and Zr-based) is close to the glass transition temperature, we propose a systematic study of topological and chemical organizations of constituent atoms in shear bands during deformation. Since shear transformation zone (STZ) is the basic flow unit in metallic glasses, the kinetics for the STZs clustering and transformation into nanoclusters (or medium-range-order domains) will be studied. The effect of the presence of these nanoclusters on shear band nucleation and propagation will be particularly identified. Critical shear band nuclei as a function of material parameters, such as size, shape, and chemical compositions, will be investigated. A mechanistic model to describe the shear band interactions with nanoclusters and other structural features, for example, another shear band and volumetric defects (e.g., nanovoids) and the effect of these interactions on plasticity, will be established. Parallel molecular simulations will be performed to aid in and validate experimental results, particularly in binary systems, e.g., Cu-Zr.

Experimentally, we will use instrumented nanoindentation technique to characterize shear band emission from a highly localized, deformed, region at various indentation rates and temperatures. The atomistic structure in shear bands will, then, be examined using combined spherical aberration-corrected (Cs-corrected) high-resolution transmission electron microscopy and high-intensity x-ray microdiffraction methods. Chemical ordering and segregation will be examined using Atom Probe Field Ion Microscopy (APFIM). Extensive efforts have been made to improve plasticity in BMGs and one of the important conclusions is that the ductility of BMGs increases as the sample size is reduced. We will conduct experiments to understand this size effect in correlation to shear band formation. Miniature samples with characteristic dimension in the nanometer range will be machined using focus ion beam (FIB) techniques. Subsequently, microcompression will be carried out to investigate the possible change of deformation mode in these miniature specimens. We also anticipate another size effect in crystalline-amorphous nanolaminates. Specifically, when the individual thickness of the amorphous layer in a crystalline-amorphous nanolaminate is less than the critical size of shear band nucleus, shear band will be difficult to form and catastrophic failure can be prevented. We will therefore attempt to synthesize and, subsequently, test these specimens to verify our conjecture. Parallel molecular simulations will also be conducted to validate experimental results. Shear band nucleation and propagation, and the interaction with the amorphous-crystalline interfaces will be simulated for micropillar and nanolaminates samples. We plan to offer a comprehensive understanding of the nature of shear band formation and shear band interaction with structural features in metallic glasses at an atomistic level.

Recent Progress

Since localized shear bands play the pivotal role in the deformation of metallic glasses, in a manner similar to dislocations in crystalline solids, the main effort of this research is to understand the interplay of structure and property of shear bands in plastic deformation.

Effect of the nanoindentation rate and the transition of deformation mode [6, 10]

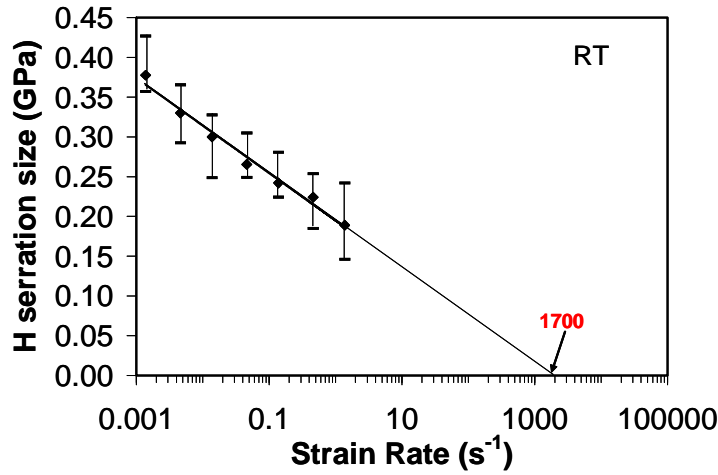
We investigated the nanoindentation behavior of $\text{Au}_{49}\text{Ag}_{5.5}\text{Pd}_{2.3}\text{Cu}_{26.9}\text{Si}_{16.3}$ bulk metallic glass samples at loading rates ranging from 0.03 to 300 mN/s and observed notable displacement bursts which were associated with shear band emission. A quantitative equation was developed between the size of displacement burst, Δh , and indentation depth, h :

$$\Delta h = \frac{24.5\Delta H}{2K_m} h \quad (1)$$

where ΔH is the hardness serration due to displacement burst and K_m is a material constant, to describe accurately the size of displacement burst as a function of the indentation depth h (so called “scaling effect”). Using a free volume model, and under the conditions of a fixed temperature and stress (or hardness), we derived an equation:

$$[\ln(\dot{\epsilon}) - A] \propto \Delta H \quad (2)$$

where $\dot{\epsilon}$ is the strain rate and A is a constant. This equation predicts that hardness serration caused by displacement burst is expected to decrease exponentially with the strain rate. Experimental data obtained from nanoindenting Au-BMG confirm this prediction, as shown in the following figure.



The result also predicts that, when strain rate is higher than a critical value of $\dot{\epsilon}_c = 1700 \text{ s}^{-1}$, there will be no hardness serration, thus no displacement burst. In other words, multiple shear bandings will occur and material will flow homogeneously. However, experimentally, the strain rate of 1700 s^{-1} is beyond the range of an existing nanoindenter. Thus, we conducted a simulation study and showed that, if the imposed strain rate is over $\dot{\epsilon}_c$, the shear band spacing would become so small that the entire sample would virtually behave like one major shear band. Actually, shear band propagates extremely fast and typically at a strain rate of about 1700 s^{-1} . When such a strain rate is imposed on a sample, the sample must be deformed homogeneously in space.

Microcompression of bulk metallic glasses [12,14]

To investigate the sample size effect, we fabricated micro-pillars with diameters between 1 and $3.8 \mu\text{m}$ from Mg-based and Zr-based metallic glasses using focus ion beam, and subsequently tested in compression. The strength of the micropillars was found to be in the range of 1342-1580 MPa, or 60-100% increment over the bulk specimens. The increase in strength is a result of the fact that the micropillars have a lower defect population, thus less probability to initiate shear bands. Qualitatively, we rationalize the increase in strength using the Weibull equation for brittle materials, assuming the characteristic flaw causing fracture in both millimeter and micron samples are the same:

$$P_f = 1 - \exp\left[-V\left(\frac{\sigma - \sigma_u}{\sigma_o}\right)^m\right] \quad (3)$$

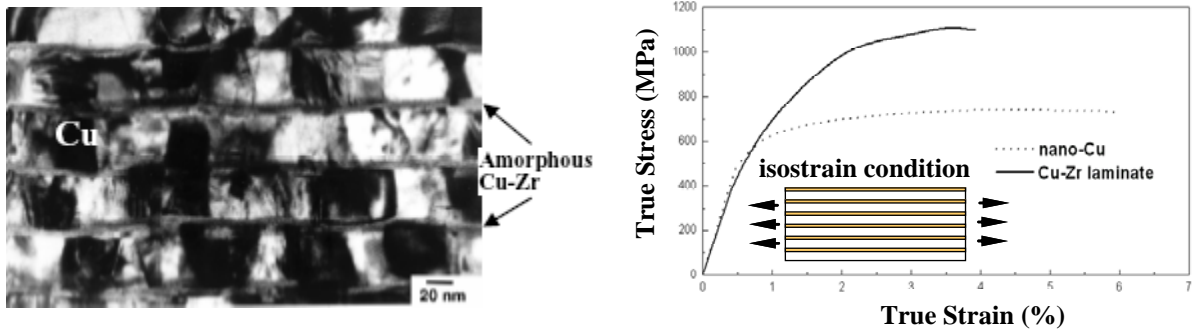
where P_f is the probability of failure, σ_o is a scaling parameter, m is the Weibull modulus and V is the volume of the tested sample. The parameter σ_u denotes the stress at which there is a zero failure probability, and is usually taken to be zero. At a fixed value of P_f , since $V \propto d^3$, where d is the diameter of the compression sample, we obtain

$$d^3 \sigma^m = \text{constant} \quad (4)$$

At a typical value of $m=35$ for BMG, the strength of the $1\mu\text{m}$ Mg-BMG samples is predicted to be about 1500MPa, which is actually close to the measured value of 1580MPa. Another important result obtained from this microcompression study is the fact that the number of shear bands increases with the sample size and strain rates, which is consistent with our early simulations [10].

Future Plans

In principle, shear banding in amorphous alloys includes two steps: shear band nucleation and propagation. Since shear band propagation is fast ($\sim 2000\text{s}^{-1}$), the rate controlling process for shear banding in metallic glasses must be the nucleation. This lead us to predict that if the characteristic dimension of an amorphous phase is less than the critical nucleus size, it would be extremely difficult to initiate localized shear band and, thus, delay fracture. In one of our recent works (Ref 9), using a free volume model combined with experimental data, we estimated the critical size of nucleus for shear band nucleation to be about 20nm. Thus, a question arises as to what if the characteristic length dimension of an amorphous phase is smaller than 20nm, the shear band spacing? Such materials do exist and can be synthesized. In fact, in 1999 we used solid-state amorphization to synthesize an amorphous/crystalline Cu-Zr laminate, with the amorphous layer thinner than 10nm, and subsequently tested it *in tension*. The laminate not only exhibited strong work hardening but also a remarkable tensile elongation of 4%. Both the nanolayered structure and the mechanical properties of the Cu-Zr nanolaminates are shown in the figure below. None of any monolithic metallic glass has ever exhibited tensile ductility. Thus, our result was a surprise and a satisfactory explanation was not given. Until recently we began to realize that we have overlooked the importance of shear band nucleation.



In the coming year, we plan to fabricate amorphous-crystalline Cu-Zr nanolayers. The thickness and, thus, volume fraction of the amorphous layer can be controlled by appropriately adjusting the relative thickness of the nanolayers. This would allow us to validate our conjecture that amorphous phase with limited thickness can bypass shear band nucleation and prevent catastrophic failure. It is worth noting that, from a scientific viewpoint, amorphous-crystalline nanolayers created by solid-state amorphization also offer us a great opportunity for the fundamental study of dislocation-interface interactions.

We recently conducted *in situ* compression test with a “ductile” Zr-base bulk metallic glass at low strain rates. The dominant mode of deformation was single shear. A direct comparison of the load-displacement data and video images indicated the flow serration commonly observed in compression at a low strain rate actually represented intermittent sample slides, rather than the

tradition belief that serration was caused by random emission of individual shear bands. This observation is very significant for it suggests existing shear bands are the preferential sites for further shear band emission; this progressive shear band emission causes the final fracture. In addition, according to the literature, “improved plasticity” in metallic glasses was only observed at low strain rates ($<10^{-4} \text{ s}^{-1}$). If our observation of Zr-BMG is a generalized case, then the reported improvement is probably a record of inhomogeneous sample sliding, rather than uniform deformation by random emission of multiple shear bands. In the coming year, we will continue performing *in situ* compression tests with different metallic glass systems to confirm this conjecture.

Publications of DOE sponsored research

1. B. Yang, L. Riester, and T.G. Nieh, ‘Strain hardening in a bulk metallic glass under nanoindentation,’ *Scripta Mater.* **54**, 1277–1280 (2006).
2. B. Yang, M. Morrison, P.K. Liaw, C.T. Liu, R. A. Buchanan, and T.G. Nieh, ‘Temperature evolution of nano-scale shear band in bulk metallic glasses,’ *J. Mater. Res.* **21**(4), 915-922 (2006).
3. Akihiko Hirata, Yoshihiko Hirotsu, Tadakatsu Ohkubo, Nobuo Tanaka, and T. G. Nieh, ‘Local atomic structure of Pd-Ni-P bulk metallic glass examined by high-resolution electron microscopy and electron diffraction,’ *Intermetallics*, **14**(8-9), 903-907 (2006).
4. B. Yang, C. T. Liu, and T. G. Nieh, ‘Unified equation for the strength of bulk metallic glasses,’ *App. Phys. Lett.* **88**(22), no. 221911 (2006).
5. J. P. Chu, C. L. Chiang, H. Wijaya, R. T. Huang, C. W. Wu, B. Zhang, W. H. Wang, and T. G. Nieh, ‘Compressive deformation of a bulk Ce-based metallic glass,’ *Scripta Mater.* **55**, 227-230 (2006)
6. B. Yang and T. G. Nieh, ‘Effect of nanoindentation rate on the shear band formation in an Au-based bulk metallic glass,’ *Acta Mater.* **55**(1), 295-300 (2007).
7. J. P. Chu, H. Wijaya, C. W. Wu, T. R. Tsai, C. S. Wei, T. G. Nieh, and J. Wadsworth, ‘Nanoimprint of gratings with a bulk metallic glass,’ *Appl. Phys. Lett.*, **90**(3) no. 034101 (2007).
8. Akihiko Hirata, Yoshihiko Hirotsu, T.G. Nieh, Tadakatsu Ohkubo, and Nobuo Tanaka, ‘Direct imaging of local atomic ordering in a Pd–Ni–P bulk metallic glass using Cs-corrected transmission electron microscopy,’ *Ultramicroscopy*, **107**, 116-125 (2007).
9. B. Yang, J. Wadsworth, and T.G. Nieh, ‘Thermal activation in Au-based bulk metallic glass characterized by high-temperature nanoindentation,’ *Appl. Phys. Lett.*, **90**, 061911 (2007).
10. Y.F. Gao, B. Yang, and T.G. Nieh, ‘Thermomechanical instability analysis of inhomogeneous deformation in amorphous alloys,’ *Acta Mater.* **55**, 2319–2327 (2007).
11. K. Wang, T. Fujita, M.W. Chen, T.G. Nieh, H. Okada, K. Koyama, W. Zhang, and A. Inoue ‘Electrical conductivity of a bulk metallic glass composite,’ *Appl. Phys. Lett.*, **91**, 154101 (2007).
12. C.J. Lee, J.C. Huang, and T.G. Nieh, ‘Sample size effect and micro-compression of Mg₆₅Cu₂₅Gd₁₀ metallic glass,’ *Appl. Phys. Lett.*, **91**, 161913, 2007.
13. Y.C. Chang, T.H. Hung, H.M. Chen, J.C. Huang, T.G. Nieh, and C.J. Lee, ‘Viscous flow behavior and thermal properties of bulk amorphous Mg₅₈Cu₃₁Y₁₁ alloy,’ *Intermetallics*, **15**, 1303-1308 (2007).
14. Y.H. Lai, C.J. Lee, Y.T. Cheng, H.S. Chou, H.M. Chen, X.H. Du, C.I. Chang, J.C. Huang, J.S.C. Jang, S.R. Jian, and T.G. Nieh, ‘Bulk and microscale compressive behavior of a Zr-based metallic glass,’ *Scripta Mater.* **2008**. - accepted
15. L. Wang, S.X. Song, and T.G. Nieh, ‘Assessing plastic shear resistance of bulk metallic glasses under nanoindentation’, *Appl. Phys. Lett.* **2008**. - accepted
16. S.X. Song, J.S.C. Jang, and T.G. Nieh, ‘Analyses of shear band emission in a Mg-based bulk metallic glass deformed at different nanoindentation rates,’ *Intermetallics*, **2008**. - accepted
17. Y. C. Chang, J. C. Huang, Y. T. Cheng and C. J. Lee, X.H. Du, and T.G. Nieh, ‘On the fragility and thermomechanical properties of Mg-Cu-Gd-(B) bulk metallic glasses,’ *J. Appl. Phys.* **2008**. - accepted
18. K. Wang, T. Fujita, D. Pan, T. G. Nieh, A. Inoue, D. H. Kim, and M.W. Chen, ‘Interface structure and properties of a brass-reinforced Ni₅₉Zr₂₀Ti₁₆Si₂Sn₃ bulk metallic glass composite’, *Acta Mater.* **2008**. - accepted

Mechanical Properties of Materials with Nanometer Scale Microstructures (DOE Grant DE-FG02-04-ER46163)

Principal Investigator: Professor William D. Nix (nix@stanford.edu)
Department of Materials Science and Engineering
416 Escondido Mall, Building 550
Stanford University, Stanford California 94305

Program Scope

Nanomechanical devices are certain to play an important role in future technologies. Already sensors and actuators based on MEMS technologies are common and new devices based on NEMS are just around the corner. These developments are part of a decades-long trend to build useful engineering devices and structures on a smaller and smaller scale. The creation of such structures and devices calls for an understanding of the mechanical properties of materials at these small length scales. In the macroscale (bulk), the mechanical properties of materials are commonly described by single valued parameters (eg. yield stress, hardness, etc), which are largely independent of the size of the specimen. However, as specimens are reduced in size to the scale of the microstructure, their mechanical properties deviate very significantly from those of bulk materials. This calls for the study of mechanical properties of materials in small volumes. Our current attention is focused on studying the mechanical properties of crystalline materials at the sub-micron scale by nanoindentation and micropillar compression.

Recent Progress

When crystalline materials are mechanically deformed in small volumes, higher stresses are needed for plastic flow. This has been called the “smaller is stronger” phenomenon and has been widely observed. Various size-dependent strengthening mechanisms have been proposed to account for such effects, often involving strain gradients. It has been argued that the indentation size effect (ISE) can be understood in terms of the hardening associated with strain gradients and the associated geometrically necessary dislocations. In order to verify this mechanism, we have probed indentations of different sizes on the (111) surface of a Cu single crystal to look for the expected lattice curvatures. Using a Scanning X-ray Microdiffraction (μ SXRD) technique, the indentation-induced lattice rotations were directly measured by the streaking of X-ray Laue spots associated with the indentations. The magnitude of the lattice rotations was found to be independent of indentation size, which is consistent with the basic tenets of the ISE model based on geometrically necessary dislocations. Moreover, using the μ SXRD data, together with an ISE model, we could estimate the effective radius of the indentation plastic zone; we found that the estimate falls in a sensible range, as determined by finite element analysis. Using these results, an estimate of the average dislocation densities within the plastic zone have been made; the findings are consistent with the ISE arising from the dependence of the dislocation density on the depth of indentation.

In recent years we have conducted uniaxial compression experiments on micrometer size pillars of single crystal gold and found surprisingly strong size effects, even though no significant strain gradients are present and the crystals are not initially dislocation free. We have argued that these size effects are caused by *dislocation starvation hardening*, with dislocations leaving the crystal more quickly than they multiply and leading to the requirement of continual dislocation nucleation during the course of deformation. A new length scale for plasticity, the distance a dislocation travels before it creates another, arises naturally in this treatment. Hardening of crystals smaller than this characteristic size is expected to be dominated by dislocation starvation while crystals much larger than this size should exhibit conventional dislocation plasticity.

In an effort to shed new light on the size effects in the micropillar experiments, we have conducted a search for strain gradients in deformed single-crystal micropillars of gold, using a submicron white-beam (Laue) X-ray diffraction technique. We have shown that, both before and after uniaxial compression, no evidence of either significant lattice curvature or subgrain structure can be found. We find that the Laue spots for these small pillars are not broadened at all by extensive compressive deformation, in contrast to the extensive broadening of Laue spots in deformed bulk metals. This is consistent with the idea that dislocations in such small pillars leave the crystal before they can interact with each other and that the high strengths of these pillars are related to dislocation starvation and not to ordinary strain hardening.

We have recently applied the micropillar compression technique to determine the mechanical properties of epitaxial Al-Al₃Sc multilayers and have discovered new deformation behavior not seen before. In all previous work on metal multilayers the strength properties have been determined either by nanoindentation (hardness) testing or by microtensile testing. While these methods give a clear picture of the very high strengths of these materials, they do not permit a very extensive look at the flow properties past the yield strain, because hardness testing does not reveal the stress-strain response and because fracture usually occurs shortly after yielding in tensile tests. By applying the micropillar compression technique to Al-Al₃Sc we have, for the first time, been able to follow the plastic flow behavior to large strains. We find that finely structured multilayers have very high strengths, as expected, but also that these materials do not strain harden! Instead, these multilayers show extensive strain softening shortly after yielding. This is manifested in the shape of the stress-strain curves and by the shapes of the deformed pillars. The strongest pillars, which show the largest amount of strain softening, deform very inhomogeneously, with mushroom-like features forming at the tops of the pillars where extensive strain softening occurs. This new and unexpected deformation mode is very important and requires further investigation.

The large amount of scatter in our initial Au micropillar experiments and the different overall shapes of our stress-strain curves compared to those published by Volkert and Lilleodden has motivated us to conduct new micropillar compression experiments using a (001) epitaxial film of Au grown onto a (001) MgO substrate. The micropillars made using this epitaxial film have a very well defined length (the thickness of the Au film) and the pillars cannot push into the substrate as they can when the underlying substrate is a soft Au crystal. The scatter for these new experiments is much reduced, but the overall shape of the stress-strain curves is unchanged from our previous work.

Future Plans

Our studies of length scale effects on mechanical properties of crystalline materials will be continued in the future.

1. We plan to conduct systematic studies of the compression deformation properties of single crystal gold pillars grown epitaxially onto MgO substrates by sputter deposition. By controlling the geometry of the arrangement of sputtering guns we can grow films in which the thickness of the film varies across the surface of the substrate. This will then permit the fabrication of micropillars of different diameters while keeping the length to diameter ratio (L/D) constant. This experiment is expected to eliminate the possible effect of a changing L/D ratio on the size dependence of plasticity in micropillars.
2. In an effort to completely remove the possible effects of gallium implantation and ion damage on the mechanical properties of micropillars we will study the plastic deformation properties of gold microcrystals made without FIB machining. We are collaborating with Prof. Eugen Rabkin of the Technion who will deposit very thin films of gold onto sapphire and form microcrystals by annealing the structure at high temperatures to effect dewetting of the film (in the liquid state) and subsequent solidification and crystal growth on cooling. This process is known to produce pristine (and faceted), sub-micron sized Au crystals on sapphire substrates. Compression of these crystals using the standard testing technique should allow us to study plasticity in small gold crystals in the absence of any FIB damage or contamination effects.
3. Because some of the theories of size-dependent plasticity depend on the existence of strong pinning points or junctions within the crystal, it seems appropriate to search for size effects in crystals where such junctions typically do not form. We plan to study strength and plastic deformation of micropillars machined from HCP Cd single crystals and oriented for basal slip. It is well known that basal slip in Cd produces almost no strain hardening because strong pinning points cannot be formed. A strong size effect would not be expected if the size effect arises primarily from the statistics of strong pinning points whereas it would be expected if the size effect is associated with dislocation starvation and the statistics of surface sources.
4. Recent work has shown that the micropillar size effect in BCC metal crystals may be less than that in FCC metals. The ease with which screw dislocations cross-slip (and multiply) in BCC metals compared to FCC metals may be responsible for this difference. In an effort to shed new light on this we plan to grow epitaxial films of vanadium onto MgO substrates by sputter deposition and to make and test micropillars using these films. Vanadium has been chosen for this work because it has a sufficiently low atomic number to allow in situ TEM studies of pillar compression (to be conducted in collaboration with Dr. Andy Minor at the National Center for Electron Microscopy at LBL in Berkeley).

Recent Publications (2005-2007)

1. J.N. Florando and W.D. Nix, "A microbeam bending method for studying stress-strain relations for metal thin films on silicon substrates," *J. Mech. Phys and Solids*, **53**, 619-638 (2005).
2. Dae-han Choi and W.D. Nix, "Anelastic behavior of Copper thin films on Silicon substrates: Damping associated with dislocations," *Acta Materialia*, **54**, 679-687 (2006).
3. Julia R. Greer, Warren C. Oliver and William D. Nix, "Size Dependence of Mechanical Properties of Gold at the Micron Scale in the Absence of Strain Gradients," *Acta Materialia*, **53**, 1821-1830 (2005).
4. Julia R. Greer and William D. Nix, "Size Dependence of Mechanical Properties of Gold at the Sub-Micron Scale," *Applied Physics A: Materials Science and Processing*, **80**, 1625-1629 (2005).
5. Y. Liang, W.D. Nix, P.B. Griffin and J.D. Plummer, JD, "Critical thickness enhancement of epitaxial SiGe films grown on small structures," *Journal of Applied Physics*, **97**, 043519-1-043519-7 (2005).
6. E.T. Lilleodden and W.D. Nix, "Microstructural length-scale effects in the nanoindentation behavior of thin gold films," *Acta Materialia*, **54**, no.6, p.1583-1593 (2006).
7. S.M. Han, R. Saha and W.D. Nix, "Determining hardness of thin films in elastically mismatched film-on-substrate systems using nanoindentation," *Acta Materialia*, **54**, no.6, p.1571-1581 (2006).
8. Junlan Wang, Jie Lian, Julia R. Greer, William D. Nix and Kyung-Suk Kim, "Size effect in contact compression of nano- and microscale pyramid structures," *Acta Materialia*, **54**, no.15, p.3973-3982 (2006).
9. J.R. Greer and W.D. Nix, "Nanoscale gold pillars strengthened through dislocation starvation," *Physical Review B*, **73**, no.24, p.245410-1-6 (2006).
10. William D. Nix, Julia R. Greer, Gang Feng and Erica T. Lilleodden, "Deformation at the Nanometer and Micrometer Length Scales: Effects of Strain Gradients and Dislocation Starvation," *Thin Solid Films*, **515**, 3152-3157 (2007).
11. F. Zhang, R. Saha, Y. Huang, W.D. Nix, K.C. Hwang, S. Qu and M. Li, "Indentation of a hard film on a soft substrate: Strain gradient hardening effects," *International Journal of Plasticity*, **23**, 25-43 (2007).
12. A.S. Budiman, S.M. Han, J.R. Greer, N. Tamura, J.R. Patel† and W.D. Nix, "A search for evidence of strain gradient hardening in Au submicron pillars under uniaxial compression using synchrotron x-ray diffraction," *Acta Materialia*, **56**, 602-608 (2008).

Understanding Size Effects in Cleavage Cracking in Thin Film Materials

DOE Award No.: DE-FG02-07ER46355

Principle Investigator: Yu Qiao, Assoc. Prof. of Mater. Sci. & Struct. Eng.
9500 Gilman Dr. MC 0085, La Jolla, 92093-0085
(Phone: 858-534-3388; Email: yqiao@ucsd.edu)

Institution: The University of California, San Diego

Project Title: Understanding Size Effect in Cleavage Cracking in Thin Film Materials

Program Scope

The reliability of polycrystalline thin films is essential to assuring safe performance of micro/nano-electromechanical systems. Usually, they are of through-thickness grain structures and are brittle at working temperatures, and therefore their fracture properties are dominated by the resistances offered by grain boundaries to cleavage cracking. As a cleavage crack front propagates across a high-angle grain boundary, it would first penetrate across a number of break-through points, and the persistent grain boundary areas would then be separated through shear fracture or ligament bending. It is, therefore, envisioned that as the film thickness is smaller than the characteristic distance between the break-through points, which is often in the range of 0.5-5 microns, the crack front transmission can be significantly confined by the film surfaces, leading to an either beneficial or detrimental size effect. That is, the fracture toughness of the polycrystalline thin film is not a material constant; rather, it highly depends on the film thickness. Since this important phenomenon has not received the necessary attention, we propose to carry out a systematic study on fracture resistances of bicrystal silicon films. The film thickness will range from 1 to 1000 microns, and the crystallographic orientations across the grain boundaries will be controlled precisely so that the size effect and the geometrical factors can be analyzed separately. The study will start with thick films. Once the crack front transmission process is relatively well understood, it will be extended to thin films. This project will shed light on crack-boundary interactions in confining microenvironments, which has both great scientific interest and immense technological importance to the development of fine-structured devices.

Recent Progress

In order to understand and improve fracture resistance of thin films, a boron-doped polycrystalline silicon was investigated as a close analogue to all many intrinsically brittle materials. The as-received material was in wafer form, with the thickness of 4 mm and the diameter of 200 mm. The grain size was in the range of 5-15 μm . The silicon wafer was heated in a tube furnace at 450 °C for 0.5 h, followed by partial quenching in cold water, through which a large number of thermal cracks were produced. Under a XTL-VI stereo trinocular microscope, the cracks arrested by through-thickness grain boundaries were identified, and 15×15 mm rectangle pieces surrounding the crack tips were harvested and sliced into 200 μm thick films by electrical discharge machining (EDM). In each group of pre-cracked films, the grains were of identical crystallographic orientations. The films were cleaned in a mixture of 4 parts of 98% sulfuric acid and 1 part of 30% hydrogen peroxide at 90 °C for 15 min, rinsed in deionized water, and slightly etched for 10 min. The etchant contained 7% of hydrofluoric acid, 75% of nitric acid, and 18% of acetic acid. After rinsing in ethanol, the films were dried in a vacuum furnace at 100

°C for 30 min, and then modified in a 20% toluene solution of chlorotrimethylsilane at 90 °C for 5 days, so that the pre-crack surfaces as well as the film surfaces were covered by a dense layer of hydrophobic silane groups. The surface treated films were mechanically polished to about 150 μm thick, and finally thinned to 1-30 μm through chemical etching in the hydrofluoric acid etchant. During etching, the sample was placed in a porous teflon container and the etchant was driven by an Omega FPU-500 peristaltic pump to flow across the sample surface at a constant rate of 30 ml/min. The etching rate was 3-5 μm/min. Since the pre-crack surfaces were protected by the silane layer, the crack tips remained sharp and clear. Prior to the tensile test, the samples were thermal treated at 350°C in vacuum for 12 h and thoroughly cleaned in acetone and ethanol.

The thin film samples were then mounted on a microtesting machine, with both ends fixed on testing stages by a Loctite-411 glue. The testing machine was custom designed, capable of applying a tensile load at a rate of 10 μm/sec, with the resolutions of load and displacement of 0.3 μN and 20 nm, respectively. The fracture surfaces were observed in a FEI XL30 environmental scanning electron microscope (SEM), as shown in Figs.1 and 2. Using the measured peak load, F_p , of grain boundary failure, the boundary toughness was calculated in the framework of linear elastic fracture mechanics: $K_{gb} = (F_p / wt) \sqrt{\pi a} \cdot f$, where w and t are the width and the thickness of the thin film sample, respectively; a is the precrack length, and $f = 1.12 - 1.39(a/w) + 7.3(a/w)^2 - 13(a/w)^3 + 14(a/w)^4$ is the geometry factor. The results are shown in Fig.3.

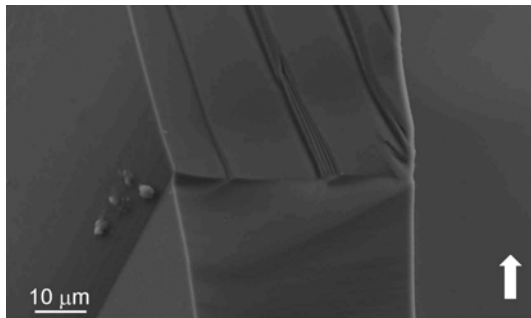


Fig.1 Cleavage cracking across a through-thickness grain boundary in a thick-films sample. The arrow indicates the crack propagation direction.

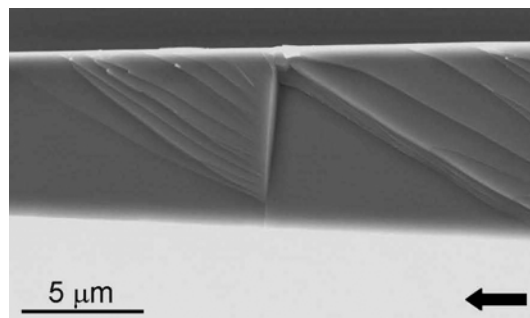


Fig.2 Cleavage cracking across a through-thickness grain boundary in a thin-film sample. The arrow indicates the crack propagation direction.

Altogether four groups of thin-film samples were investigated, with the film thicknesses varying in the range of 2 to 15 μm. In each sample, along the grain boundary there is only one BTP. In the same group, all the samples are sliced from the same pre-cracked bicrystal. Thus, they are of the same crystallographic orientation. Clearly, K_{gb} increases with t . For instance, for group 1 samples, the fracture toughness of grain boundary increases by about 20% as t rises from 2.4 μm to 12.5 μm. For group 2 samples, as the film thickness increases from 3-4 μm to about 10 μm, the boundary toughness increases by nearly 30%. The data of group 4 samples show that as the film thickness is larger than 20 μm, the grain boundary toughness is no longer size dependent, which converges to the behavior of thick films. According to literature data, the fracture toughness of crystallographic plane of single crystal silicon is about 0.9-1.1 Mpa·m^{1/2}, nearly 40% smaller than the measured thick-film boundary toughness. Through Eq.(1), the value of C can be determined as 3.4, close to the experimental data of large bicrystals. Note that since the crystalline structures of the silicon sample is nearly perfect, at the small length scale of the current study, the size dependent caused by the weakest-link effect should be

negligible. Even if the weakest-link effect were detectable, it should cause a decrease in K_{gb} as the film becomes thicker. As t rises, the increase in K_{gb} directly reflects the PGBI effect.

The size sensitivity of fracture toughness of group 1 samples is weaker than that of the other 3 groups, which may be attributed to that their crystallographic misorientation angles, especially the twist angle, are the smallest. When the twist angle is small, as film thickness varies, the change in PGBI area is less pronounced, and thus the associated variation in fracture work is less evident. Note that, even though the twist angles of groups 2, 3, and 4 are quite different, their K_{gb} - t relationships are somewhat similar, indicating that as the twist angle exceeds a critical range, the PGBI area is sufficiently large so that direct shear separation is difficult. The crack front first penetrates across the boundary and propagates forward in grain "A". The PGBI is left behind the advancing front, acting as tough reinforcements bridging the fracture flanks together. Consequently, the criteria of unstable crack growth in grain "A" is not directly dependent on θ . Because mixed-mode fracture is unfavorable, the critical range of twist angle should be relatively small.

In addition, a few irregular cracking modes at grain boundaries were analyzed. For instance, it was noticed that other than the crystallographic orientation, the orientation of the grain boundary plane also plays a critical role. With respect to the initial crack surface, if the inclination angle is relatively small, the crack tends to penetrate across the boundary; if the angle is large, the crack may either bifurcate along the boundary or turn back on another crystallographic plane. The former is triggered by crack front transmission, and the latter may result in a higher critical crack growth driving force.

Other than grain boundaries, twin boundaries are also of a toughening effect. Depending on the orientation of cleavage plan and the twin system, the crack surface may either be planar or become jerky across the first boundary, while across the second boundary the cleavage ridges tend to re-combine back into a single plane. The crack behavior at the first twin boundary is considerably influenced by the twin width, indicating that the anisotropy of crack-tip stress field is essential.

To better understand the experimental results, a number of theoretical and computational analyses have been performed on the fracture toughness of grain boundaries of various properties. If the boundary is sufficiently tough such that it would not yield even after the cracking trapping effect is fully overcome, the boundary fracture resistance can be estimated as

$$\frac{G_{tot}}{G_{sc}} = \left\{ \frac{w}{t} + \left[2.4 - 0.3 \frac{t}{w} \right]^2 \cdot \left(1 - \frac{w}{t} \right) \right\} \frac{1}{\cos \theta \cdot \cos \varphi} + \beta \frac{\tan \theta}{4} \frac{t}{w} \left[1 - \left(\frac{w}{t} \right)^2 \right] \quad (1)$$

where G_{tot} is the boundary resistance; G_{sc} is the resistance of a single crystal; t is the film thickness; θ and φ are the twist and tilt misorientation angles, respectively; and w and β are material constants. Equation (2) gives the upper estimate. If the grain boundary is relatively weak so that it is separated simultaneously as the cleavage front bypasses it, its fracture

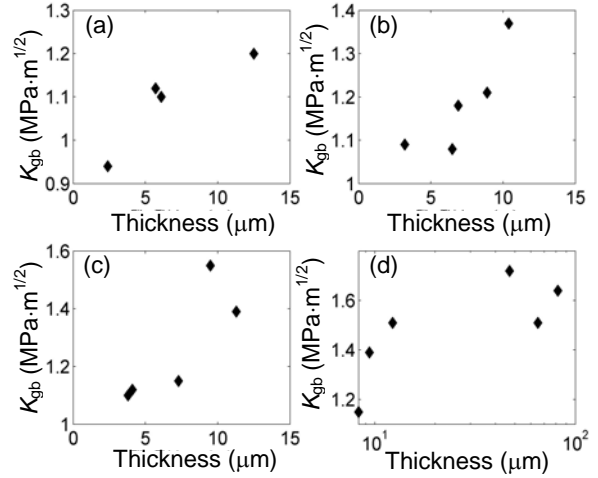


Fig.3 The measured grain boundary toughness, K_{gb} , as a function of the film thickness, t . (a) Group 1 samples, with the twist angle, θ , and the tilt angles, ϕ , being 4.3° and 5.6° , respectively. (b) Group 2 samples ($\theta = 11.1^\circ$, $\phi = 4.2^\circ$). (c) Group 3 samples ($\theta = 7.6^\circ$, $\phi = 12.4^\circ$). (d) Group 4 samples ($\theta = 9.1^\circ$, $\phi = 17.2^\circ$).

resistance can be assessed in the framework of R-curve analysis, which provides the lower estimate. The experimental data scatter nicely in between these two limits, suggesting that the grain boundaries under investigation are separated apart through a mixed mode.

Future Plans

In the final year of this project, all the work discussed in the proposal will be completed, except the finite element analysis that has become relatively less critical with the theoretical analyses being performed. If possible, a temperature chamber will be developed so that the microfracture experiment can be carried out at a series of temperatures ranging from 300 to 600 °C, so that the effects of dislocation activities can be examined. The assumption that films of multiple grain layers tend to be tougher will be tested against experimental data. The thin film behavior under bending moments will be analyzed so as to investigate mixed fracture modes. A soft-coating technique has been developed and will be applied in our experiment to gain a better control of crack propagation.

List of Publications

1. Qiao, Y; Kong, X. Cleavage resistance of fine-structured materials. *Met. Mater. Inter.* **12**, 27-30 (2006).
2. Chen, J; Qiao, Y. Mixed-mode cleavage front branching at a high-angle grain boundary. *Scripta Mater.* **56**, 1027-1030 (2007).
3. Chen, J; Qiao, Y. Secondary cracking at grain boundaries in silicon thin films. *Scripta Mater.* **57**, 1069-1072 (2007)
4. Qiao, Y; Kong, X. On size effect of cleavage cracking in polycrystalline thin films. *Mech. Mater.* **39**, 746-752 (2007).
5. Chen, J.; Qiao, Y. Characteristic length scale in cleavage cracking across high-angle grain boundary. *Comput. Mater. Sci.*, in the press.
6. Chen, J.; Qiao, Y. Interaction of cleavage ridges with grain boundaries in polysilicon films. *Appl. Phys. A*, in the press.
7. Chen, J.; Kong, X.; Chakravarthula, S. S.; Qiao, Y. Grain boundary separation in transgranular cleavage cracking. *Mater. Res. Innov.*, in the press.
8. Qiao, Y.; Chen, J.; Kong, X.; Chakravarthula, S. S. Energy equilibrium of cleavage front transmission across a high-angle grain boundary in a free-standing silicon thin film. *Eng. Fract. Mech.*, in the press.
9. Chen, J.; Lu, W.; Qiao, Y. Penetration of cleavage front across a high angle grain boundary. *Mech. Res. Commun.*, under review.
10. Chen, J.; Qiao Y. A size effect in cleavage cracking in free standing polysilicon thin film. *Acta Mater.*, under review.
11. Chen, J.; Qiao, Y. Cleavage cracking across triple grain boundary junctions in free standing silicon thin film. *J. Mater. Res.*, under review.
12. Chen, J.; Lu, W.; Qiao, Y. Resistance to cleavage cracking of grain boundary arrays in free standing thin film, under preparation.
13. Chen, J.; Qiao, Y. Bifurcation and deviation of cleavage paths at through-thickness grain boundaries. *Met. Mater. Trans. A*, under review.

The Coupling between Interfacial Charge and Mechanical Deformation at High Temperatures in Ceramics

DE-FG02-07ER46403

PI: Rishi Raj

Department of Mechanical Engineering

University of Colorado at Boulder

Boulder, CO 80309-0427

rishi.raj@colorado.edu

(303)492-1029

Recently there has been a convergence of observations that have demonstrated that electrical fields can couple with stress-induced phenomena in ceramics at high temperatures. These phenomena often appear related to grain boundary diffusion in ceramics. Examples are: (i) a lower flow stress at a given strain rate and temperature when an electrical field is applied in experiments of creep and superplasticity in ceramics (Yang and Conrad, 1997-99), (ii) microwave enhanced sintering, and (iii) spark-plasma-sintering (SPS). There is circumstantial evidence that the application of electrical fields depresses grain growth. The objective of this research program is to understand the basic science underlying one or more of these observations.

A principal question that we are addressing is whether the phenomena listed above arise from the influence of applied electrical fields on (a) the *driving force* for diffusional transport, or (b) the *kinetics* of diffusional transport, or (c) both thermodynamics and kinetics. For instance, the driving force can arise from an applied stress, or by the sintering stress, or from grain growth. The thermodynamic approach stems from the results of a uniaxial experiment at high temperatures in zirconia, where the applied load generates a potential difference between the loaded and the unloaded faces of the specimen (Pannikatt and Raj, 1997). The concept for the kinetic explanation arises from a theoretical model that suggests that the space charge generated near grain boundaries due to non-stoichiometric compositions of charged species segregated to the boundary, can have a very significant effect on the kinetics of diffusional transport (Jamnik and Raj, 1996).

A critical question to be addressed in this program is whether the electro-mechanical coupling arises predominantly from the thermodynamic driving force or from a kinetic effect.

A combination of experiments and modeling will be employed in this research program, where experiments are carried out to prove or to disprove fundamental questions. For example, the thermodynamic explanation would suggest that the influence of the electrical field depends on the direction of the applied field (we are studying how the effect on creep behavior changes when the sign of the applied field is reversed, and when the applied field is parallel or perpendicular to the direction of uniaxial loading). The applied stress can have a deviatoric component (as in uniaxial loading) and a

hydrostatic component (as in sintering), while the electrical field is a vector quantity. A thermodynamic explanation may be expected to have reciprocity. That is, if applies stress can generate an electrical potential, then it may be possible to induce strain simply by applying an electrical field.

One of the possible kinetic models for studying the electro-mechanical effect at high temperatures is that the applied field has an influence on the space charge in the Debye layers adjacent to the grain boundaries. The influence of interfacial space charge (or double layers) on ionic transport is a traditional topic in solid state electrochemistry. However, the coupling between an applied stress as well as an electrical field on interfacial transport, is a new topic that we are exploring in the current program. Experiments are being designed with thin film zirconia specimens to study the effect of stress as well as applied fields on ionic transport to study this electro-mechanical coupling.

Finally, over the longer term we seek to understand if there is common underlying science in the seemingly disparate phenomena such as creep, free sintering, microwave-sintering, and SPS sintering of ceramics. All of these phenomena share the transport of charged species at grain boundaries, although the method used to electrically activate the grain boundaries varies from one experiment to another. It would be fair to say that while microwaves and SPS have definitely been shown to enhance densification, a clear and generally accepted fundamental understanding of the underlying mechanisms is still missing. We hope that the work in this program would lead to such clarifications.

Mechanical Behavior in Lithium Aluminum Silicate Composites

PI: Ivar Reimanis
Metallurgical and Materials Engineering Department
Colorado School of Mines
Golden, CO 80401
USA

Email: reimanis@mines.edu

Program Scope

A novel material behavior was recently observed in a class of low coefficient of thermal expansion (CTE) ceramic composites in which cracking is accompanied by high energy release, leading to multi-particle ejection. High energy particle ejection lasting up to several minutes is observed in composites comprising β -eucryptite (LiAlSiO_4) when they are subjected to compressive loads such as those underneath an indenter. Figure 1 shows an image of particles ejecting from a β -eucryptite composite taken with a high speed camera. It is hypothesized that the spontaneous particle ejection is driven by a recently discovered pressure-induced phase transformation in β -eucryptite. Research is performed to establish the critical parameters required to control the phenomenon, so that it may ultimately be employed in new applications, and so it may be used to better understand structure-property relations in β -eucryptite based composites. Ion implantation studies will be carried out to study how radiation-induced damage tolerance may be altered by a phase transformation. In addition to potential uses in nuclear applications, preliminary experimental results suggest the process can be utilized to create a new, phase-transformation-toughened ceramic. Because β -eucryptite exhibits unusual behavior – for example, it has an average negative coefficient of thermal expansion and is also a superionic conductor – the proposed work is expected to advance fundamental understanding concerning structure-property relations in ceramics. In addition, the potential use of β -eucryptite materials in a wide variety of engineering applications has not been realized because fundamental studies on its behavior are lacking.

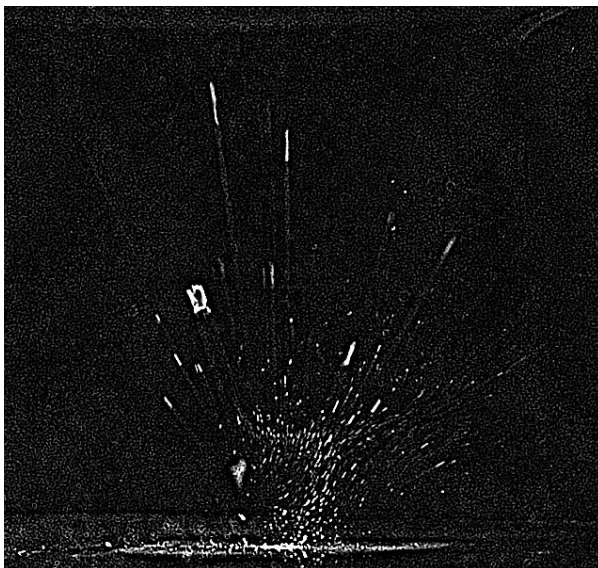


Figure 1. High speed photographic image (1000 frames/sec) of particles being ejected from a β -eucryptite composite that has experienced a 30 Kg Vickers indentation.

Recent Progress

In-situ indentation experiments with Raman spectroscopy have been performed on β -eucryptite and its composites to establish that a phase transformation occurs during indentation. These experiments were performed by a Colorado School of Mines Ph.D. student with Dr. Michael Lance at the High Temperature Materials Laboratory at Oak Ridge National laboratory. A diamond platen approximately 100 μm in diameter was used to apply an indentation-like load on the specimen surface. Figure 2 shows an example of data obtained. Shown are scans taken at different loads beginning at 1.5 Kg (corresponding to ~ 1.25 GPa uniaxial applied stress and -0.71 GPa hydrostatic under the indent) and increasing to 6.5 Kg (~ 6.24 GPa uniaxial applied stress to -5.07 GPa hydrostatic stress under the indent). The appearance of a new peak (~ 520 cm^{-1}) at a distinct load, and its disappearance upon unloading (not shown here) helps to confirm the hypothesis that β -eucryptite transforms to ϵ -eucryptite during indentation. Unfortunately, to the knowledge of the PI and co-workers, this is the first Raman spectra obtained for what is likely the phase ϵ -eucryptite, and thus it is not possible to unambiguously determine that the peak arises from molecular arrangements in the ϵ -eucryptite structure.

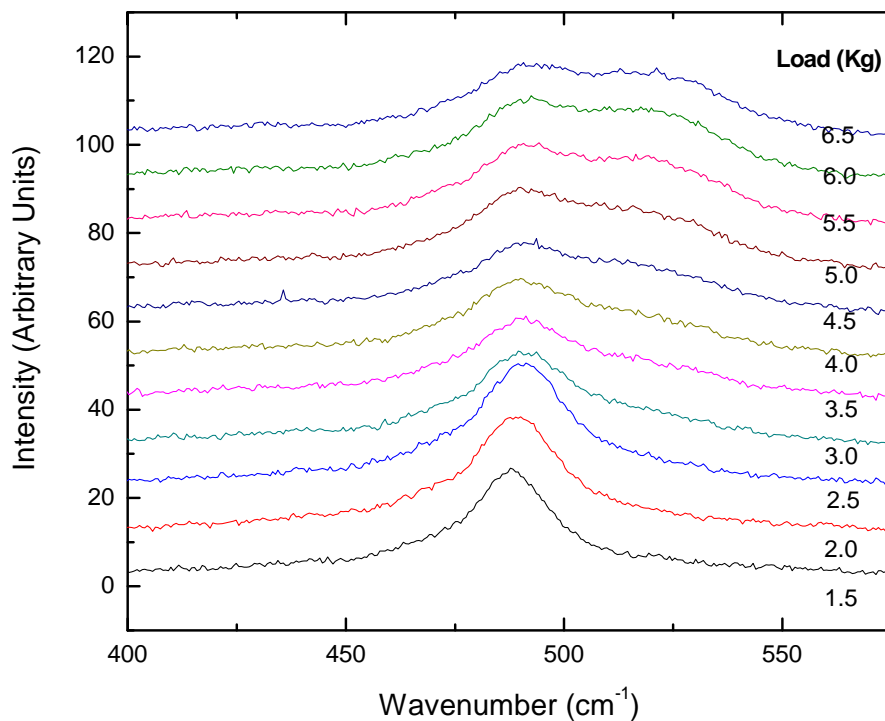


Figure 2. Raman spectra taken from β -eucryptite loaded with a diamond platen to different loads (given in Kg). The formation of a distinct peak at approximately 520 cm^{-1} is apparent.

Future Plans

Mechanical testing Fracture toughness testing will be performed on β -eucryptite and its composites to determine 1) whether or not it is susceptible to moisture-assisted subcritical crack growth and 2) to evaluate whether or not toughness enhancements are possible in a composite comprising eucryptite and zirconia. Indentation coupled with acoustic emission is also being used as a method to establish whether or a phase transformation is associated with particle ejecta.

Irradiation studies To evaluate the mechanisms of amorphization, specimens will be ion-implanted with Kr^{++} and Ne^+ ions to simulate irradiation. The implantation and analysis will be performed with collaborators at LANL.

Modeling Numerical modeling employing object oriented finite element modeling (with collaborators at NIST) will be performed to establish residual stress distributions in β -eucryptite and its composites and eventually, to examine the possibilities of employing transformation toughening. The PI is looking for collaborators to perform molecular dynamics simulations of β - and ϵ -eucryptite in order to correlate the Raman spectra with structure.

The U.S. Department of Energy, Office of Science, Office of Basic Energy Sciences
Mechanical Behavior and Radiation Effects of Materials Contractors Meeting

Elisa Riedo, Grant Number: DE-FG02-06ER46293

School of Physics, GeorgiaTech, 837 State Street, Atlanta, GA 30332-0430 USA

elisa.riedo@physics.gatech.edu

“NanoMechanics: Elasticity and Friction in Nano-Objects”

The goal of this research is to study the nanoscopic mechanical properties, namely elasticity and friction, of C nanotubes, oxide nanobelts, oxide nanowires and vertical forests of nanotubes and oxide nanorods. Gaining an atomistic insight of these properties we open up the possibility to produce nanomaterials with tailored size, shape, chemistry and structure for optimum mechanical performances.

Recent Progress

Zinc oxide (ZnO) has drawn considerable interest because of its semiconducting and piezoelectric properties. A rich variety of ZnO nanostructures, such as nanocombs, nanorings, nanosprings, nanobelts, nanowires and nanocages can be synthesized. ZnO nanostructures have applications as field-effect transistors, gas sensors, field-emission displays and nanoelectromechanical systems (NEMS). All these applications require the knowledge and the ability to control the mechanical behavior of ZnO nanostructures. In particular, it is of crucial importance to understand the size dependence of the elastic properties.

In general, size dependent effects can be found when the volume of a nanostructure is so small that surface effects start to be relevant. This usually happens for dimensions smaller than tens of nanometers, while for larger sizes the Young's modulus approaches its bulk value. For example, the Young's modulus of carbon nanotubes increases significantly with decreasing size for diameters smaller than 4 nm. Conversely, the modulus of GaN nanowires increases with increasing diameter reaching the bulk value at 84 nm. The origin of the elastic modulus size dependence has been related to different effects, such as the presence of defects and the balance between surface and bulk properties as the surface to volume ratio varies.

The elastic properties of ZnO nanostructures and their size dependence have been previously investigated by means of transmission electron microscopy (TEM) and atomic force microscopy (AFM). The Young's modulus of ZnO nanowires was found to decrease dramatically with increasing diameter, reaching the ZnO bulk value for diameters larger than 120 nm. This behavior was attributed to a surface stiffening effect dominating at large surface-to-volume ratios. The Young's modulus of ZnO nanobelts with a wide range of lateral dimensions, ranging from 20 to 230 nm in thickness and 30 to 700 nm in width, was also measured. Previous studies yielded a wide spread of modulus values between 30 and 160 GPa, without a clear dependence on their thickness t , width w or surface-to-volume ratio. Molecular dynamics simulations showed a noticeable size dependence of the elastic properties only for ZnO nanobelts with lateral dimensions below 4 nm, for which the effects of surface stresses become significant.

In this research, the elastic properties of ZnO nanobelts are investigated with an AFM by means of the modulated nanoindentation technique. Their Young's modulus is found to decrease significantly from about 100 GPa to 10 GPa, as the width-to-thickness ratio increases from 1.2 to 10.3. This behavior is explained by a growth-direction dependent aspect ratio and the presence of stacking faults in nanobelts growing along particular directions.

In the modulated nanoindentation technique a modulated signal induces a normal oscillation of the scanner supporting the sample, while the normal force is monitored by the deflection of the cantilever.

The frequency of the oscillations was set at 1.384 kHz and the amplitude was maintained low at 1.5 Å to remain in the sticking regime. This modulated nanoindentation technique has been tested on a silicon substrate, yielding an average value of 143 GPa. The same silicon tip (PointProbe NCHR from Nanoworld), of radius around 60 nm, was used for the images and the modulated nanoindentation experiments. The normal cantilever spring constant, 33 N/m, was calibrated using the method of Sader *et al.*.

The ZnO nanobelts were prepared by physical vapor deposition, following the procedure described by Pan *et al.*, and deposited on a flat silicon substrate. The nanobelts were characterized by TEM and AFM (Veeco CP-II). TEM images and electron diffraction patterns show that the ZnO nanobelts have a wurtzite structure and grow mainly along [0001] without defects or dislocations. There are indications that a few of these nanobelts are actually nanowires, i.e. no rectangular or square cross section. Less common growth directions are $[01\bar{1}0]$ and $[2\bar{1}\bar{1}0]$. Nanobelts grown along these directions present the polar (0001) surface at the side surfaces. This nanobelt presents a single stacking fault running parallel to the (0001) surface over the entire length of the nanobelt, consistent with previous observations of stacking faults parallel to the (0001) surface.

The distribution of the nanobelts growth direction is somehow reflected in the size and shape distribution of the nanobelts as observed by AFM. A statistical study of 137 nanobelts shows that 85% of them have a width-to-thickness ratio, w/t , smaller than 3. Among these nanobelts, 27% present a circular/polygonal cross section, characteristic of nanowires. For these nanowires, the average w/t is $w/t = 1.4 \pm 0.2$. Finally, only 15% of the nanobelts have $3 < w/t < 10$.

In order to investigate the size dependence of the elastic properties of ZnO nanobelts, the Young's modulus, E_{NB} , of 14 different nanostructures (nanobelts or nanowires) was measured as a function of surface-to-volume ratio, w , and t . No clear correlation has been found between E_{NB} and surface-to-volume ratio, w , and t . The surface-to-volume ratio is defined here as the ratio between the perimeter and the area of the cross section. Since most of the nanobelts are more than 100 μm long (the smallest length being 40 μm), the error due to end effects is less than 1%. Among the nanobelts studied here, a few have similar w or t , but different w/t . For example, two nanobelts with comparable thicknesses, $t = 174$ nm and $t = 161$ nm but different w/t of 1.94 and 7.01, have average moduli of 69 GPa and 20 GPa, respectively. Similarly, two nanobelts with $w \sim 1000$ nm but $w/t = 2.22$ and 8.21, have average moduli of 50 GPa and 8 GPa, respectively. These results suggest that the key parameter controlling the elastic properties of the nanobelts is the width-to-thickness ratio.

Fig. 4 shows E_{NB} against w/t for ZnO nanobelts. A clear tendency emerges from this graph, showing that the Young's modulus decreases from about 100 GPa to about 10 GPa as w/t increases from 1.2 to 10.3. A sharp decrease is observed for ratios between 2 and 3, while for ratios over 3 the Young's modulus remains constant. The w/t dependence of the Young's modulus presented in Fig. 4 is highlighted in this paper for the first time. It is noted that data previously reported in the literature agree with the results shown here (see supplementary material). The results compiled from Refs. 13 to 16 indicate that the highest Young's moduli, above 100 GPa, were measured for nanobelts with the smallest

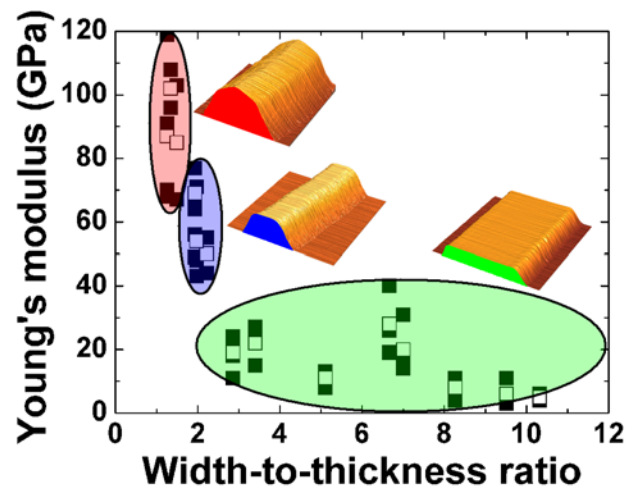


Figure 1. Young's modulus of ZnO nanostructures as a function of width-to-thickness ratio.

w/t , usually lower than 1.5. Yum *et al.* measured the elastic modulus of four ZnO nanobelts with $1.4 < w/t < 4.4$ and obtained $85 > E_{NB} > 38$ GPa, with $E_{NB} = 85$ GPa corresponding to $w/t = 1.4$. The results presented here are also consistent with the conclusions of other works, in which the elastic modulus is almost constant and equal to about 30 GPa for nanobelts with w/t ranging from 2 to 9.

In order to understand the origin of the low elastic modulus of nanobelts with high w/t , surface effects and the possibility of a structural phase transition were investigated. Chen *et al.* explained the size dependence of ZnO nanowires moduli by considering the nanowire as a composite wire composed of a core with a modulus similar to the bulk and a shell with a higher modulus. The observed increase of the modulus with a decreasing diameter of the wires is thus explained in terms of composite modulus where the higher shell modulus dominates at large surface-to-volume ratios. However, the surface to volume ratio reported in our study is more than one order of magnitude smaller than the value required for noticeable surface effects in their investigation (0.004 - 0.032 compared with 0.08 nm^{-1}).

A structural phase transition can lead to a sudden stress drop and therefore an apparently low Young's modulus in the nanobelts. At a pressure around 9 GPa, a phase transition was observed in ZnO crystals [22] and theoretical studies suggested that the phase transition pressure could be as low as 6 GPa. Considering a maximum load F of 200 nN used in our experiments, $E^* = 75$ GPa, a tip radius of 60 nm, Equation (3) would give a contact radius of 5 nm, and thus a maximum pressure of only 3 GPa. Indeed, no hysteresis or sudden force variations have been observed in our experiments when the tip is approaching or retracting during the indentation process. A power law fit of the force-indentation depth curve yields an exponent of 1.50 ± 0.05 , in excellent agreement with the value $3/2$, predicted by the Hertz contact mechanics model.

Since no surface effects or structural phase transitions can be invoked to explain the observed w/t dependence, it is necessary to understand if w/t is related to any structural property of the nanobelts. Recent X-ray diffraction results on single ZnO nanobelts suggest a relationship between w/t and the growth direction. Nanobelts with $w/t = 8.5$ and 8.7 grew along $[01 \bar{1} 0]$, i.e. perpendicular to $[0001]$ and with a polar narrow side surface, while nanobelts with $w/t = 1.5$ and 2.1 grew along $[0001]$. These findings are also consistent with the TEM and AFM measurements and suggest that high w/t is less common and is associated to a less common growth direction, i.e. $[2 \bar{1} \bar{1} 0]$ or $[01 \bar{1} 0]$.

However, in bulk ZnO, the Young's modulus along $[0001]$ is expected to be close to the one along a perpendicular direction, i.e. $[2 \bar{1} \bar{1} 0]$ or $[01 \bar{1} 0]$ [27]. By means of a commercial indentation system with a $1.5 \mu\text{m}$ diamond tip, the Young's moduli along the $[0001]$ and $[01 \bar{1} 0]$ directions were measured to be 163 GPa and 143 GPa, respectively. This result was confirmed by applying the modulated nanoindentation technique presented here to two ZnO bulk samples (MTI Corporation). The measured moduli are $E = 180$ GPa for the sample oriented (0001) and $E = 153$ GPa for the sample oriented $(01 \bar{1} 0)$.

TEM measurements indicate that nanobelts or nanowires grown along $[0001]$ are free of dislocations and stacking faults, while nanobelts grown along $[01 \bar{1} 0]$ and $[2 \bar{1} \bar{1} 0]$ with the polar (0001) surface as the narrower side surface exhibit stacking faults parallel to the (0001) surface over the entire length of the nanobelts. We conclude that the low Young's modulus in nanobelts with high w/t is due to the presence of planar defects in nanobelts grown along $[01 \bar{1} 0]$ or $[2 \bar{1} \bar{1} 0]$ and identified as high w/t nanobelts. A similar role of the planar defects has been recently shown in WO_3 nanowires, where the Young's modulus decreases from about 300 GPa (bulk value) to 100 GPa, as the diameter of the nanowire increases from 16 nm to 53 nm. The cause of this behavior was attributed to a size dependent defect concentration.

The origin of a larger Young's modulus for nanobelts with $w/t = 1$ as compared with nanobelts with $w/t = 2$ is still unclear. However, we remark that the majority of the nanobelts presenting the highest

modulus values were identified as nanowires from AFM topography measurements. The symmetry of the structure seems thus to play a role.

In summary, the Young's modulus of ZnO nanobelts with a width-to-thickness ratio between 1.2 and 10.3 was measured by AFM using the modulated nanoindentation technique. We show that the modulus decreases with increasing width-to-thickness ratio from about 100 GPa to about 10 GPa. This unusual aspect ratio dependence is explained in terms of a growth direction dependent aspect ratio and the presence of stacking faults in nanobelts growing along particular directions. Our findings open the way to tailor the mechanical properties of the nanobelts in a controlled manner over a wide range of elastic modulus values.

Planned activities for next year

At present we are installing a new confocal micro-Raman system that we want to couple with our atomic force microscope (AFM) in order to study in situ the mechanical properties and the structural properties of different nano-objects including nanotubes and ZnO nanobelts. We are also planning to study the frictional properties of carbon nanotubes by sliding an AFM tip over an individual nanotube lying on a hard surface. The tribological properties will be related to the structural and geometrical properties of the nanotubes. Finally, we are performing nanoindentation measurements on silver nano wires and we are working in collaboration with Prof. Ken Gall who mimics our experiments by means of molecular dynamics simulations.

Papers published in referred journals on work supported by DOE

- 1.D. B. Wang, M. Lucas, R. Szoszkiewicz, E. Riedo, T. Okada, S. C. Jones, S. R. Marder, Lee, W. P. King, and "Local wettability modification by thermochemical nanolithography with write-read-overwrite capability", **Appl. Phys. Lett.** 91, 243104 (2007)
- 2.R. Szoszkiewicz, T. Okada, S. C. Jones, T.-D. Li, W. P. King, S. R. Marder and E. Riedo "High-speed, thermochemical nanolithography with sub-15 nm feature size", **Nano Letters** 7, 1064 (2007)
- 3.M. Lucas, W. Mai, J.H. Song, Z.L. Wang and E. Riedo "Aspect ratio dependence of the elastic properties of ZnO nanobelts", **Nano Letters** 7, 1314 (2007).
- 4.T.-D. Li, J. Gao, R. Szoszkiewicz, U. Landman and E. Riedo "Structured and viscous water in subnanometer gaps", **Phys. Rev. B** 75, 115415 (2007).
- 5.M. Lucas, W. Mai, J.H. Song, Z.L. Wang and E. Riedo "Size dependence of the mechanical properties of ZnO nanobelts", **Philos. Mag.** 87, 2135 (2007).

Book chapters

- 1.M. Lucas, T. Li, and E. Riedo. "Nano and Giga Challenges for Information Technology". Springer, Heidelberg Publications, NanoScience and Technology Series 2008.
- 2.R. Szoszkiewicz and E. Riedo, "Applied Scanning Probe Methods V". Springer, Heidelberg Publications, NanoScience and Technology Series 2007.
- 3.L. Merchan, R. Szoszkiewicz and E. Riedo, "Fundamentals of Friction and Wear on the nanoscale". Springer, Heidelberg Publications, 2007.

DOE DE-FG02-07ER46393, Cornell University

Continuum Plasticity: From Grain Boundaries and Coarsening to Cellular Structures and Recrystallization,

James P. Sethna, sethna@lassp.cornell.edu, Laboratory of Atomic and Solid State Physics, Clark Hall, Cornell University, Ithaca, NY 14853-2501
February 29, 2008, for period 6/14/2007-6/13/2008

Program Scope:

We are developing a continuum way of describing the annealing and bending of crystals that connects between the macroscopic behavior and the microscopic atoms and defects (dislocations) in the material. Such a continuum dislocation model should not only avoid explicitly dealing with myriads of atoms or dislocations, but also should predict and explain the behavior which emerges on the mesoscale. Until recent work by the principle investigator, no continuum dislocation model has been shown even to form the basic wall structures into which dislocations naturally organize. Our model suggests that both grain boundary formation (at high temperatures) and the formation of cell wall dislocation structures (at low temperatures) happen as a kind of shock formation, related mathematically to sonic booms and traffic jams. Our model provides a new, elegant framework with the potential for simulating and explaining much of the evolution of single-phase materials.

The three objectives of our research are (1) To extend our model into a minimalist continuum theory of dislocation dynamics, providing fundamental insights into the basic phenomena that emerge under external deformation – wall formation, the different stages of plasticity, grain coarsening, cell refinement, ductile fracture, and recrystallization. (2) To test the predictions against more microscopic simulations and experiments, and to facilitate and inspire new experimental and simulation tests by others. (3) To engage talented students and researchers with interests in field theory, differential geometry, and the mathematics of singularity formation into this exciting area.

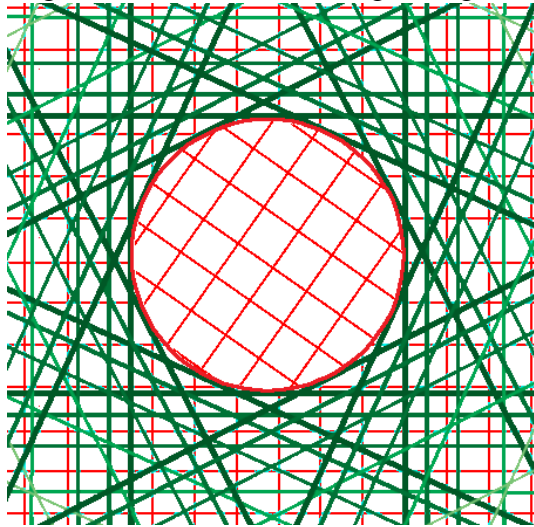
The theoretical methods we use are based on elegant mathematics and fundamental physics. Our continuum field originates in the topological theory of defects in crystals, and describes the differential geometry of the deformed crystal. Our evolution law emerges naturally from the laws of motion of the more microscopic individual dislocations under their mutual interactions and the external stress. Our numerical methods include both the finite-difference methods used by physicists and the finite-element methods preferred by engineers (better for complicated shapes like cracks and airplanes); we use special upwind and Fourier techniques for dealing with the shock formation. Our software will include flexible language structures to steer the complex simulation on parallel computers.

The proposed research will provide a theoretical framework for inspiring and interpreting the results of new experiments and large-scale simulations of materials deformation in the coming years – a longstanding strength of the Department of Energy and the national labs. If successful, our theory could eventually become a unified model for addressing practical problems in metallurgy – how the morphology and properties of a material depend upon its beating and heating history.

Recent Progress:

In the year preceding the beginning of my DOE funding, Limkumnerd and I made substantial progress on three theoretical aspects of our plasticity model, which became two publications.

(1) Pursuing the near-field asymptotics of wall formation in the theory, we discovered for the case of grain boundaries (allowing both glide and climb) that our model had an amazing number of analytical relationships between different parameters in the asymptotic expansion. Limkumnerd finally discovered an amazing mapping, which reduces the nine-parameter plasticity model to a one-parameter Burger's equation. This mapping provides both a tidy derivation of the variety of relationships, and a rigorous derivation of the wall formation for the model for this particular case.



A circular grain boundary decomposed into a series of flat walls whose density decays away from the center of the cylindrical cell. Selected for inclusion in a new figures section for Physical Review B.

(2) Much of the most interesting numerical work on discrete dislocation dynamics is in two dimensions and involves only one or two slip systems. Exploring the predictions of our model, suitably modified to include only one slip system, we found that grain-boundary and cell-wall formation does not occur (in agreement with the simulations). Instead, we discovered a new type of wall, formed as a transient structure, where the dislocation density jumped discontinuously (i.e., not a delta-function in the dislocation density, but rather a step function).

(3) Limkumnerd and I also discovered several properties of continuum dislocation density theory that were not tied to our proposed dynamical evolution law. These focused on the relationship between grain boundaries, rotations, and stress-free states. Limkumnerd showed that there were a large number of stress-free states in the model – including in particular any superposition of grain boundaries (dislocation walls satisfying the Frank conditions). These stress-free states, we showed, could be characterized either in terms of a continuous distribution of straight grain boundaries, or in terms of a continuous rotational field. One of the figures from this paper was selected for a new “covers” section for Physical Review B (left).

I then spent fall semester '07 on sabbatical in Europe, where contact was made with a few groups working on plasticity and a long-term collaboration was started. I had an excellent, brief visit with Erik van der Giessen's group at the University of Groningen in the Netherlands, where my former graduate student Surachate Limkumnerd was a post-doc at the time, with in-depth conversations with group members working on discrete dislocation dynamics, and long discussions with Erik and Limkumnerd about their statistical theory for multiple-slip. I had a brief and illuminating visit at Risø National Laboratory in Denmark, with the plasticity group there, meeting in particular with Wolfgang Pantleon. I spent a month at DTU in Denmark visiting Karsten Jacobsen and Jens Nørskov in CAMD, becoming immersed in physics of likely long-term interest to DOE (catalysis, transport in nanosystems, developing methods to estimate errors in electronic structure calculations) but not currently relevant to this grant.

The long-term collaboration was established with Stefano Zapperi during a month visit with him in Turin. Zapperi is one of the leaders in the field of avalanches and critical fluctuations (crackling noise), and has been a key figure in the recent use of these methods to understand fluctuations in plastic deformation. Indeed, I view the wall formation that we study and the crackling noise observed in recent experiments and simulations as the two key features in plasticity that motivate and foreshadow theoretical progress in the field. Indeed, before (and unrelated to) my arrival, Zapperi wrote an article for Science on simulations of crackling noise in the deformation of nanowires, on which I was invited to write a Science Perspectives companion article. Zapperi and I are now collaborating on a number of projects involving the analysis of simulations and experimental data, of potential interest to this project.

Since returning from sabbatical in late January, I have been working with two graduate students (Yong Chen and Woo Song Choi), have ordered a fast multi-core computer to run the next stage of simulations, and have hired a post-doc for next year (Stefanos Papanikolaou). In the fall semester Yong Chen translated Limkumnerd's C++ code into Python and began to optimize it. Chen last month explored the effects of strong dependence of the dislocation mobility on the density (similar to the methods used by the more traditional dislocation density theories used by Dawson and colleagues for incorporating work hardening). These, Chen found, led to the formation of larger number of lower-angle grain boundaries; the wall formation persisted even when dislocation entanglement was introduced in this fashion, but wall aggregation and coalescence was impeded by the reduced mobility. This month Chen is implementing a rotation-field observer into the code, and will use it to study the misorientation angle distributions to compare with the scaling analysis of experiments by Darcy Hughes and collaborators.

In the month and a half that Woo Song Choi has been involved in the project, he has been exploring methods of optimizing and parallelizing the code. By implementing a C++ multiply-add function that is called from Python, he has both substantially increased the speed of the serial code and implemented a multithreaded implementation that is the first step toward fully utilizing the eight cores in the new machine.

Publications:

No publications citing this grant have been published so far in the grant period.

Two publications that describe work relevant to this project were published between submission of the proposal and the beginning of the grant period:

["Shocks and slip systems: Predictions from a mesoscale theory of continuum dislocation dynamics"](#), Surachate Limkumnerd and James P. Sethna, *J. Mech. Phys. Solids* (2007), doi:10.1016/j.jmps.2007.08.008.

["Stress-free states of continuum dislocation fields: Rotations, grain boundaries, and the Nye dislocation density tensor"](#), Surachate Limkumnerd and James P. Sethna, *Phys. Rev. B* **75**, 224121 (2007).

Also, I wrote a Science Perspectives article which would have acknowledged DOE if it were allowed by the journal:

["Crackling Wires"](#), James P. Sethna, *Science* 318 (5848), 207-208 (12 October 2007).

People supported by project:

Yong Chen is a Physics graduate student who has worked on the project since September '07. His stipend for the first semester (while I was on sabbatical) was supported by a teaching assistantship; this semester he is being paid by the grant.

Woo Song Choi is a graduate student in Physics that has been working on the project for about one and a half months; I recruited him somewhat after I arrived back in the US. He is being supported by a teaching assistantship this semester.

Stefanos Papanikolaou, a talented current graduate student at the University of Illinois at Urbana, will join the group in August 2008 as a post-doctoral associate, supported by this grant. Stefanos will also be attending the Washington contractor's meeting with me.

Future Plans for coming year:

Before the contractor's meeting, we intend to set up the new computer and optimize the multithreaded code. We will develop and test the observers for rotation fields and grain boundary locations in one and two dimensions. I expect we may have results for the misorientation angle distributions and grain sizes for large one-dimensional simulations of both refinement and coarsening by the meeting, and may have initial results in two or even three dimensions.

In the subsequent year we will (a) systematically extract predictions for mechanisms of refinement, (b) study interplay of grain rotation and merging in coarsening, (c) complete and publish large-scale simulations of coarsening and refinement, (d) implement a scattering observer to calculate Fourier-space predictions for X-ray and neutron scattering experiments, (e) make concrete experimental predictions for X-ray scattering experiments probing stress jumps and dislocation evolution in early stages of polygonalization and in later stages of hardening.

Shape memory in nanoscale metallic alloys

Alexander Thompson, Karthik Guda Vishnu, and Alejandro Strachan

School of Materials Engineering, Purdue University, West Lafayette, Indiana 47907

Email: strachan@purdue.edu. Phone: (765) 496-3551

Motivation and scope of proposed work

Active materials with nanoscale dimensions are highly desirable in a variety of emerging technologies including nanofluidics and nanoelectronics. Shape memory materials would be ideal candidates for a large number of these applications where changes in conformation or actuation-sensing capabilities are required; however, **it is not yet known whether current shape memory alloys (SMAs) retain their “memory effect” when their size is reduced to the nanoscale or, more generally, how size and dimensionality affect their performance.** This situation stems from a lack of a detailed understanding of the molecular level processes that govern the behavior of SMAs. The unique properties of these alloys, shape memory and superelasticity, stem from a diffusion-less structural transition (denoted martensite) that results in a complex microstructure; this microstructure plays a key role in the response of the material. Nanoscale SMA specimens are expected to develop nanostructures very different from macroscopic ones and their behavior remains uncharacterized. Thus **we propose to use electronic structure calculations and large-scale molecular dynamics (MD) to characterize the size and dimensionality dependence of the martensitic nanostructure of nanoscale NiTi alloys and the resulting thermo-mechanical response** including shape memory and superelasticity, and **computationally explore avenues to optimize the performance of nanoscale SMA samples** for applications that require active components.

We propose to develop a *first principles*-based approach to *predict* the behavior of nanoscale NiTi alloys consisting of three main components:

- ***Ab initio* quantum mechanical (QM)** calculations (including equations of state of various crystal structures) will be performed to characterize atomic interactions from first principles.
- The QM data will be used to parameterize a **many-body inter-atomic potential** for large-scale MD that captures the relative stability of the various phases and their elastic properties.
- **Large-scale MD simulations** to characterize: the martensitic transformation, resulting nano-structure, and mechanical response as a function of dimensionality (clusters, wires, slabs and bulk) and size.

A successful project will provide a **fundamental understanding of whether shape memory is possible in nanoscale samples of current materials and a quantitative characterization of the role of size and dimensionality on performance**, providing the knowledge-base for the design and optimization of active components for next generation nano- and micro-devices.

Role of size and geometry on martensite microstructure in Zr

We use MD to characterize the martensitic microstructure in Zr nanoscale wires (nanowires) when the austenite phase (bcc) transforms into martensite (fcc) upon cooling. Our focus is to understand how size and geometry affect the resulting martensitic microstructure.

The bcc to hcp transition involves an orthotropic transformation where a bcc $\{111\}$ planes transforms into an hcp closed packed plane, see Figure 1. During the transformation the plane involved undergoes a compression of 13.3% along the $\langle 100 \rangle_{\text{bcc}}$ direction contained in it and expansions of 6.06% along its $\langle 110 \rangle_{\text{bcc}}$ direction; an expansion along the $\langle 110 \rangle_{\text{bcc}}$ direction normal to the plane leads to an hcp structure with perfect c/a . The transition requires, in addition, the relaxation of the atomic positions.

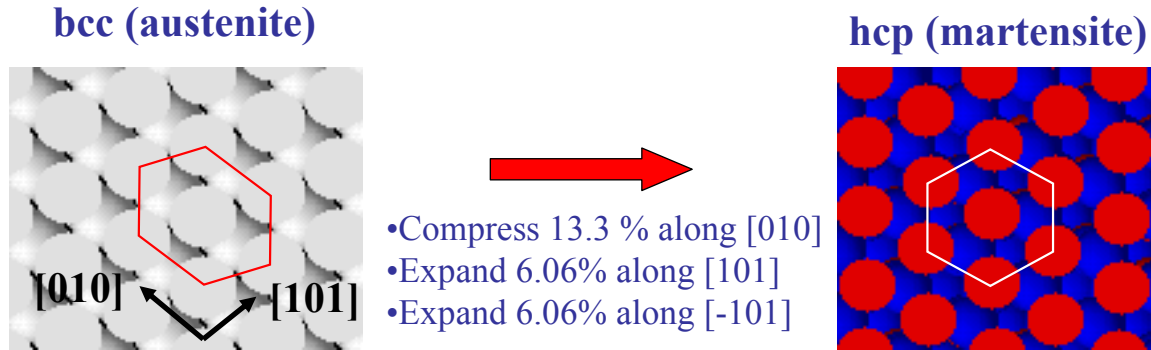


Figure 1: bcc to hcp transition; a bcc $\{110\}$ plane transforms into an hcp closed packed plane.

The initial structures of our simulations consist of $\langle 111 \rangle$ wires, see Figure 2, with radii between 15 Å and 45 Å and lengths up to almost 1000 Å and impose periodic boundary conditions along their axes; $\langle 111 \rangle$ wires can expose three closed-packed $\{110\}$ surfaces and consequently are the most stable ones. In order to characterize the martensitic microstructure the simulation temperature is gradually decreased from $T=1450\text{K}$ to $T=300\text{K}$ in 25 K decrements either every 10 or 40 ps. The temperature of the simulations is controlled by a Nose-Hoover thermostat. The resulting microstructure at 300 K is analyzed based on the number of neighbors of each atom and the angles between such bonds. This allows us to characterize the local environment of each atom and classify then into one of the following categories: hcp, fcc, surface [less than 11 nearest neighbors (nn)] and defective (11 and 13 nn, as well as those with 12 nn that can not be classified as fcc or hcp).

As shown in Figure 2(b) six possible domains can form, each corresponding to a $\langle 110 \rangle$ direction. Three of these directions are normal to the wire axis and the associated domains will be denoted “radial”; the other three $\langle 110 \rangle$ directions make an angle of 35.26° and the resulting domains will be

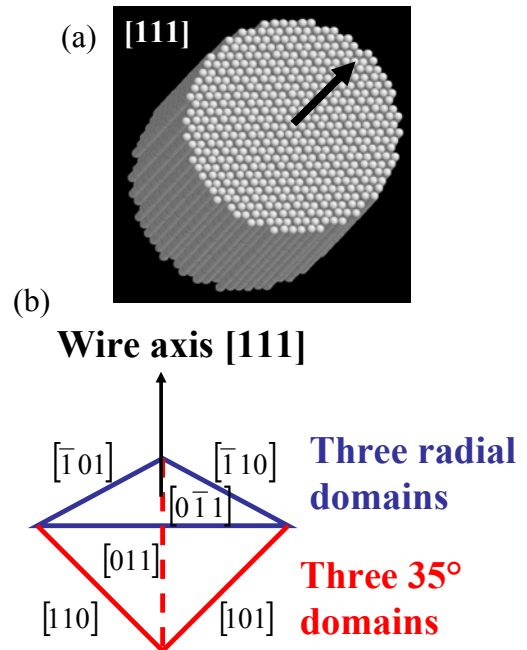


Figure 2: (a) snapshot of a $[111]$ bcc Zr wire used as initial conditions for MD simulation. (b) orientation of the six $\langle 110 \rangle$ directions; each of the corresponding planes can transform into an hcp closed packed plane leading to six possible domains; three radial ones and three at 35° .

dubbed “35°”.

Figure 3(a) shows the martensite structure that results from cooling wires of various sizes, we observe both single- and multi-domain structures containing radial and 35° domains. Multi-domain structures lead to changes in the shape of the nanowires with a bending angle that depends of the type of domains that intersect at the boundary. Figure 3(b) shows the resulting microstructure as a function of wire radius and length. We can see that small wires result in single-domain structures (empty symbols); as the radius of the wires is increased we observe multiple radial domains. For a long and thin wire we observe multiple 35° domains and multiple-domain structures with both radial and 35° domains are observed for long and thick wires.

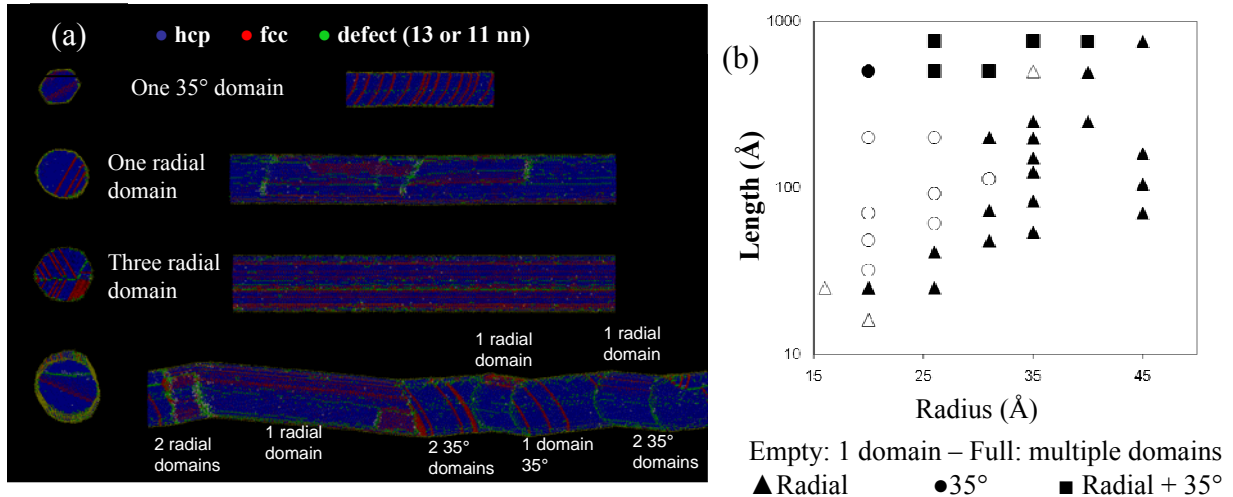


Figure 3. Left: Various martensite structures resulting from MD cooling simulations. The number and character of the domains is indicated. Right: map of martensite microstructure as a function of wire radius and length.

Our results show that the domain structure resulting from martensitic phase transitions depends strongly on size and geometry indicating the potential viability of using geometrical considerations to tailor the microstructure and, consequently, properties of nanoscale shape memory materials.

Current and future work

Due to the symmetry of its austenite and martensite phases Zr does not exhibit shape memory and we are currently working the NiTi alloys that do exhibit this behavior as well as superelasticity. We have performed extensive *ab initio* simulations, using density functional theory within the generalized gradient approximation (DFT-GGA), to characterize the various crystal structures responsible for the behavior of NiTi. Table 1 summarizes our results of equilibrium structures and relative energies of NiTi in B2, B19, B19' and R phases; our results are in good agreement with previous calculations and experiments. We are currently extending these calculations to characterize the various phases under applied mechanical loads to characterize structural changes and relative phase stability under stress.

We will use these DFT-GGA calculations to parameterize many body interatomic potentials that we will use with large-scale MD to characterize the role of size, geometry, and dimensionality on martensite structure and properties of NiTi alloys.

PHASE	SPACE GROUP	Lattice parameters (Bohr)	Lattice angles	X_{Ni}, Y_{Ni}	X_{Ti}, Y_{Ti}	Relative energy (eV per formula unit)
B2	Pm3m	5.68972 Bohr	90	0, 0	0, 0	0
R PHASE	P3	C = 9.855 A = 13.937	120	----	-----	-0.027
B19	Pmcm	A = 5.248 b = 8.754 C = 7.977	90	0, 0.06698011	0, 0.033453	-0.051
B19'	P21/m	a = 5.481 B = 8.858 C = 7.577	97.8	0.0418, 0.071044	0.07299, 0.0269	-0.081

Table 1: DFT-GGA results for equilibrium structure and relative energetics for various phases of NiTi.

Summary

Our simulations indicate that dimensionality, size and geometry play important roles in determining the martensitic structure of materials enabling the possibility of using these variables to tailor materials response. We are currently working on the development of accurate, first principles-based interatomic potentials for NiTi that will be used in large-scale MD simulations designed to characterize the martensitic phase transformation and thermo-mechanical properties of nanoscale NiTi specimens.

Electrical, mechanical and thermal properties of single molecules

Nongjian (NJ) Tao
Arizona State University,
Tempe, AZ 85287-3503
Email: njtao@asu.edu

Program Scope

Building a device using a single or a few molecules is one of the ultimate goals in technology. Owing to many unique electronic properties of molecules, electronic applications have been a focus of molecular devices. In addition to wonderful electronic properties, many molecules have attractive electromechanical, thermal electrical and molecular recognition properties that are fundamentally different from conventional bulk materials, which may lead to new devices. An interesting electromechanical effect that has been studied by us is single molecule piezoresistivity. In contrast to bulk materials, piezoresistivity in single molecules is much greater in magnitude. Electromechanical effects arise from the coupling of electrons to the ionic degree of freedom of molecules. This coupling takes place also in the form of excitation and absorption of phonons, which can be studied by inelastic tunneling spectroscopy. The excited phonons eventually dissipate energy and result in local heating of the molecule. We have observed evidence of the current-induced heat generation in single molecules. The reverse process, conversion of thermal energy to electrical energy, has also been demonstrated recently by other groups in single molecules. These findings led us to propose to study the interplay between electrical, mechanical and thermal properties of single molecules. Our objectives are:

- Determine the lifetime and stability of a single molecule bound to two electrodes;
- Study local heating and cooling in single molecule junctions due to electron-phonon and electron-electron interactions;
- Measure electron-phonon interactions in single molecule wires;
- Explore piezoelectric properties of single molecules.

We believe that this study will provide us with new insight into the electron transport properties of molecules, as well as necessary knowledge and skills for future device applications.

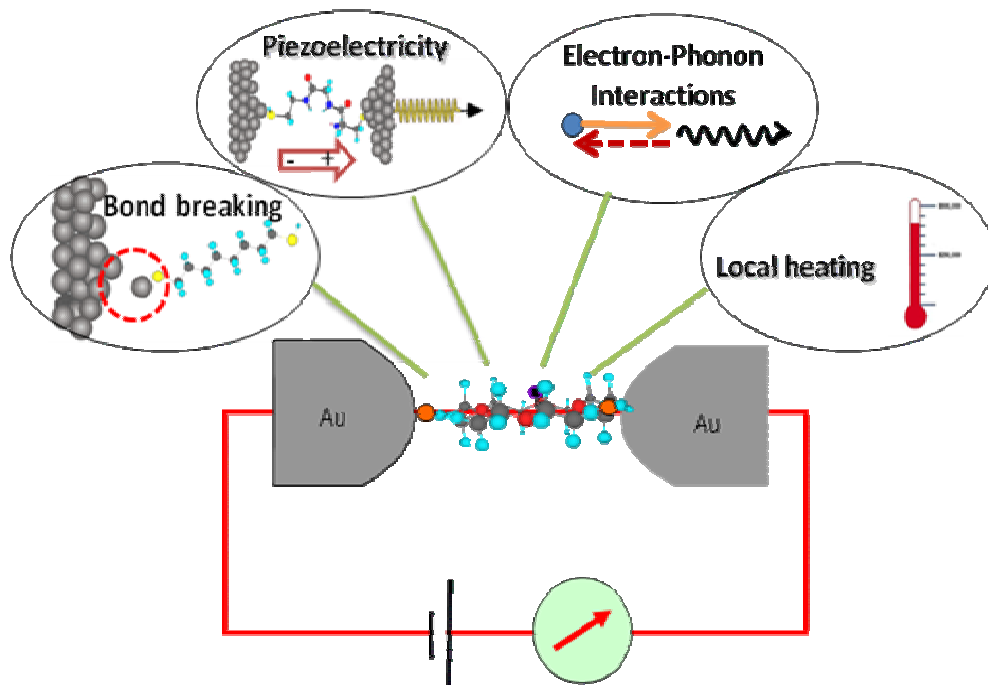


Fig. 1 A molecule electrically “wired” to two electrodes serves a model system for studying charge transport in single molecules and basic building block for developing device applications. This project focuses on the electrical, thermal and mechanical properties of single molecules, in order to achieve a better understanding of charge transport and to explore new functions of single molecules.

Progress Report

We have studied electromechanical properties of single molecules, molecular recognition properties of peptides and development of stable and controllable method to study single molecules. During the course of study, we have expanded the scope to address critical and relevant issues related to the molecule-electrode interface and current-induced local heating in single molecules, and study charge transport in single DNA molecules. We summarized some of the findings here.

Piezoresistivity in single molecules

We studied piezoresistivity in both saturated n-alkanedithiol chains and conjugated oligothiophenedithiol molecules with 3 and 4 thiophene repeating units (abbreviated as 3T1DT, and 4T1DT, respectively). The n-alkane chains are linear molecule consisting of n carbons. These molecules have large LUMO-HOMO gaps and are considered to be poorly conducting. The piezoresistive effect was found to be $\sim 10\%$ per nN, which is attributed to the elongation of the molecule upon stretching (Figs. 2a and c). In contrast, the oligothiophene molecules have much smaller HOMO-LUMO gaps and are more conductive than the alkane chains. Like the alkane chains, the conductance of oligothiophene molecules decrease upon stretching, but the piezoresistive effect is $\sim 45\%$ per nN, much greater than that of alkane chains (Figs. 2b and d). Since oligothiophenes are structurally much more rigid than alkanes, the contribution due to geometrical elongation is negligible. The observed large piezoresistive effect in oligothiophenes is attributed to an increase in the HOMO-LUMO gaps upon stretching, which is expected based on Peierls' instability model. Both the alkanedithiol and oligothiophenedithiol junctions break down when the force is increased to ~ 1.5 nN. The breakdown takes place at the molecule-electrode (gold) contacts, which inspired us to investigate the molecule-electrode binding strength.

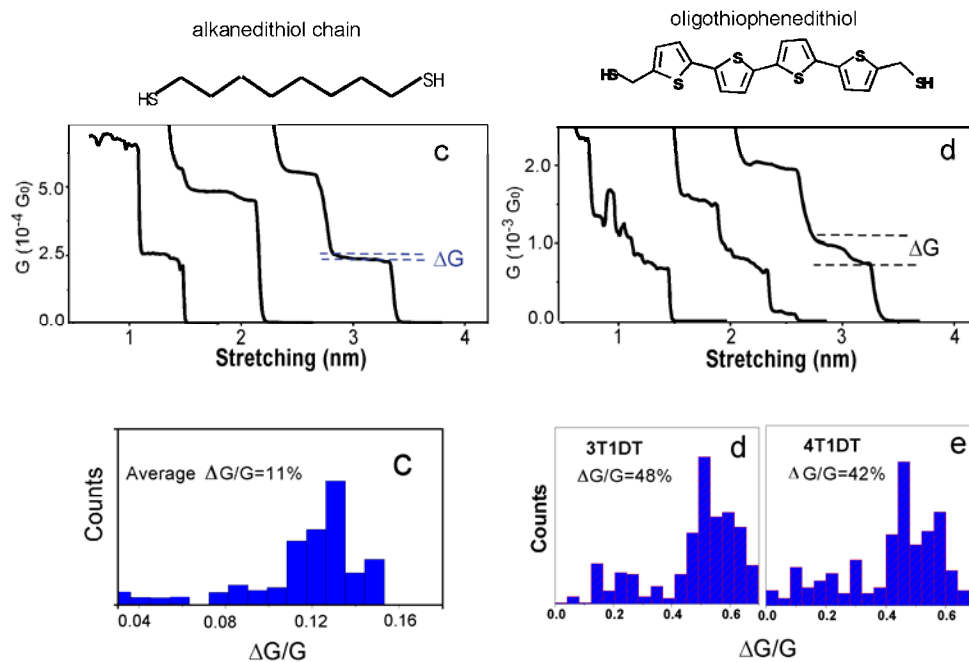


Fig.2. (a-b) Transient conductance curves recorded during the stretching of individual alkanedithiol (a) and 4T1DT (b) junctions, respectively. The force-induced conductance changes of the last molecules are marked by ΔG . (c-e) Histograms of the force-induced conductance changes, $\Delta G/G$, for alkanedithiol (c), 4T1DT (d) and 4T1DT (e) molecules, respectively.

Molecule-electrode binding strength

For molecules terminated with dithiol linkers, the weakest link is Au-Au at the molecule-electrode contact. We have studied the breakdown of Au-Au bond by simultaneously measuring the force and conductance of individual molecular junctions using a C-AFM (Fig. 3). There is a fairly large variation in the measured breakdown force, but the histogram constructed from thousands of individual measurements shows a peak, which gives the average breakdown force required to break a molecular junction. We have determined the average force as a function of stretching rate. The breakdown force increases linearly with the logarithm of stretching rate, and then reaches a plateau. This behavior is well described by a thermodynamic bond-breaking model. A comparative study of Au-Au atomic point contacts indicates that the breakdown of the molecular junctions takes place at Au-Au

bonds near the molecule-electrode contact. By fitting the force vs. stretching rate data with the thermodynamic model, the lifetime (0.1s) and binding energy (~ 0.66 eV) were extracted. Both quantities are found to have broad distributions, owing to large variations in the molecule-electrode contact geometry. Although the molecular junctions are short lived on average, certain contact geometries are considerably more stable. The technique developed here makes it possible to systematically study the lifetime and stability of molecular junctions formed with various linker groups and electrode materials.

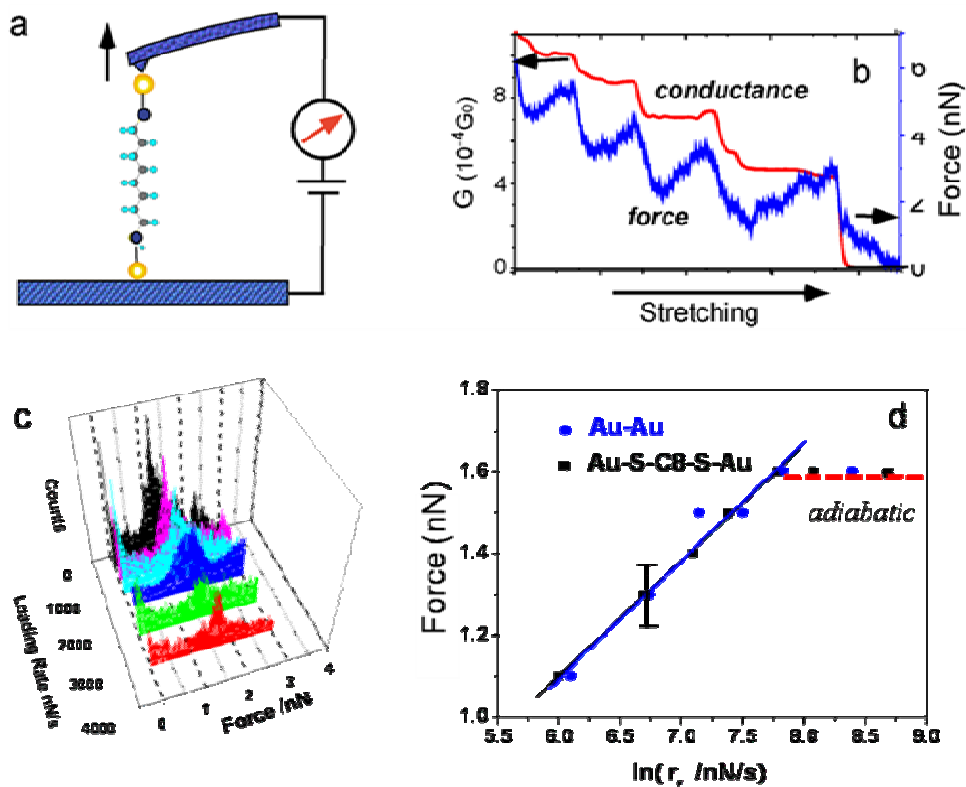


Fig.3. (a) Simultaneous conductance and force measurement of a molecular junction during breakdown using a conducting AFM setup. (b) As the individual molecules break, the conductance decreases in a stepwise fashion (red), and associated with each conductance step the force (blue) also decreases abruptly. (c) Force histograms at different stretching rates (different colors). (d) Average breakdown forces for single alkanedithiol (black dots) and Au-Au contact (blue dots) vs. stretching rate. The force increases and then reaches a plateau with stretching rate as predicted by the thermodynamic theory. Both C8 and Au point contact behave in the same way, indicating the breakdown in both cases taking place at the Au-Au bond.

Local heating effect on the stability of molecular junctions

We have developed an experimental approach to determine the local temperature in a single molecule junction by measuring the breakdown force. Since the breakdown process is thermally activated, the average breakdown force is sensitive to the local temperature of the molecule-electrode contact, which allows us to determine the effective local temperature of the molecular junction. We found that the local temperature increases with the bias voltage and reaches ~ 50 K above room temperature at a bias voltage of 1 V (Fig. 4). When increasing the bias above 1 V, the molecule junction becomes increasingly unstable. In collaboration with Prof. Di Ventra at UC San Diego, we have also performed first-principles calculation of the local temperature and current-induced forces on the same molecule, and found good agreement with the experimental findings. This success opens the door to the study of current-induced local heating in various molecules and possible electron-electron induced cooling effect in single molecular junctions.

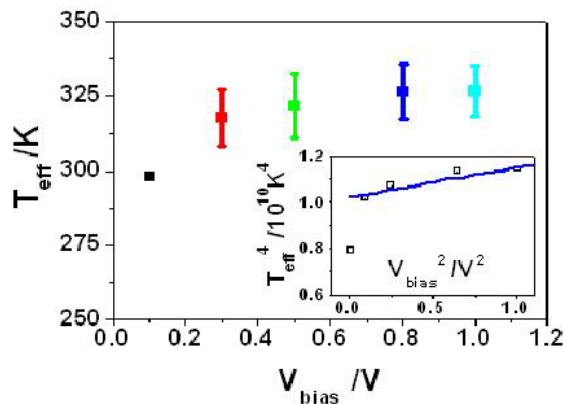


Fig. 4 Effective local temperature of a single molecule junction measured from the breakdown force.

Future Plan

We will focus on electron transport, mechanical and thermal properties, as well as the interplay between these properties in single molecules. In addition to deepen the understanding of the previous findings, we will explore new phenomena, including bond breaking and reformation, electron-electron induced local cooling, electron-phonon interactions in single molecule and single molecule piezoelectricity.

Publications

1. Z.F. Huang, F. Chen, R. D'Agosta, P. A. Bennett, M. Di Ventra and N.J. Tao, "Local-Heating in Single Molecule Junctions: Evidence of Electron-Phonon and Electron-Electron Interactions, Nature Nanotechnology, in revision, 2, 698-703 (2007).
2. Fang Chen, Zhifeng Huang, N.J. Tao, "Forming single molecular junctions between ITO electrodes", Appl. Phys. Lett., 91, 162106(2007).
3. Xiulan Li, Joshua Hihath, Fang Chen, Takuya Masuda, Ling Zang and N.J. Tao, "Thermally Activated Electron Transport in Single Redox molecules", J. Am. Chem. Soc., 129, 11535-11542 (2007).
4. Zhifeng Huang, Feng Chen, Peter A. Bennett and Nongjian Tao "Single Molecule Junctions Formed via Au-Thiol Contact: Stability and Breakdown Mechanism", J. Am. Chem. Soc., 129, 13225-13231(2007).
5. J. Hihath, F. Chen, P.M. Zhang and N.J. Tao, "Thermal and Electrochemical Gate Effects on DNA Conductance", J. Phys., 19, 215202-215221(2007).
6. F. Chen, J. Hihath, Z.F. Huang, X.L. Li and N.J. Tao, "Measurement of single molecule conductance", Annual Review of Physical Chemistry, 58, 535-564(2007).
7. F. Chen, X.L. Li, J. Hihath, Z.F. Huang and N.J. Tao, "Effect of Anchoring Groups in Single Molecule Conductance A Comparative Study of Thiol-, Amine- and Carboxylic Acid-Terminated Molecules", J. Am. Chem. Soc., 128, 15874-15881 (2006)
8. N.J. Tao, "Electron transport in molecular junctions", Nature Nanotech.,1, 173-181(2006).
9. Z.F. Huang, B.Q. Xu, Y.C. Chen, M. Di Ventra and N.J. Tao, "Current Induced Local heating in Single Molecule Junctions", NanoLett., 6, 1240-1244(2006).
10. X.Y. Xiao, D. Brune, J. He, S.M Lindsay, C. B Gorman; N.J. Tao, "Redox-Gated Electron Transport in Electrically Wired Ferrocene Molecules" Chemical Physics, 326, 138-143(2006).
11. X.L. Li, B.Q. Xu, X.Y. Xiao, X.M. Yang, L. Zang and N.J. Tao, "Controlling Charge Transport in Single Molecules using Electrochemical Gate", Faraday Discussions, 131, 11-120(2006).
12. J. Hihath, B.Q. Xu, P.M. Zhang, and N.J. Tao, "Study of Nucleotide Polymorphisms via Electrical Conductance Measurements", Proc. Natl Acad. Sci., 102, 16979-16983(2005).
13. B.Q. Xu, X.L. Li, X.Y. Xiao, H. Sakaguchi and N.J. Tao "Electromechanical and Conductance Switching Properties of Single Oligothiophene Molecules", NanoLett., 5, 1491-1495(2005).
14. X.L. Li, B.Q. Xu, X.Y. Xiao, J. Hihath and N.J. Tao, "Measurement of Electron Transport Properties of Single Molecules", J. Jpn. Appl. Phys., 44, 5344-5347(2005).
15. N.J. Tao, "Measurement and Control of Single Molecule Conductance", J. Material Chem., invited *Highlight* article, 5, 3260-3263(2005).
16. B.Q. Xu, X.Y. Xiao, X.M. Yang, L. Zang and N.J. Tao, "Large Gate Current Modulation in a Room Temperature Single Molecule Transistor", J. Am. Chem. Soc., 127, 2386-2387(2005).

**Multiscale Modeling of Dislocation Behavior in Non-Magnetic Transition Metals and
Ferromagnetic Iron
Grant no. DE-PG02-98ER45702**

V. Vitek

Department of Materials Science and Engineering, University of Pennsylvania,
Philadelphia, PA 19104
e-mail: vitek@seas.upenn.edu

1. Scope of the program

The principal goal of this project is to advance scientific insight into the deformation and fracture mechanisms in body-centered-cubic (BCC) transition metals: molybdenum, tantalum, niobium, tungsten and iron. The motivation for this study is two-fold. First, BCC transition metals and their alloys are the most important materials employed in technologies associated with energy production and conversion. Iron, naturally, dominates since it is the principal component of steels that are and will remain the core materials. Recently, nuclear power generation has been moving to a new stage and both advanced nuclear and future fusion power plants require structural components that will accumulate radiation damage amounting to ~100dpa. Hence, the need to investigate deformation and fracture behavior in the presence of large concentrations of self-interstitial atoms (SIAs). Secondly, from the perspective of fundamental science, these materials belong to the class of metals in which the bonding has a mixed nearly free electron and covalent character. The latter is mediated by the *d*-electrons that control the stability of structures and, moreover, in the case of iron magnetism plays an important role. This presents a formidable challenge for atomic level studies of extended defects, such as dislocations and interfaces that govern mechanical properties of materials.

The link between bonding on atomic scale and the mechanical response of a material on the scales ranging from nano to macro can only be established via a multiscale approach. In this project the first step of such multiscale scheme is the atomic level simulation of the glide of dislocations at 0K, first in perfect crystals of transition metals and later in crystals with self-interstitials. Modeling on atomistic level is then followed by two steps on mesoscopic level. First, we formulate a yield criterion that includes all the components of the stress tensor that were found to be consequential in atomistic studies and applies to any $\{111\}\{101\}$ slip system in a given BCC metal. The important stress components are, beside the Schmid stress, shear stresses parallel to the slip direction in planes other than the glide plane and shear stresses perpendicular to the slip direction. This new yield criterion, which is not based on the Schmid law and is of non-associated type, can then be employed in continuum crystal plasticity and represents a basis for development of new yield criteria for polycrystals [1, 2].

The second very important step is inclusion of temperature and strain rate effects into the yield criteria. This involves development of a mesoscopic model of dislocation glide at finite temperatures via formation and propagation of pairs of kinks. At this point the previously advanced dislocation models are utilized [3, 4]. However, the novel concept is that the Peierls potential is regarded as a function of the applied stress tensor and its form is extracted from atomistic studies of the dependence of the Peierls stress on this tensor. Hence, the stress dependence of the dislocation velocity, which represents the dislocation mobility law, involves the full stress tensor rather than the Schmid stress only. Finally, this mesoscopic model is included into the above mentioned yield criterion that ultimately comprises the effects of temperature and strain rate.

The essential precursor of any atomistic studies is a description of atomic interactions that reflects correctly the physics of bonding in a given material. We employ the bond-order potentials (BOPs) that represent the bond energy exactly within the tight-binding approximation to the electronic structure and retain the angular character of bonding. This is essential in transition metals where the bonding is principally driven by the interaction between the localized valence *d*-electrons. Apart from the proper quantum mechanical character, another significant advantage of BOPs is that modeling can be performed in real space without the use of periodic boundary conditions. This broadens significantly the range of solvable problems. Hence, a substantial part of the research is devoted to the development and testing of BOPs. While for the non-magnetic transition metals, tantalum and niobium, we follow the same path as in our previous studies of molybdenum and tungsten, the situation is very different in the case of magnetic iron. It has been proposed recently that the Stoner model of band magnetism [5] can be employed to develop BOPs for magnetic metals [6]. It is one of the primary objectives of this research to construct, test and apply BOPs for iron in studies of dislocations, interstitials and their interactions. This development is done in close collaboration with Professor Pettifor and his group at Oxford, with Dr. Nguyen-Manh and his colleagues at the Culham Science Center in the U. K and with Drs. Elsässer and Mrovec at the Fraunhofer Institute in Freiburg, Germany.

2. Recent Progress

2.1. Construction of bond-order potentials (BOPs)

Within the BOPs scheme the binding energy, E^B , is approximated as $E^B = E^{\text{pair}} + E^{\text{core}} + E^{\text{cov}}$, where E^{pair} is the pairwise contribution arising from the overall overlap repulsion, E^{core} a many-body repulsion that originates from the strong repulsion which the valence s and p electrons experience and E^{cov} is the bonding energy arising from the partially filled d-band. The latter part is fitted so as to reproduce DFT based calculated bond integrals as functions of the separation of atoms. The former two parts are fitted to reproduce the lattice parameter, cohesive energy and elastic moduli. The constructed potentials are extensively tested by probing the stability of the BCC structure relative to alternative crystal structures, evaluating the energy for highly distorted structures encountered along tetragonal, trigonal, orthorhombic and hexagonal transformation paths, calculating γ -surfaces and phonon dispersion curves. Details of these procedures and constructed BOPs for molybdenum and tungsten are found in recent publications based on this research [7, 8].

2.2. Atomistic study of the glide of $1/2\langle 111 \rangle$ screw dislocations

Detailed investigation of the glide of the $1/2[111]$ dislocation in Mo and W under the effect of shear, tensile and compressive stresses was completed. The most important finding is that the Peierls stress, identified

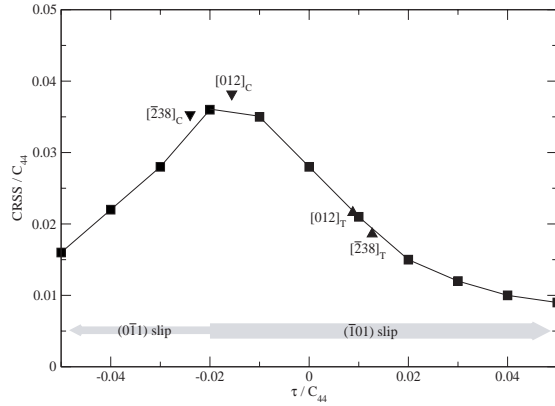


Fig. 1. Peierls stress (CRSS) for W vs shear stress, τ , perpendicular to the Burgers vector

with the critical resolved shear stress (CRSS) in the maximum resolved shear stress plane (MRSSP) depends not only on the orientation of the MRSSP, which leads to the well-known twinning-antitwining asymmetry, but also on the shear stress perpendicular to the Burgers vector. This is shown in Fig. 1 where the CRSS for W is plotted as a function of the shear stress, τ , perpendicular to the Burgers vector, when the MRSSP coincides with the $(\bar{1}01)$ plane. The positive τ lowers the corresponding Peierls stress, while the negative τ makes the slip more difficult. The reason is that in the former case τ extends the core into the $(\bar{1}01)$ plane, while in the latter case the core is constricted on the $(\bar{1}01)$ plane and extended onto

$(0\bar{1}1)$ and $(\bar{1}10)$ planes. For large negative values of τ this extension becomes so overwhelming that the dislocation starts to glide on one of these planes although the corresponding Schmid factors are half of that for the $(\bar{1}01)$ $[111]$ slip system. The conclusion of this study is that for the $(\bar{1}01)$ $[111]$ slip system the CRSS relates to the two shear stresses parallel to the Burgers vector, $\sigma^{(\bar{1}01)}$ and $\sigma^{(0\bar{1}1)}$, and two shear stresses perpendicular to the Burgers vector, $\tau^{(\bar{1}01)}$ and $\tau^{(0\bar{1}1)}$. In a single crystal this finding applies, of course, equally to all twelve $\langle 111 \rangle \{101\}$ slip system since they are crystallographically equivalent.

2.3. Analytical yield criterion for single crystals

Following the original suggestion in [9, 10] and using the findings of the atomistic calculations, we formulate the following yield criterion for any $\langle 111 \rangle \{101\}$ system and a general loading by an applied stress tensor Σ_c^{app} defined in the cube axes.

$$\mathbf{m} \Sigma_c^{\text{app}} \mathbf{n} + a_1 \mathbf{m} \Sigma_c^{\text{app}} \mathbf{n}_1 + a_2 (\mathbf{n} \times \mathbf{m}) \Sigma_c^{\text{app}} \mathbf{n} + a_3 (\mathbf{n}_1 \times \mathbf{m}) \Sigma_c^{\text{app}} \mathbf{n}_1 = \tau_{\text{cr}}^*$$

where \mathbf{m} is the unit vector in the slip direction, \mathbf{n} the unit vector perpendicular to the reference plane, and \mathbf{n}_1 the unit vector perpendicular to the $\{110\}$ plane in the zone of \mathbf{m} that makes the angle -60° with the reference plane. The coefficients a_1, a_2, a_3 , as well as τ_{cr}^* , are all adjustable parameters that are ascertained by fitting the CRSS vs the orientation of the MRSSP and CRSS vs τ dependencies determined by atomistic calculations. Fig. 2 shows the yield loci of the yield surfaces projected into the deviatoric plane obtained using the above yield criterion for Mo and W, respectively. For comparison we also show as the dotted

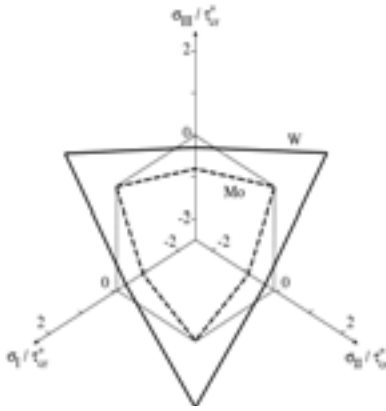


Fig. 2 The yield loci in the deviatoric plane

polygon the yield locus that is obtained from the Schmid law ($a_1=a_2=a_3=0$). The remarkable difference between the yield loci obtained from the yield criterion and that corresponding to the Schmid law demonstrates the breakdown of the Schmid law in both molybdenum and tungsten. However, in molybdenum this is caused by a combination of the twinning-antitwinning asymmetry of shearing parallel to the slip direction and the effect of the shear stresses perpendicular to the slip direction, while in tungsten only the latter plays role. This analysis was applied to the case of uniaxial loading and a remarkable agreement with experimental observations [11-13] was attained.

2.4. Temperature and strain rate dependence of the yield stress

The approach we follow employs the usual dislocation models of kink-pair formation [3, 4] but the new concept is that the Peierls barrier is a function of the full applied stress tensor. The Peierls barrier and its dependence on the applied stress tensor are extracted from the results of 0K atomistic calculations that provide a broad

data base for the dependence of the Peierls stress on the externally applied stresses. Since the Peierls stress is related to the maximum derivative of the Peierls barrier this data base allows us to reconstruct the Peierls barrier with high confidence. Once the Peierls barrier is known the activation enthalpy of kink-pair formation, $H(\boldsymbol{\sigma})$, is determined using the above mentioned models, as a function of the stress tensor $\boldsymbol{\sigma}$. The yield stress dependence on temperature and strain rate is then determined from the relation $H(\boldsymbol{\sigma}) = k_B T \ln(\dot{\epsilon}_0 / \dot{\epsilon})$, where T is the temperature and $\dot{\epsilon}$ the strain rate; $\dot{\epsilon}_0$ is an appropriately chosen constant. Comparison between calculated and measured [14] temperature dependence of the yield stress of tungsten loaded in tension along the $[\bar{1}49]$ axis at the strain rate $\dot{\epsilon} = 8.5 \times 10^{-4} \text{ sec}^{-1}$ is shown in Fig. 3. The excellent agreement was obtained by choosing $\dot{\epsilon}_0 = 3.7 \times 10^{10} \text{ s}^{-1}$ that leads to a reasonable mobile dislocation density.

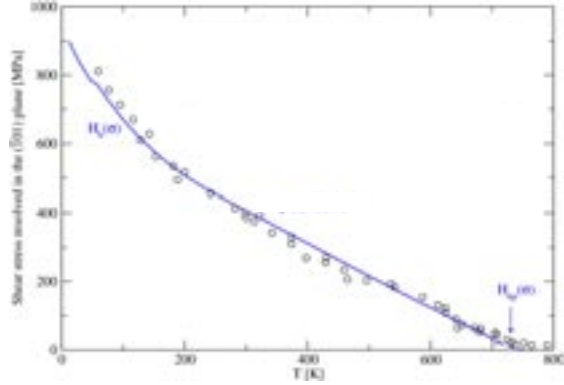


Fig. 3 Calculated temperature dependence of the yield stress (curve) of W compared with the experimental data (circles) of [14]

3. Future research

As alluded to in Section 2.1, a significant effort is being devoted to the development of the BOPs, presently for Ta, Nb and Fe; potentials for Mo and W were developed in our earlier studies [7,8]. The reason for concentrating on Ta and Nb is a relatively extensive availability of experimental data on deformation behavior of single crystals of these metals, so that our theoretical results can be linked with experiments. An example is the recent study of tantalum in Ref.[14]. Similarly, construction of the BOP for Fe, which involves supplementing the binding energy by a term depending on magnetic moments, is in progress. This is an important step for future studies of SIAs and their effect on dislocation behavior since in Fe, owing to ferromagnetism, the SIA configuration is $\langle 110 \rangle$ dumbbell while in all other BCC transition metals it is $\langle 111 \rangle$ dumbbell [6]. Hence, the interaction between dislocation and SIAs may be significantly different in Fe than in other BCC transition metals.

Atomistic modeling of the structure and glide of $1/2\langle 111 \rangle$ screw dislocations in non-magnetic BCC transition metals (Nb, Ta) and ferromagnetic BCC iron will be carried out in the way briefly described in Section 2.2, once the corresponding BOPs have been developed. In parallel we will carry out atomistic studies of the interaction between screw dislocations and SIAs, in particular their effect on the Peierls stress and glide geometry. This study is central for understanding the effect of radiation damage on deformation behavior that is a pivotal issue for materials that are employed in nuclear energy systems.

The results of the above atomistic studies will be employed in formulation of yield criteria, as outlined in Section 2.3, and in advancement of the models of the thermally activated dislocation glide, briefly described in Section 2.4. The latter provide the mobility rules for dislocations and introduce on the

macroscopic level temperature and strain rate dependencies into the yield stress. This course of research represents multi-scale modeling that inputs the most important aspects of atomic bonding via BOPs, identifies the governing features and stress responses of dislocations at atomic level and formulates temperature and strain rate dependent yield criteria for engineering studies of the plastic response of materials to complex loading, temperature variation and strain rate, as well as possible effects of irradiation.

4. Publications resulting from the DOE sponsored research: 2005-2007

1. M. J. Cawkwell, D. Nguyen-Manh, C. Woodward, D. G. Pettifor and V. Vitek: *Origin of Brittle Cleavage in Iridium*, Science **309**, 1059-62, 2005.
2. D. Nguyen-Manh, M. J. Cawkwell, R. Gröger, M. Mrovec, R. Porizek, D. G. Pettifor and V. Vitek: *Dislocations in Materials with Mixed Covalent and Metallic Bonding*, Mat. Sci. Eng. A **400-401**, 68-71, 2005.
3. M. J. Cawkwell, M. Mrovec, Duc Nguyen-Manh, D. G. Pettifor and V. Vitek: *A Bond-Order Potential Incorporating Analytic Screening Functions for the Molybdenum Silicides*, in "Integrative and Interdisciplinary Aspects of Intermetallics", edited by M.J. Mills, H. Clemens, C-L. Fu, H. Inui, MRS Symposium Proceedings, Vol. **842**, p. S2.8.1-6, 2005.
4. M. Sob, M. Friák, D. Legut and V. Vitek: *Theoretical Strength, Magnetism and Stability of Metals and Intermetallics* in "Complex Inorganic Solids - Structural, Stability, and Magnetic Properties of Alloys", edited by P.E.A. Turchi, A. Gonis, K. Rajan, and A. Meike, Springer, Berlin, pp. 307-326, 2005.
5. R. Gröger and V. Vitek: *Breakdown of the Schmid Law in BCC Molybdenum Related to the Effect of Shear Stress Perpendicular to the Slip Direction*, Materials Science Forum **482**, 123-126, 2005.
6. M. Sob, J. Pokluda, M. Cerny, P. Sandera and V. Vitek: *Theoretical Strength of Metals and Intermetallics from First Principles*, Materials Science Forum **482**, 33-38, 2005.
7. V. Vitek: *Dislocation Cores and Unconventional Properties of Plastic Behavior*, Handbook of Materials Modeling Vol. I: Methods and Models, edited by S. Yip, Springer, pp. 2883-2896, 2005.
8. M. J. Cawkwell, D. Nguyen-Manh, D. G. Pettifor and V. Vitek: *Construction, Assessment, and Application of a Bond-Order Potential for Iridium*, Phys. Rev. B **74**, 064104 – 13, 2006.
9. R. Gröger and V. Vitek: *Effect of Non-Glide stresses on Deformation of BCC Metals at Finite temperatures*, Proceedings Third International Conference Multiscale Materials Modeling, editor. P. Gumbsch, Fraunhofer IRB Verlag, p. 571-574, 2006.
10. M. J. Cawkwell, C. Woodward, D. Nguyen-Manh, D. G. Pettifor and V. Vitek: *Atomistic Study of Athermal Cross-Slip and its Impact on the Mechanical Properties of Iridium*, Acta Materialia **55**, 161-169, 2007.
11. R. Gröger and V. Vitek: *Explanation of the discrepancy between the measured and atomistically calculated yield stresses in body-centered cubic metals*, Philos. Mag. Lett., **87**, 113–120, 2007.
12. M. Mrovec, R. Gröger, A. G. Bailey, D. Nguyen-Manh, C. Elsässer and V. Vitek: *Bond-order potential for simulations of extended defects in tungsten*, Phys. Rev. B, **75**, 104119 - 16, 2007.
13. M. Aoki, D. Nguyen-Manh, D. G. Pettifor and V. Vitek: *Atom-Based Bond-Order Potentials for Modeling Mechanical Properties of Metals*, Prog. Mater. Science, **52**, 154-195, 2007.
14. D. Nguyen-Manh, V. Vitek and A.P. Horsfield: *Bond Screening: A Challenge for Modelling of Intermetallics and Fusion Materials*, Prog. Mater. Science, **52**, 255–298, 2007.
15. V. Vitek and V. Paidar: *Non-planar dislocation cores: A ubiquitous phenomenon affecting mechanical properties of crystalline materials*, Dislocations in Solids, edited by J. P. Hirth, in print, 2008.

References

- [1] Bassani JL and Racherla V, in Gumbsch P, eds., *Proceedings Third International Conference Multiscale Materials Modeling*, vol. Freiburg: Fraunhofer IRB Verlag, 2006, p. 13.
- [2] Racherla V and Bassani JL, *Modelling and Simulation in Mat. Sci. Eng.* 2007; 15: S297.
- [3] Seeger A, *Philos. Mag.* 1956; 1: 651.
- [4] Dorn JE and Rajnak S, *Trans. TMS-AIME* 1964; 230: 1052.
- [5] Stoner EC, *Proc. Roy. Soc. London A* 1939; 165: 372.
- [6] Liu GQ, Nguyen-Manh D, Liu BG and Pettifor DG, *Phys. Rev. B* 2005; 7117: 4115.
- [7] Mrovec M, NguyenManh D, Pettifor DG and Vitek V, *Phys. Rev. B* 2004; 6909: 4115.
- [8] Mrovec M, Gröger R, Bailey AG, NguyenManh D, Elsässer C and Vitek V, *Phys. Rev. B* 2007; 75: 104119.
- [9] Qin Q and Bassani JL, *J. Mech. Phys. Sol.* 1992; 40: 813.
- [10] Qin Q and Bassani JL, *J. Mech. Phys. Sol.* 1992; 40: 835.
- [11] Hollang L, Hommel M and Seeger A, *Phys. Stat. Sol. (a)* 1997; 160: 329.
- [12] Hollang L and Seeger A, *Materials Transactions, JIM* 2000; 40: 141.
- [13] Hollang L, Brunner D and Seeger A, *Mat. Sci. Eng. A* 2001; 319: 233.
- [14] Brunner D and Glebovsky V, *Mater Lett* 2000; 44: 144.
- [15] Lassila, D. H., LeBlanc, M. M., and Rhee, M. in *MRS Symp. Proc.*, Vol. 779, 2003, p W2.9.1–2.9.12.

NANOSTRUCTURE PATTERNING UNDER ENERGETIC PARTICLE BEAMS: RADIATION EFFECTS VERSUS SELF-ORGANIZATION

Lumin Wang

Department of Nuclear Engineering & Radiological Sciences, and Department of Materials
Science & Engineering, University of Michigan, Ann Arbor, MI 48109-2104
e-mail: lmwang@umich.edu

Ordered arrays of nanoparticles or nano-scale cavities and nano-fibers of uniform thickness are desirable for applications in advanced optical, photonic and magnetic information storage devices. It has been demonstrated that various types of these nanostructures can be obtained by energetic particle irradiation. However, the mechanisms responsible for these nanoscale phenomena are not yet well understood at present and that prevented the application of some of the irradiation induced spectacular nanostructures. For example, irradiation induced voids or gas bubbles have been observed to arrange into a three dimensional superlattice in a variety of materials under ion irradiation, but they seem to occur only in very narrow experimental conditions. Many of the previously reported results could not be repeated due to the lack of understanding of the key controlling parameters. This research is aimed at exploring the unique experimental conditions for creating such nanostructures with energetic particle beam irradiation and the fundamental scientific basis for these irradiation induced self-organization processes. The nanostructures interested in this research include irradiation induced two or three dimensional arrays of nanoparticles or nanocavities either on top of material surfaces or beneath the irradiated surface, and irradiation induced formation of nano-porous structures with uniform nano-fibers in semiconducting materials. Our previous research has provided important data for creating such nanostructures in a group of materials (e.g., CaF_2 , Ge and GaSb) with electron and ion beam irradiation, and further indicated that there might be a universal intrinsic material science responsible for all these “self-organized” nanostructure observed under the particle beam irradiation.

Some of the key observations and their indications are highlighted below: (1) Using in situ TEM and other advanced analytical TEM techniques, we have analyzed the dynamic process of three-dimensional nano-scale defect cluster superlattice in electron irradiated calcium fluoride. We have identified that the defect clusters are true fluorine gas bubbles resulted from electron irradiation induced decomposition of the material (Fig. 1). The formation of such nano-arrays is sensitive to the energy of the electron beam and the irradiation temperature. (2) Two dimensional ordered arrays of nanoparticles of various elements on the surface of various materials have been obtained under low energy ion irradiation (a few keV to 30 keV) (Fig. 2). The ion energy and incident angle have been found to be the most important parameters that controls the uniformity of the nanoparticle size and their ordering. Although the controlling mechanisms for these ordered nanoparticle arrays involve sputtering and redeposition of sputtered atoms, a great similarity has been found in the nanoparticle organization process with the formation of three dimensional nanocavity arrays observed under the irradiated surface (Fig. 3). (3) Photoluminescent patterns that are made of uniform

sized nano-fibers have been produced on the surface of germanium and GaSb by focused ion beam. Although the micron-sized patterns were directly written by the focused ion beam, the nanofibers within the irradiated areas are formed apparently due to a self-organization mechanism. With the application of high energy ions, we can make the nanofibers imbedded under an intact surface layer (Fig. 4). Finally, a theoretical model under development for explaining the formation mechanism of the uniform nanofibers has also generated other irradiation induced nanopatterns indicating all these irradiation induced nanostructures may be controlled by a same fundamental mechanism.

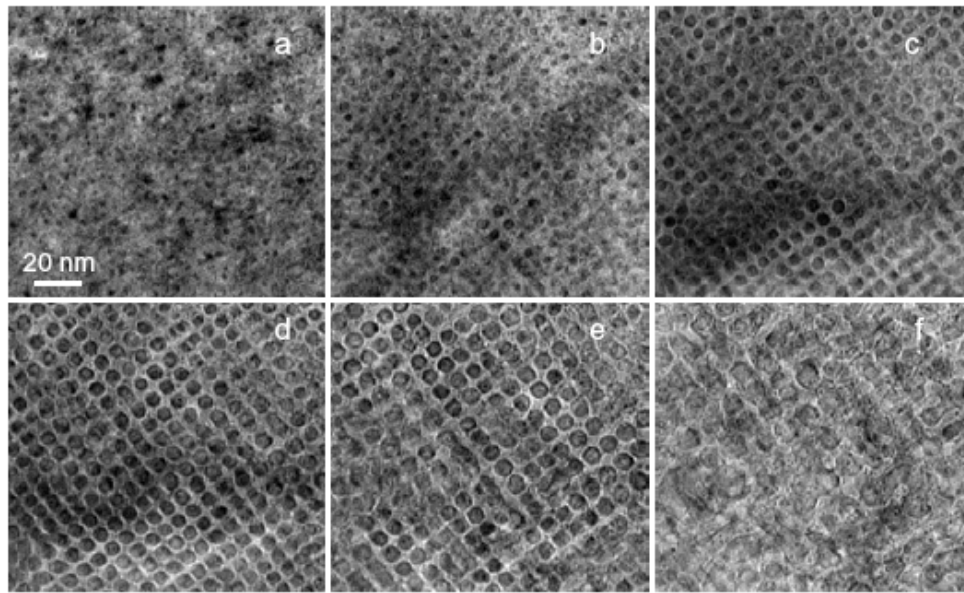


Fig. 1. Overfocused bright-field TEM images of fluorine bubbles in CaF_2 during *in situ* TEM with electron fluence of (a) $5 \times 10^{19} \text{e}^-/\text{cm}^2$, (b) $4.5 \times 10^{20} \text{e}^-/\text{cm}^2$, (c) $1.2 \times 10^{21} \text{e}^-/\text{cm}^2$, (d) $2 \times 10^{21} \text{e}^-/\text{cm}^2$, (e) $3 \times 10^{21} \text{e}^-/\text{cm}^2$, (f) $4 \times 10^{21} \text{e}^-/\text{cm}^2$. A superlattice of fluorine bubbles has developed through a self-organization process. (T.H. Ding, Ph.D. Thesis, to be published)

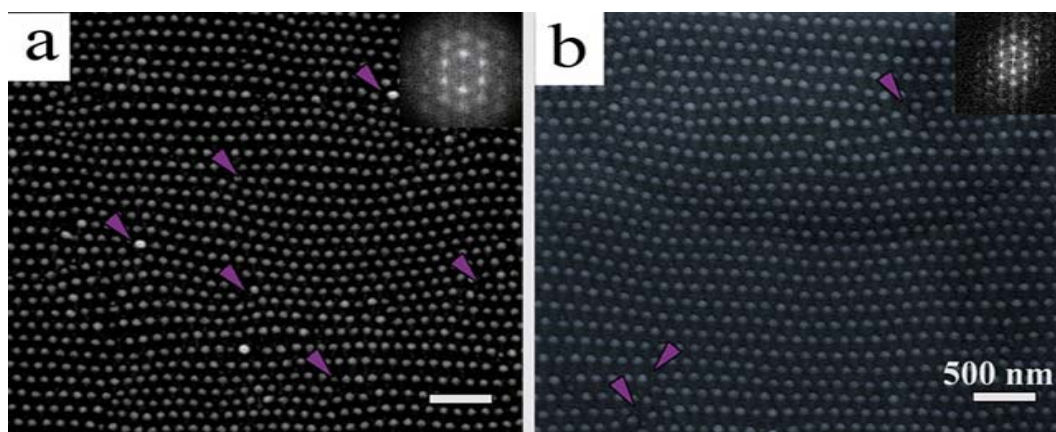


Fig. 2. SEM images showing ordered arrays of Ga nanodroplet on the surface of Ga ion bombarded GaAs surface. The uniformity and the degree of order of the nanodroplets depend on the ion energy and incident angle of the ions. The Ga ion energy was 5 keV with an incident angle of 35° for achieving the above structures (Q. Wei et al., *Physical Review Letters*, 2008).

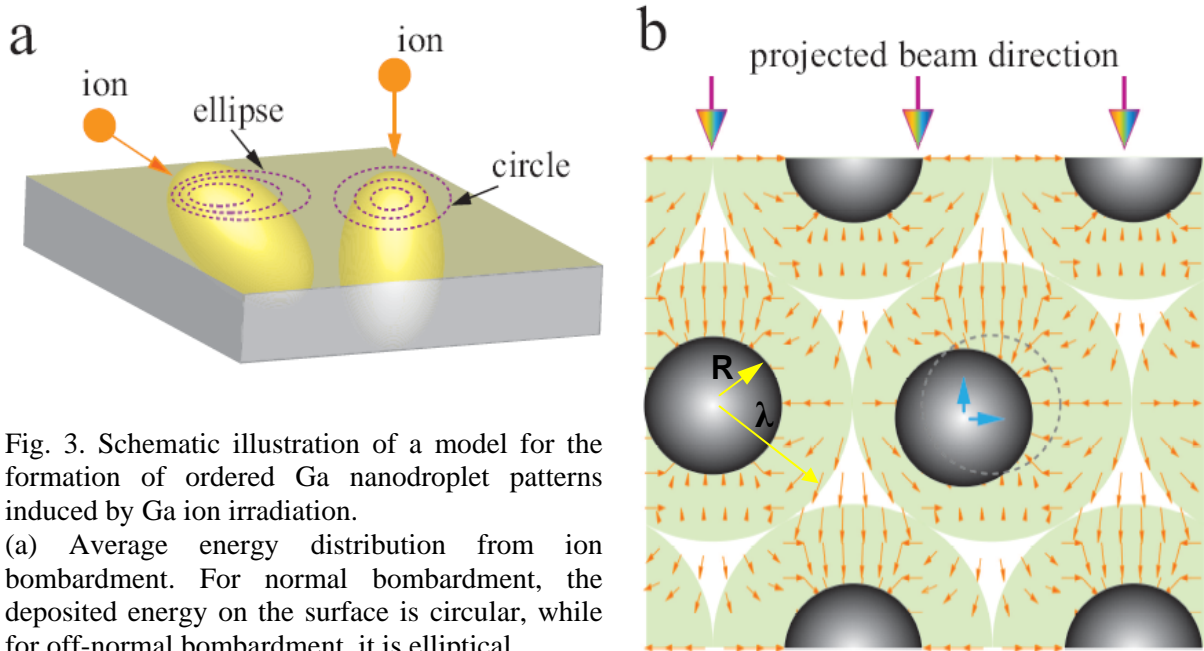


Fig. 3. Schematic illustration of a model for the formation of ordered Ga nanodroplet patterns induced by Ga ion irradiation.

(a) Average energy distribution from ion bombardment. For normal bombardment, the deposited energy on the surface is circular, while for off-normal bombardment, it is elliptical.

(b) Atom supply and movement directions that cause an off-center Ga droplet to move to the center of nanoparticle lattice. Small arrows represent the direction and magnitude of local Ga atom migration induced by the ion beam on the surface. Blue arrows inside the droplet indicate the moving direction of the droplet, and dashed circle shows the final position of partially aligned droplets (Q. Wei, et al., *PRL*, 2008). This model resembles a model proposed for the formation of three dimensional superlattice of nanovoids.

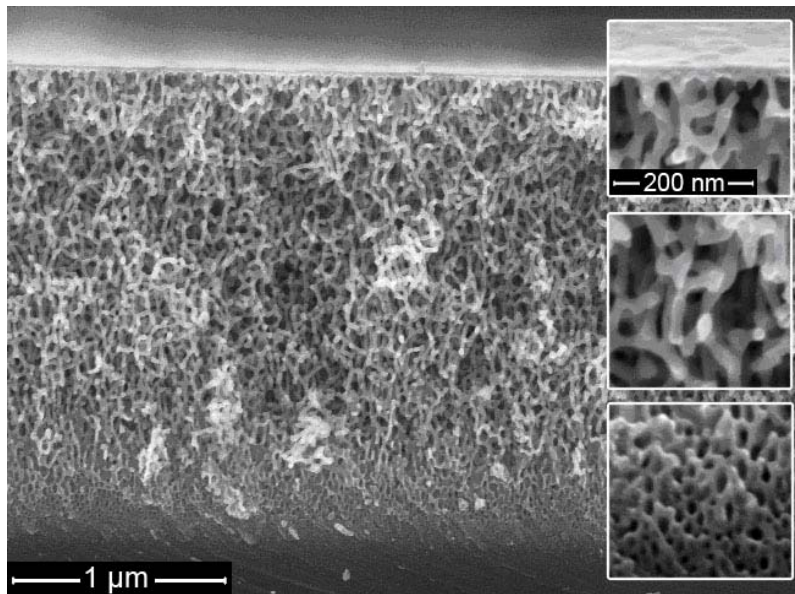


Fig. 4. Cross-sectional SEM image of GaSb fiber layers. Material was irradiated with 1 MeV Au⁺ to 1×10^{14} ions/cm². Insets show (a) the surface layer (tilted to 10° off axis), (b) the presence of fully formed fibers, and (c) a transition regime in which the fibers blend into the substrate. Main scale bar is 1 μm, inset bar is 100 nm. (A. Perez-Bergquist et al., *Small*, in press)

The future work of this project includes new experiments on more materials with more experimental conditions as well as theoretical modeling and computer simulation. Our aim is to discover and prove a universal controlling mechanism for the nano-scale self-organization phenomenon observed under energetic particle irradiation, and further identify the exact role of irradiation in these processes. Based on that, we will further seek the control of size, morphology and the nature of the nano-clusters in the patterned arrays and study their physical properties and stability under various environments.

Recent Publications:

1. S. Zhu, S.X. Wang, L.M. Wang, R.C. Ewing and X.T. Zu, Behavior of implanted strontium in yttria-stabilized zirconia, *Applied Physics Letters* 90 (2007) 171915-1-3.
2. Qiangmin Wei, K. Sun and Lumin Wang, Formation of GaAs nanocones by focused ion beam, Proceedings Microscopy and Microanalysis 2007 (Fort Lauderdale, FL, August 5-9, 2007, Cambridge University Press), *Microscopy and Microanalysis* 13 (2007) 602-603.
3. Qiangmin Wei, Jie Lian, Sha Zhu, Weixing Li, Kai Sun, Lumin Wang, Ordered nanocrystals on argon ion sputtered polymer film, *Chemical Physics Letters* 452 (2008) 204-208.
4. Q.M. Wei, J. Lian, W. Lu and L.M. Wang, Ordered Ga nanodroplets on GaAs surface induced by focused ion beam, *Physical Review Letters* 100 (2008) 076103.
5. Kun-Dar Li, H.Y. Xiao, and L.M. Wang, Computer simulation study of defect formation and migration energy in calcium fluoride, *Nuclear Instr. & Meth. B*, in press.
6. Alejandro Perez-Bergquist, Sha Zhu, Kai Sun, Xia Xiang, Yanwen Zhang, and Lumin Wang, Embedded nanofibers induced by high energy ion irradiation of bulk GaSb, *Small* (2008) in press.
7. Qiangmin Wei, Weixing Li, Kai Sun, J. Lian and Lumin Wang, Morphological instability of Cu nanolines induced by Ga⁺-ion bombardment: in situ scanning electron microscopy and theoretical model, *Journal of Applied Physics* (2008) in press.

Near Surface Plasticity and its Applications in Surface Treatment

Honghui Yu (PI), Mazen Diab

Mechanical Engineering Department, The City College of the City University of New York
Steinman Hall, Convent Ave at 140th street, New York, NY 10031

yu@ccny.cuny.edu

Program Scope and Definition

When an iron plate was peened by a large amount of stainless steel balls in a vacuum chamber that was vibrated at an ultrasonic frequency, in a short period time, a nano-structured surface layer was formed. It is also observed that railway tracks and wheels have a nano-crystalline layer near surface too.

Numerous engineering applications involve contact and sliding. There is always a microscopic layer near surface that is plastically deformed. Understanding the microstructure evolution and dislocation pattern formation near surface is extremely important. However, the area is relatively under represented, especially in the theoretical part. There are very few theoretical works trying to understand the fundamental mechanisms involved.

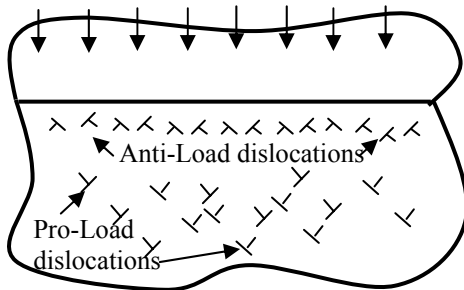


Fig. 1 Segregation of anti- and pro-load dislocations

Before this project, in collaboration with Y.F. Gao and K.S. Kim, we studied a simple unit process, in which a stepped surface is under a contact load and dislocation is allowed to nucleate from the step. We found two types of dislocations existing near surface. One type, called *anti-load dislocation*, is pushed closer to the step as the load increases. And another type, *pro-load dislocations*, is pushed even further away from the step as the load increases. The results indicate the segregation of similar dislocation under the normal contact load (Fig. 1). The segregation of the anti-load dislocations generates a sub-layer of

tensile stress. And because the pro-load dislocations are easily driven away from the step into the bulk, they produce a much thicker layer of compressive stress.

This project continues studying dislocations near surface. We adopt two approaches. One is to devise simple theoretical models to study the fundamental dislocation processes near surface and to gain basic physical understanding. The other is to develop a fast numerical code to simulate the dislocation segregation and pattern formation near surface when it is under rough contact. Especially, we are going to deal with the cases that have very high dislocation density and to study the interactions among different parts of the surface.

Recent progress

An integral formulation for finite body with dislocations

To simulate dislocation motion, it is essential to have a tool that can calculate stress field quickly. Compared with finite element method, boundary element method has fewer degrees of freedom and is easier to refine mesh when it is needed. Based on Stroh formalism for general anisotropic material, we derived the following equation for a finite body which has many dislocations inside¹,

$$0 = \oint_{\partial\Omega} \mathbf{A} \cdot \langle \ln(\zeta_\alpha - \zeta_\alpha^0) \rangle \cdot \mathbf{L}^{-1} \cdot (\mathbf{B} + \bar{\mathbf{B}})^{-1} \cdot \left(\frac{d\mathbf{u}}{ds} + i\bar{\mathbf{B}} \cdot \mathbf{t} \right) \Big|_\zeta ds - \sum_{k=1}^n \mathbf{A} \cdot \langle \ln(z_\alpha^{(k)} - \zeta_\alpha^0) \rangle \cdot \mathbf{L}^{-1} \cdot (\mathbf{B} + \bar{\mathbf{B}})^{-1} \cdot \mathbf{b}^{(k)} \quad (1)$$

where matrixes \mathbf{A} and \mathbf{L} were defined by Stroh, $\mathbf{B} = i\mathbf{A}\mathbf{L}^{-1}$ ($i = \sqrt{-1}$), $\langle \cdot \rangle$ represents a diagonal matrix whose α -th diagonal element is listed inside. The equation establishes the relation between the displacement \mathbf{u} and traction \mathbf{t} along the boundary, more interesting, the effect of dislocation is directly included in the last term. In Equ. (1), $\mathbf{b}^{(k)}$ is the Burgers vector of k -th dislocation. Note that the derivative of the displacement along the boundary du/ds is used instead of displacement \mathbf{u} . The corresponding integral kernel has weaker singularity than that in the conventional Boundary Element Method(BEM). Similar treatment is used when calculating the stress at an interior point, so that the stress calculation is accurate even at places very close to the boundary. For an isotropic material, \mathbf{A} and \mathbf{L} are both singular, but matrix \mathbf{B} still exists. By taking limit from anisotropic material to isotropic, we have the following equation for isotropic materials,

$$\oint_{\partial\Omega} \left\{ \log(\zeta - \zeta_0) \mathbf{I} + \frac{y - y_0}{\zeta - \zeta_0} \cdot \frac{1}{2\mu} \begin{bmatrix} 1 & i \\ i & -1 \end{bmatrix} \right\} \cdot \left[i \frac{d\mathbf{u}}{ds} - \bar{\mathbf{B}} \cdot \mathbf{t} \right] \Big|_\zeta ds - \sum_{k=1}^n \left\{ \log(z^{(k)} - \zeta_0) \mathbf{I} + \frac{y^{(k)} - y_0}{z^{(k)} - \zeta_0} \cdot \frac{1}{2\mu} \begin{bmatrix} 1 & i \\ i & -1 \end{bmatrix} \right\} \cdot \mathbf{b}^{(k)} = 0. \quad (2)$$

A new boundary element method²

Equ. (1) or (2) can be solved numerically using boundary element method. In our numerical implementation, we interpolate du/ds directly by its values at the nodal points of each element. By doing so, the degrees of freedom are much fewer than that if interpolating \mathbf{u} . The following example is solved to check the accuracy of the program.

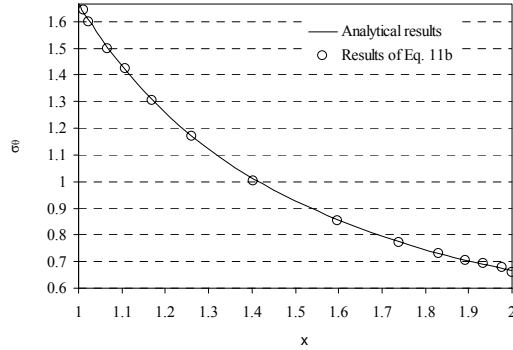
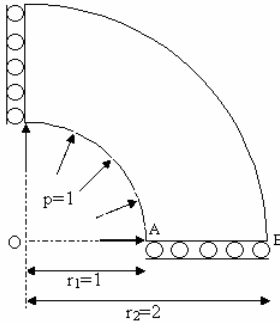


Fig. 2a: Pressurized Thick-Walled Cylinder. Fig. 2b: Distribution of Hoop Stress.

In the conventional BEM, due to the higher order singularity of the integral kernel, accurate calculation of stress near the external boundary is very difficult. In our new treatment, such difficulty is eliminated, as shown in the example above.

Application to dislocation dynamics

In Eqs. (1) and (2), contributions from dislocations are directly included. Linear superposition technique, which was usually used in literature for problems having finite boundary, is no longer needed. After solving the boundary displacement or traction, the driving

force for each dislocation can be calculated. Combine the stress solver with an algorithm in dislocation dynamics, we can simulate dislocation motion in solid. A typical problem, a unit cell of polycrystalline under pure shear, is simulated to test the new program. The model is similar to the one studied by Balint et al. The average stress in the cell is calculated through a boundary integration. When dislocations are generated and move in the solid body, a non-linear stress-strain relation is obtained. Use the results, we obtain the flow stress, the Hall-Petch exponent and another fitting parameter k . They are all very close to the values obtained by Balint et al.

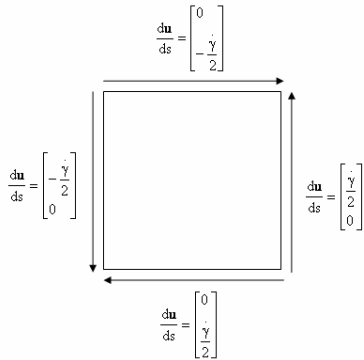
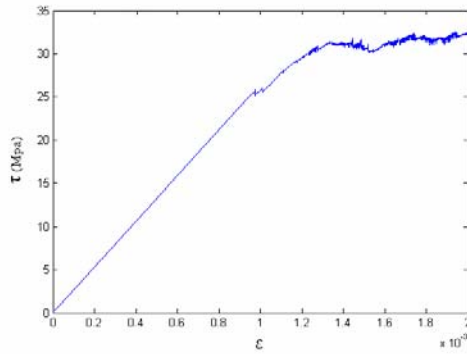


Fig. 3a: A unit cell under pure shear loading



3b: Stress v.s Strain

Some Fundamental Problems in Contact

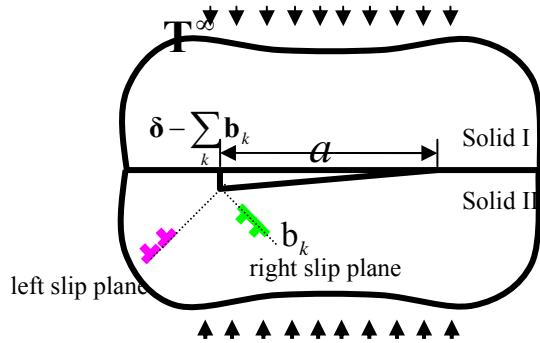
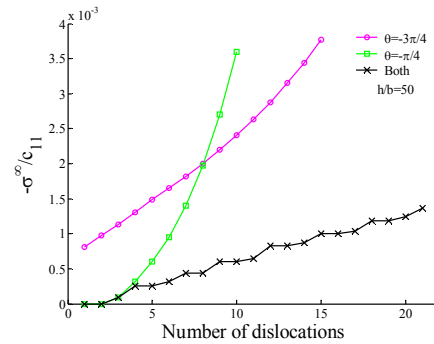


Fig. 4a: A stepped surface under contact loading



4b: Remote stress v.s. number of dislocations

1) *Latent softening*. In collaboration with Y.F. Gao and K.S. Kim³, the contact hardening behavior due to multiple dislocations is studied (Fig. 4a). Dislocations nucleated from a surface step are stabilized and piled up. The pileup leads to the contact hardening behavior. The hardening curves in Fig. 4b correspond to the cases when pile-up occurs in right slip plane only ($\theta = -\pi/4$), left slip plane only ($\theta = -3\pi/4$), and both. When both of the two slip planes operate, we get a significant drop of the hardening curve, as shown by the curve with cross markers. We call the phenomenon “latent softening”. The curve also shows that the dislocation pileup on one slip plane can even cause spontaneous dislocation nucleation on the other slip plane without further increase of the contact load.

2) Dislocation nucleation from surface source

In our previous investigation, we used Rice-Thompson model as dislocation nucleation criterion. In this study, we use a cohesive zone model to describe the sliding slip plane where the dislocations initiate. Apply Equ. (1), we have

$$\mathbf{t}|_{\zeta_0} = -2 \operatorname{Re} \left\{ \frac{1}{\pi i} \oint_{\partial\Omega} \mathbf{L} \cdot \left\langle (C_0 + p_\alpha S_0) / (\zeta_\alpha - \zeta_\alpha^0) \right\rangle \cdot \mathbf{L}^{-1} \cdot (\mathbf{B} + \bar{\mathbf{B}})^{-1} \cdot \left[i \frac{d\mathbf{u}}{ds} - \bar{\mathbf{B}} \cdot \mathbf{t} \right] \Big|_{\zeta} ds \right. \\ \left. + \frac{1}{\pi} \int_{\text{slip-plane}} \mathbf{L} \cdot \left\langle (C_0 + p_\alpha S_0) / (\zeta_\alpha - \zeta_\alpha^0) \right\rangle \cdot \mathbf{L}^{-1} \cdot (\mathbf{B} + \bar{\mathbf{B}})^{-1} \cdot \frac{d\Delta\mathbf{u}}{ds} \Big|_{\zeta} ds \right\}, \quad (3)$$

where $\Delta\mathbf{u}$ is the displacement jump across the slip plane, and the integral on the slip plane is from interior toward surface. Along the slip plane, the traction is related to the displacement jump through a cohesive law, which is derived from a potential function. By solving Equ. (3), we obtain the displacement jump across the slip plane. A dislocation is nucleated when a ripple of displacement jump becomes unstable.

Future plan

1) Formulation for cases with very high dislocation density

Modeling the evolution of many strongly interacting dislocations is a many-body problem. When the number of dislocations increases, the computation time increases drastically. Due to the $1/r$ singularity of the theoretical stress field near a dislocation, the interaction between the two dislocations that are very close becomes artificial. Some stochastic models might be combined with our current formulation to determine the resolved shear stress on dislocations. We can use dislocation density ρ to represent dislocation distribution inside the body. The smeared stress field can be obtained by first solving a boundary integral equation,

$$0 = \oint_{\partial\Omega} \mathbf{A} \cdot \left\langle \ln(\zeta_\alpha - \zeta_\alpha^0) \right\rangle \cdot \mathbf{L}^{-1} \cdot (\mathbf{B} + \bar{\mathbf{B}})^{-1} \cdot \left(\frac{d\mathbf{u}}{ds} + i\bar{\mathbf{B}} \cdot \mathbf{t} \right) \Big|_{\zeta} ds \\ - \int_{\Omega} \mathbf{A} \cdot \left\langle \ln(z_\alpha - \zeta_\alpha^0) \right\rangle \cdot \mathbf{L}^{-1} \cdot (\mathbf{B} + \bar{\mathbf{B}})^{-1} \cdot \left(\sum_i \mathbf{b}^{(i)} \rho^{(i)} \right) dA \quad (4)$$

where $\mathbf{b}^{(i)}$ and $\rho^{(i)}$ are the Burgers vector and dislocation density of i -th type dislocation. At any interior point, the resolved shear stress is the smeared average stress plus a random term, which is a function of the dislocation density. The flux of each dislocation type is proportional to the resolved shear stress and dislocation density, the change of dislocation density over time is related to the derivative of the flux in the slip plane direction and the new dislocations generated by the source, which is a random number having a distribution function depending on the shear stress. Thus, the evolution of dislocation density can be calculated.

2) Dislocation pattern and segregation near surface using high density model

The new model will be used to study the dislocation segregation and pattern formation near surface due to contact load. Many fundamental problems need be answered. Such as what determines the length scale in the organized pattern, the thickness of the tensile layer near surface, and the long range interaction among different asperities of the contacting surface, etc.

References

- Yu, H. H. (2008) A boundary element method for dislocation dynamics: part 1 formulation.
 Diab, M. and Yu, H.H. (2008), A boundary element method for dislocation dynamics: part 2 numerical implementation.
 Gao, Y.F., Yu, H.H. and Kim, K.S. (2008), Micro-plasticity of surface steps under adhesive contact: Part II – Multipledislocation mediated contact hardening

Investigating Deformation and Failure Mechanisms in Nanoscale Multilayer Metallic Composites

PI's: H. M. Zbib, D. F. Bahr, and S. Medyanik

(zbib@wsu.edu , dbahr@wsu.edu, Medyanik@wsu.edu)

Washington State University, Pullman, WA 99164-2920

F. Akasheh, Tuskegee University (fakasheh@tuskegee.edu)

Other WSU personal working on the project: I. Mastorakos (Research Associate)

Graduate Students: Shuai Shao (PhD), Nicole Overman (MS), Cory Overman (MS),

In collaboration with A. Misra and R.G. Hoagland, LANL

Extended Abstract

Currently, experimental and theoretical research on bimetallic NMM composites is available in the literature, some of which is based on going collaboration between LANL and WSU on the monotonic loading of bimetallic NMM composites [1-3], including the Cu-Ni and Cu-Nb system. In the current investigation, we are developing a multiscale modeling approach combined with novel biaxial loading experiments to study deformation and failure mechanisms under cyclic loading in **trimetallic NMM** composites. Based on bimetallic systems, the interactions of dislocations with the interfaces between the metallic layers is the controlling factor in the deformation of these systems. Adding a third metallic layer, with different elastic constants, lattice parameters, and crystal structure than the other two layers will provide added control of the residual stresses, interfacial energies, and image forces that will act on dislocations as they interact with the interfaces, alternatively making it easier or harder for dislocations to cross the boundaries.

The goal of this investigation is to advance our fundamental understanding of deformation, damage, and failure mechanisms under cyclic loading of NMM composites. As a step forward, we aim to explore the fatigue behavior of trimetallic NMM composites comprising hybrid coherent/incoherent interfaces. Towards this end our investigation involves fabricating a **trimetallic systems** based on **Cu-Ni-Nb**, experimentally examining their behavior under both monotonic and cyclic loading, and a modeling effort based on a multiscale approach.

The testing techniques includes a biaxial bulge testing experiment for both loading conditions, which is more similar to the loading conditions found on coatings than the current uniaxial stretching and uniaxial bending experiments used to measure their response.

The modeling effort uses a multiscale approach to understand the interactions of individual defects with the interfaces as well as to understand the complex interactions of many dislocations. The primary tools for modeling are molecular dynamics to study dislocation-interface interactions, and discrete dislocation dynamics to investigate the behavior of large dislocation systems. The dislocation structures predicted from the modeling will be compared to those found experimentally using electron and scanning probe microscopy.

A coordinated experimental, computational and theoretical effort is underway. The following is a summary of progress since the start of the project in fall of 2007.

Experiments

Bulge testing to determine both elastic and plastic properties in multilayer metallic films allows for both biaxial and uniaxial testing. Our challenge in adapting this test to the systems of interest is to (1) account for the substrate supporting the structure, (2) remove the substrate for free-standing film testing and (3) carry out fatigue testing on these structures. Initial testing on Cu-Nb bilayers (fabricated at LANL) of 20 nm thickness, with a total thickness of 2000 nm, is shown in the pressure – deflection shown in Figure 1. The film is supported by a micromachined Si / SiO₂ window 4mm square and 2000 nm thick . The ability to pressurize a membrane to a specific deflection is important in this research for determining both the residual stress in the membrane, which is accumulated during processing, and the stiffness of the membrane. The membrane is pressurized with a bellows to a specified deflection, which can be either in a “positive” or “negative” direction, allowing for very accurate determination of the residual stress. The residual stress and biaxial modulus of the substrate were found to be 17.5 MPa and 163.8 GPa respectively (as would be expected for this composite substrate), while the residual stress for the film and substrate was 30MPa with a biaxial modulus of 164.8GPa.

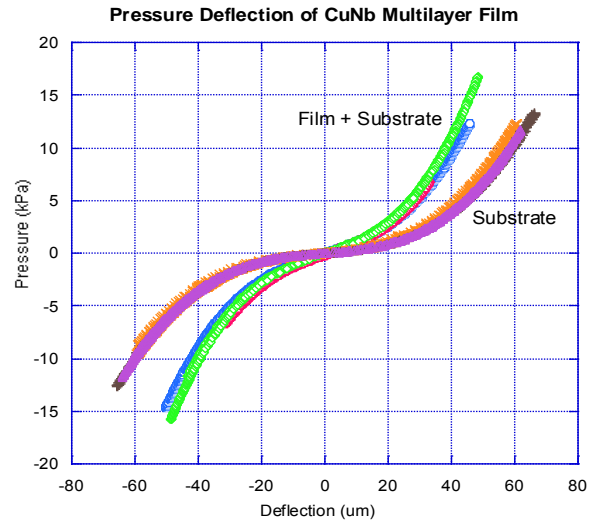


Figure 1. Pressure-deflection of Cu-Nb bilayers

Work in Progress and future work includes the following.

- Testing freestanding films, and dynamic testing at specified frequencies (100's of Hz) to evaluate the fatigue response of the material.
- Fabricate and characterize trimetallic NMM composites
- Testing of the trimetallic system Cu-Ni-Nb.

Molecular Dynamics Analyses

Our objective here is to use MD simulations to: 1) study the influence of individual layer thickness of bi- and tri-layer structures to the interfacial energy, and 2) to modify the molecular dynamic code to model indentation experiments for multilayered metallic composites. The MD code we are using is based on the Embedded Atom Method (EAM). Within this framework, the total internal energy of a system of N atoms is expressed as a sum of two terms: (i) $F(\rho_i)$, the embedding energy required to place atom i in an electron density ρ_i , and (ii) $\varphi(r_{ij})$, the two-body potential between atoms i and j. r_{ij} is the separation distance between atoms i and j and ρ_i is the host electron density at atom i due to all other atoms. The host electron density is approximated as the sum of the electron densities $f(r_{ij})$ of all individual atoms j. Therefore, we need to determine three individual functions: $F(\rho_i)$, $\varphi(r_{ij})$ and $f(r_{ij})$.

We started our study by first finding the appropriate potentials for each material used. In general, the three functions described above are given in the form of spline functions [4,5]. However, these functions cannot be used for alloys since the functions describe the atomic energy of the bulk pure materials at equilibrium. Therefore, we needed analytical functions that can be used also for alloys. The method we used is a combination of two theories. The first is developed by Cai and Ye [6] for fcc metals and the second is developed by Johnson and Oh [7] for bcc metals. Furthermore, an EAM model with two types of atoms (say a and b), needs two density functions $f_a(r)$ and $f_b(r)$, two embedding energy functions $F_a(\rho)$ and $F_b(\rho)$, and three pair potential functions $\varphi_{aa}(r)$, $\varphi_{bb}(r)$ and $\varphi_{ab}(r)$. The first six functions

are the functions used for the monoatomic systems. The remaining function $\varphi_{ab}(r)$ is assumed to be a density-weighted combination of monoatomic pair potentials [8]. After the atomic potentials were developed, Cu-Ni and Cu-Nb bilayer structures were formed and relaxed to equilibrium. Figure 2 shows the relaxed configuration of the Cu-Nb bilayer.

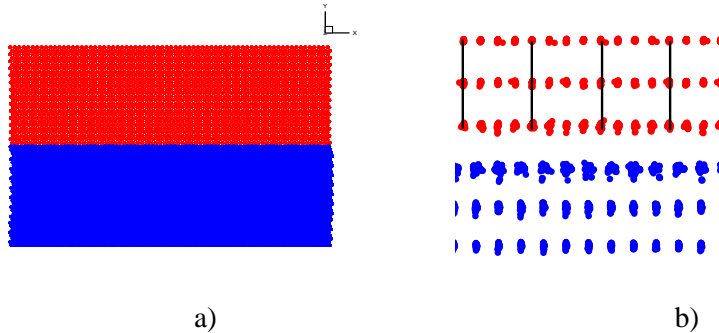


Figure 2: (a) Relaxed Cu-Nb bilayer. Cu is at the bottom (red) and Nb on the top (blue). The orientation is as follows: Cu (x-axis [1 1 -2], y-axis [1 1 1]), Nb (x-axis [-1 -1 2], y-axis [1 -1 0]). (b) Magnification of the interfacial area along z-axis (Cu [1 -1 0] and Nb [1 1 1] directions). Due to the big difference ($\sim 9\%$) between the lattice constants of Cu and Nb, the Nb layer has more atomic columns than the Cu. The result is an extra atomic columns inside the Nb.

Work in progress :

- a. Combining the above materials to study trimetallic Cu-Ni-Nb systems.
- b. Modifying the molecular dynamics code to model indentation experiments for multilayered metallic composites. The objective here to use indentation to generate dislocations at and near the surface that will propagate through the layers.
- c. Creating bi-metallic and tri-metallic multilayered atomistic systems with a number of different geometries and crystallographic orientations. (currently in progress)

Future work:

- a. Calculate interfacial energy for different combinations of layers (Cu-Ni-Nb systems) and different layer thicknesses.
- b. Introduce dislocations and calculate the interfacial energy for different layer thicknesses.
- c. Investigate the dislocation behavior inside the middle layer under uniaxial tension and compression.
- d. Study the dislocation propagation through the interface.
- e. Analyze possibilities for interface strengthening mechanisms.
- f. Introduce a nano-crack and investigate crack-dislocation interaction under uniaxial tension and compression.

Dislocation dynamics analysis for heterogeneous layered structures

Current 3D codes in dislocation dynamics do not address the following two critical issues faced in the analysis of multilayered structure,

- a. Image stresses (resulting from the difference in elastic properties of the different layering materials): Depending on the bimetal system, such forces can be significant in repelling/attracting threading channeling dislocations away from/towards the interfaces; thus influencing the effective layer thickness and dislocation reactions at the interfaces. In the case of nanoscale trimetallic systems, such effects become more complicated and cannot be easily predicted based on bimetal results and a computational approach becomes necessary
- b. Dislocation-interface interactions: Depending on the crystal and/or orientation of the materials on either sides of the interface (coherent or incoherent), dislocations impinging on the interface can

either pile-up or transmit. Upon transmission, additional forces due to the formation of a ledge are experienced.

To address those issues, our DD framework [9] has already been modified so that the simulation cell can be made up of any number of layers each having its own crystal structure, orientation and materials properties. To account for image stress, the multiscale coupling of continuum FEA analysis and DD is utilized. In the case of two materials, the image force in material 2 due to a dislocation in material 1 σ_{img}^{21} , is determined from an eigenstress of the form: $\sigma_{img}^{21} = (C_2 - C_1)\varepsilon^{\infty 1}$ along with superposition principle [9], where C_i is the elastic stiffness tensor of material i and $\varepsilon^{\infty 1}$ is the dislocation strain field as if the whole domain was made from material 1. A demonstration of this calculation is shown in Figure 3. The top and bottom layers are made of Cu and Ni, respectively. An edge dislocation (line along y-axis and Burgers vector along the x-axis) exists at the center just below the interface in material 2. The stress contours represent the image stress due to the difference in shear modulus of Cu and Ni.

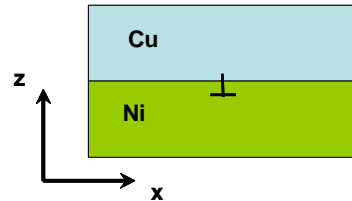
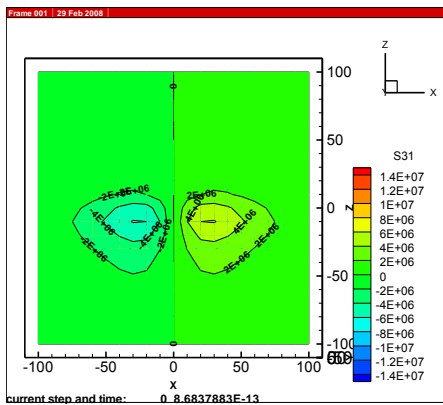


Figure 3. Image stress of an edge dislocation near the interface in Cu-Ni system.

Work in progress and Future work:

- Modifications made to the DD framework to allow for the specification of interface properties. For example, if the interface is incoherent, the interface can be made impenetrable to dislocation. In the case of coherent systems, an additional force can be imposed on a dislocation attempting to cross the interface. Additional rules as observed in MD simulations, like dislocation core spreading and trapping at the interface can also be implemented in DD (work in progress)
- Perform DD analysis of dislocation mechanisms in trimetallic NMM composites
- Establish DD Models of interface dislocations and disconnections
- Analyze Interface crack-dislocation interaction coupled with DD

References

- F. Akasheh, H.M. Zbib, J.P. Hirth, R.G. Hoagland, and A. Misra, J. Appl. Phys., 101 (2007).
- F. Akasheh, H.M. Zbib, J.P. Hirth, R.G. Hoagland, and A. Misra, J. Appl. Phys., 102 (2007).
- F. Akasheh, and H.M. Zbib, in: Multiscale Modeling and Simulation of Composite Materials and Structures, Eds, Y. Kwon, D. Allen and R. Talreja, Springer, (2007).
- M.S. Daw and I. Baskes, Phys. Rev. Lett. 50, 1285 (1983)
- M.S. Daw and I. Baskes, Phys. Rev. B 29, 6443 (1984).
- J Cai and Y. Ye, Phys. Rev. B 54, 8398 (1996).
- R.A. Johnson and D.J. Oh, J. Mater. Res. 4, 1195 (1989)
- R.A. Johnson, Phys. Rev. B 39, 12554 (1989)
- H.M. Zbib, and T. Diaz de la Rubia, Int. J. Plasticity, 18, 1133 (2002).

Laboratory Projects

Microstructural Design of Advanced Ceramics

Paul F. Becher
Oak Ridge National Laboratory
Materials Science and Technology Division
MS 6068
P. O. Box 2008
Oak Ridge, TN 37831
becherpf@ornl.gov

Collaborators: Gayle S. Painter, Klaus van Benthem and Hua-Tay Lin, Materials Science and Technology Division, Oak Ridge National Laboratory and Naoya Shibata, Institute of Engineering Innovation, University of Tokyo, Tokyo, Japan

Program Scope: The processing of bulk ceramics typically involves small additions of compounds that promote densification of a compact of powders of the main constituent. Aside from enhancing densification, these additions often can modify the microstructure and/or properties of the resultant ceramic. However, the specific mechanisms by which these changes occur are not well understood because the elucidation of such is complicated by the fact that ceramics are quite complex systems where multiple elements and crystalline and non-crystalline phases are present. However, understanding the role of such additives in the development of microstructural characteristics across multiple length scales from atomic to macroscopic processes provides a critical path for tailoring ceramics to achieve unique properties for application in severe environments. This can be achieved only by combining theory and atomic scale observations to define the behavior of additive atoms in conjunction with experimental studies of their effects on microstructural evolution and the impact on the properties of ceramics. It is this approach that forms the basis of this task, which involves contributions from multiple collaborators.

Recent Progress: Our previous aberration-corrected scanning transmission electron microscopy (STEM) results provided the first direct image of additive rare earth atoms segregated to sites on smooth prismatic β - Si_3N_4 grain surfaces [1], which have now been confirmed by several groups [2]. The observed ordering of the adsorption sites corresponds with those predicted from the first-ever first-principles total energy calculations to address this issue [3,4]. Subsequent imaging of larger amorphous regions at multi-grain junctions revealed that the rare earth atoms assembled in layers parallel to the prism surfaces of the Si_3N_4 grains extending several monolayers out into the amorphous pocket exhibiting increasing degree of disorder with distance from the β - Si_3N_4 surface [5, 6]. Within these nanometer thick intergranular films, ordering is also observed but is limited to the grain surface, with the bulk of the intergranular film exhibiting no distinct structure or ordering. On the other hand, measurements of site-specific binding strengths of the adsorbing atoms have until now eluded researchers. Recently, electron beam irradiation during scanning transmission electron microscopy (STEM) has been used to probe the relative abundance and stabilities of rare earth adsorption sites in polycrystalline silicon nitride ceramics. Site-specific binding strengths of gadolinium at the interface plane between Si_3N_4 grains and the adjacent amorphous triple pockets were found to be consistent with theoretical predictions [6].

Typically, ordered adsorption of the rare earths within the intergranular film region has only been observed at one of the grain interfaces, likely a result of misorientation between adjacent grains. This raised the issue of how general was the nature of the rare earth adsorption. In addition, the question as to whether or not the addition of additional densification additives will alter the rare adsorption behavior and/or the microstructural evolution must be considered. Recent observations have revealed ordered rare earth adsorption occurs at the interfaces of each of the opposing grains within Si_3N_4 ceramics and is not altered by other additives (e.g., MgO , Al_2O_3 or SiO_2), confirming the general nature of the adsorption behavior [7].

The fundamental significance of these findings centers on the fact that nanometer thick intergranular films are pervasive in polycrystalline ceramic materials, and their structure is typically determined by total energy minimization under steric (geometric) constraints. In such complex materials, it is also necessary to take full account of other conditions, (e.g., chemical composition, sintering temperatures and dispersion interactions). The segregation and adsorption behaviors of different elemental species subjected to various temperature conditions and the resulting crystalline/amorphous interfacial configurations have now been shown in this study to critically control phase transformation and microstructural evolution in ceramics and, hence, their mechanical properties [8,9].

In the case of Si_3N_4 ceramics, a phase transformation must take place during the densification, which strongly impacts the onset of the evolution of the final microstructure. The temperature at which the transformation initiates in the presence of a combination of MgO and RE_2O_3 densification additives is found to decrease with increasing atomic number of the rare earth (RE), Figure 1. This behavior coincides with the predicted and observed decrease in the affinity of the rare earth to segregate to and adsorb on the prism planes of hexagonal prism-shaped beta grains with increase in the atomic number of the RE. In addition, when RE adsorption is diminished, the attachment of Si (and N) on the smooth prism planes is enhanced, which increases diametrical growth rates that are reaction-rate limited. Combined with the typically fast [0001] growth, it is this augmented grain growth that contributes towards the initiation of the alpha-beta transformation at lower temperatures.

While the nature of the secondary densification addition (e.g., MgO, Al_2O_3 or SiO_2) does not affect the RE adsorption behavior, results show that the viscosity of the amorphous phase formed by the additives increases when MgO is replaced by Al_2O_3 and Al_2O_3 is replaced by SiO_2 [10,11]. This increase in viscosity of the amorphous phase during densification is responsible for the substantial increase in the temperature range over which the transformation occurs when MgO is replaced by SiO_2 [9]. Increasing the temperature range for the phase transformation (e.g., by replacing La_2O_3 by Lu_2O_3 or replacing MgO by SiO_2) will inhibit the formation of large elongated beta grains for each temperature-time condition [9].

By understanding the explicit role of the additives at the atomic scale and their impact on physical processes that occur during densification, one can now tailor the processing conditions for the specific additives employed to develop, in this case, a self-reinforced microstructure in silicon nitride ceramics. The proof of the concepts developed is demonstrated by the fact that silicon nitride ceramics containing the combination of the rare earth oxides and magnesia could be produced where each exhibited fracture strengths in excess of 1 GPa and fracture toughness values in the range of 10 to 15 $\text{MPa}\cdot\text{m}^{1/2}$ at room temperature combined with excellent strength retention at 1200°C (e.g., >800 MPa).

Future Plans: Papers on the influence of secondary additives (Al_2O_3 or SiO_2 as compared to MgO) on the adsorption behavior of rare earth additives and the impact on phase transformation and microstructural evolution in silicon nitride ceramics will be submitted to refereed journals. Extension of these fundamental concepts to other ceramic systems will be addressed in future studies. This task terminates at the end of FY 2008.

References

1. N. Shibata, S. J. Pennycook, T. R. Gosnell, G. S. Painter, W. A. Shelton, and P. F. Becher, "Observation of Rare Earth Segregation in Silicon Nitride Ceramics at Sub-Nanometer Dimensions," *Nature*, 428:730-33 (2004).
2. C. Dwyer, A. Ziegler, N. Shibata, G. B. Winkelmann, R. L. Satet, M. J. Hoffmann, M. K. Cinibulk, P. F. Becher, G. S. Painter, N. D. Browning, D. J. H. Cockayne, R. O. Ritchie, and S. J. Pennycook, "Interfacial Structure in Silicon Nitride Sintered with Lanthanide Oxides," *J. Mater. Sci.*, **41** 4405-12 (2006).

3. G. S. Painter, P. F. Becher, W. A. Shelton, R. L. Satet, and M. J. Hoffmann, "Differential Binding Model: Effects of Rare-Earths on β -Si₃N₄ Grain Growth and Microstructure," *Phys. Rev. B.*, 70:144108 (2004).
4. N. Shibata, G. S. Painter, R. L. Satet, M. J. Hoffmann, S. J. Pennycook and P. F. Becher, "Rare Earth Adsorption at Intergranular Interfaces in Silicon Nitride Ceramics: Sub-Nanometer Observations and Theory," *Phys. Rev. B.*, **72**, 140101 R-1 to -4 (2005).
5. N. Shibata, G. S. Painter, P. F. Becher and S. J. Pennycook, "Atomic Ordering at an Amorphous /Crystal Interface," *Appl. Phys. Lett.*, **89** 051908-1 to -3 (2006).
6. K. van Benthem, G. S. Painter F. W. Averill S. J. Pennycook and P. F. Becher, "Experimental Probe of Adsorbate Binding Energies at Internal Crystalline/Amorphous Interfaces," *Appl. Phys. Lett.*, submitted.
7. N. Shibata, P. F. Becher, G. S. Painter, "Interfacial Adsorption of Rare Earths in Si₃N₄ Ceramics Containing Minor MgO, Al₂O₃ or SiO₂ Additions," to be published.
8. P. F. Becher, G. S. Painter, N. Shibata, R. L. Satet, M. J. Hoffmann, and S. J. Pennycook, "Influence of Additives on Anisotropic Grain Growth in Silicon Nitride Ceramics," *Mater. Sci. Engr'g A*, 422: 85-91 (2006) - Invited.
9. P. F. Becher, G. S. Painter, N. Shibata, S. B. Waters and H.-T. Lin, "Effects of Rare Earth (RE) Intergranular Adsorption on the Phase Transformation, Microstructure Evolution and Mechanical Properties in Silicon Nitride with RE₂O₃ + MgO Additives: RE = La, Gd, Lu," *J. Am. Ceram. Soc.*, accepted.
10. P. F. Becher, M. K. Ferber, L. Riester, and S. B. Waters M. J. Hoffmann and R. Satet, "The Influence of Mg Substitution for Al on the Properties of SiREMe Oxynitride Glasses," *J. Non-Cryst. Solids*, 333(2) 124-8 (2004).
11. G. Pezzotti, K. Ota, Y. Yamamoto and H.-T. Lin, "Elementary Mechanisms Behind the High-Temperature Deformation Behavior of Lutetium-Doped Silicon Nitride," *J. Am. Ceram. Soc.*, 86(3) 471-74 (2003).

Publications from this this project, 2005-2007

1. Publications 2,4,5,8 and 9 above.
2. G. S. Painter and P. F. Becher, "Microstructural Design of Ceramics: Theory and Experiment," in *Ceramics Science and Technology, Vol. I*, edited by Prof. Ralf Riedel and Prof. I-Wei Chen, Wiley-VCH Weinheim, 2008.
3. V. Fouquet, F. Paumier, M. J. Guittet, M. Gautier-Soyer, R. Satet, M. Hoffmann, P.F. Becher, and G.S. Painter, Composition and local bonding in RE-Si-M-O-N (M = Mg, Al; RE = La, Lu) Glasses," *Appl. Surf. Sci.*, accepted.
4. H.-D. Kim, Y.-J. Park, B.-D. Han, M.-W. Park, W.-T. Bae, Y.-W. Kim, H.-T. Lin and P. F. Becher, "Fabrication of Dense Bulk Nano-Si₃N₄ Ceramics Without Secondary Crystalline Phase," *Scripta Mater.*, 54: 615-19 (2006).
5. P. F. Becher, S. Ii, Y. Ikuhara, G. S. Painter, and M. J. Lance, "Direct Observations of Debonding of Reinforcing Grains in Silicon Nitride Ceramics Sintered with Yttria Plus Alumina Additives," *J. Am. Ceram. Soc.* **88**(5), 1222-26 (2005).
6. C. H. Hsueh and C. R. Luttrell, "Recent Advances in Modeling Stress Distributions in Multilayers Subjected to Biaxial Flexure Tests," *Compos. Sci. Technol.*, 67 [2] 278–285 (2007). (invited)
7. C. H. Hsueh and G. A. Thompson, "Appraisal of Formulas for Stresses in Bilayered Dental Ceramics Subjected to Biaxial Moment Loading," *J. Dent.*, 35 [7] 600–606 (2007).
8. H. Conrad, D. Yang and P. Becher, "Effect of an Applied Electric Field on the Flow Stress of Ultrafine-Grained 2.5Y-TZP at High Temperatures," *Mater. Sci. & Engr. A*, in press.
9. Kosacki, C. M. Rouleau, P. F. Becher, J. Bentley and D. H. Lowndes, "Nanoscale Effects on the Ionic Conductivity in Highly Textured YSZ Thin Films," *Solid State Ionics*, 176: 1319-26 (2005).
10. C. H. Hsueh and P. F. Becher, "Effective Viscosity of Suspensions of Spheres," *J. Am. Ceram. Soc.*, 88(4) 1046049 (2005).

11. C.-H. Hsueh, P. Miranda and P. F. Becher, "An Improved Correlation Between Impression and Uniaxial Creep," *J. Appl. Phys.*, 99 113513-1 to -7 (2006).
12. C.-H. Hsueh, C. R. Luttrell and P. F. Becher, "Analyses of Multilayered Dental Ceramics Subjected to Biaxial Flexure Tests" *Dental Materials*, 22: 460-69 (2006).
13. C.H. Hsueh, C.R. Luttrell and P.F. Becher, "Modelling of Bonded Multilayered Disks Subjected to Biaxial Flexure Tests," *Int'l J. Solids and Structures*, 43: 6014-25 (2006).

Atomistic simulations of irradiated materials on the reactor timescales

Program title: Microstructural evolution and mechanical response of complex alloys under prolonged particle radiation

PI: Vasily Bulatov
L-367, P.O. Box 808, LLNL, Livermore, CA 94551

Scope and definition

Development of new quantitative methods for simulations of microstructure evolution in irradiated materials. New algorithms for microstructure simulations reaching length and time scales of material work-life in real reactors. This research projects responds to the need to enhance reliability of accelerated material tests in the testing facilities being developed within the R&D programs on fission and fusion reactors.

Background

Further development of nuclear energetics demands materials that can withstand harsh conditions of particle irradiation, high temperature and active chemical agents over tens of years. The only fully reliable method to evaluate the potential of a candidate material is to subject it to conditions relevant for the future reactor designs. However such is not a practical approach given that the relevant environment can be achieved only after the reactor is already built. Furthermore, even if an appropriate material testing facility were to exist, testing materials over the intervals of 50 years will never be a viable option. Thus, development of capabilities for reliable accelerated material testing becomes a critical priority for the future of nuclear energy R&D. The International Fusion Materials Irradiation Facility (IFMIF) planned for operation in 2017 illustrates the magnitude of challenges in materials development that the international community is currently trying to address. The cost of this famous project is enormous (nearly \$1B) requiring the participating nations to pool their resources.

An alternative approach to accelerated materials testing is undertaken by several research groups in Europe and Japan. As an example, JANNUS is a new multi-beam ion accelerator facility assembled by CEA (France) at the Saclay and Orsay centers. The new JANNUS facilities combine several existing ion accelerators with modern *in situ* and *ex situ* diagnostics, all at a relatively low cost. Using one of the accelerators to impart primary damage and the other accelerators to implant H and/or He₂, JANNUS can “simulate” a wide variety of irradiation conditions, including those produced in real reactors by neutron irradiation. Scheduled to start in 2008, a typical JANNUS experiment will use high particle fluxes to impart the same total damage as the material would receive over its entire work life in the future reactor. What remains unclear, both in the case of IFMIF neutron source and ion beam facilities like JANNUS, is whether the material performance observed over 6 hours of violent irradiation can be used to predict the behavior of the same material over the reactor lifetime. The premise of JANNUS and possible other future facilities for accelerated materials testing is that numerical simulations can provide a reliable connection between the accelerated tests and the material lifetime performance predictions.

There are two essential requirements to numerical simulations to be useful in this undertaking. The first is *fidelity*: the models should be based on accurately quantified mechanisms of material degradation. The second requirement is *computability*: the numerical algorithms should be as efficient as necessary to cover the relevant set of irradiation conditions in detail. If and when both conditions are met, numerical simulations will be able to serve as the bridge connecting the accelerated tests *a la* JANNUS to predictive work life material assessment. This work is a part of BES-funded project “Microstructural evolution and mechanical response of complex alloys under prolonged particle radiation” in which we develop, in collaboration with UIUC and CEA Saclay, the methods for accurate and computationally efficient simulations of damage accumulation on the time scales ranging from accelerated tests to the reactor lifetime.

Recent progress

Plethora of methods exist for computational prediction of microstructure of irradiated materials ranging from atomistic calculations of very high (chemical) accuracy to mean-field cluster-dynamics methods relying on various more or less crude approximations. As usual, the accuracy can be traded for computational efficiency. In this range, kinetic Monte Carlo (KMC) has arguably the greatest potential for accurate simulations connecting atomistic mechanisms of defect formation and motion directly to the kinetics of microstructural evolution. Numerous research efforts are now centered on obtaining accurate atomistic input to the KMC simulations of irradiated materials. The critical obstacle for the KMC approach is its low computational efficiency: current KMC simulations fall far short of the length and time scales relevant for microstructure evolution in the reactor environments. Especially wide is the time scale gap: whereas the time scale of atomistic diffusion can be of the order of nano-seconds, the resulting microstructure evolution has to be modeled on the reactor time-scale (tens of years).

The only seemingly plausible route to bridging this notorious time scale gap is to employ a coarse-grained description, such as phase-field method in which smoothly varying concentration field(s) are used to approximately represent material microstructure while the details of atomic positions in the crystal lattice are no longer considered. Remarkably, for a class of materials of interest (pure iron and dilute iron alloys), an alternative method exists that efficiently bridges the time scale gap all the while representing the material microstructure in full atomistic details. This is the method of first-passage kinetic Monte Carlo (FPKMC) developed recently by the PI and his team at LLNL.

When it comes to pure metals and dilute alloys, the main computational bottleneck for the detailed KMC simulations is the need for a very large number of Monte Carlo cycles required to bring the crystal defects (vacancies, interstitials, impurities and their clusters) into their interaction range by diffusive hops¹. As a result, simulations of radiation damage have been limited to rather small material volumes (typically no more than $1 \mu^3$) and very low irradiation doses (between 0.01 and 01 displacements per atom (dpa)). There have been several attempts to circumvent the need

¹ An additional serious difficulty arises when some of the unit mechanisms by which the model evolves have vastly different kinetic rates. Such stiffness is often, if not always, the case when it comes to simulations of material microstructures.

for the numerous diffusive hops [1,2], all of them achieve some improvements in the efficiency of KMC simulations but at a cost of their accuracy. The fundamental difficulty that neither of the earlier methods can fully address is that statistics of collisions in the system of N random walkers (diffusing crystal defects) is a difficult N -body problem in which the probability of collisions between, say, walkers 1 and 2, depends on all other $N-2$ walkers in the system. It is only in the limit of very small hops (in [1]) or vanishing time steps (in [2]) that such approximate methods become asymptotically exact. Unfortunately, in this same limit the mentioned methods lose their numerical efficiency.

Our new method FPKMC is based on the exact solutions for the first passage statistics of random walks and a time-dependent Green's function formalism [3]. Rather than relying on approximations, the method presents an exact numerical solution of the N -body problem for the statistics of collisions among N randomly diffusing particles. At the same time the method is strikingly more efficient than the approximate methods previously developed for KMC simulations of radiation damage or numerous other diffusion-controlled process. The method relies on the trick of spatial protection [4] to reduce the difficult N -body problem to a combination of much simpler 1-body and 2-body problems. The resulting FPKMC algorithm is asynchronous: every walker propagates within its personal space and time horizon. The numerical efficiency of the FPKMC algorithm derives from its ability to propagate the walkers over distances close to the average particle spacing on each Monte Carlo cycle coupled with the fact that the cost of such time step remains $O(1)$. At the same time, the algorithm is as exact as a Monte Carlo algorithm can be: for any number of walkers N , the statistics of simultaneous random walks with collisions is correctly reproduced in the limit of large number of independent Monte Carlo simulations.

We have performed numerous numerical tests in which the new method's accuracy and computational efficiency was amply demonstrated [3]. The FPKMC algorithm was shown to be capable of simulating systems with 10^9 diffusing particles and to cover time scales exceeding 200 decades, all at a modest computational cost (on a single CPU workstation). Given its accuracy and efficiency, the FPKMC algorithm seems to be ideally suited for atomistic simulations of damage accumulation in irradiated materials. In addition to circumventing the need for the numerous atomic hops, the method efficiently addresses the problem of disparate kinetic rates: in some of our recent simulations the ratio of maximum-to-minimum kinetic rates reached over 15 orders of magnitude yet the simulations remained efficient. We have recently completed an extension of the FPKMC method to simulations of damage accumulation under electron and particle (neutron, ion) irradiation. This extension required us to find efficient ways to handle, in addition to defect diffusion, the reactions of defect annihilation and agglomeration (clustering), emission of monomers from defect clusters, insertion of new defects in the form of Frenkel pairs or displacement cascades, interaction with defect sinks and others.

Our new computer code employs a general protocol for the code user to define new models for a wide range of materials under irradiation. First, the code has been tested on a set of relatively simple models of pure iron subjected to electron irradiation up to a low dose of 0.018 dpa. The method surpassed our expectations for computational performance: whereas previously the same simulations required days of continuous

computing [5], it has taken us just 10 minutes with the new method to reproduce the earlier results. Given the method's demonstrated efficiency, we continued simulations of the same model material to the doses 3 orders of magnitude higher than was previously accessible, e.g. to 20-30 dpa. We believe ours are the first ever atomistic KMC simulations of radiation damage to the doses typical of real nuclear reactors. What is even more remarkable is that the method's high efficiency is not limited to the typically high damage dose rates ($\sim 10^{-4}$ dpa/s) assumed in the earlier KMC simulations whose numerical efficiency deteriorates with the decreasing dose rates. In contrast, the new method performs admirably down to dose rates typical of real reactors (10^{-8} dpa/s) and lower.

Encouraged by this high efficiency we performed two series of simulations at two different dose rates: (series 1) at a dose rate of 10^{-4} dpa/s typical of the accelerated material tests in ion beam facilities and (series 2) at a lower dose rate of 10^{-8} dpa/s typical of the conditions in the current reactors. Each of the two series contained simulations performed at five different temperatures selected to evaluate, by numerical simulations, if the damage accumulated in iron under high rate irradiation can be used to predict the damage that will be accumulated in the same material on a much longer time scale of the actual reactors [6]. The results suggest that the rates of microstructural evolution can be enhanced by 4 orders of magnitude in the accelerated tests by raising the test temperature so that the resulting damage at an end-of-life dose (~ 20 dpa) will be approximately the same as that in the reactor conditions but a lower temperature. The observed scaling is only approximate and some differences in the resulting microstructures are clearly detectable. Nevertheless, our observations encourage us to think that accurate KMC simulations of damage accumulation in irradiated materials can be meaningfully employed for enhancing reliability of the accelerated material tests.

On-going work and future plans

Together with our collaborators at CEA Saclay we are now developing new, more accurate models of iron under multi-beam irradiation. The new models will include He, H, C and possibly other minor alloying elements. Simultaneously, we are also working on a novel computational approach of multi-resolution Monte Carlo that can potentially bridge the length and time scales gaps still existing in KMC simulations of concentrated multi-component alloys. We intend to develop several new algorithmic ideas to accelerate the overall rate of the lattice KMC by many orders of magnitude while retaining the method's accuracy as required for simulations of material microstructure on the length and time scales relevant for the future nuclear energy systems.

References

- [1] J. S. van Zon and P. R. ten Wolde, *J. Chem. Phys.* **123**, 234910 (2005).
- [2] J. Dalla Torre, J.-L. Bocquet, N.V. Doan, *et al.*, *Philos. Mag.* **85**, 549 (2005).
- [3] T. Opperstrup, V.V. Bulatov, G.H. Gilmer, *et al.*, *Phys. Rev. Lett.* **97**, 230602 (2006).
- [4] M. H. Kalos, D. Levesque, and L. Verlet, *Phys. Rev. A* **9**, 2178 (1974).
- [5] A. Barbu, C. S. Becquart, J.L. Bocquet, *et al.*, *Philos. Mag.* **85**, 541 (2005).
- [6] M.J. Caturla, T. Diaz de la Rubia, and M. Fluss. *J. Nucl. Mater.* **323**, 163 (2003).

Mechanics of Small Length Scales

David M. Follstaedt, Elizabeth A. Holm, Jianyu Huang, and John P. Sullivan
dmfolls@sandia.gov, eaholm@sandia.gov, jhuang@sandia.gov, jpsulli@sandia.gov
Sandia National Laboratories, Albuquerque, NM 87185

Program Scope:

The *Mechanics of Small Length Scales* project encompasses three major thrust areas: Mechanical Properties of Nanostructured Materials, Theory of Microstructures and Ensemble Controlled Deformation, and Mechanics and Dynamics of Nanostructured and Nanoscale Materials. These thrusts combine theory and experiment in order to obtain atom-level control and understanding of properties. Specific interests include the elastic and plastic deformation of bulk and nanostructured materials, the thermal evolution of a material's micro- and nanostructure, anelastic relaxation, and atomic-scale studies of mechanical deformation in nanoscale materials.

Recent Progress/Future Directions:

Mechanical Properties of Nanostructured Materials. This thrust area focuses on understanding the deformation mechanisms and resulting strengths of nanostructured metals, and on determining the stability of these structures.

We use special synthesis methods to produce metals with highly refined nanostructures, and then determine their strengths. For instance, we used ion implantation to form high densities of nanometer-scale oxide precipitates in metals, evaluated their strengths by combining nanoindentation with finite-element modeling, and showed that yield strength is well accounted for by the Orowan mechanism where precipitates block dislocation motion. More recently, we have shown that He bubbles (Fig. 1a) also block dislocation motion and produce similar high strengths (2.9 GPa), but by a different mechanism: the dislocations become bound to the bubbles.

We also examined the strength of fine-grained Ni (~10 nm) produced by pulsed-laser deposition, and found that Hall-Petch scaling of strength and hardness extends to such small grain sizes. Our recent collaborations with Univ. Pittsburgh (Profs. Mao and Wiezorek) and NCEM (E. Stach) used in-situ TEM to identify deformation mechanisms in this material, and found rather direct evidence that grain rotation is a prominent mechanism along with dislocation motion. We also demonstrated that individual grains in this material can undergo quite high lattice distortions. The grain agglomerates formed by the rotation appear closely related to the dimpled surfaces found when nanocrystalline metals are fractured (Fig. 1b).

The nanocrystalline Ni is found to be unstable with respect to abnormal grain growth at modest temperatures (250-400°C, work with Prof. Robertson, Univ. Illinois); see Fig. 1c. Unexpectedly, the enlarged grains contain numerous defects, including twins, stacking faults, dislocations and stacking fault tetrahedra, which are thought to be related to their growth into the nanocrystalline metal with its high density of grain boundaries. In addition to wanting to understand the stability limits of nanostructured metals, we are interested in the mechanical properties of the bimodal structures produced by the enlarged abnormal grains in the metal. The bimodal structure is expected to exhibit much greater ductility than the original nanocrystalline metal while retaining some of its high strength.

Theory of Microstructures and Ensemble Controlled Deformation. The goal of this thrust area is to combine experiment, modeling, and simulation to construct, analyze, and utilize three-dimensional (3D) polycrystalline micro- and nano-structures.

In support of the experimental work on abnormal grain growth described previously, we have extended our successful model for abnormal subgrain growth to include nanocrystalline film structures, including the appropriate geometry, crystallography, and grain boundary properties. Since surface effects are particularly relevant to nanocrystalline films, we include both geometric surface effects (i.e. the transition from equiaxed to columnar growth) as well as surface free energy anisotropy in the model. To ensure equivalence with experimental systems, we are also implementing the capability to create simulation microstructures directly from EBSD micrographs. Finally, since particle pinning is a proposed

mechanism for controlling nanocrystalline grain growth, we have studied particle effects on abnormal growth. We find that, depending on the initial conditions, particles may have a profound effect on grain evolution – or almost none at all.

Because both normal and abnormal grain growth are governed by grain boundary properties, we focus on quantifying the properties of Ni grain boundaries. In particular, we have developed an automated way to generate minimum energy grain boundary structures, which we utilize in novel molecular dynamics (MD) simulations to determine boundary energy and mobility for a large catalog of grain boundaries, as shown in Figure 2. Polycrystalline MD simulations also elucidate the interaction between grain boundaries and vacancies that may lead to defect generation. Finally, new polycrystal plasticity models will help characterize the mechanical properties of nanocrystals, with particular attention to the role of the grain size distribution on strength and ductility.

Mechanics and Dynamics of Nanostructured and Nanoscale Materials. The objective of this thrust area is to develop atomic-scale understanding of dynamic processes in materials. These include internal dissipation and defect motion during plastic deformation of nanotubes and nanowires.

Our recent experimental work in internal dissipation is focused on anelastic relaxation in nanostructured materials, including nanocrystalline Ni films and nanoporous metals. This latter activity includes collaboration with A. Misra et al. (Los Alamos National Lab) and their nanoporous materials of Au and Pt. Molecular dynamics simulation of internal dissipation in nanocrystals of silicon containing a split interstitial defect have recently been completed. Matching between the defect relaxation rate and the longitudinal acoustic wave frequency produces a unique temperature-dependent signature characteristic of this defect. Due to the importance of phonon transport and scattering in internal dissipation of nanoscale materials, a new activity has been initiated to probe boundary scattering processes in phonon transport. The experimental structure enables the measurement of differential thermal conductivity between two nanoscale specimens – a control structure and a test structure that has been modified in order to increase boundary scattering.

With the recent arrival of Jianyu Huang to Sandia (formerly of Boston College), new activities are being initiated within this thrust to image defect motion and plastic deformation in nanoscale materials with atomic scale resolution. This capability consists of a unique transmission electron microscopy + scanning probe microscopy (TEM-SPM) platform, wherein fully functional scanning probe microscopes, including a scanning tunneling microscope (STM), an atomic force microscope (AFM), and a nanoindenter, are integrated into a high resolution TEM. This platform has enabled the understanding of atomic scale deformation processes in carbon nanotubes (CNTs) and elucidated a number of novel deformation mechanisms, such as superplastic elongation, dislocation glide-induced cross-linking of nanotube walls, kink motion, the electrical transport properties of each individual wall in a multi-wall CNT, and the formation mechanisms of buckyballs [1-10]. One such example that reveals the experiment and simulation of dislocation dynamics in a CNT is shown in Fig. 3 [6]. Current experiments are focused at understanding dislocation structures, size-mediated plasticity, internal energy dissipation mechanisms, and the electrical-mechanical coupling mechanisms of CNTs and nanowires.

- [1] Huang, J.Y. et al. Superplastic carbon nanotubes - Conditions have been discovered that allow extensive deformation of rigid single-walled nanotubes. *Nature* **439**, 281-281 (2006).
- [2] Huang, J.Y. et al. Atomic-scale imaging of wall-by-wall breakdown and concurrent transport measurements in multiwall carbon nanotubes. *Physical Review Letters* **94**, 236802 (2005).
- [3] Huang, J.Y. et al. Enhanced ductile behavior of tensile-elongated individual double-walled and triple-walled carbon nanotubes at high temperatures. *Physical Review Letters* **98**, 185501 (2007).
- [4] Huang, J.Y. et al. Kink formation and motion in carbon nanotubes at high temperatures. *Physical Review Letters* **97**, 075501 (2006).
- [5] Huang, J.Y., Ding, F., Jiao, K. & Yakobson, B.I. Real time microscopy, kinetics, and mechanism of giant fullerene evaporation. *Physical Review Letters* **99**, 175503 (2007).
- [6] Huang, J.Y., Ding, F. & Yakobson, B.I. Dislocation dynamics in multiwall carbon nanotubes. *Physical Review Letters* **100**, 035503 (2008).
- [7] Huang, J.Y. Vacancy motion in carbon nanotubes. (*to be submitted*) (2008).
- [8] Huang, J.Y., Chen, S., Ren, Z.F., Chen, G. & Dresselhaus, M.S. Real-time observation of tubule formation

- from amorphous carbon nanowires under high-bias Joule heating. *Nano Letters* **6**, 1699-1705 (2006).
- [9] Huang, J.Y. In situ observation of quasimelting of diamond and reversible graphite-diamond phase transformations. *Nano Letters* **7**, 2335-2340 (2007).
- [10] Huang, J.Y., Ding, F., Jiao, K. & Yakobson, B.I. Self-templated growth of carbon-nanotube walls at high temperatures. *Small* **3**, 1735-1739 (2007).

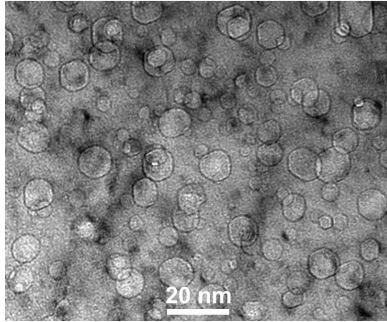


Fig. 1a. TEM image of He bubbles formed by ion implanting 5 at% He into Ni at 500°C.

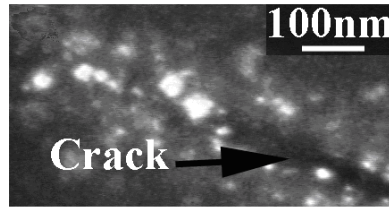


Fig. 1b. *In-situ* TEM image of crack advancing into nanocrystalline Ni, with grain agglomerates (bright, larger than nanograins) forming around it.

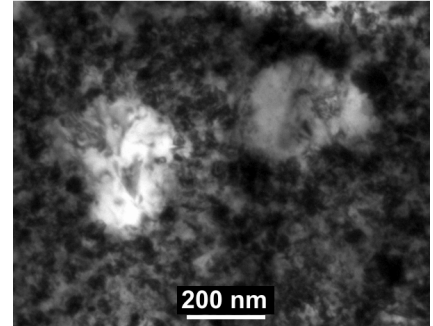


Fig. 1c. Two abnormal grains (~300nm) with internal defects growing into nanocrystalline Ni grains (10-20 nm) at 275°C.

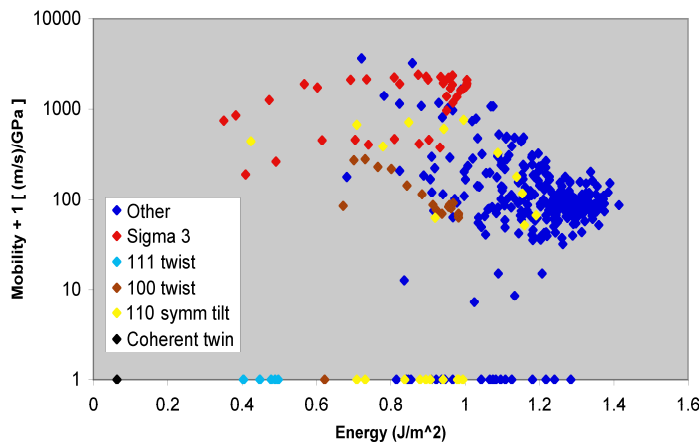


Fig. 2. Boundary mobility versus energy for 388 Ni grain boundaries, as determined from molecular dynamics simulations. Note that contrary to conventional wisdom, energy and mobility are not highly correlated.

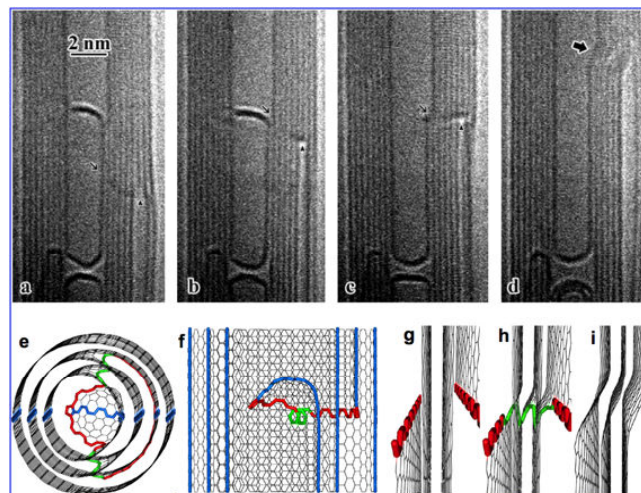


Fig. 3. In-situ dislocation dynamics in a multiwalled CNT. Arrowheads and slim arrows point out the dislocation cores and the dislocation lines, respectively. The fat arrow points out a kink. As the dislocation or kink passes by, a

nanocrack was created in (a)-(d). The core of the edge and screw dislocations in (e)-(i) is marked in red, and green, respectively. (a) A dislocation with a Burgers vector of $\frac{1}{2}[0001]$ is nucleated. (b) The dislocation climbs up. (c) A dislocation with a Burgers vector of $\frac{1}{2}[000-1]$ is formed, and it interacts with the climbing-up $\frac{1}{2}[0001]$ dislocation. (d) The $\frac{1}{2}[0001]$ dislocation annihilates with the $\frac{1}{2}[000-1]$ dislocation, forming a kink. (e)-(f) An atomic structural model of the dislocation in (c). The dislocation loop has two edge (red) and two screw components (green). The atoms marked in blue are for reference. (g)-(i) Schematic structural model explaining the kink formation due to the interaction of a $\frac{1}{2}[0001]$ and a $\frac{1}{2}[000-1]$ dislocations in graphite layers.

DOE/BES Sponsored Publications CY 2007-2008

DISLOCATION DYNAMICS IN NANOCRYSTALLINE NICKEL, Z. Shan, D. M. Follstaedt, J. M. K. Wiezorek, J. A. Knapp, E. A. Stach and S. X. Mao, *Phys. Rev. Lett.* **98**, 095502 (2007).

DEFECT STRUCTURES PRODUCED BY LOW TEMPERATURE ANNEALING OF PULSED-LASER DEPOSITED NICKEL, K. Hattar, D. M. Follstaedt, J. A. Knapp and I. M. Robertson, *Acta Mat.* **56**, 794-801 (2008).

HARDENING BY BUBBLES IN He-IMPLANTED NICKEL, J. A. Knapp, D. M. Follstaedt and S. M. Myers, *J. Appl. Phys.* **103**, 013518 (2008).

LARGE LATTICE STRAIN IN INDIVIDUAL GRAINS OF DEFORMED NANOCRYSTALLINE Ni, Z. Shan, J. M. K. Wiezorek, J. A. Knapp, D. M. Follstaedt, E. A. Stach and S. X. Mao, *Applied Physics Letters*, in press 2008.

FORMATION MECHANISM OF DIMPLED FRACTURE SURFACES OF NANOCRYSTALLINE MATERIALS, Z. Shan, J. A. Knapp, D. M. Follstaedt, J. M. K. Wiezorek, E. A. Stach and S. X. Mao, *Physical Review Letters*, in press 2008.

GRAIN BOUNDARY INTERFACE ROUGHENING TRANSITION AND ITS EFFECT ON GRAIN BOUNDARY MOBILITY FOR NON-FACETING BOUNDARIES, D. Olmsted, S. M. Foiles, E. A. Holm, *Scripta Mater.* **57**, 1161 (2007).

EFFECTS OF GRAIN BOUNDARY CONSTRAINT ON PROPERTIES OF POLYCRYSTALLINE MATERIALS, E. S. McGarrity, K. S. McGarrity, P. M. Duxbury, B. W. Reed, E. A. Holm, (2007 Annual Highlight Article) *Mod. Simul. Mater. Sci. Eng.* **15**[4] S353 (2007).

CONSTRAINT EFFECTS IN GRAIN BOUNDARY NETWORKS, E.S. McGarrity, P.M. Duxbury, E.A. Holm, and B. Reed, *Proc. 3rd Int. Conf. Multiscale Mater. Model.*, P. Gumbsch (editor) (Fraunhofer Institute, Freiburg, Germany, 2006) pp. 289-291.

ROUGHNESS SCALING IN GBE MATERIALS, P. M. Duxbury, E. S. McGarrity, and E. A. Holm, *Proc. 11th Int. Conf. Fracture*, A. Carpinteri (editor) (ICF, Turin, Italy, 2006).

MEASURING STRESS GRADIENTS BY ETCH-BACK IN ANNEALED DIAMOND-LIKE TETRAHEDRAL AMORPHOUS-CARBON THIN FILMS, T. A. Friedmann and J. P. Sullivan, submitted to *Thin Solid Films* (2007).

HIGH PERFORMANCE POLYCRYSTALLINE DIAMOND MICRO AND NANO RESONATORS, N. Sepúlveda, J. Lu, D. M. Aslam, and J. P. Sullivan, *J. MEMS*, in press (2008).

CHARACTERIZATION OF BONDING CONFIGURATION IN FURNACE ANNEALED AND LASER ANNEALED TETRAHEDRAL AMORPHOUS CARBON (TA-C) THIN FILMS, D. S. Grierson, A.V. Sumant, A. R. Konicek, T. A. Friedmann, J. P. Sullivan, and R. W. Carpick, submitted to *Phys. Rev. B* (2008).

NANOMECHANICAL RESONATOR ARRAYS IN ONE AND TWO DIMENSIONS, J. P. Sullivan, D. A. Czaplewski, T. A. Friedmann, and J. R. Wendt, submitted to *Int. J. Nano Systems and Tech.* (2008).

Multiscale Mechanical Properties and Alloy Design

Principal Investigators

E. P. George, H. Bei, J. R. Morris, C. T. Liu, J. A. Horton
Materials Science and Technology Division, Oak Ridge National Laboratory, 1 Bethel Valley Road, Oak Ridge, TN 37831-6115. Email: georgeep@ornl.gov, beih@ornl.gov, morrisj@ornl.gov, liuct@ornl.gov, hortonja@ornl.gov

Principal Collaborators

G. M. Pharr, Y. F. Gao, Department of Materials Science and Engineering, University of Tennessee

Program Scope

This program aims to develop fundamental understanding of mechanical behavior across multiple length scales in metals and alloys. Of special interest are new mechanical phenomena, including size effects on mechanical properties, unusually high ductility in B2-structured rare-earth ordered alloys, magnetic effects on strength and ductility, and pseudoelasticity in the absence of obvious structural transformations. Interesting size effects occur at several different length scales, but our near-term focus is on small-scale mechanical behavior. Over the long term, our goal is to understand the physical mechanisms of interaction across multiple length scales in multiphase alloy systems. The observed relationships between mechanical properties and microstructural features (controlled, as needed, by innovative processing techniques and characterized by state-of-the-art microanalytical tools) are used to model deformation and fracture processes. This understanding leads to the formulation of broad scientific principles for the design of advanced metallic materials for use in a variety of next-generation energy production and conversion applications.

Recent Progress

Because of space limitations it will not be possible to describe fully our recent research progress; rather only selected highlights are provided below. A partial list of publications resulting from this work is provided at the end of this abstract.

Small-scale mechanical behavior

In many cases one needs to be able to measure and understand the mechanical behavior of small volumes of materials including, for example, structural materials in which the constituent phases can have length scales of a few nanometers to hundreds of nanometers. It is also necessary sometimes to know how mechanical properties vary from point to point in a complex structural component, in order to understand both how properties evolved from prior processing and to predict future service behavior. To accomplish this, spatially resolved mechanical tests can be performed *in situ*, e.g., by micro/nanoindentation, or *ex situ* by micro-machining small-scale specimens from the regions of interest and conducting micro-compression/tensile tests. Regardless of the manner in which the tests are performed, it is important to understand how the measured mechanical properties are influenced by the small length scales of the tested materials.

Recently, a new micro-compression test was developed to measure the small-scale mechanical behavior of free-standing pillars [1]. Using this method, micro-pillars with sizes down to a few hundred nanometers have been fabricated and tested in compression [e.g., 2]. The compression testing is typically conducted in a modified nanoindentation system equipped with a flat-tip indenter and, as in the case of bulk compression tests, is believed to largely avoid strain-gradient effects, although recent tensile tests on long-gage-length specimens [3] suggest that end effects can influence the measured strengths. Several methods can be used to fabricate micro-pillars for compression testing, but the most common technique is fabrication from bulk materials by focused ion beam (FIB) milling.

Recently, we developed an alternative technique to produce single crystal micro-pillars that avoids FIB milling. Our technique involves directional solidification of eutectic alloys to produce long-aspect-ratio fibrous composites, followed by etching away of the matrix to expose the fibers as free-standing micro-pillars [4]. By controlling the directional solidification rate, the spacing and size of the pillars can be systematically varied, as shown in Fig. 1. In the case of NiAl-Mo eutectics, the matrix has the composition Ni-45Al (at.%) and the pillars, which are approximately square in cross-section, have the composition Mo-10Al-4Ni (at.%). The matrix and fiber are both single crystals and grow along $\langle 100 \rangle$ with $\{110\}$ interfaces.

Compression tests of these Mo-alloy micro-pillars showed that, after an initial elastic regime, they all yielded at shear stresses close to the theoretical strength ($\sim \mu/26$, where μ is the shear modulus), independent of size for sizes in the range 360~1000 nm [5]. Figure 2 shows representative load-displacement curves along with images

of several pillars before compression. Only those tests where the flat-punch indenter landed squarely on individual pillars were included in our analysis. Table 1 summarizes the yield strength data from a number of valid tests on pillars of different sizes which shows that the directionally solidified Mo-alloy micropillars behave like dislocation-free materials.

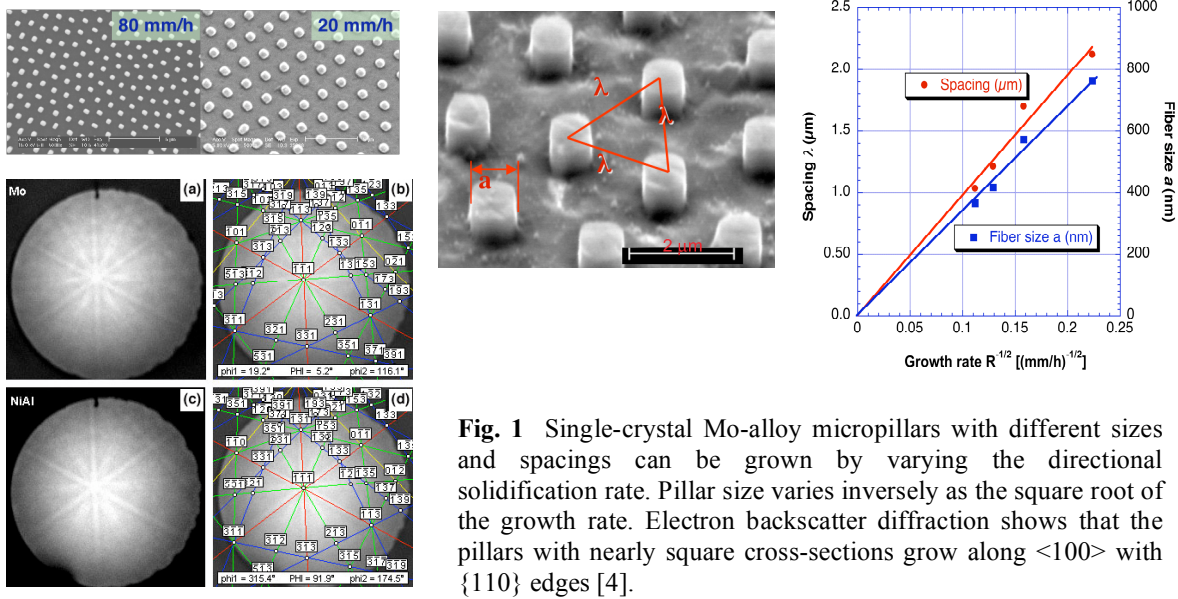


Fig. 1 Single-crystal Mo-alloy micropillars with different sizes and spacings can be grown by varying the directional solidification rate. Pillar size varies inversely as the square root of the growth rate. Electron backscatter diffraction shows that the pillars with nearly square cross-sections grow along $\langle 100 \rangle$ with $\{110\}$ edges [4].

Because the directionally solidified micro-pillars behave like dislocation-free materials, they provide a unique opportunity to probe dislocation nucleation events. Additionally, by comparing their yield strengths with the pop-in stresses obtained from nanoindentation experiments we showed recently [6] that it is possible to experimentally distinguish between homogeneous and heterogeneous dislocation nucleation. In nanoindentation tests, the stress state is nonuniform, and the resolved shear stress on potential slip systems reaches a maximum underneath the contact. Therefore, dislocation nucleation is expected to occur inside the solid. In micro-pillar compression tests, on the other hand, the stress field is, in principle, uniform, and dislocation nucleation can occur anywhere in the gage section including at free surfaces and edges. Consequently, in nanoindentation, dislocation nucleation is likely to occur homogeneously in the bulk, as full dislocation loops but, during micro-pillar compression, it is expected to occur heterogeneously at surfaces and edges, as half or quarter dislocation loops.

To verify this, nanoindentation was performed on bulk single crystals and free standing short micro-pillars using indenters with 178 and 580-nm tip radii. As shown in Table 2, the critical shear stress for dislocation nucleation during nanoindentation is $\sim 1/8$ of the shear modulus for two different Mo-alloy single crystals (Mo-3Nb and Mo-10Al-4Ni). The corresponding stress in uniaxially compressed Mo-10Al-4Ni micropillars is $\sim 1/26$ of the shear modulus. Our analysis shows that this strength difference is due to the higher critical stress required to nucleate a full dislocation loop homogeneously in the bulk as opposed to a half or quarter loop heterogeneously at a surface or edge.

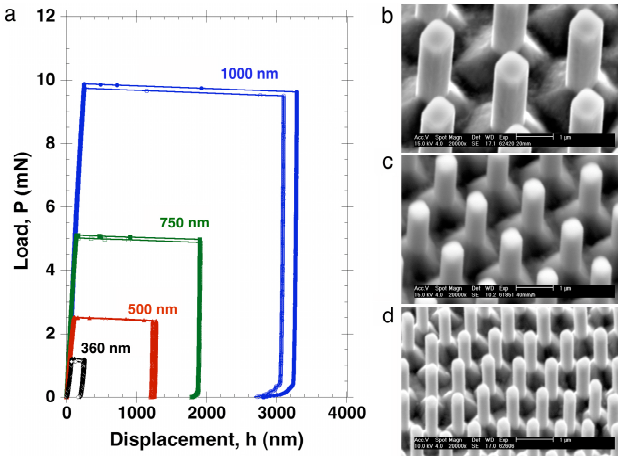


Fig. 2 Micro-compression tests of Mo-alloy pillars with sizes in the range 360-1000 nm: (a) Compressive load-displacement curves; SEM images of micropillars with nominal edge dimensions of (b) 750 nm, (c) 500 nm, and (d) 360 nm [5].

Table 1. Summary of compressive yield strengths of Mo alloy micro-pillars. The pillars all yielded at ~ 9 GPa (i.e., at $\sim \mu/26$) independent of size [5].

Nominal pillar size, a [μm]	Number of valid tests	Measured area, A [μm^2]	Compressive yield strength [GPa]
1.00	5	1.00 ± 0.02	9.17 ± 0.44
0.75	4	0.58 ± 0.02	9.24 ± 0.77
0.50	12	0.26 ± 0.02	9.30 ± 0.48
0.36	9	0.13 ± 0.02	9.18 ± 1.16

Table 2 Mechanical properties of Mo-alloy single crystals evaluated from nanoindentation and micro-pillar compression tests. The shear strength (τ_{max}) is calculated by using the pop-in load and the slip system that has the maximum resolved shear stress [6].

	$P_{\text{pop-in}}$ (mN)	τ_{max} (GPa)	τ_{max}/μ	μ/τ_{max}
<i>Nanoindentation</i>				
Bulk Mo-3Nb ($R=580\text{nm}$)	3.08 (mean)	15.1	0.116	8.62
	3.29 (upper bound)	15.4	0.119	8.43
Bulk Mo-3Nb ($R=178\text{nm}$)	0.329 (mean)	15.7	0.121	8.27
	0.359 (upper bound)	16.2	0.125	8.03
Pillar Mo-10Al-4Ni ($R=178\text{nm}$)	0.31 (mean)	14.8	0.123	8.13
<i>Micro-compression</i>				
Pillar Mo-10Al-4Ni	n/a	4.6	0.038	26.2

Understanding the fundamentals of unusual ductility in B2 rare-earth alloys

Promoting ductility in polycrystalline, highly ordered B2 alloys has been a long-time goal. Recently, there have been several reports of ductility in such compounds, particularly in rare-earth based materials such as YAg. These materials are line compounds, with high anti-phase boundary (APB) energies; however, they can exhibit significant tensile elongations. The origins of this unusual behavior are not understood, in particular the mechanisms of deformation. Understanding this may lead to new strategies for optimizing other B2 materials as well.

We have recently demonstrated that observed deformation modes in these systems are possibly related to phase transformations to other crystal structures, in particular to the B33 CrB-type structure and the related B27 FeB-type structure [7]. *Ab initio* calculations show that these structures compete closely with the B2 structure, resulting in low stacking fault energies on the B2 $\{110\}$ planes. The transformation from B2 to B33 is shown to be related to that in shape memory alloys such as NiTi. We predict that the B2 $\langle 100 \rangle$ dislocations may be dissociated, due to a low stacking fault energy on $\{110\}$ planes, with a stacking fault that produces local stacking similar to the B33 crystal phase that closely competes in these systems. Such dissociations have been observed in the low-temperature NiTi phase, and in similar materials including ZrCo. We have also used *ab initio* calculations to demonstrate that ZrCo, a B2 compound with reasonable ductility, also has the B33 phase as a ground state, with a small barrier to transformation. This barrier may explain why this phase has not been observed experimentally, though it has been observed in related ternary alloys and in ZrCo near crack tips. This suggests that these materials may exhibit transformation toughening.

Future Plans

Pillars produced by directional solidification offer a unique opportunity to investigate small-scale mechanical behavior because we can systematically introduce dislocations by room-temperature pre-straining to study the effects of initial dislocation structure on pillar behavior without the confounding effects of other defects that may be present in FIB-milled pillars. To this end, we plan to pre-strain the NiAl-Mo composites to different amounts and then etch away the matrix to reveal free-standing pillars with different sizes and dislocation densities. Micro-compression experiments on such pillars will allow us to probe the transition from discrete to collective dislocation behavior. Complementary nanoindentation experiments to shed further light on this transition are also planned.

Our calculations have shown that pseudo-binary systems may provide a convenient approach to test the effect of B2/B33/B27 relative phase stability on ductility. For example, YNi is B27 at all temperatures, while YZn is B2 at all temperatures with a large energy difference between the B2 phase and the competing structures. $\text{YNi}_{0.5}\text{Zn}_{0.5}$ is predicted to have phase stability similar to that of YCu, which exhibits significant tensile ductility. Thus, by tuning the composition, the phase stability may also be tuned, and effects on ductility may be measured. This approach will be used experimentally to examine these materials. Further calculations will focus on transformation pathways and generalized stacking fault surfaces, as well as the development of empirical atomistic potentials to allow examination of dislocation core structure and other defect properties in these materials.

References

1. M. D. Uchic, D. M. Dimiduk, J. N. Florando, and W. D. Nix, *Science* **305** (2004) 986-989.
2. J. R. Greer and W. D. Nix, *Phys. Rev. B* **73** (2006) 245410.
3. D. Kiener, W. Grosinger, G. Dehm, and R. Pippan, *Acta Mater.* **56** (2008) 580-592.
4. H. Bei and E. P. George, *Acta Mater.* **53** (2005) 69-77.
5. H. Bei, S. Shim, E. P. George, M. K. Miller, E. G. Herbert, and G. M. Pharr, *Scr. Mater.* **57** (2007) 397-400.
6. H. Bei, Y. F. Gao, S. Shim, E. P. George, and G. M. Pharr, *Phys. Rev. B* **77** (2008), 060103(R).
7. J. R. Morris and Y. Y. Ye, *Acta Mater.* (2008), submitted.

Partial list of DOE Sponsored Publications in 2005-2007

1. H. Bei, S. Shim, E. P. George, M. K. Miller, and G. M. Pharr, "Effects of focused ion beam milling on the nanomechanical behavior of a molybdenum-alloy single crystal," *Appl. Phys. Lett.* **91** (2007) 011915.
2. L. Yang, X. L. Wang, C. T. Liu, J. A. Fernandez-Baca, C. L. Fu, J. W. Richardson, and D. Shi, "Neutron diffraction study of the structure and low-temperature phase transformation in ternary NiAl+M alloys," *Scr. Mater.* **56** (2007) 911-914.
3. Y. Yamamoto, M. P. Brady, Z. P. Lu, P. J. Maziasz, C. T. Liu, B. A. Pint, K. L. More, H. M. Meyer, and E. A. Payzant, "Creep-resistant, Al_2O_3 -forming austenitic stainless steels," *Science* **316** (2007) 433-436.
4. Y. Liu, H. Bei, C. T. Liu, and E. P. George, "Cooling-rate induced softening in a Zr50Cu50 bulk metallic glass," *Appl. Phys. Lett.* **90** (2007) 071909.
5. C. T. Liu, C. L. Fu, M. F. Chisholm, J. R. Thompson, M. Krcmar, and X. L. Wang, "Magnetism and solid solution effects in NiAl (40% Al) alloys," *Prog. Mater. Sci.* **52** (2007) 352-370.
6. J. R. Morris, Y. Y. Ye, M. Krcmar and C. L. Fu, "The Role of Phase Stability in Ductile, Ordered B2 Intermetallics," in *Advanced Intermetallic-Based Alloys*, edited by J. Wieszorek, C.L. Fu, H. Clemens, M. Takeyama, D. Morris, MRS Proceedings, **980**, II06-10 (2007).
7. M. Krcmar, C. L. Fu and J. R. Morris, "Structural transformations and improved ductility in ordered FeCo and ZrCo intermetallics," in *Advanced Intermetallic-Based Alloys*, edited by J. Wieszorek, C.L. Fu, H. Clemens, M. Takeyama, D. Morris, MRS Proceedings, **980**, II02-03 (2007).
8. O. N. C. Uwakweh and C. T. Liu, "Mossbauer effect measurement evidence for magnetic transition in ordered Fe-doped NiAl," *Intermetallics* **15** (2007) 98-102.
9. D. Wu, I. Baker, P. R. Munroe, and E. P. George, "The yield strength anomaly of single-slip-oriented Fe-Al single crystals," *Intermetallics* **15** (2007) 103-107.
10. J. H. Strader, S. Shim, H. Bei, W. C. Oliver, and G. M. Pharr, "An experimental evaluation of the constant s relating the contact stiffness to the contact area in nanoindentation," *Philos. Mag.* **86** (2006) 5285-5298.
11. H. Bei, S. Xie, and E. P. George, "Softening caused by profuse shear banding in a bulk metallic glass," *Phys. Rev. Lett.* **96** (2006) 105503.
12. H. Bei, E. P. George, J. L. Hay, and G. M. Pharr, "Influence of Indenter Tip Geometry on Elastic Deformation During Nanoindentation," *Phys. Rev. Lett.* **95** (2005) 045501.
13. K. M. Youssef, R. O. Scattergood, K. L. Murty, J. A. Horton, and C. C. Koch, "Ultrahigh strength and high ductility of bulk nanocrystalline copper," *Appl. Phys. Lett.* **87** (2005) 091904.
14. J. R. Morris, Y. Y. Ye, and M. H. Yoo, "First-principles examination of the (1012) twin boundary in hcp metals," *Philos. Mag.* **85** (2005) 233-238.

On the relevance of interfaces to the properties of nanolayered composites

R. G. Hoagland^a, A. Misra^b, M. J. Demkowicz^a, and J. Wang^a

hoagland@lanl.gov

^aMST Division and ^bMPA Division

Los Alamos National Laboratory

Los Alamos, NM 87545

Atomic environments—structural units defined by the relative configuration of an atom and its neighbors—inside and in the vicinity of an interface may be distinctly different from those in the neighboring perfect crystals. Some interfaces have structures that are easily inferred such as a $\Sigma 3$ symmetric twin boundary in an fcc crystal. Most other interfaces possess atomic structures that are not so “intuitive” and may require many variables to adequately define the atomic configuration in and near the interface. Such interfaces are much more interesting than the simple twin interface, because they often possess many metastable states for a given set of macroscopic degrees-of-freedom. These various states may differ in energy, but by relatively small amounts, and may be separated by small energy barriers. Consequently, they may easily change state, and, therefore, configuration, in response to changes in stress, temperature, and composition. These easy configurational changes enable such multi-state interfaces to actively participate in and influence a broad array of reactions and processes. In this talk we will focus on the atomic structure of interfaces in incommensurate systems and present some new results showing the relevance of this structure to dislocation and point defect interactions. These results help to explain the behavior of nanolayered composites.

New x-ray and neutron tools for exploring local structures in materials

Gene E. Ice

Materials Science and Technology Division, Oak Ridge National Laboratory

Powerful characterization tools have emerged over the last decade, made possible by intense new x-ray and neutron facilities. These characterization tools offer unprecedented opportunities to explore underlying structures in materials and how these structures control materials properties. Here we briefly describe three related characterization techniques that directly impact research interests in the *Mechanical Behavior and Radiation Effects Core Research Area*: (1) nondestructive 3D micro-imaging of mesoscale crystal structures for studies of deformation, grain growth and fracture; (2) micro-diffuse scattering for sensitive studies of radiation damage and defects in small or polycrystal samples, or in dangerous or hard to produce crystals; and (3) micro-beam neutron diffraction for characterization of fragile crystal structures, for measurements of samples in extreme environments and for studies of heterogeneous samples with both low and high Z components. The new information from these techniques can guide and challenge theory and can provide detailed tests of state-of-the-art models of materials behavior. The talk will give examples of recent results and evolving capabilities, will highlight some ongoing mysteries where striking experimental results are not yet understood and will humbly suggest research where fruitful collaborations are likely. Ultimately the aim of the talk is to promote a deepening dialog with the leaders in the *Mechanical Behavior and Radiation Effects Core Research Area*, and to advertise emerging experimental capabilities that can impact ongoing and future research programs.

Stable Nanoclusters in Metallic Matrices

C. T. Liu,^{1,2} C. L. Fu,¹ M. K. Miller,¹ J. H. Schneibel,¹ M. J. Mills,³ X. L. Wang,¹ M. Krcmar¹
liuct@ornl.gov, fucl@ornl.gov, millermk@ornl.gov, schneibeljh@ornl.gov, millsmj@er6s1.eng.ohio-state.edu

¹Oak Ridge National Laboratory, Oak Ridge TN 37830

²University of Tennessee, Knoxville, TN 37996-2200

³Ohio State University, Columbus Ohio 43210

Program Scope

The goal of this project is to attain a fundamental understanding of the formation mechanism, thermal stability, and hardening mechanism of stable nanoclusters in metallic matrices. This work is motivated by observation of remarkably stable nanoclusters (2-4 nm in diameter) in Fe-based ferritic alloys (e.g., 14YWT, Fe-14Cr-3.0W-0.46Ti-0.3Y₂O₃, wt%) prepared by mechanical alloying. These nanoclusters are enriched with Ti, Y, and O atoms with the composition best described by (Ti₄₀Y₁₀)(O₅₀), as determined by atom probe analyses. The clusters are surprisingly stable during long-term creep tests at 650-900°C, and they are responsible for reducing the creep rate by six orders of magnitude. The study of the scientific mechanisms underlying these stable nanoclusters is expected to identify novel material states that are capable of extending the useful temperature range of nanophase materials from ambient to elevated temperatures.

The unusual thermal stability of the nanoclusters in 14YWT has been the major focus of the research to date. While initial study has been with Fe-based alloys, with the intention to use our emerging knowledge to predict and verify other metallic systems containing potentially stable nanoclusters to extend our mechanistic understanding of this phenomena. This research is composed of two major tasks: (1) theoretical and experimental studies of the formation mechanism and thermal stability of stable nanoclusters in metallic systems using atom-scale characterization tools and first-principles calculations, and (2) experimental and modeling studies of hardening mechanisms of stable nanoclusters at ambient and elevated temperatures.

Recent Progress

Direct quenching combined with atom probe analyses revealed that nanoclusters in ferritic alloys were stable at temperatures as high as 1400°C (0.91T_m). The ultra-high stability of these nanoclusters was confirmed by in-situ small-angle neutron scattering up to 1400°C. Atom probe tomography of several conditions of the 14YWT alloy revealed that the grain boundaries were also decorated with an enhanced number density of the Ti-, Y- and O-enriched nanoclusters [1], as shown in the atom maps in Fig. 1. The density of nanoclusters was sufficiently high ($> 10^{24} \text{ m}^{-3}$) that impingement of some of the nanoclusters was apparent. Visual inspection indicated that the nanoclusters on the grain boundaries were similar in size to those in the grain interior. No significant difference in the composition of the nanoclusters in the grain interior and on the grain boundaries was detected. The grain boundaries were also found to be enriched in Cr, W and C over an ~4 nm wide region centered on the grain boundary, with maximum levels of 20 at. % Cr, 2 % W, and 0.4 % C, respectively. These nanoclusters may form preferentially at the grain boundaries either due to the inhomogeneous distribution of solute at the grain boundaries or due to enhanced nucleation and diffusion along them [2].

Design-by-atoms calculations based on first-principles calculations were used to determine the interaction of solute atoms on the Fe lattice [3]. Oxygen, confined as an interstitial, showed an exceptionally high affinity for vacancies, an effect enhanced by spin-polarization. This O-vacancy mechanism enables the nucleation of O-enriched nanoclusters that attract solutes with high O-affinities (Ti and Y). The stability of these nanoclusters is a consequence of the fact that defects and solutes with high individual formation energies can collectively form a bound state system of low energy and high stability. In order to nucleate the nanoclusters on the Fe lattice, the binding energy of an O atom [$E_b(\text{O})$] in the cluster has to be lower than the heat of formation of the TiO₂ oxide phase. We note that there is a

large energy difference between $E_b(O)$ in defect-free Fe (-0.6 eV) and the heat of formation (per O) of TiO_2 (-4.3 eV). As noted in Fig. 2, vacancies play a pivotal role in reducing this energy difference. Specifically, we find that $E_b(O)$ in an O-vacancy pair (O:V) increases by as much as 3.2 eV as the neighboring Fe atoms are progressively replaced by Ti atoms. This is because the O:V pair has an unusually high binding energy and Ti has a higher affinity for O than Fe. Figure 2 also indicates a further increase in $E_b(O)$ by approximately 0.4 eV due to the interaction between O:V pairs in the presence of Ti. Thus, the total increase of $E_b(O)$ for an O atom in an O:V pair in the presence of Ti solutes can be as large as 3.6 eV, which is surprisingly close to the energy difference (3.7 eV) between $E_b(O)$ in defect-free Fe and the heat of formation of TiO_2 . Our further calculations indeed indicate that small additions of the large atom, Y, increase $E_b(O)$ by ~ 0.7 eV, enabling the formation of nanoclusters instead of TiO_2 .

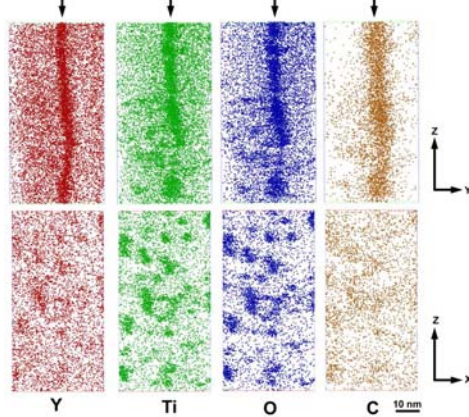


Fig. 1. 4-nm thick atom map slices of a grain boundary region in 14YWT ferritic alloy hot extruded and annealed for 1h at 1000°C (top: grain boundary edge-on; bottom: side view).

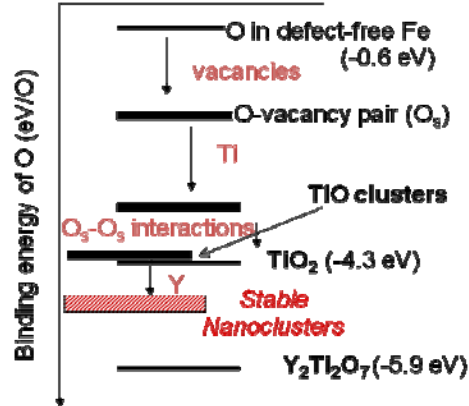


Fig. 2. Schematic representation of oxygen binding energy levels in defect-free Fe, in O-vacancy pair, and in clusters. For reference, the corresponding energy levels of oxide phases are also shown. [31]

It should be noted that the ternary oxide phase $Y_2Ti_2O_7$ is a very stable compound with the calculated formation energy of -5.9 eV per oxygen atom. Consequently, the energy of O atoms in the nanoclusters can hardly become lower than the formation energy of the $Y_2Ti_2O_7$ oxide phase in the presence of Y. If too much Y is present, the $Y_2Ti_2O_7$ oxide phase is likely to precipitate. Therefore, the conditions for stable nanoclusters require a well-dispersed Y distribution with more Ti than Y in the nanoclusters.

A magnetism-induced O confinement is identified as one of the significantly contributing sources (by 1.1 eV) to this unusually strong O-vacancy binding. For O in an interstitial octahedral site of defect-free Fe, there exists strong spatial confinement of charge with localization in the core region of the O atom. Now, with creation of a nearest-neighbor vacancy, the O charge confinement is alleviated by electron delocalization into the newly-created volume: as a result, the electronic kinetic energy is reduced and the O-vacancy binding is greatly enhanced.

To provide experimental evidence that vacancies play a key role in the stability of nanoclusters in 14YWT [3,4], position lifetime spectroscopy was used to detect vacancy cluster formation in three samples: (1) 14YWT with nanoclusters, (2) a cast alloy with the same composition as (1) but containing no nanoclusters, and (3) a powder metallurgy alloy with the same composition as (1) but containing neither Y nor nanoclusters. Vacancy clusters that are equivalent to 4-6 vacancies were found to be associated only with the nanocluster sample. The observed vacancy clusters are consistent with the theoretic prediction that the vacancies are a constitutive element vital to the formation of nanoclusters in 14YWT.

Characterization of structural features reveals that the mechanical behavior of 14YWT can be affected by nanoclusters in the grain interior, grain boundaries decorated with nanoclusters, and grain size, each of which may contribute to the hardening in different proportions at different temperatures. At present, we

are attempting to identify each individual role in hardening. After hot extrusion and annealing (1 h/1000°C), the grain size of the 14YWT alloy is ~100 nm, i.e., it is an ultra-fine grained (UFG) material [5]. This suggests that there are at least two contributions to its room temperature strength: the strengthening due to the nanoclusters, and the strengthening due to the small grain size (Hall-Petch strengthening). Annealing for 24 h at 1200°C resulted in a grain size well above 100 μm, while the nanocluster population remained essentially unchanged (as revealed by small angle neutron scattering). The UFG material was much stronger at room temperature than the coarse-grained material: the 0.2% compressive yield stresses were ~2040 and ~840 MPa, respectively. Based on experimental results for UFG ferritic steels, this is not unexpected – the Hall-Petch contribution for the difference in the grain sizes can be more than ~1500 MPa. Surprisingly, however, the UFG material was not weak in compression-creep testing at 800°C (0.7T_m), where superplasticity or diffusional creep would be expected, but exhibited instead very high creep strength. By testing at temperatures to 1050°C, we finally found conditions for which the UFG material is weaker than the coarse-grained one (see Fig. 3). We suspect that the nanoclusters on the grain boundaries are responsible for the remarkable resistance of the grain boundaries against sliding and diffusion at high temperatures. Note that both materials have the same strength at 950°C. More work is needed to develop the mechanistic underpinnings of these observations.

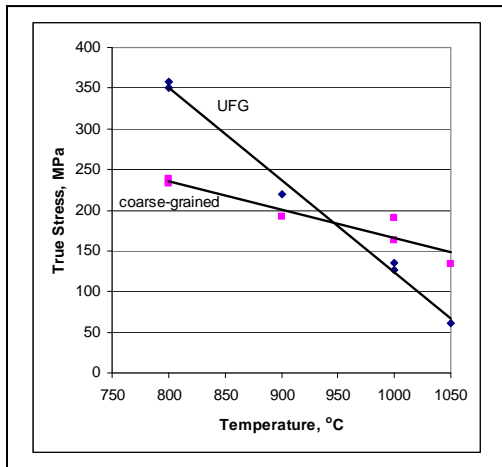


Fig. 3. Creep strength of 14YWT at a strain rate of 10^{-5} s^{-1} and 5% plastic strain. The UFG material was annealed for 1 h at 1000°C, while the coarse-grained material was annealed for 24 h at 1200°C.

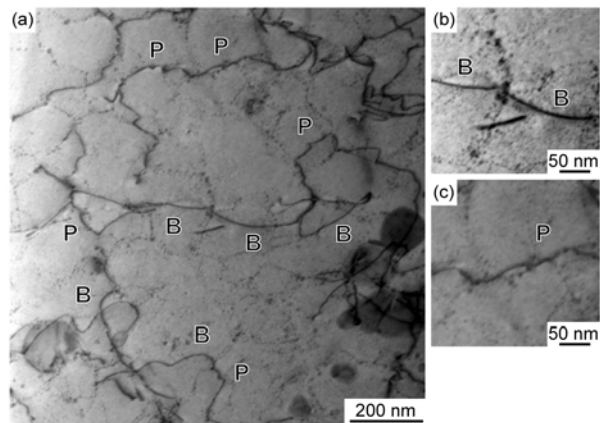


Fig. 4. BF-STEM micrographs for the 5-d annealed and crept sample; (a) an overview for the dislocation structure in a large grain; (b) a dislocation bowing between a nanocluster cell and (c) a dislocation fully pinned against the nanocluster cell. [6]

Detailed characterization of microstructure and dislocation structure has been conducted on the 14YWT alloy after creep deformation at 800°C.[6] A stable grain structure is maintained in the UFG material even following extended creep testing at 800°C. Remarkably, in spite of the ultra-fine grain size (~100 nm), the alloy exhibits excellent creep resistance, suggesting that there is no significant grain boundary sliding (GBS). Nanoclusters appear to decorate the initial grain boundaries and provide significant impediment to GBS. During long-term annealing at 1000°C and after subsequent creep testing at 800°C, extensive anomalous grain growth (AGG) was observed. However, the minimum creep rates of the 14YWT samples are similar even though they possess vastly different grain structures. In the coarse grains, the dislocations are strongly impeded by the presence of nanocluster cells (see Fig. 4) which originally form on the grain boundaries of the UFG structure. These nanocluster cells are crucial for the retention of creep strength even after AGG has occurred. Further studies will focus on the interaction of mobile dislocation with individual nanoclusters and nanocluster cells on initial grain boundaries.

Future plans

- To better understand nanocluster formation and stability, atomic scale tools will be used to characterize the nanoclusters in the bulk and on grain boundaries after isothermal annealing at a

series of different high temperatures and times to determine evolution behavior of the nanoclusters, to determine crystalline structure of nanoclusters, and to construct 2D and 3D concentrations and radial concentration maps of the solute distribution in the nanoclusters. Furthermore, novel techniques of positron lifetime spectroscopy and coincidence Doppler broadening of annihilation radiation (2D-DBAR) will be used to characterize the size, concentration and chemical environment of vacancies in nanocluster materials.

- We will continue to investigate the interplay between magnetism and cluster size (structures and symmetries) and the local structures of vacancy complexes in these nanoclusters by first-principles calculations. Calculations to date have been on relatively small cluster systems, examining many possible configurations. Future work includes further studies at this size, plus larger-scale calculations. Additionally, we plan to examine composition effects, at different alloying additions with strong oxygen affinity (such as Zr), and at structures in different host lattices to test our emerging mechanistic understanding.
- Kinetic Monte Carlo simulations will be used to monitor the flow of solute atoms and the kinetic process of nanocluster formation.
- We will develop a better understanding of the effect of nanocluster decoration on grain boundary sliding in the nanocluster material. To do so, we will produce an alloy with the same composition and same ultrafine grain size (~100 nm) as the 14YWT alloy, but without nanoclusters. Without nanoclusters at the grain boundaries, we expect this alloy to be very weak in creep at elevated temperatures (i.e., we expect it to be superplastic). Then we will characterize and compare the grain boundaries in this alloy and the 14YWT in order to identify the reasons for the substantial differences in their mechanical behavior.
- We will continue efforts to understand and quantify dislocation/nanocluster interactions. The present results indicate that the nanocluster cells in the large grains are the predominant inhibitor of dislocation movement, via climb by-pass or detachment, whereas the fine clusters between them simply add a frictional stress. To confirm this scenario, in-situ TEM heating/straining experiments at ORNL will be conducted in order to directly observe the nature of dislocation movement in the large grains. Once confirmed a frictional stress parameter from the ultra-fine nanoclusters and an Orowan-based bowing stress from the nanocluster cells can be incorporated into a physics-based creep model.
- Currently mechanical alloying is the sole way to produce the nanocluster material. Because of technical difficulties and high-cost issues with mechanical alloying, innovative methods will be investigated for effective fabrication of nanocluster materials.

References (Only publications of DOE Sponsored research in 2005 to 2007)

- [1] M. K. Miller, D. T. Hoelzer, E. A. Kenik and K. F. Russell, "Stability of ferritic MA/ODS alloys at high temperatures", *Intermetallics*, 13 (2005) 387-392.
- [2] M. K. Miller, K. F. Russell and D. T. Hoelzer, "Characterization of precipitation in MA/ODS ferritic steels" *J. Nucl. Mater.*, 351 (2006) 261-268.
- [3] C. L. Fu, M. Krcmar, G. S. Painter, and X. Chen, "Vacancy Mechanism of High Oxygen Solubility and Nucleation of Stable Oxygen-Enriched Clusters in Fe," *Phys. Rev. Lett.* 99, 225502 (2007).
- [4] M. K. Miller, C. L. Fu, M. Krcmar, D. T. Hoelzer, C. T. Liu, "The vacancies as a constitutive element for the design of nanocluster-strengthened ferritic steels", *J. Shanghai Metallic Mater.* (accepted)
- [5] J. H. Schneibel, C. T. Liu, D. T. Hoelzer, M. J. Mills, P. Sarosi, T. Hayashi, U. Wendt and H. Heyse, "Development of porosity in an oxide dispersion-strengthened ferritic alloy containing nanoscale oxide particles", *Scripta Mater.* 57, 1040-1043, 2007.
- [6] T. Hayashi, P. M. Sarosi, J. H. Schneibel, M. J. Mills, "Creep response and deformation process in nanocluster-strengthened ferritic steels, *Acta Mater.*, 2008 (in print)

Deformation Physics of Ultra-fine Scale Materials

Amit Misra

<amisra@lanl.gov>

Los Alamos National Laboratory, MS K771,
Los Alamos, NM 87545.

Program scope

As the characteristic length scales of the microstructure (e.g., grain size) in a material that control the mechanical properties are reduced to the nanometer range, the strength is enhanced to unprecedented levels, often approaching the theoretical limits defined for perfect crystals. For example, nanoscale composites made at LANL from ordinary soft metals such as Cu, Ni, Nb, etc with strengths of a few tens of MPa in the bulk can achieve strengths in excess of 2000 MPa. More importantly, the conventional descriptions relating mechanical properties to the microstructural dimensions do not extrapolate to nanometer dimensions. The mechanisms that determine strength and failure limits of nano-scale materials represent new realms of mechanical behavior. Development of fundamental understanding of the unusual mechanical behavior (e.g., super strong) of nanostructured materials, unexplained by conventional continuum-scale models, is the grand challenge pursued by this core research program. In response to this grand challenge, the specific objectives of this program are to understand: (1) the origins of ultra-high strengths in nanometer-scale layered composites, (2) the ultimate strength limit achieved via tailoring of length scales and atomic structures and energetics of interfaces, (3) role of interfaces in slip transmission and dislocation storage, (4) post-yield behavior, associated with plastic flow stability, work hardening, and fracture mechanisms, (5) thermal stability, and (6) stabilization of new or unusual atomic arrangements in nanometer-scale composites.

Our research team at LANL has successfully adopted a highly synergistic combination of state-of-the-art atomistic modeling and cutting-edge experimental methods that are able to probe the details of the deformation mechanisms in metallic nanolayered composites. Specifically, the integrated approach consists of nanoscale synthesis by physical vapor deposition (PVD), nanomechanical testing, high-resolution transmission electron microscopy (HRTEM), x-ray diffraction (XRD), dislocation theory and molecular dynamics (MD) simulations. For a systematic scientific study following the objectives listed above, the PVD synthesis route offers a number of advantages. First, any two (or more) metals (or ceramics) can be alternately deposited to produce a layered composite. Second, the individual layer thicknesses can be controlled to within an atomic layer (unlike many techniques that produce a distribution in grain sizes). Third, the products have high-purity, and are porosity-free. Fourth, self-supported samples with total thicknesses of tens of micrometers, or more, are readily synthesized. We perform nanomechanical characterization by nanoindentation, microtensile testing, micropillar compression and large strain deformation via cold rolling. Our nano-scale characterization of the as-synthesized and deformed materials utilizes world-class HRTEM and XRD capabilities at LANL. Atomistic simulations using the best state-of-the-art computational schemes are used to examine the critical unit processes that are involved in the deformation of these materials. Such calculations help to elucidate the new types of deformation mechanisms that are discovered in these composites.

Besides the PI, the research team involves R.G. Hoagland (co-PI, LANL), F. Spaepen (Harvard University, co-investigator), J.D. Embury (McMaster University, Canada and LANL

consultant) and J.P. Hirth (LANL consultant). The program also involves the following LANL staff: J. Wang (atomistic modeling, post-doctoral researcher), M.J. Demkowicz (atomistic modeling, LANL Director's post-doctoral fellow, TSM effective April'08), N.A. Mara (experiments, LANL Director's post-doctoral fellow, TSM effective April'08), D. Bhattacharyya (TEM, 50% effort, post-doctoral researcher), and O. Anderoglu (Texas A&M university, summer GRA). We have collaborated with other BES-funded staff at LANL: Can Aydiner (LANL Director's postdoc fellow) and D. Brown (Lujan neutron scattering center, *in situ* tensile testing in synchrotron beams), M. Nastasi (CINT, residual stresses in ion-synthesized materials), M.I. Baskes (MD simulations), and C.N. Tome (polycrystal plasticity modeling). In addition, we have significant external collaborations, e.g., H.M. Zbib and D. Bahr (Washington State University, dislocation dynamics simulations), A.K. Mukherjee (UC-Davis, high temperature tensile testing of metallic multilayers), T. Ungar (Budapest, Hungary, XRD peak profile analysis), and P. M. Anderson (Ohio State University, dislocation models of multilayer strength).

Recent Progress

Significant technical accomplishments from the last three years are summarized below:

1) New methodologies were developed to perform TEM on FIB-sectioned foils from beneath the nano-indenters in multilayers. Such detailed microscopy characterization has shown extensive plastic deformability of 5 nm layers without any cracking (Fig. 1).

3) New approaches were developed to experimentally measure the stress-strain curves of Cu-Nb multilayers that have individual layer thicknesses of a few to a couple tens of nanometers. In earlier work on multilayers, uniaxial tensile testing was limited to coarser layer thickness of greater than 50 nm, and hardness measurement was the only available test method at lower layer thickness. We measured flow stress approaching 2.5 GPa and deformability exceeding 25% at layer thickness of 5 nm via compression testing of focused-ion-beam (FIB) micro-pillars. *In situ* tensile tests, performed under synchrotron radiation at APS (Argonne), simultaneously measure elastic strains in the two layers along with the total strains and stresses and reveal co-deformation of approximately 25 nm thick Cu and Nb layers.

3) Experiments on Cu/metallic glass (palladium silicide) multilayers revealed significant plasticity in nanometer-scale metallic glasses constrained by nano-scale metal (Cu) layers, whereas in the bulk form, metallic glasses fail via

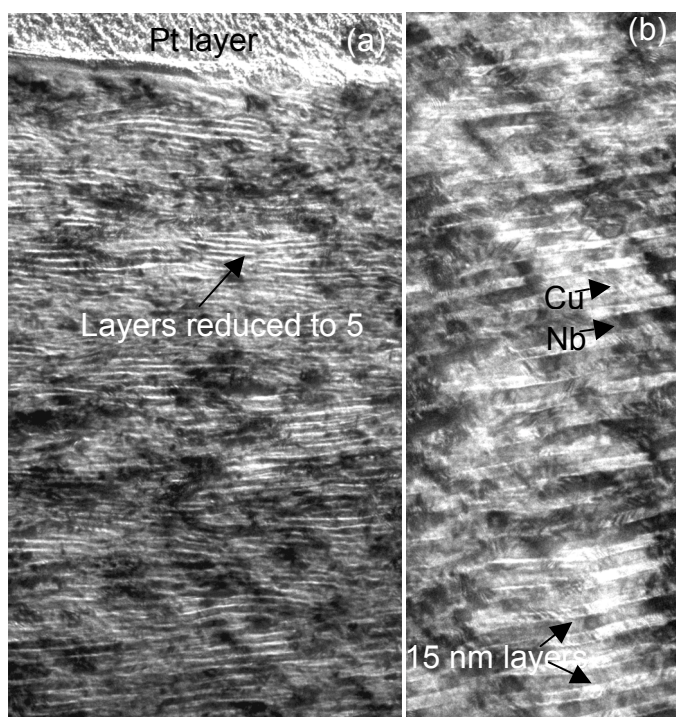


Fig. 1 TEM cross-section from (a) directly below a hardness indent, and (b) some distance below the indent tip. The initial layer thickness was ≈ 15 nm. The indented surface is coated with Pt prior to FIB machining.

highly localized shear bands. 50 nm Cu / 10 nm Pd-Si multilayers samples were rolled to elongations in excess of 200%. This work is in collaboration with Frans Spaepen at Harvard University.

4) Atomistic modeling was used to reveal the complex atomic structures of incoherent fcc-bcc Cu-Nb interfaces. We have discovered several metastable atomic structures for this interface. We also explored the glide dislocation interaction with these interfaces. In particular, the dislocation core spreading at these weak interfaces was found to be the key factor that determined the unusually large barrier to slip transmission for these interfaces.

5) Dislocation dynamics simulations (sub-contract with Hussein Zbib at Washington State University) were used to study the complex glide dislocation – interface dislocation interactions, in both parallel and orthogonal configurations, during confined layer slip in fcc-fcc systems. Unit processes, such as cross-slip of a glide dislocation approaching an orthogonal interface dislocation, studied via discrete dislocation modeling are consistent with experimental observations and provide insight on the work hardening and recovery mechanisms during confined layer slip.

6) This program has lead to several spin-off projects at LANL.

- Fatigue of nanolayered composites: We designed and built a novel resonance-frequency device to measure fatigue behavior of nanolayered composites. For the first time, it has been shown that nanolayered materials exhibit large increases in fatigue endurance limit compared to bulk materials due to suppression of damage accumulation during cyclic straining.

- Radiation damage tolerance of nanolayered composites: Interfaces act as obstacles to slip and sinks for radiation-induced defects. Hence, nanolayered composites provide orders of magnitude increase in strength and enhanced radiation damage tolerance compared to bulk materials.

- Nano-twinned metals: In certain composites of alternating Cu and austenitic stainless steel layers *we discovered that the steel layer had a preferred orientation of twins normal to the growth direction with an average spacing of only a few nanometers*. Pursuing this observation further, we found that films made entirely of austenitic stainless steel could be produced containing nanometer thick twinned structures. These films possess strengths that are over an order of magnitude greater than bulk austenitic stainless steel, consistent with atomistic model predictions for twinned interfaces. In a spin-off project, we are studying controlled synthesis of nano-twinned structures in physical vapor deposited metals.

Future Plans

- Exploration of the unusual deformation mechanisms that give rise to ultra-high strengths and high deformability in crystalline/amorphous and metal / ceramic (e.g., metal-nitride) multi-layers using a combination of TEM (including *in situ* studies) and atomistic modeling.

- Atomistic modeling will be used to elucidate shear localization mechanisms in nano-layered systems with layer thickness less than approximately 5 nm. Experiments such as TEM investigation of regions beneath nano-indentations and compressed micro-pillars will be used to elucidate the deformation behavior at comparable length scales.

- We will explore the *optimization* of interface structure and strength by examining the strengthening and mechanical stability of bimodal multilayers with alternate arrangement of 10 nm and 100 nm bilayer periods, for both metal-metal and metal-nitride systems.
- Atomic scale modeling will be conducted to explore a set of systems containing a range of interfacial shear strengths. These studies will seek to probe the relative importance of interface structure on the slip transmission.
- Dislocation dynamics simulations will model the dislocation interactions pertaining to confined layer slip to provide insight on the work hardening, dislocation storage, and recovery mechanisms.

Selected recent publications (over 80 publications total since FY2000)

1. M.J. Demkowicz, R.G. Hoagland, J.P. Hirth, *Interface structure and radiation damage resistance in Cu-Nb multilayer nanocomposites*, PHYSICAL REVIEW LETTERS, in press.
2. Demkowicz MJ, Wang J, Hoagland RG, *Interfaces between dissimilar crystalline solids*, in Dislocation in Solids, ed. Hirth JP, (2008) in press.
3. A. Misra, *Mechanical Behavior of Metallic Nanolaminates*, NANOSTRUCTURE CONTROL OF MATERIALS ed. by A J Hill and R H J Hannink, Woodhead Publishing Co., UK, pp. 146-176, (2006).
4. A. Misra, M.J. Demkowicz, X. Zhang and R.G. Hoagland, "*Radiation damage tolerance of ultra-high strength nanolayered composites*", JOM, **59**, 62, September 2007 (invited overview).
5. A. Misra, R.G. Hoagland, "*Plastic Flow Stability of Metallic Nanolaminate Composites*", JOURNAL OF MATERIALS SCIENCE, invited paper for a special issue on Nanomaterials, **42**, 1765 (2007).
6. A. Misra, M.J. Demkowicz, J. Wang and R.G. Hoagland, *Multiscale Modeling of Plastic Deformation of Metallic Nanolayered Composites*, JOM, April 2008.
7. N.A. Mara, D. Bhattacharyya, P. Dickerson, R.G. Hoagland, A. Misra, "*Deformability of ultra-high strength 5 nm Cu/Nb nanolayered composites*", APPLIED PHYSICS LETTERS, in press.
8. D. Bhattacharyya, N.A. Mara, A. Misra and R.G. Hoagland, "*Nanoindentation and microstructural studies of Al-TiN multilayers*", SCRIPTA MATERIALIA, in press.
9. J. Wang, R.G. Hoagland and A. Misra, *Atomistic Simulations of the Shear Strength and Sliding Mechanisms of Copper-Niobium Interfaces*, ACTA MATERIALIA, accepted.
10. F. Akasheh, H.M. Zbib, J.P. Hirth, R.G. Hoagland and A. Misra, "*Interactions between glide dislocations and parallel interfacial dislocations in nanoscale strained layers*", JOURNAL OF APPLIED PHYSICS, **102**, 034314 (2007).
11. A. Donohue, F. Spaepen, R.G. Hoagland and A. Misra, "*Suppression of the shear band instability during plastic flow of confined metallic glass ultra-thin films*", APPLIED PHYSICS LETTERS, **91**, 241905 (2007).
12. Y.-C.Wang, A. Misra and R.G. Hoagland, "*Fatigue properties of nanoscale Cu/Nb multilayers*", SCRIPTA MATERIALIA, **54**, 1593 (2006).
13. R.G. Hoagland, J.P. Hirth and A. Misra, "*On the role of weak interfaces in blocking slip in nanoscale layered composites*", PHILOSOPHICAL MAGAZINE, **86**, 3537 (2006).
14. A. Misra, X. Zhang, D. Hammon, R.G. Hoagland, "*Work hardening in rolled nanolayered metallic composites*", ACTA MATERIALIA, **53**, 221 (2005).
15. A. Misra, J.P. Hirth and R.G. Hoagland, "*Length-scale-dependent Deformation Mechanisms in Incoherent Metallic Multilayered Composites*", ACTA MATERIALIA, **53**, 4817 (2005).

LBLN MECHANICAL BEHAVIOR OF MATERIALS PROGRAM

R. O. Ritchie (PI), A. P. Tomsia, E. Saiz, D. C. Chrzan, and J. W. Ager

Materials Sciences Division, Lawrence Berkeley National Laboratory

University of California, Berkeley, CA 94720. email: roritchie@lbl.gov

Program Scope: This program is focused on developing an understanding of the mechanical behavior of next generation structural materials, in particular involving mechanical properties that are influenced by factors operating at a wide range of length scales. Our long-term goal is to design, synthesize, and characterize (structurally and mechanically) a new series of hierarchical/hybrid structural materials, whose unique properties derive from architectures controlled over length scales from nano to macro dimensions. The inspiration for these structures is biological; our goal is to defeat the “law of mixtures” (as in Nature) by devising complex hierarchical structures comprising weak constituents into strong and tough hybrid materials, displaying far superior properties than their individual constituents. The research combines mechanistic understanding of structural behavior, principally damage tolerance, at multiple length scales, the ability to synthesize such materials, the control of structural features, particularly interfaces, at the nanoscale, the ability to *mechanically* characterize such structures at all dimensions, and the evaluation of the suitability of these (non-biological) structures/systems for technological application.

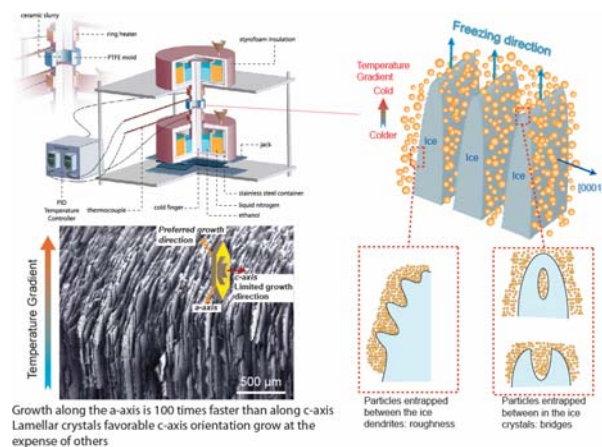


Figure 1. A novel experimental setup is used to directionally freeze concentrated ceramic suspensions while promoting the formation of lamellar ice crystals. The ice expels the ceramic particles as it grows. After sublimating the water, the result is a layered, homogeneous ceramic scaffold. By controlling the freezing kinetics and the composition of the suspension it is possible to tailor the architecture of the material at multiple length scales to replicate some of the unique micro-structural features behind the mechanical response of biological materials (*e.g.*, the lamellae roughness or the bridges between lamellae).

Recent Progress: The development of novel structural materials and the maintenance of their integrity remains a central feature of preserving and enhancing our standard of living. Strategic technological fields such as transportation or the production of energy demand new lightweight tough materials able to operate in extreme environments. The materials response, in particular the mechanical performance, is invariably defined by the structure at widely differing length scales. Examples of this are the dimensions that affect deformation *vs.* fracture. Deformation may be influenced by characteristic dimensions in the realm of nano- to micrometers, such as a Burgers vector or precipitate spacing, whereas the fracture properties generally involve mechanistic phenomena that occur over much larger size-scales. Nowhere is this more apparent than with biological composites such as nacre or bone. Natural materials are sophisticated composites whose properties are invariably far

superior to their individual constituent phases. This unique response derives from an architectural design that spans nanoscale to macroscopic dimensions, with precisely and carefully engineered interfaces. The fracture resistance of such materials originates from toughening mechanisms at each of these dimensions. Few structural engineering materials have such structural hierarchy, yet biology's message is clear – unique mechanical properties can be achieved through mechanisms acting at multiple length scales.

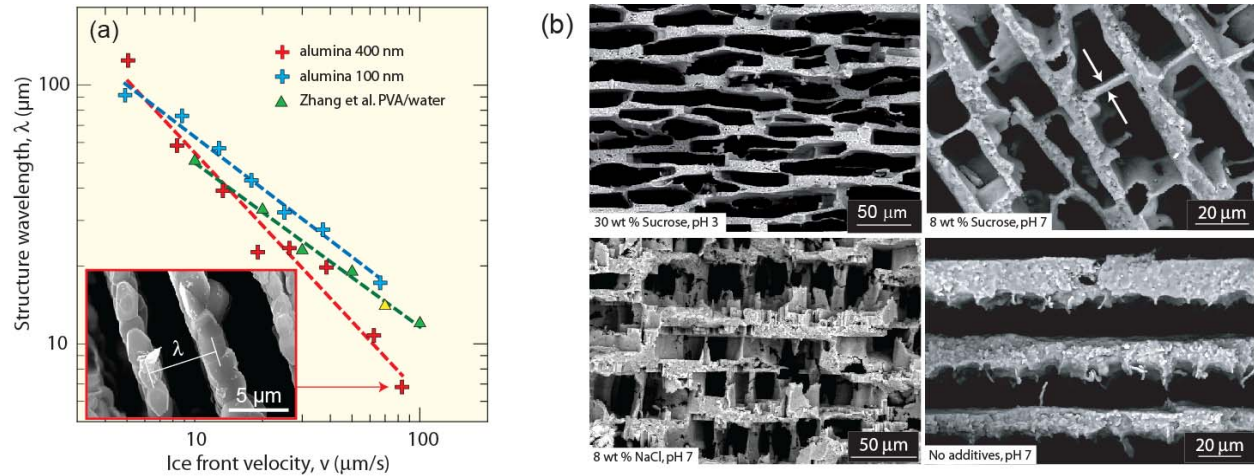


Figure 2. (a) The lamellae thickness can be controlled by controlling the velocity of the freezing front, $\lambda \propto v^{-n}$ ($n=1$ for 400 nm particles, and $2/3$ for 100 nm). Materials with lamellae as thin as 1-2 μm (very close to the 0.5 μm value of nacre) ordered over macroscopic dimensions can be fabricated in practical sizes. (b) The roughness of the lamellae (that replicate the roughness of the ice crystals) can be manipulated from the submicron to the micron levels by using additives that vary the solid-liquid interfacial tension and the phase diagram of the solvent. In concentrated suspensions the growing ice crystals can split and trap ceramic particles. The trapped particles generate inorganic bridges between lamellae (white arrows) whose size and distribution can also be manipulated using additives. It has been shown how both the roughness and bridges play a critical role on the mechanical response of the natural material.

The notion of biomimicry and hierarchical organization has received much interest in the materials communities; however, advances have been few if any, primarily due to the lack of fabrication techniques able to produce such materials in practical dimensions. Our laboratory has worked on these much needed processing technologies. We have developed a technique, *freeze casting*, which uses the intricate microstructure of ice to template the microstructure of complex ceramic scaffolds (Figs. 1- 2). These scaffolds are subsequently infiltrated using liquid or vapor-based techniques with a second “soft” phase (either a polymer or a metal) to fabricate hybrid composites with a architecture that mimics that of nacre at multiple length scales.

We have used freeze casting to fabricate model polymer/ceramic (PMMA/ Al_2O_3) and metal/ceramic (Al-Si/ Al_2O_3) hybrid materials with fine lamellar architectures. Brick and mortar microstructures with high ceramic contents (up to 80 vol%) have been also fabricated by combining freeze casting and hot uniaxial pressing. The objective is to combine a strong and hard (ceramic) phase with a “lubricating” (polymer or metal) layer in between to permit relaxation of stresses. These hybrid materials have a sophisticated mechanical response that replicates natural organic/inorganic composites at many levels. Their bending load-displacement data exhibit a gradually decreasing load after the elastic limit, characteristic of

stable cracking. Furthermore, PMMA/Al₂O₃ materials show remarkable R-curve behavior displaying fracture toughnesses approaching 30 MPa√m with yield strengths of 200 MPa. These toughness properties are one order of magnitude better than what can be expected from the “rule of mixtures” bounds or that of the individual constituent phases (Fig. 3). In fact, they approach the values for aluminum alloys while exhibiting lower density and higher stiffness (Fig. 4).

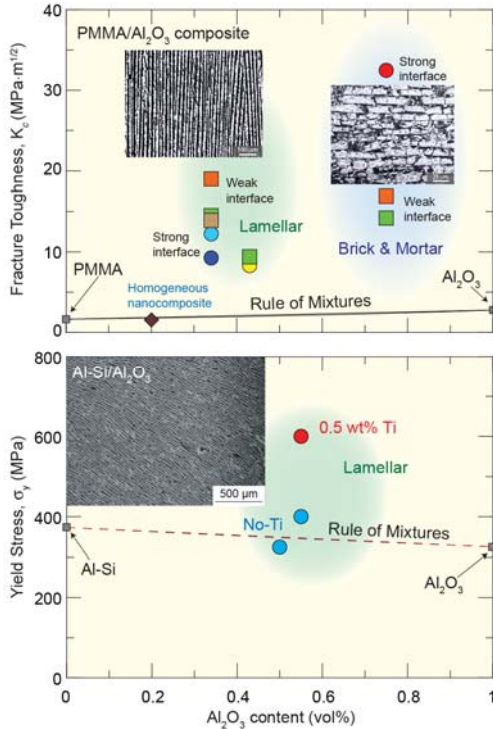


Figure 3. The mechanical properties of the hybrid materials are significantly higher of what could be expected from the simple “rule of mixtures” relationships from their components; moreover, adhesion at the soft/hard interface plays a critical role. Note how the toughness of the homogeneous PMMA/Al₂O₃ nanocomposite is much lower than that of the hierarchical material.

Modeling efforts of these materials have focused on 2-D Burrige-Knopoff-like (B-K) models for studying statistical aspects of the hybrid material deformation across multiple length scales. As toughness correlates with the delocalization of damage, we need to understand aspects of the model that can influence the spatial distribution of damage. A simple model for “brick and mortar” structures based on linear springs bonding the inorganic “bricks” predicts localized damage and hence premature failure. However, springs that show jumps in the load-displacement curve lead to damage distributed throughout the sample, similar to that observed in traditional B-K models. Further, the magnitudes of the damage within local regions display a power-law distribution akin to those observed in earthquake models. Therefore the physical properties of the springs (at molecular to nano levels) play a defining role in the macroscopic properties. We are developing a statistical mechanics model for the polymer springs that bond the inorganic bricks, and use it to estimate the constitutive response of many polymer strands acting in parallel. The predicted response displays the nonlinear behavior necessary to generate distributed damage that has been observed in the natural composites.

The results show that a promising route to developing new structural materials is to understand the mechanisms that control mechanical behavior over multiple dimensions in solids with complex, hierarchical architectures. Studies that “bridge the length-scales” are popular but have been largely based in mechanics rather than mechanistic understanding. Without discovery of mechanisms, new material design is merely empirical. We believe that we have a novel approach to fabricate in practical dimensions hybrid/hierarchical structures whose unique properties derive from architectures controlled multi-dimensions. This combination of processing, modeling, structural and mechanical characterization at all relevant dimensions will enable new design criteria that will lead to novel families of structural materials with unprecedented combination of mechanical properties.

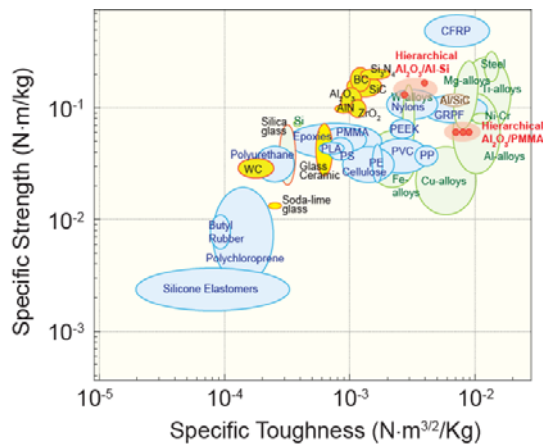


Figure 4. Comparing the properties of the hybrid hierarchical composites with other engineering materials emphasizes their unique mechanical response. Using a hierarchical design it is possible to fabricate a composite of two conventional materials with modest mechanical properties (Al_2O_3 and PMMA) that exhibit a response comparable to aluminum alloys. In the future we will extend these design concepts to other material combinations to achieve unique properties. Preliminary results with the toughness and particularly strength of Al-Si/ Al_2O_3 materials are already extremely promising.

Selected Publications

D. H. Alsem, R. Timmerman, B. L. Boyce, E. A. Stach, J. Th. M. De Hosson, R. O. Ritchie, "Fatigue failure in micron-scale polycrystalline silicon films", *J. Appl. Phys.*, **101**, 2007, pp. 013515.

D. H. Alsem, O. N. Pierron, E. A. Stach, C. L. Muhlstein, R. O. Ritchie, "Mechanisms for fatigue of micron-scale silicon structural films", *Adv. Engin. Mater.*, **9**, 2007, pp. 15-30.

D. H. Alsem, E. A. Stach, M. T. Dugger, M. Enachescu, R. O. Ritchie, "An electron microscopy study of wear in polysilicon microelectromechanical systems", *Thin Solid Films*, **515**, 2007, 3259-66.

R. Yu, X. F. Zhang, L. C. De Jonghe, and R. O. Ritchie, "Elastic constants and tensile properties of Al_2O_3 by density functional calculations", *Phys. Rev. B*, **75**, 2007, 104114.

A. Ziegler, M. K. Cinibulk, C. Kisielowski, R. O. Ritchie, "Atomic-scale observation of the grain-boundary structure of Yb-doped silicon nitride ceramics", *Appl. Phys. Lett.*, **91**, 2007, 141906.

J. W. Foulk III, R. M. Cannon, G. C. Johnson, P. A. Klein, R. O. Ritchie, "A micromechanical basis for partitioning the evolution of grain bridging in brittle materials", *J. Mech. Phys Solids*, **55**, 2007, 719-743.

J. C. Card, R. M. Cannon, E. Saiz, A. P. Tomsia, R. O. Ritchie, "Of the physics of moisture-induced cracking in metal-glass (copper/silica) interfaces", *J. Appl. Phys.*, **102**, 2007, 053516-12.

S. Deville, E. Saiz, A. P. Tomsia, "Ice-templated porous alumina structures" *Acta Mater.*, **55**, 2007, 1965.

A. Gauffier, E. Saiz, E., A. P. Tomsia, P. Y. Hou. "The wetting behavior of NiAl and NiPtAl on polycrystalline alumina" *J. Mater. Sci.*, **42**, 2007, 9524-28.

E. Saiz, A. P. Tomsia, N. Rauch, N., C. Scheu, M. Rühle, M. Benhassine, D. Seveno, J. De Coninck, J., S. Lopez-Esteban. "Nonreactive spreading at high temperature", *Phys. Rev. E*, **76**, 2007, 041602.

A. Ziegler, J. C. Idrobo, C. Kisielowski, N. D. Browning, R. O. Ritchie, "Atomic-Resolution Observation of Semi-Crystalline Intergranular Thin Films in Silicon Nitride", *Appl. Phys. Lett.*, **88**, 2006, 141919.

V. Schroeder, R. O. Ritchie, "Stress-Corrosion Fatigue-Crack Growth in a Zr-Based Bulk Amorphous Metal", *Acta Mater.*, **54**, 2006, 1785-94.

C. W. Dwyer, A. Ziegler, N. Shibata, G. B. Winkelman, R. L. Satet, M. J. Hoffmann, M. K. Cinibulk, P. F. Becher, G. S. Painter, N. D. Browning, D. J. H. Cockayne, R. O. Ritchie, S. J. Pennycook, "Interfacial Structure in Silicon Nitride Sintered with Lanthanide Oxide", *J. Mater. Sci.*, **41**, 2006, 4405-12.

L. Gremillard, E. Saiz, V. Radmilovic, A. P. Tomsia, "Role of titanium on the reactive spreading of lead-free solders on alumina." *J. Mater. Res.*, **21**, 2006, pp. 3222-33.

S. Deville, E. Saiz, R. K. Nalla, A. P. Tomsia, "Freezing as a Path to Build Complex Composites," *Science*, **311**, 2006, 515-18.

J. C. Idrobo, H. Iddir, S. Ögüt, A. Ziegler, N. D. Browning, R. O. Ritchie, "Ab Initio Structural Energetics of $\beta\text{-Si}_3\text{N}_4$ Surfaces", *Phys. Rev. B*, **72**, 2005, 241301.

M. H. Jhon, A. M. Glaeser, D. C. Chrzan, "Computational Study of Stacking Faults in Sapphire," *Phys. Rev. B*, **71**, 2005, 214101.

Program Title

RADIATION DAMAGE EFFECTS IN CERAMICS AND NON-METALS

(FWP 09SCPE409)

Principal InvestigatorsKurt E. Sickafus,
Blas P. Uberuaga**Mailing Address**Los Alamos National Laboratory
MS-G755
Los Alamos, NM 87545**E-mail Address**kurt@lanl.gov
blas@lanl.gov**Program Scope**

The goal of this program is to understand radiation damage effects in ceramics exposed to energetic particles. Radiation damage studies of ceramics involve: (1) prediction of microstructural evolution in ceramics exposed to radiation; and (2) identification of physical aspects of ceramics that are effective in promoting radiation resistance. Our ultimate goal is to design new radiation-resistant ceramics. We conduct irradiation tests on single-, poly- and nano-crystalline ceramics, in order to evaluate their irradiation damage response. We perform computer simulations of damage evolution in ceramics to promote our understanding of radiation damage phenomena in these materials. In particular, we apply accelerated molecular dynamics techniques to reach experimentally-relevant time scales in our simulations. This allows us to assess defect mobility, annihilation and aggregation with the goal of predicting radiation damage in non-metallic, ionic materials. For example, we have found that radiation-induced interstitial clusters in some ceramics can be very mobile. This high mobility impacts such phenomenon as the interaction between collision cascades, which in turn, impacts the radiation damage accumulation rate. We expect radiation resistant ceramics to find application in existing fission reactors, in future fusion reactors or accelerator-based reactors, or as actinide-host ceramic fuel-forms and waste-forms.

Recent Progress*I. Predicting radiation damage trends in ceramics*

We have developed a method to predict trends in radiation damage resistance (specifically, stability against amorphization transformations) for oxide ceramics with varying chemistries (specifically, multi-component $A_xB_yO_z$ oxides, where A and B represent metal cations and O represents oxygen anions), but with similarities in crystal structure. The method is based on the postulate that ceramic compounds with natural tendencies to accommodate lattice disorder should exhibit superior structural stability in a radiation environment. We tested this hypothesis on compounds with crystal structures closely related to the *fluorite* (CaF_2) crystal structure. In a recent paper published in the journal *Nature Materials* [Sickafus et al. *Nature Mater.* 2007], we predicted differences in the irradiation damage response of iso-structural oxides known as delta (δ) phase compounds, with stoichiometries given by $A_4B_3O_{12}$. We based these predictions on the calculated energies of formation of point defects on both the cation and anion sublattices in these materials. We tested these predictions using ion irradiation experiments and found that $A_4B_3O_{12}$ compounds with low point defect formation energies had the highest structural stabilities (namely, they exhibit resistance to amorphization), while compounds with high point defect formation energies are less stable in a displacive radiation environment. These

results are in agreement with trends found previously for *pyrochlore* compounds (compounds with stoichiometry $A_2B_2O_7$), which suggests possible “*universal*” applications for these predictive methods.

II. Enhanced radiation tolerance in nanocrystalline compounds

We recently discovered a substantial enhancement in radiation-induced amorphization resistance for single-phased nanocrystalline (NC) versus large-grained polycrystalline (PC) compounds (specifically for NC versus PC magnesium gallate spinel, $MgGa_2O_4$) [Shen et al. *Appl. Phys. Lett.* 2007]. We irradiated both NC and PC $MgGa_2O_4$ with high doses of heavy ions and found that PC $MgGa_2O_4$ is rather readily amorphized (under low temperature irradiation conditions), while NC $MgGa_2O_4$ remains unchanged by ion irradiation. To our knowledge, this is the first experimental study to reveal radiation resistant properties (specifically, amorphization resistance) in a single-phase, NC material. These results have important implications for the development of advanced, highly robust materials for applications in extreme environments (e.g., nuclear reactors). Our study also provides an opportunity to advance our theoretical understanding of radiation damage phenomena, by developing atomistic models that reveal the mechanisms underlying these unanticipated results.

III. Modeling defect diffusion in complex oxides

One key component to understanding how materials evolve in a radiation environment is defect kinetics. Defects – vacancies, interstitials, and clusters of both – necessarily are formed under irradiation. Their mobility will govern how larger scale features, including voids and loops, are formed and evolve. We have used atomistic computer simulation (molecular dynamics (MD) and accelerated molecular dynamics (AMD)) methods to systematically investigate the mechanisms by which ions are transported in materials such as MgO, spinel, bixbyite, fluorite, perovskites and pyrochlores. We have discovered that interstitial clusters in materials that have a 1:1 stoichiometry, such as MgO, exhibit extremely high diffusivities. In contrast, clusters in more complex oxides such as $MgAl_2O_4$ spinel do have a tendency to aggregate, but do not diffuse in a highly concerted way as they do in MgO. However, spinel is surprising in that Al ions preferentially migrate on the Mg sublattice. Furthermore, we have examined the role that disorder plays in defect diffusion, again using spinel as a model compound [Uberuaga et al. *Phys. Rev. B* 2007]. The disorder in such materials effectively creates traps to oxygen transport. Thus, the overall diffusivity of oxygen is decreased as cation disorder is increased in the material (we anticipate these trends with increasing radiation dose). In addition, we have examined how impurities, which are always present in real materials, trap defects and defect clusters, also retarding their diffusion. Such effects would have consequences on radiation damage evolution, as defects are less able to find sinks and other defects to form aggregates.

Future Plans

I. Experiments on irradiated ceramics with potential for use in nuclear reactor applications

We intend to examine radiation damage-induced microstructural evolution in materials subjected to both ionization and displacive radiation at high temperatures (so-called *spectrum effects*). The high temperature experiments are necessary to study radiation damage recovery and especially to mimic environmental conditions similar to those experienced by ceramics that may function as either fuel materials or structural materials in advanced, high-temperature nuclear reactors. Our studies will greatly improve our understanding of fundamental mechanisms associated with the radiation-induced swelling in complex ceramic materials.

We will use a wide range of characterization techniques to probe a variety of materials’ radiation effects, from atomic point defect formation (such as interstitials and vacancies), to macroscopic property alterations, including thermal conductivity degradation and increases (or decreases) in mechanical hardness. Our main experimental characterization expertise has always been in transmission electron microscopy (TEM) and X-ray diffraction (XRD) techniques, and we will continue to emphasize these techniques in our future work. But the primary goal of our studies is to establish linkages between our theoretical predictions of materials’ radiation damage behavior at the

atomic scale and the effects that we observe experimentally. With this in mind, we will employ any and all experimental characterization techniques necessary to best relate to our theoretical efforts.

We will emphasize experimental studies of radiation-induced microstructural evolution in oxides including *spinels* (MgAl_2O_4 , MgGa_2O_4 , etc.) and *fluorites* (ZrO_2 , CeO_2 , HfO_2 , ThO_2 , and UO_2 , as well as mixtures of these dioxides with lanthanides, Ln_2O_3). We will simulate neutron-induced displacement damage and fission product damage using selected irradiating ion species and ion energies.

II. Atomistic computer simulations of initial stages of microstructural evolution in oxide ceramics

As mentioned earlier, our theoretical effort has revealed several interesting and key insights into the behavior of defects in ceramics as relates to their radiation resistance. Over the next few years, we will focus on understanding the early formation of microstructural features in irradiated oxides, including interstitial loops and vacancy voids. These larger-scale features are observable in TEM experiments and thus offer the best opportunity for connecting theory and experiment. In order to do this, we will develop higher level modeling capabilities. In the past, we have used chemical rate theory to explore the impact that mobile clusters have on the predicted loop size in MgO. We have begun development of a kinetic Monte Carlo (KMC) capability that will allow us to more directly incorporate the results from MD and AMD simulations, allowing us to determine the role that atomic-scale diffusive processes have on the formation and structure of loops and voids.

With regard to the specific areas of materials research, we will focus on the following: 1) determine the types and numbers of defects produced during collision cascades in fluorite-related materials, such as bixbyites and δ -phase materials; and 2) develop KMC capabilities to look at the insipient formation of voids and loops in oxide materials. Regarding this last point, we will compare and contrast materials such as MgO and spinel in which the kinetic behavior of defects are very different. Once these capabilities are mature, we will apply them to fluorite-derivative materials. These efforts will allow us to understand how elemental defect properties control larger microstructural features.

References (DOE/OBES-sponsored research publications, 2006-present)

2006

A.R. Cleave, R.W. Grimes, R. Smith, B.P. Uberuaga and K.E. Sickafus, Nucl. Instrum. and Meth. B **250** (2006) 28.

B.P. Uberuaga, R. Smith, A.R. Cleave, R.W. Grimes, A.F. Voter and K.E. Sickafus, Nucl. Instrum. and Meth. B **250** (2006) 12.

C.R. Stanek, B.P. Uberuaga, K.J. McClellan, M. R. Levy, R.W. Grimes, Phys. Stat. Sol. C **4** (2007) 984.

C.R. Stanek, J.A. Valdez, K.E. Sickafus, K.J. McClellan and R.W. Grimes, Ceram. Eng. Sci. Proc. **27** (5) (2006) 162.

D. Bacorisen, R. Smith, J.A. Ball, R.W. Grimes, B.P. Uberuaga and K.E. Sickafus, Nucl. Instrum. and Meth. B **250** (2006) 36.

D. Bacorisen, R. Smith, B.P. Uberuaga, K.E. Sickafus, J.A. Ball and R.W. Grimes, Phys. Rev. B **74** (2006) 214105.

E.R. Batista, J. Heyd, R.G. Hennig, B.P. Uberuaga, R.L. Martin, G.E. Scuseria, C.J. Umrigar, and J.W. Wilkins, Phys. Rev. B **74** (2006) 121102.

J.A. Valdez, M. Tang and K.E. Sickafus, Nucl. Instrum. and Meth. B **250** (2006) 148.

J.K. Lee, H.S. Jung, J.A. Valdez, M.F. Hundley, J.D. Thompson, K.E. Sickafus, M. Nastasi, D.W. Hamby, D.A. Lucca, Nucl. Instrum. and Meth. B **250** (2006) 279.

K. Omae, I.-T. Bae, M. Naito, M. Ishimaru, Y. Hirotsu, J.A. Valdez and K.E. Sickafus, Nucl. Instrum. and Meth. B **250** (2006) 300.

M. Ishimaru, I.-T. Bae, A. Hirata, Y. Hirotsu, J.A. Valdez and K.E. Sickafus, Nucl. Instrum. and Meth. B **242** (2006) 473.

“A multi-scale study of the role of microstructure in the deformation behavior of hexagonal materials”

FWP Number: 09SCPE401

Principal Investigator: Dr Carlos N. Tomé

MST-8, LANL, MS-G755
Los Alamos National Laboratory
Los Alamos, NM 87545
phone: 505-665-0892, e-mail: tome@lanl.gov

Program Scope

This program is a comprehensive study of the connection between microstructural features (dislocations, twins, grain boundaries and twin boundaries) and the observed mechanical response of Hexagonal Close Packed (HCP) metallic aggregates. This research plan interconnects modeling, simulation, and experimental studies at length scales that go from the atomistic to the continuum. It draws on a range of LANL characterization and modeling tools, individual and institutional expertise, and on the unique neutron diffraction capabilities of the BES funded spectrometers SMARTS and HIPPO at the Los Alamos Lujan Center. Part of the proposed research involves using the synchrotron source at Argonne National Lab. **The goals of this project are: a) to provide insight into the basic crystallographic mechanisms of deformation in HCP and their role in deformation and fracture; b) to develop a predictive capability of mechanical response based on such mechanisms.**

Recent progress

The systems analyzed in this project are: pure Zr, Mg alloy AZ31 and, to a lesser extent, Be and Hf. All of them shear plastically via several slip and twin modes, whose relative contribution to deformation varies with temperature, strain rate, and polycrystal texture. In this project we use loading histories involving changes in direction and temperature as a paradigm to reveal the role of microstructure in hardening. The load-change procedure is particularly revealing when dealing with twinning, because twins induced during the pre-load stage act as barriers to dislocations or to other twins during the reload stage.

Two recent publications [Proust et al, Acta, 2007; Beyerlein and Tomé, IJP, 2007] provide a summary of the advances done in this project in what concerns developing crystallographically based constitutive laws of plastic response. These results represent the state-of-the-art in what concerns constitutive description of this class of materials. Specifically, we utilize experimental information about evolution of texture, hardening, and volume fraction of twinning to build up macroscopic constitutive models, function of temperature, rate and texture. TEM and MD provide information on active slip and twin systems, de-twinning, twin morphology, and twin-dislocation interactions. Such information is accounted for by the meso-scale model representing the grains. *The invited talk to this Contractors Meeting by Irene Beyerlein will describe such progress.*

Also as part of this program we perform in-situ neutron diffraction during tensile, compressive and cyclic testing of Zr, Mg and Be. We characterize the active deformation systems, their activation stresses, twinning, de-twinning, and the evolution of internal stresses. We have developed a symbiotic procedure between these experiments and polycrystal elasto-plastic simulations [Agnew et al, Acta, 2006], which we use to infer basic information about crystallographic mechanisms. An important progress in this area is our experimental

measurement - and incorporation into grain models - of the stress relaxation associated with twin activation in Mg [Clausen et al, Acta, 2008].

The microscopic scale component of this project comprises TEM, EBSD, Molecular Dynamics and Dislocation simulations. TEM has been instrumental in characterizing active slip and twin systems in Zr and Mg as a function of temperature. One of the relevant results of this characterization is the identification of slip and secondary twinning inside primary twins, which explains the ductility observed in these HCP aggregates despite the scarcity of 'soft' deformation modes [McCabe et al, Phil Mag, 2006]. An important contribution of this project was the development of an automated EBSD technique for quantifying twinning in deformed aggregates [McCabe et al, IJP, 2008; Proust et al, Met Trans, 2008]. The latter information is invaluable both, for understanding quantitatively the contribution of twinning to deformation, and to provide benchmarks against which to compare the prediction of our constitutive models.

Molecular Dynamics has been applied to understand the interaction between dislocation and twin interfaces (relevant to understanding hardening) and has started being used to study the atomistic mechanisms leading to twin nucleation, a process still not understood in HCP. Dislocation simulations have been applied to analyze whether dislocation dissociations can be energetically favorable to induce twin nucleation. *Preliminary results of this microscopic theoretical treatment are going to be presented in a Poster by Capolungo, Wang et al. during this Contractors Meeting.*

Future plans

During the previous phase of this project we have been able to achieve a reasonable grasp of the meso (grain) and macro (aggregate) characterization of plasticity in HCP. In the next phase we foresee to focus more intensely in the microscopic aspects, in order to both, improve our basic understanding of the deformation mechanisms, and incorporate more physics and less empiricism in our multiscale constitutive models.

For such purpose we have started to use synchrotron X-ray diffraction for detailed characterization of the stress evolution associated with twin nucleation and propagation in individual grains of Mg. In addition, we expect that cyclic experiments done in Zr and Mg under neutron irradiation will yield information on: evolution of dislocation structures in HCP materials, twin & de-twin processes, build-up of internal stress. Such information (relevant for example to Bauschinger effects) will be interpreted and implemented into meso-scale models of intragranular structures.

We have started recently doing in-situ TEM on FIB tensile specimens, with the intention of characterizing dislocation reactions at twin interfaces, which is one of the basic mechanisms behind the observed hardening response of HCP materials.

Twin nucleation is a necessary stage at the initiation of deformation, but it is also an elusive mechanism for experimental characterization. We have started using Molecular Dynamics (MD) and dislocation theory for studying the atomistic and dislocation processes associated with twin nucleation in HCP. As with all the other microscopic information, we expect this information to find its way into mechanisms and microstructure based models of hardening.

We plan, in the short term, to use the expertise acquired in this project for starting a study of shape memory alloys. Transformations induced by load, temperature and magnetic fields – all combined - will be characterized using the unique capabilities of the SMARTS neutron diffractometer at LANL. Polycrystal-based constitutive models for describing this class of materials are still in their infancy. We believe that we can extend the Visco Plastic and Elasto Plastic models, plus the twin transformation models, done for this project, to provide a much needed theoretical tool for interpreting the diffraction experiments and for learning about the basic processes taking place during the shape memory effect.

DOE sponsored publications 2006-2007

- S.R. Agnew, D.W. Brown, and C.N. Tomé, “Validating a Polycrystal Model for the Elasto-Plastic Response of Magnesium Alloy AZ31 Using In-situ Neutron Diffraction,” *Acta Mater.*, vol. **54** (2006) 4841-4852.
- M.I. Baskes, S.G. Srinivasan, S. Valone, R.G. Hoagland, “Multi-state Modified Embedded Atom Method”, *Phys. Rev. B*, vol. **75** (2007) p. 94113.
- I.J. Beyerlein and C.N. Tomé, “Modeling directional anisotropy in grains subjected to large strains and strain path changes”, *Ultrafine Grained Materials IV. Edited by Y.T. Zhu, T.G. Langdon, Z. Horita, M.J. Zehetbauer, S.L. Semiatin and T.C. Lowe*. TMS (The Minerals, Metals & Materials Society) (2006) pp. 63-71.
- I. J. Beyerlein and C. N. Tomé, “Modeling transients in the mechanical response of copper due to strain path changes”, *Int. Journal of Plasticity* **23** (2007) 640-664
- I. J. Beyerlein and C. N. Tomé, “Modeling compression and tension reloads in copper pre-strained by rolling”, *Materials Science Forum* 539-543 (2007) 3383-88.
- I. J. Beyerlein, L. S. Tóth, C. N. Tomé, and S. Suwas, “Role of twinning on texture evolution of silver during equal channel angular extrusion”, *Philosophical Mag.* **87** (2007) 885-906.
- I. J. Beyerlein, D. J. Alexander and C. N. Tomé, “Plastic Anisotropy in Aluminum and Copper pre-strained by Equal Channel Angular Extrusion (ECAE)”, *Journal of Materials Science* **42** (2007) 1733-1750.
- I.J. Beyerlein and C.N. Tomé, “A dislocation based constitutive law for pure Zr including temperature effects”, *Int. Journal of Plasticity* **24** (2008) 867-895
- D.W. Brown, A. Jain, S.R. Agnew and B. Clausen, "Twinning and Detwinning During Cyclic Deformation of Mg Alloy AZ31B", *Materials Science Forum*, vol. 539-543, pp. 3407-3413 (2007)
- E. Cerreta, C.A. Yablinsky, G.T. Gray III, S.C. Vogel, and D.W. Brown, “The Influence of Grain Size and Texture on the Mechanical Response of High Purity Hafnium” *Materials Science and Engineering A*, **456** (2007) 243-251.
- E. Cerreta, G.T. Gray III, and C.P. Trujillo, “The Influence of Peak Shock Pressure on the Quasi-static Reload Response of Hafnium” *Journal de Physique IV*, **134** (2006) 1029-1034.
- E. Cerreta, G.T. Gray, A.C. Lawson, C.E. Morris, T.A. Mason, R.S. Hixson, and P.A. Rigg, “The Influence of Oxygen Content on the Pressure Induced Phase Transformation and Shock Hardening of Titanium” *Journal of Applied Physics*, **100** (2006) 0135301-9.
- B. Clausen, C.N. Tomé, D.W. Brown and S.R. Agnew, "Reorientation and Stress Relaxation due to Twinning: Modeling and Experimental Characterization for Mg", *Acta Mater.* (2008) in press.
- A. Jain and S.R. Agnew, “Modeling the Temperature Dependent Effect of Twinning on the Behavior of Magnesium Alloy AZ31B Sheet,” *Mater. Science Eng. A*, in press.
- A. Jain, D.W. Brown, and S.R. Agnew, “Twinning and Detwinning Cyclic Deformation of Mg Alloy AZ31B,” *Mater. Sci. Forum*, (2007), 539-543
- A. Jain and S.R. Agnew, “Effect of Twinning on the Mechanical Behavior of a Magnesium Alloy Sheet During Strain Path Changes,” *Magnesium Technology 2006*, Eds. A. Luo, N. Nealameggham, R.S. Beals, (TMS: Warrendale, PA:2006) 219-224.
- G.C. Kaschner, C.N. Tomé, R.J. McCabe, A. Misra, S.C. Vogel, and D.W. Brown. “Exploring the Dislocation/Twin Interactions in Zirconium”, *Mat Sci Eng A* **463** (2007) 122-127.
- G.C. Kaschner, C.N. Tomé, I.J. Beyerlein, S.C. Vogel, D.W. Brown, R.J. McCabe. “Role of Twinning in the Hardening Response of Zirconium during Temperature Reloads” *Acta Mat.* **54** (2006) 2887-2896.
- Y.M. Kim, B.J. Lee and M.I. Baskes, “Modified embedded-atom method interatomic potentials for Ti and Zr”, *Phys. Rev. B*, vol.**74** (2006) p.14101

- R.A. Lebensohn, C.N. Tomé and P. Ponte Castañeda, “Self-consistent modeling of the mechanical behavior of viscoplastic polycrystals incorporating intragranular field fluctuations”, *Philosophical Magazine* **87** (2007) 4287-4322
- R.J. McCabe, E.K. Cerreta, A. Misra, G.C. Kaschner, C.N. Tomé. “Effects of Texture, Temperature, and Strain on the Deformation Modes of Zirconium”, *Phil Mag* **86** (2006) 3595-3611.
- R.J. McCabe, G. Proust, E.K. Cerreta, A. Misra, “Quantitative Analysis of Deformation Twinning in Zirconium,” *Int. J. of Plasticity* (2008) in press.
- G. Proust, R.J. McCabe, J.T. Rogers, “Improvements on the Automated Twin Identification Technique using Electron Backscatter Diffraction Data,” *Met. Trans* (2008) in press.
- G. Proust, C.N. Tomé, and G.C. Kaschner. “Modeling Texture, Twinning, and Hardening Evolution During Deformation of Hexagonal Materials”, *Acta Materialia* vol. **55** (2007) 2137-2148.
- B. Raesinia, C.W. Sinclair, W.J. Poole, C.N. Tomé, “On the impact of grain size distribution on plastic behaviour of polycrystalline metals”, *MSMSE* 16 (2008), in press.
- C. A. Yablinsky, E. Cerreta, and G. T. Gray,” The Influence of Twinning on the Work Hardening Behavior of Hafnium”, *Metallurgical and Materials Transactions A* (in press).
- C.A. Yablinsky, E. Cerreta, G.T. Gray, S.C. Vogel, and D.W. Brown, “The Effect of Twinning on the Work Hardening Behavior and Microstructural Evolution of Hafnium” *Metallurgical and Materials Transactions A*, **37** (2006) 1907-1915.
- G. G. Yapici, I. J. Beyerlein, I. Karaman, C. N. Tomé, “Tension-Compression Asymmetry in Severely Deformed Pure Copper”, *Acta Materialia* **55** (2007) 4603-4613.

Defects and Defect Processes in Ceramics

William J. Weber, Principal Investigator
Email: bill.weber@pnl.gov

Ram Devanathan, Fei Gao, Weilin Jiang, and Yanwen Zhang
Co-Principal Investigators

Pacific Northwest National Laboratory
P.O. Box 999, Mail Stop K8-87, Richland, WA 99352

Program Scope: Experimental and computational methods are synergistically integrated to study defects and the dynamic processes associated with defect formation and migration, defect-defect interactions, and the evolution of nanostructures and phase transformations, including effects of localized electronic excitations. Defect formation, defect configurations, defect migration, defect interactions, and kinetics of defect processes are experimentally investigated as functions of temperature, time and environmental conditions, as well as studied using density functional theory, *ab initio* molecular dynamics, classical molecular dynamics, and kinetic Monte Carlo techniques. The objective is to develop fundamental understanding and models of electronic excitations, atomic-level defects, defect/property relationships, and dynamics of defect processes in ceramic structures that support the development of predictive models of materials behavior over multiple length and time scales.

Recent Progress: Research has: 1) developed basic understanding and predictive models of defect processes and irradiation damage in covalent and ionic ceramics over multiple scales; 2) quantified ionization-induced recovery processes in ceramics; 3) developed improved interatomic potentials for SiC, ZrSiO₄, UO₂; 4) developed computational models for defect recovery and recrystallization in SiC; 5) used *ab initio* molecular dynamics to evaluate threshold displacement processes, charge transfer and charge-assisted defect formation in SiC and GaN; 6) developed computational models of thermo-mechanical properties of GaN nanotubes and nanowires; and 7) determined electronic stopping power of ions in ceramics and identified deficiencies in current stopping power models.

Future Plans: Future research includes experimental and computational efforts to systematically study the effects of dynamic localized electronic excitations, induced by ionizing radiation, on defect annealing, recrystallization, and hydrogen/helium diffusion. Work on developing a fundamental understanding and models of the complex correlations of electronic and atomic dynamic processes, as well as materials behavior far from equilibrium. Study defect-interface interactions, gas transport, and radiation effects in nanostructured ceramics.

Peer-Reviewed Journal Publications (2005 – 2008):

1. Y. Zhang, W. J. Weber, A. Razpet, and G. Possnert, **Electronic Stopping Powers for He, Be and F in Au**, *Nucl. Instrum. and Methods in Physics Res.* **B 227** [4]: 479-484 (2005).
2. Y. Zhang, F. Gao, W. Jiang, D. E. McCready, and W. J. Weber, **Studies of Damage Accumulation in 4H Silicon-Carbide by Ion-Channelling Techniques**, *Materials Science Forum* **475-479**: 1341-1344 (2005).
3. W. J. Weber, F. Gao, R. Devanathan, W. Jiang, and Y. Zhang, **Defects and Ion-Solid Interactions in Silicon Carbide**, *Materials Science Forum* **475-479**: 1345-1350 (2005).
4. F. Gao, E. J. Bylaska, and W. J. Weber, **Defect Properties in GaN: Ab Initio and Empirical Potential Calculations**, *Materials Science Forum* **475-479**: 3087-3090 (2005).
5. M. Posselt, F. Gao, and D. Zwicker, **Migration of Di- and Tri-Interstitials in Silicon**, *Nucl. Instrum. and Methods in Physics Res.* **B 228** [1-4]: 212-217 (2005).
6. L. R. Corrales, A. Chartier, and R. Devanathan, **Excess Kinetic Energy Dissipation in Materials**, *Nucl. Instrum. and Methods in Physics Res.* **B 228** [1-4]: 274-281 (2005).
7. F. Gao, R. Devanathan, Y. Zhang, and W. J. Weber, **Annealing Simulations of Nano-Sized Amorphous Structures in SiC**, *Nucl. Instrum. and Methods in Physics Res.* **B 228** [1-4]: 282-287 (2005).
8. H. L. Heinisch and W. J. Weber, **Computational Model of Alpha-Decay Damage Accumulation in Zircon**, *Nucl. Instrum. and Methods in Physics Res.* **B 228** [1-4]: 293-298 (2005).
9. R. Devanathan, L. R. Corrales, W. J. Weber, A. Chartier, and C. Meis, **Molecular Dynamics Simulation of Defect Production in Collision Cascades in Zircon**, *Nucl. Instrum. and Methods in Physics Res.* **B 228** [1-4]: 299-303 (2005).

10. P. Nachimuthu, S. Thevuthasan, V. Shutthanandan, E. M. Adams, W. J. Weber, B. D. Begg, D. K. Shuh, D. W. Lindle, E. M. Gullikson, and R. C. C. Perera, **Near-Edge X-ray Absorption Fine-Structure Study of Ion-Beam-Induced Phase Transformation in $Gd_2(Ti_{1-y}Zr_y)_2O_7$** , *J. Applied Physics* **97**: 033518 (2005).
11. A. Chartier, C. Meis, J.-P. Crocombette, W. J. Weber, and L. R. Corrales, **Molecular Dynamic Simulation of Disorder Induced Amorphization in Pyrochlores**, *Physical Review Letters* **94**: 025505 (2005).
12. P. Nachimuthu, S. Thevuthasan, E. M. Adams, W. J. Weber, B. D. Begg, B. S. Mun, D. K. Shuh, D. W. Lindle, E. M. Gullikson, and R. C. C. Perera, **Near-Edge X-ray Absorption Fine Structure Study of Disorder in $Gd_2(Ti_{1-y}Zr_y)_2O_7$** , *J. Physical Chemistry B* **109** [4]: 1337-1339 (2005).
13. F. Gao and W. J. Weber, **Atomic-Level Computer Simulation of SiC: Defect Accumulation, Mechanical Properties and Defect Recovery**, *Philosophical Magazine* **85** [4-7]: 509-518 (2005).
14. W. Jiang, V. Shutthanandan, S. Thevuthasan, C. M. Wang and W. J. Weber, **Nitrogen Analysis Using Energetic Ion Beams**, *Surface and Interface Analysis* **37** [4]: 374-378 (2005).
15. W. Jiang, W. J. Weber, C. M. Wang, J. S. Young, L. A. Boatner, J. Lian, L. M. Wang, and R. C. Ewing, **Cadmium Nanowire Formation Induced by Ion Irradiation**, *Advanced Materials* **17** [13]: 1602-1606 (2005).
16. M. Posselt, F. Gao, and D. Zwicker, **Atomistic Study of the Migration of Di- and Tri-Interstitials in Silicon**, *Physical Review B* **71**: 245202 (2005).
17. Y. Zhang, W. J. Weber, D. E. McCready, D. A. Grove, J. Jensen, and G. Possnert, **Experimental Determination of Electronic Stopping for Ions in Silicon Dioxide**, *Applied Physics Letters* **87**: 104103 (2005).
18. B. S. Thomas, N. A. Marks, L. R. Corrales, and R. Devanathan, **Threshold Displacement Energies in Rutile TiO_2 : A Molecular Dynamics Simulation Study**, *Nucl. Instrum. and Methods in Physics Res. B* **239** [3]: 191-201 (2005).
19. Y. Zhang, J. Lian, C. M. Wang, W. Jiang, R. C. Ewing, and W. J. Weber, **Ion-Induced Damage Accumulation and Electron-Beam-Enhanced Recrystallization in $SrTiO_3$** , *Physical Review B* **72**: 094112 (2005).
20. R. Devanathan and W. J. Weber, **Insights into the Radiation Response of Pyrochlores from Calculations of Threshold Displacement Events**, *J. Applied Physics* **98**: 086110 (2005).
21. W. Jiang, W. J. Weber, and L. A. Boatner, **Accumulation and Recovery of Disorder in Au^{2+} -Irradiated $Cd_2Nb_2O_7$** , *Nucl. Instrum. and Methods in Physics Res. B* **241** [1-4]: 372-376 (2005).
22. C. M. Wang, Y. Zhang, V. Shutthanandan, D. R. Baer, W. J. Weber, L. E. Thomas, S. Thevuthasan, and G. Duscher, **Self-Assembling of Nanocavities in TiO_2 Dispersed with Au Nanoclusters**, *Physical Review B* **72**: 245221 (2005).
23. Y. Zhang, W. J. Weber, A. Razpet, and G. Possnert, **Electronic Stopping Powers for Be, Ca and Ti in SiC**, *Nucl. Instrum. and Methods in Physics Res. B* **242** [1-2]: 82-84 (2006).
24. C. M. Wang, V. Shutthanandan, Y. Zhang, S. Thevuthasan, L.E. Thomas, W. J. Weber, and G. Duscher, **Atomic-Level Imaging of Au Nanocluster Dispersed in TiO_2 and $SrTiO_3$** , *Nucl. Instrum. and Methods in Physics Res. B* **242** [1-2]: 380-382 (2006).
25. W. Jiang and W. J. Weber, **Effect of Irradiation Temperature on Dynamic Recovery in Gallium Nitride**, *Nucl. Instrum. and Methods in Physics Res. B* **242** [1-2]: 431-433 (2006).
26. Y. Zhang et al. **Formation of Cobalt Silicide Films by Ion Beam Deposition**, *Nucl. Instrum. and Methods in Physics Res. B* **242** [1-2]: 602-604 (2006).
27. R. M. Van Ginhoven, A. Chartier, C. Meis, W. J. Weber, and L. R. Corrales, **Theoretical Study of Helium Insertion and Diffusion in 3C-SiC**, *J. Nuclear Materials* **348** [1-2]: 51-59 (2006).
28. S. Thevuthasan, V. Shutthanandan, and Y. Zhang, **Applications of High Energy Ion Beam Techniques in Environmental Science: Investigation Associated with Glass and Ceramic Waste Forms**, *J. Electron Spectroscopy and Related Phenomena* **150** [2-3]: 195-207 (2006).
29. J.-P. Crocombette, A. Chartier, and W. J. Weber, **Atomistic Simulation of Amorphization Thermokinetics in Lanthanum Pyrozirconate**, *Applied Physics Letters* **88**: 051912 (2006).
30. W. Jiang, V. Shutthanandan, Y. Zhang, S. Thevuthasan, W. J. Weber, and G. J. Exarhos, **Hydrogen Behavior in Mg^{+} -Implanted Graphite**, *J. Materials Research* **21** [4]: 811-815 (2006).
31. M. Posselt, F. Gao, and W. J. Weber, **Atomistic Simulations on the Thermal Stability of the Antisite Pair in 3C- and 4H-SiC**, *Physical Review B* **73**: 125206 (2006).
32. E. J. Bylaska, K. Tsemekhman, and F. Gao, **New Development of Self-Interaction Corrected DFT for Extended Systems Applied to the Calculation of Native Defects in 3C-SiC**, *Physica Scripta* **T124**: 86-90 (2006).
33. F. Gao, R. Devanathan, Y. Zhang, M. Posselt, and W. J. Weber, **Atomic-Level Simulation of Epitaxial Recrystallization and Phase Transformation in SiC**, *J. Materials Research* **21** [6]: 1420-1426 (2006).

34. T. A. G. Wiss, J.-P. Hiernaut, P. M. G. Damen, S. Lutique, R. Fromknecht, and W. J. Weber, **Helium Behaviour in Waste Conditioning Matrices during Thermal Annealing**, *J. Nuclear Materials* **352** [1-3]: 202-208 (2006).
35. Y. Zhang, J. Jensen, G. Possnert, D. A. Grove, D. E. McCready, B. W. Arey, and W. J. Weber, **Electronic Stopping Forces of Heavy Ions in Metal Oxides**, *Nucl. Instrum. and Methods in Physics Res.* **B 249** [1-2]: 18-21 (2006).
36. L. R. Corrales and R. Devanathan, **Characterization of Energy Conservation in Primary Knock-On Atom Cascades: Ballistic Phase Effects on Variable Time Steps**, *Nucl. Instrum. and Methods in Physics Res.* **250** [1-2]: 6-11 (2006).
37. W. Jiang, Y. Zhang, W. J. Weber, J. Lian, and R. C. Ewing, **Direct Evidence of N Aggregation and Diffusion in Au⁺ Irradiated GaN**, *Applied Physics Letters* **89**: 021903 (2006).
38. A. Chartier, J.-P. Crocombette, C. Meis, W. J. Weber, and L. R. Corrales, **Radiation Effects in Lanthanum Pyrozoirconate**, *Nucl. Instrum. and Methods in Physics Res.* **B 250** [1-2]: 17-23 (2006).
39. R. Devanathan, L. R. Corrales, W. J. Weber, A. Chartier, and C. Meis, **Atomistic Simulation of Collision Cascades in Zircon**, *Nucl. Instrum. and Methods in Physics Res.* **B 250** [1-2]: 46-49 (2006).
40. F. Gao, R. Devanathan, T. Oda, and W. J. Weber, **Development of Partial-Charge Potential for GaN**, *Nucl. Instrum. and Methods in Physics Res.* **B 250** [1-2]: 50-53 (2006).
41. Y. Zhang, W. J. Weber, D. A. Grove, J. Jensen, and G. Possnert, **Electronic Stopping Powers for Heavy Ions in Niobium and Tantalum Pentoxides**, *Nucl. Instrum. and Methods in Physics Res.* **B 250** [1-2]: 62-65 (2006).
42. J. Lian, W. J. Weber, W. Jiang, L. M. Wang, L. A. Boatner, and R. C. Ewing, **Radiation-Induced Effects in Pyrochlore and Nanoscale Materials Engineering**, *Nucl. Instrum. and Methods in Physics Res.* **B 250** [1-2]: 128-136 (2006).
43. W. Jiang, W. J. Weber, J. S. Young, L. A. Boatner, J. Lian, L. M. Wang, and R. C. Ewing, **Irradiation-Induced Nanostructures in Cadmium Niobate Pyrochlores**, *Nucl. Instrum. and Methods in Physics Res.* **B 250** [1-2]: 188-191 (2006).
44. J. Nie, H. Y. Xiao, X. Zu, and F. Gao, **First principles calculations on Na and K-adsorbed diamond(100) surface**, *Chemical Physics* **326** [2-3]: 308-314 (2006).
45. Y. Zhang, W. J. Weber, V. Shutthanandan, and S. Thevuthasan, **Non-linear Damage Accumulation in Au-irradiated SrTiO₃**, *Nucl. Instrum. and Methods in Physics Res.* **B 251** [1]: 127-132 (2006).
46. F. Gao, Y. Zhang, M. Posselt, and W. J. Weber, **Atomic-Level Simulations of Epitaxial Recrystallization and Amorphous-to-Crystalline Transition in 4H-SiC**, *Physical Review* **B 74**: 104108 (2006).
47. Z. Wang, X. Zu, F. Gao, and W. J. Weber, **Atomic-Level Study of Melting Behavior of GaN Nanotubes**, *J. Applied Physics* **100**: 063503 (2006).
48. R. Devanathan, L. R. Corrales, W. J. Weber, A. Chartier, and C. Meis, **Molecular Dynamics Simulation of Energetic Uranium Recoil Damage in Zircon**, *Molecular Simulation* **32** [12-13]: 1069-1077 (2006).
49. Y. Zhang, C. M. Wang, M. H. Engelhard, and W. J. Weber, **Irradiation Behavior of SrTiO₃ at Temperatures Close to the Critical Temperature for Amorphization**, *J. Applied Physics* **100**: 113533 (2006).
50. J. Du, R. Devanathan, L. R. Corrales, W. J. Weber, and A. N. Cormack, **Short- and Medium-Range Structure of Amorphous Zircon from Molecular Dynamics Simulations**, *Physical Review* **B 74**: 214204 (2006).
51. Z. Wang, X. Zu, F. Gao, and W. J. Weber, **Atomistic Simulation of Brittle to Ductile Transition in GaN Nanotubes**, *Applied Physics Letters* **89**: 243123 (2006).
52. W. Jiang, Y. Zhang, V. Shutthanandan, S. Thevuthasan, and W. J. Weber, **Temperature Response of ¹³C Atoms in Amorphized 6H-SiC**, *Applied Physics Letters* **89**: 261902 (2006).
53. I.-T. Bae, Y. Zhang, W. J. Weber, M. Higuchi, and L. A. Giannuzzi, **Electron-Beam Induced Recrystallization in Amorphous Apatite**, *Applied Physics Letters* **90**: 021912 (2007).
54. W. Jiang, Y. Zhang, M. H. Engelhard, W. J. Weber, G. J. Exarhos, J. Lian, and R. C. Ewing, **Behavior of Si and C Atoms in Ion Amorphized SiC**, *J. Applied Physics* **101**: 023524 (2007).
55. J.-P. Crocombette, G. Dumazer, N. Q. Hoang, F. Gao, and W. J. Weber, **Molecular Dynamics Modeling of the Thermal Conductivity of SiC as a Function of Cascade Overlap**, *J. Applied Physics* **101**: 023527 (2007).
56. R. Devanathan, F. Gao, and W. J. Weber, **Atomistic Modeling of Amorphous Silicon Carbide using a Bond-Order Potential**, *Nucl. Instrum. and Methods in Physics Res.* **B 255** [1]: 130-135 (2007).
57. F. Gao, Y. Zhang, R. Devanathan, M. Posselt, and W. J. Weber, **Atomistic Simulations of Epitaxial Recrystallization in 4H-SiC along the [0001] Direction**, *Nucl. Instrum. and Methods in Physics Res.* **B 255** [1]: 136-140 (2007).
58. R. Devanathan, P. Durham, J. Du, L. R. Corrales, and E. M. Bringa, **Molecular Dynamics Simulation of Amorphization in Forsterite by Cosmic Rays**, *Nucl. Instrum. and Methods in Physics Res.* **B 255** [1]: 172-176 (2007).

59. Z. Wang, X. Zu, F. Gao, and W. J. Weber, **Size Dependence of Melting of GaN Nanowires with Triangular Cross Sections**, *J. Applied Physics* **101**: 043511 (2007).
60. Z. Wang, X. Zu, F. Gao, and W. J. Weber, **Atomistic Study of the Melting Behavior of Single Crystalline Wurtzite Gallium Nitride Nanowires**, *J. Materials Research* **22** [3]: 742-747 (2007).
61. I.-T. Bae, W. J. Weber, M. Ishimaru, and Y. Hirotsu, **Effect of Ionization Rates on Dynamic Recovery Processes during Electron-Beam Irradiation of 6H-SiC**, *Applied Physics Letters* **90**: 121910 (2007).
62. R. Devanathan and W. J. Weber, **Radiation Effects in a Model Ceramic for Nuclear Waste Disposal**, *JOM* **59**: 32-35 (2007).
63. W. M. Zhang, Y. G. Wang, J. Li, J. M. Xue, H. Ji, Q. Ouyang, J. Xu, and Y. Zhang, **Controllable Shrinking and Shaping of Silicon Nitride Nanopores under Electron Irradiation**, *Applied Physics Letters* **90**: 163102 (2007).
64. Z. Wang, X. T. Zu, F. Gao, W. J. Weber, and J.-P. Crocombette, **Atomistic Simulation of the Size and Orientation Dependences of Thermal Conductivity in GaN Nanowires**, *Applied Physics Letters* **90**: 161923 (2007).
65. Z. Wang, F. Gao, J.-P. Crocombette, X. T. Zu, L. Yang, and W. J. Weber, **Thermal Conductivity of GaN Nanotubes Simulated by Nonequilibrium Molecular Dynamics**, *Physical Review B* **75**: 153303 (2007).
66. F. Gao, J. Du, E. J. Bylaska, M. Posselt, and W. J. Weber, **Ab Initio Atomic Simulations of Antisite Pair Recovery in Cubic Silicon Carbide**, *Applied Physics Letters* **90**: 221915 (2007).
67. Z. Wang, X. Zu, L. Yang, F. Gao, and W. J. Weber, **Atomistic Simulations of the Size, Orientation and Temperature Dependence of Tensile Behavior in GaN Nanowires**, *Physical Review B* **76**: 045310 (2007).
68. Y. Zhang, J. Jensen, G. Possnert, D. A. Grove, I.-T. Bae, and W. J. Weber, **Stopping Power Measurements of He Ions in Si and SiC by Time of Flight Spectrometry**, *Nucl. Instrum. and Methods in Physics Res. B* **261** [1-2]: 1180-1183 (2007).
69. T. Oda, Y. Oya, S. Tanaka, and W. J. Weber, **Validation of Potential Models for Li₂O in Classical Molecular Dynamics Simulation**, *J. Nuclear Materials* **367-370**: 263-268 (2007).
70. W. Jiang, I.-T. Bae, and W. J. Weber, **Disordering and Dopant Behaviour in Au⁺-Ion-Irradiated AlN**, *Journal of Physics: Condensed Matter* **19**: 356207 (2007).
71. W. Jiang, P. Nachimuthu, W. J. Weber, and L. Ginzburgsky, **Variation in Lattice Parameters of 6H-SiC Irradiated to Extremely Low Doses**, *Applied Physics Letters* **91**: 091918 (2007).
72. N. Li, H. Y. Xiao, X. T. Zu, L. M. Wang, R. C. Ewing, J. Lian, and F. Gao, **First-Principles Study of Electronic Properties of La₂Hf₂O₇ and Gd₂Hf₂O₇**, *J. Applied Physics* **102**: 063704 (2007).
73. L. Ma, Y. Wang, J. Xue, Q. Chen, W. Zhang, and Y. Zhang, **Energy Loss and Straggling of MeV Ions through Biological Samples**, *J. Applied Physics* **102**: 084702 (2007).
74. Z. Rong, F. Gao, W. J. Weber, and G. Hobler, **Monte Carlo Simulations of Defect Recovery within a 10 keV Collision Cascade in 3C-SiC**, *J. Applied Physics* **102**: 103508 (2007).
75. Z. Wang, X. T. Zu, F. Gao, and W. J. Weber, **Mechanical Behavior of Gallium Nitride Nanotubes under Combined Tension-Torsion: An Atomistic Simulation**, *J. Applied Physics* **103**: 013505 (2008).
76. R. Devanathan and W. J. Weber, **Dynamic Annealing of Defects in Irradiated Zirconia-based Ceramics**, *J. Materials Research* (March, 2008) in press.
77. I.-T. Bae, Y. Zhang, W. J. Weber, M. Ishimaru, Y. Hirotsu, and M. Higuchi, **Ionization-Induced Effects in Amorphous Apatite at Elevated Temperatures**, *J. Materials Research* (April, 2008) in press.
78. Y. Zhang, I.-T. Bae, and W. J. Weber, **Atomic Collision and Ionization Effects in Oxides**, *Nucl. Instrum. and Methods in Physics Res. B* (2008) in press.
79. W. J. Weber, L. Wang, Y. Zhang, W. Jiang, and I. Bae, **Effects of Dynamic Recovery on Amorphization Kinetics in 6H-SiC**, *Nucl. Instrum. and Methods in Physics Res. B* (2008) in press.
80. I.-T. Bae, Y. Zhang, W. J. Weber, M. Ishimaru, Y. Hirotsu, and M. Higuchi, **Temperature Dependence of Electron-Beam Induced Effects in Amorphous Apatite**, *Nucl. Instrum. and Methods in Physics Res. B* (2008) in press.
81. Z. J. Chen, H. Y. Xiao, X. T. Zu, L. M. Wang, F. Gao, J. Lian, and R. C. Ewing, **Structural and Bonding Properties of Stannate Pyrochlores: A Density Functional Theory Investigation**, *Computational Material Science* (2008) in press.
82. Z. Wang, X. T. Zu, L. Yang, F. Gao, and W. J. Weber, **Orientation and Temperature Dependence of the Tensile Behavior of GaN Nanowires: An Atomistic Study**, *Journal of Materials Science: Materials in Electronics* (2008) in press.
83. F. Gao, Y. Zhang, M. Posselt, and W. J. Weber, **Computational Study of Anisotropic Epitaxial Recrystallization in 4H-SiC**, *J. Physics: Condens. Matter* **20** (2008) in press.

Author Index

Author Index

Averback, R.	3	Morris, J. R.	94
Ager, J. W.	108	Müllner, P.	29
Akasheh, F.	78	Ngai, M. Y.	23
Bahr, D. F.	78	Nieh, T. G.	33
Becher, P. F.	82	Nix, W. D.	37
Bei, H.	94	Overman, C.	78
Bellon, P.	3	Overman, N.	78
Bulatov, V.	86	Painter, G. S.	82
Chrzan, D. C.	108	Pharr, G. M.	94
Chu, W-K.	7	Qiao, Y.	41
Dauskardt, R. H.	10	Raj, R.	45
Demkowicz, M. J.	98	Reimanis, I.	47
Devanathan, R.	119	Riedo, E.	50
Diab, M.	74	Ritchie, R. O.	108
Dunand, D. C.	11	Saiz, E.	108
Ewing, R. C.	15	Schneibel, J. H.	100
Follstaedt, D. M.	90	Seidman, D. N.	11
Fu, C. L.	100	Sethna, J. P.	54
Gao, F.	119	Shao, S.	78
Gao, Y. F.	94	Shibata, N.	82
George, E. P.	94	Sickafus, K. E.	112
Hoagland, R. G.	78, 98	Strachan, A.	58
Holm, E. A.	90	Sullivan, J. P.	90
Horton, J. A.	94	Tao, N. J.	62
Huang, J.	90	Thompson, A.	58
Ice, G. E.	99	Tomé, C. N.	115
Jiang, W.	119	Tomsia, A. P.	108
Kameda, J.	27	Uberuaga, B. P.	112
Koslowski, M.	19	van Benthem, K.	82
Krcmar, M.	100	Van Swygenhoven, H.	1
Krische, M. J.	23	Vishnu, K. G.	58
Lian, J.	15	Vitek, V.	66
Liechti, K. M.	23	Volkert, C. A.	2
Lin, H-T.	82	Wakamatsu, M.	23
Liu, C. T.	94, 100	Wang, J.	98
Liu, X. Y.	27	Wang, L.	15, 70
Mastorakos, I.	78	Wang, X. L.	100
McMahon, Jr., C. J.	27	Weber, W. J.	119
Medyanik, S.	78	Xu, D.	23
Miller, M. K.	100	Yu, H-h.	74
Mills, M. J.	100	Zbib, H. M.	78
Misra, A.	78, 98, 104	Zhang, Y.	119

Participant List

Participant List		
Firstname	Lastname	Organization
Firas	Akasheh	Tuskegee University
Christie	Ashton	Office of Basic Energy Sciences
Robert	Averback	University of Illinois
David	Bahr	Washington State University
Ian	Baker	Dartmouth College
Paul	Becher	Oak Ridge National Laboratory
Hongbin	Bei	Oak Ridge National Laboratory
Pascal	Bellon	University of Illinois
Irene	Beyerlein	Los Alamos National Laboratory
Vasily	Bulatov	Lawrence Livermore National Laboratory
Laurent	Capolungo	Los Alamos National Laboratory
Daryl	Chrzan	Lawrence Berkeley National Laboratory
Wei-Kan	Chu	Univ. of Houston
Bill	Corwin	Oak Ridge National Laboratory
Reinhold	Dauskardt	Stanford University
Michael	Demkowicz	Los Alamos National Laboratory
David	Dunand	Northwestern University
Rodney	Ewing	University of Michigan
Yanfei	Gao	University of Tennessee and Oak Ridge National Laboratory
Easo	George	Oak Ridge National Laboratory
Kevin	Hemker	Johns Hopkins University
Richard	Hoagland	Los Alamos National Laboratory
Elizabeth	Holm	Sandia National Laboratories
Jianyu	Huang	Sandia National Laboratory
Gene	Ice	Materials Science and Technology Division ORNL
Alexander H.	King	Ames Laboratory
Wayne	King	Lawrence Livermore National Laboratory
Refik	Kortan	US DOE Office of Basic Energy Sciences
Marisol	Koslowski	Purdue University
Richard	LeSar	Iowa State University
Jie	Lian	University of Michigan
Kenneth	Liechti	University of Texas at Austin
C.T.	Liu	UT/ORNL
Marcel	Lucas	Georgia Tech
Nathan	Mara	Los Alamos National Laboratory
Charles	McMahon	University of Pennsylvania
Andrew	Minor	Lawrence Berkeley National Laboratory
Amit	Misra	Los Alamos National Laboratory
Peter	Mullner	Boise State University
T.G.	Nieh	University of Tennessee
William	Nix	Stanford University
David	Olmsted	Sandia National Laboratories
Stefanos	Papanikolaou	University of Illinois
Yu	Qiao	Univ California, San Diego
Rishi	Raj	University of Colorado at Boulder
Ivar	Reimanis	Colorado School of Mines
Elisa	Riedo	Georgia Institute of Technology
Robert	Ritchie	Lawrence Berkeley National Laboratory
Ian	Robertson	University of Illinois
James	Sethna	Physics, Cornell University
Kurt	Sickafus	Los Alamos National Laboratory
Jerry	Simmons	Sandia National Labs

Alejandro	Strachan	Purdue University
John	Sullivan	Sandia National Laboratories
Nongjian	Tao	Arizona State University
Carlos	Tomé	Los Alamos National Laboratory
Peter	Tortorelli	Oak Ridge National Laboratory
Blas	Uberuaga	Los Alamos National Laboratory
Helena	Van Swygenhoven	Paul Scherrer Institute, Switzerland
John	Vetrano	Basic Energy Sciences
Vaclav	Vitek	University of Pennsylvania
Cynthia	Volkert	University of Göttingen, Germany
Lumin	Wang	University of Michigan
William	Weber	Pacific Northwest National Laboratory
Richard	Wright	Idaho National Laboratory
Honghui	Yu	The City University of New York
Hussein	Zbib	Washington State University
Yanwen	Zhang	Pacific Northwest National Laboratory
Steven	Zinkle	Oak Ridge National Laboratory